

JPL Publication 88-22

Proceedings of the Twelfth NASA Propagation Experimenters Meeting (NAPEX XII)

Held at Syracuse University,
Syracuse, New York, June 9-10, 1988

Faramaz Davarian
Editor

(NASA-CR-182796) PROCEEDINGS OF THE TWELFTH
NASA PROPAGATION EXPERIMENTERS MEETING
(NAPEX 12) (Jet Propulsion Lab.) 180 p
CSCL 20N

N89-11074
--THRU--
N89-11094
Unclass
G3/32 0167357

August 1988

NASA

National Aeronautics and
Space Administration

Jet Propulsion Laboratory
California Institute of Technology
Pasadena, California



Proceedings of the Twelfth NASA Propagation Experimenters Meeting (NAPEX XII)

Held at Syracuse University,
Syracuse, New York, June 9–10, 1988

Faramaz Davarian
Editor

August 1988



National Aeronautics and
Space Administration

Jet Propulsion Laboratory
California Institute of Technology
Pasadena, California

This publication was prepared by the Jet Propulsion Laboratory, California Institute of Technology, under a contract with the National Aeronautics and Space Administration.

PREFACE

The NASA Propagation Experimenters Meeting (NAPEX) is a forum convened to discuss the studies supported by the NASA Propagation Program. The reports delivered at this meeting by the management and the investigators of the program summarize the recent activities as well as plans for the future. Representatives from domestic and international organizations who conduct radio wave propagation studies are invited to NAPEX for discussions and exchange of information. This proceedings records the content of NAPEX XII.

NAPEX XII, which took place on June 10, 1988, at Syracuse, New York, was organized into one non-technical opening session and three technical sessions. NASA and JPL managers of the program addressed the audience in the opening session. The first technical session, chaired by Dr. William Rafferty of JPL, was devoted to mobile satellite propagation. A total of six presentations were made at this session. The second technical session examined the propagation effects for frequencies above 10 GHz and included six papers. Dr. David Rogers of Comsat Laboratories was the session chairman. The last technical session, which was chaired by myself, addressed new developments in the Propagation Program. Six presentations were delivered at the last session.

I would like to express my appreciation to the participants of NAPEX XII, especially to those international participants who had to travel from such distant countries as Canada, Denmark, Japan, the Netherlands, and the United Kingdom to attend our meeting. The efforts of Dr. Ernest Smith of the University of Colorado in assisting me to organize the meeting as well as the banquet, which took place during the evening of June 9, are acknowledged. I would also like to thank Mr. John Kiebler of NASA Headquarters for his uninterrupted support of the Propagation Program: Thanks to Mr. Kiebler's efforts, the Propagation Program is enjoying a moderate expansion. Many thanks are extended to Professors Arlon Adams and Tapan Sarkar of Syracuse University for hosting NAPEX XII on campus.

NAPEX XIII is planned for June 1989 in San Jose, California.

Faramaz Davarian
Project Manager
NASA Propagation Program

ABSTRACT

The NASA Propagation Experimenters Meeting (NAPEX), supported by the NASA Propagation Program, is convened annually to discuss studies made on radio wave propagation by investigators from domestic and international organizations. NAPEX XII was held on June 9 and 10, 1988, at Syracuse University, New York, and consisted of representatives from Canada, Denmark, Japan, the Netherlands, United Kingdom, and the United States. The meeting was organized into three technical sessions: The first was devoted to mobile satellite propagation; the second examined the propagation effects for frequencies above 10 GHz; and the third addressed new developments in the Propagation Program.

CONTENTS

INTRODUCTORY REMARKS AND FUTURE TRENDS	1
F. Davarian	
PIFEX PROPAGATION EXPERIMENTS	5
R.F. Emerson, J.B. Berner, and L.G.L. Ho	
PIFEX DATA AND ARCHIVAL FORMATS	11
J.B. Berner	
RESULTS OF 1987 MSS HELICOPTER PROPAGATION EXPERIMENT AT UHF AND L BAND IN CENTRAL MARYLAND	18
J. Goldhirsh and W.J. Vogel	
IMSS PROPAGATION MODELING AT VIRGINIA TECH	27
W.L. Stutzman, R.M. Barts, and C.W. Bostian	
PRELIMINARY RESULTS OF MARECS-A MEASUREMENTS IN CENTRAL MARYLAND AND PLANS FOR 1988 MSS EXPERIMENT IN AUSTRALIA	36
W.J. Vogel and J. Goldhirsh	
ETS-V PROPAGATION EXPERIMENTS IN JAPAN	47
S. Ohmori	
MOBILE SATELLITE PROPAGATION MEASUREMENTS AND MODELING: A REVIEW OF RESULTS FOR SYSTEMS ENGINEERS	55
W.L. Stutzman, editor	
PROPAGATION HANDBOOK, FREQUENCIES ABOVE 10 GHz	70
L.J. Ippolito	
RESULTS OF APL RAIN GAUGE NETWORK MEASUREMENTS IN MID-ATLANTIC COAST REGION AND COMPARISONS OF DISTRIBUTIONS WITH CCIR MODELS	81
J. Goldhirsh, N. Gebo, and J. Rowland	
INTERFERENCE BY RAIN SCATTER	91
R.K. Crane	
MILLIMETER-WAVE STUDIES	103
K.C. Allen	
GROUND-BASED RADIOMETRIC OBSERVATIONS OF EMISSION AND ATTENUATION AT 20.6, 31.65, AND 90.0 GHz	114
E.R. Westwater, J.B. Snider, and M.J. Falls	
LASER COMMUNICATION THROUGH THE ATMOSPHERE	126
K. Shaik and J.H. Churnside	

PLAN OF PROPAGATION AND COMMUNICATION EXPERIMENTS USING ETS-VI	132
S. Ohmori	
PLAN OF ADVANCED SATELLITE COMMUNICATIONS EXPERIMENT USING ETS-VI	138
T. Shiomi	
OPEX-OLYMPUS PROPAGATION EXPERIMENT	140
G. Brussaard	
ACTS AND OLYMPUS PROPAGATION EXPERIMENTS	146
C.W. Bostian and K.R. Baker	
A DIGITAL BEACON RECEIVER	157
P.D. Ransome	
OLYMPUS BEACON RECEIVER	164
J. Ostergaard	
THE PROPAGATION INFORMATION CENTER AT THE UNIVERSITY OF COLORADO	169
E.K. Smith and W.L. Flock	

NAPEX ATTENDEES - JUNE 10, 1988, SYRACUSE, NEW YORK

Prof. & Mrs. Arlon T. Adams
Syracuse University
III Link Hall
Syracuse, NY 13210
(315) 423-4397

Mr. and Mrs. John Butterworth
Communications Research Centre
P. O. Box 11490, Station H
Ottawa, Ontario K2H 8S2
CANADA
(613) 998-2559/TELEX 053-4143

Mr. Kenneth C. Allen
ITS/NTIA, Radio Bldg.
325 Broadway
Boulder, CO 80303
(303) 497-3412/FTS 320-3412

Dr. Richard L. Campbell
Michigan Technical University
Dept. of Electrical Engineering
Houghton, MI 49931
(906) 487-2848

Mr. Ken R. Baker
Virginia Tech.
Dept. of Electrical Engineering
Blacksburg, VA 24061
(703) 961-6834

Dr. James H. Churnside
Mail Code R/E/WP1
NOAA Wave Propagation Laboratory
325 Broadway
Boulder, CO 80303
(303) 497-6744

Mr. Melvin Barmat
Telecommunications Inc.
1899 L Street NW
Suite 1010
Washington, DC 20006
(202) 467-6400

Prof. Robert K. Crane
Thayer School of Engineering
Dartmouth College
Hanover, NH 03755
(603) 646-3843

Mr. R. Michael Barts
Virginia Tech.
Dept. of Electrical Engineering
Blacksburg, VA 24061
(703) 961-6834

Dr. Faramaz Davarian
Mail Stop 200-111
Jet Propulsion Laboratory
4800 Oak Grove Drive
Pasadena, CA 91109
(818) 354-4820

Prof. Charles W. Bostian
Virginia Tech.
Dept. of Electrical Engineering
Blacksburg, VA 24061
(703) 961-6834

Dr. Khaled Dessouky
Mail Stop 161-228
Jet Propulsion Laboratory
4800 oak Grove Drive
Pasadena, CA 91109
(818) 354-0412

Dr. Gert Brussaard
Technical University of Eindhoven
THE NETHERLANDS

Mr. Richard F. Emerson
Mail Stop 238-420
Jet Propulsion Laboratory
4800 Oak Grove Drive
Pasadena, CA 91109
(818) 354-3834

Dr. Shingo Ohmori,
Communications Research Laboratory
Ministry of Posts and
Telecommunications
Kashima, Ibaraki 314
JAPAN
0299-82-1211/FAX 0299-83-5728

Prof. Warren L. Flock
ECE Dept.
University of Colorado
Campus Box 425
Boulder, CO 80309-00425
(303) 492-7012

Mr. Jens Ostergaard
ElektronikCentralen
Venlighedsvej 4
DK-2970 Hoersholm
DENMARK
(02) 867722/TELEX 37121

Dr. Julius Goldhirsh
Johns Hopkins University
Applied Physics Lab
Johns Hopkins Road
Laurel, MD 20707
(301) 953-5042

Dr. William Rafferty
Mail Stop 238-420
Jet Propulsion Laboratory
4800 Oak Grove Drive
Pasadena, CA 91109
(818) 354-5095

Miss Loretta Ho
Mail Stop 200-111
Jet Propulsion Laboratory
4800 Oak Grove Drive
Pasadena, CA 91109
(818) 354-1724

Mr. Peter D. Ransome
Signal Processing Ltd.
Cambridge Science Park
Milton Road
Cambridge CB4 4GJ,
ENGLAND
(0223) 358357/TELEX 817360

Dr. Louis J. Ippolito
Westinghouse Electric Corporation
Mail Stop 4240
P.O. Box 1897
Baltimore, MD 21203
(301) 765-2603

Dr. David V. Rogers
COMSAT Labs
22300 COMSAT Drive
Clarksburg, MD 20871
(301) 428-4411

Mr. John Kiebler
NASA Headquarters
Code ECC
600 Independence Ave.
Washington, DC 20546
(202) 453-1515

Mr. Charles Ruggier
Mail Stop 200-111
Jet Propulsion Laboratory
4800 Oak Grove Drive
Pasadena, CA 91109
(818) 354-1823

Dr. Ben Segal
Communications Research Centre
P.O. Box 11490, Station H
Ottawa, Ontario K2H 8S2
CANADA
(613) 596-9697/TELEX 053-4143

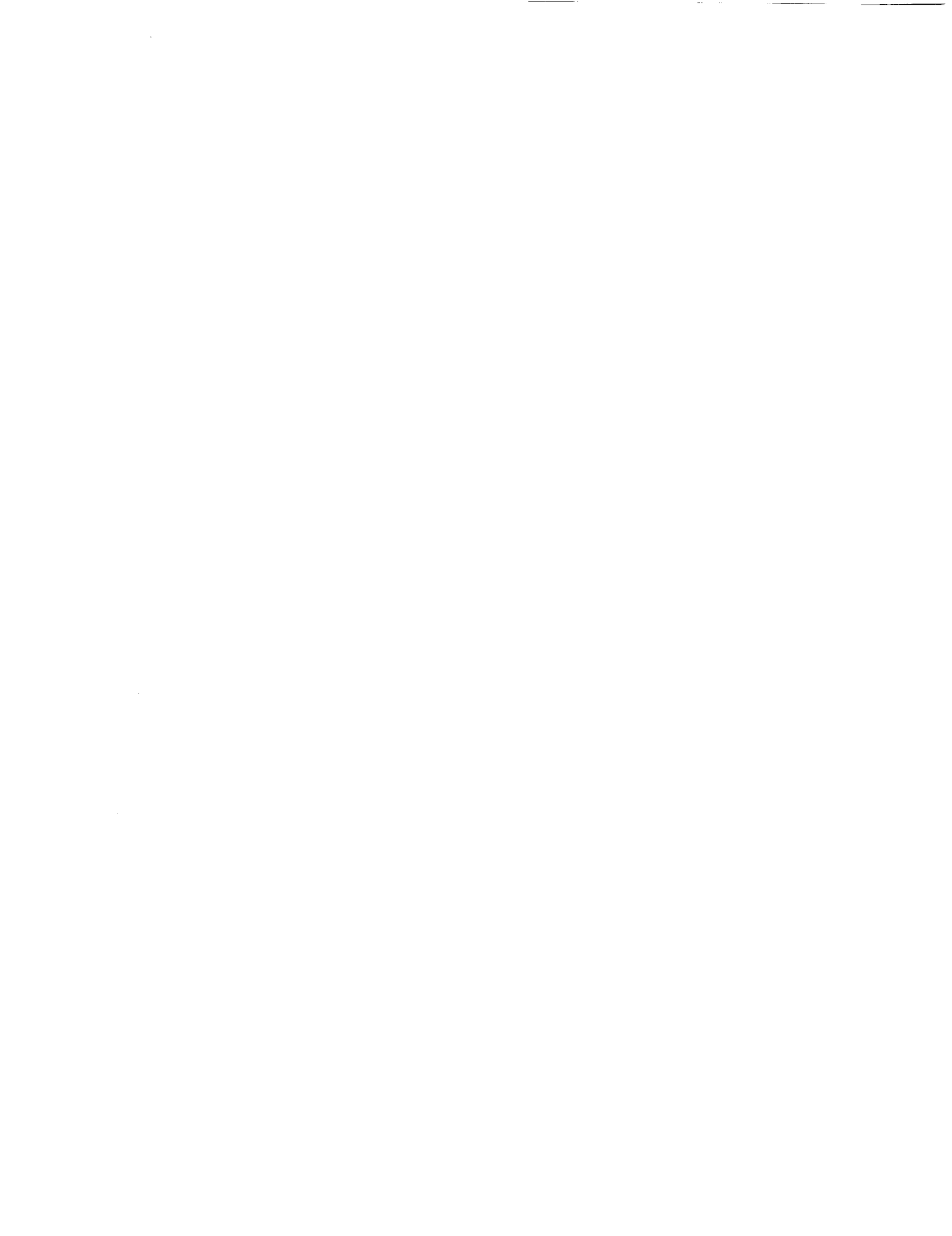
Dr. Kamran Shaik
Mail Stop 161-228
Jet Propulsion Laboratory
4800 Oak Grove Dr.
Pasadena, CA 91109
(818) 354-9176

Dr. Ernest K. Smith
University of Colorado
Dept. of Electrical Engineering
Campus Box 425
Boulder, CO 80309-00425
(303) 492-7123

Prof. Warren Stutzman
Virginia Tech.
Dept. of Electrical Engineering
Blacksburg, VA 24061
(703) 961-6834

Dr. Wolfhard J. Vogel
University of Texas
Electrical Engineering Research Lab
10100 Burnet Road
Austin, TX 78758
(512) 471-8608

Dr. Edgeworth R. Westwater
Wave Propagation Laboratory
NOAA/ERL/WPL, Dept. of Commerce
325 Broadway
Boulder, CO 80303
(303) 497-6527



INTRODUCTORY REMARKS AND FUTURE TRENDS

Faramaz Davarian
Jet Propulsion Laboratory
California Institute of Technology
4800 Oak Grove Drive
Pasadena, California 91109

The Propagation Studies and Measurements Program is mandated by NASA to perform propagation studies to investigate Earth/space communication links. The program objectives are to aid NASA's Applications Programs, and to support the communications satellite industry, particularly emerging services. This program achieves its objectives by studying the effects of propagation and noise on Earth/space communications, disseminating its findings, and participating in the CCIR study groups.

RECOMMENDATIONS OF THE REVIEW PANEL

The Propagation Program was reviewed by a panel of experts in September 1986. The program review resulted in a document which was published in February 1987 describing the panel findings and suggestions. The panel had prepared a hearty list of fourteen recommendations. These recommendations address all aspects of the program and were taken quite seriously by the program management at JPL. The following examples demonstrate our reaction to certain panel instructions.

Recommendations 2 and 3 stress the need for a) cooperation with other centers of propagation studies, and b) monitoring of the work conducted in such centers. In response to these recommendations, I made a few trips which took me to Boulder, Colorado; Tokyo, Japan; and Noordwijk, the Netherlands. In Boulder, arrangements were made for cooperation with the Wave Propagation Laboratory of NOAA, and the Institute for Telecommunications Sciences of NTIA. In Tokyo, I visited the Communications Research Laboratory and the KDD laboratory. My discussions at CRL, where Dr. Kim Dinh of Aussat was also present, resulted in our plans to participate in an experiment later this year (September 1988) in Australia. This experiment is addressed on page 36 of this issue. The purpose of my trip to Noordwijk was to attend the Olympus Propagation Experimenters meeting. Our plan for participation in the Olympus Experiment is discussed on page 146 of this issue.

Recommendation 6 concerned practical scenarios for mobile satellite propagation measurements. From the beginning of our activity in the area of mobile satellite, we had to rely on simulated space platforms because we had no access to satellite beacons. Since the panel recommendations were published, this has changed: We made our first satellite experiment in December 1987, which is reported on page 36 of this document. And as was

mentioned earlier, we are planning to go to Australia in September 1988 to participate in a realistic mobile satellite experiment.

Recommendation 8 considers radiometric techniques and cloud effects. A joint effort with the Wave Propagation Laboratory is currently addressing this topic as can be learned from the article on page 114 of this issue.

A study of optical propagation was addressed in Recommendation 14. The article on page 126 is in response to this recommendation.

FUTURE TRENDS

Certain areas will be emphasized in our program in FY '89. These areas include:

- a) Participation in Earth/space propagation experiments where signals transmitted from spacecraft will be used for making field measurements.
- b) Studies in Ka and millimeter-wave frequencies.
- c) Radiometric techniques for making noise measurements and studying cloud effects.
- d) Investigation of new and emerging satellite communications services.
- e) CCIR participation.
- f) Cooperation with other centers of propagation studies.

A major effort that started in FY '88 and is expected to gain momentum in FY '89 is the Olympus and ACTS studies. We have established an excellent relationship with the propagation community in ESA, as a result of which we have been invited to join the Olympus Propagation Experimenters (OPEX) to conduct propagation measurements. Currently, we are preparing for participation in the Olympus experiment. Our plans call for construction of a beacon receiver, recording and processing of data in accordance with the OPEX standard format, exchanging propagation data with other experimenters, participation in the CODE exercise, testing of uplink power control schemes, etc.

We believe that the Olympus experiment will prepare us for making positive contributions to the ACTS Program. Our full participation in ACTS by the year 1992 is foreseen.

Our activities in the mobile satellite area will experience certain changes. Our effort regarding mobile satellite software

channel simulation will be reduced. No more non-spacecraft platform measurements are planned. The emphasis will be given to the following areas: studies and field measurements using satellite beacons, model improvement, and CCIR contributions. We must publicize the results of our work and receive feedback from the users. At the same time we must make sure that our models receive wide acceptance. We should pay attention to new areas in mobile and personal satellite services. Considering our limited budget, we need to identify study areas which will produce the biggest return for the same investment.

REVIEW AND REPORTING

All investigators of the Propagation Program get together in the yearly NAPEX meeting to report on their progress and plans. The NAPEX meeting is intended to have wide coverage and includes every aspect of the program without necessarily getting into too many details. To complement the NAPEX meeting, workshops on specific topics are organized. For example, in October 1987, we had a workshop on mobile satellite at JPL. We will organize other workshops in the future, examples of which are workshop on ACTS propagation, workshop on propagation studies for frequencies above 10 GHz, etc.

Last May, the Propagation Program organized a session on propagation for the mobile satellite conference in Pasadena which was sponsored by JPL. A number of the Propagation Program investigators along with other participants made a total of eight presentations. This type of activity is aimed at publicizing our program and providing an opportunity to the potential users to hear what we have to say and give us feedback. An invited paper which reviews propagation measurements and models was presented by Warren Stutzman in the conference. Because of the great relevance of this paper to our interest in mobile satellite communications, it has been reprinted on page 55 of this issue. Review papers of this type are greatly encouraged because of their ease of use by system engineers.

We periodically update the two NASA Propagation Handbooks. The new revision of the handbook on frequencies below 10 GHz was published in December 1987. Due to its popularity, we are already running out of handbook copies and soon will reprint some more. The revision was performed by Warren Flock of the University of Colorado. The handbook on frequencies above 10 GHz is in its fourth revision and soon will be published, see paper on page 70. The NASA handbooks are excellent vehicles for dissemination of information and education of the propagation community.

We also disseminate our findings via publishing peer-reviewed papers, making conference presentations, issuing reports, etc. Our newly formed Information Center at the University of Colorado

will play a major role in informing the community of our activities by making user surveys and publishing a quarterly newsletter. The Information Center will also keep us up to date on the activities of other centers of propagation studies.

As was mentioned earlier, the Propagation Program was reviewed by a panel of experts less than two years ago. We are thinking of continuing this type of program review in some form or other. A periodic review every four years may be the answer.

In Summary, the elements of our program review and reporting are:

- 1) NAPEX meetings
- 2) Workshops
- 3) Conference and journal papers
- 4) Reports and publications
- 5) Organization of conference sessions and short courses
- 6) CCIR participation
- 7) Periodic panel review
- 8) Information center --newsletter, user survey, etc.
- 9) Interaction with other centers of propagation studies
- 10) NASA Propagation Handbooks

PiFEx Propagation Experiments

Richard F. Emerson
 Jeff B. Berner
 Loretta L. G. Ho

Jet Propulsion Laboratory
 4800 Oak Grove Drive
 Pasadena, California 91109

ABSTRACT

The Pilot Field Experiments (PiFEx) have provided considerable data (more than 1 gigabyte) on the performance of MSAT-X equipment and subsystems. These data have been used to optimize performance of the system. Data has also been collected on propagation effects using a satellite beacon operating at L-Band. Preliminary results show good agreement with earlier work.

INTRODUCTION

This paper presents an overview of the Pilot Field Experiments (PiFEx) performed under the Mobile Satellite Experiment Program (MSAT-X) at JPL. The first section is a brief history of PiFEx and plans for further experiments. The second is a discussion of some results from the Satellite 1a experiment held last August.

PiFEx: Past, Present, and Future

The Pilot Field Experiments were developed to provide an orderly transition from the development of a system architecture, and the equipment necessary to implement that architecture, to a prototype system for demonstrations and user experiments. PiFEx was started in November of 1985 with the expectation of demonstrating a major portion of the technologies under development at JPL by the first quarter of 1987. While the main thrust of PiFEx has been the performance evaluation of the equipment, it was realized that measurements of the propagation environment should be an essential part of the activity. The mobile laboratory, referred to as the Propagation Measurement Van, was designed and built to support both the engineering and propagation experiments (Emerson, 1987).

The first in the PiFEx series (Tower 1) was performed at the Wave Propagation Laboratory facility in Erie, Colorado. These experiments were primarily engineering in nature. In addition to the verification of system integration, the performance of the JPL developed Mechanically Steered Antenna and the data modulation technique were evaluated. While static tests had been performed at JPL, these were the first tests where a mobile environment approximating the satellite link was available. Even here the ability to evaluate the open loop tracking performance of the antenna, using a turn rate sensor, was severely limited. However, valuable experience was gained during this activity. A description of Tower 1 was published in the MSAT-X Quarterly series (Emerson et al., 1988).

The second PiFEx activity (Satellite 1a) was conducted on roads and freeways between JPL, in Pasadena, and Santa Barbara, California. While, again, the primary purpose was to evaluate equipment performance in a realistic environment, special attention was given to selecting sites where useful propagation data could also be obtained. The original plan was to use a signal from a Pacific Operational Region INMARSAT transponder. Scheduling difficulties precluded this. However, there was a beacon signal available on a MARISAT satellite. The level of this beacon is somewhat less (~ 4.0 dB) than desired (Parkyn, 1987 and Sue, 1987). This, combined with the low elevation angle to the satellite (~ 13 degrees), provided a test beyond the worst case limit of design. Again, the evaluation of performance of the JPL Mechanically Steered Antenna was the primary purpose of the experiment. The secondary, but equally important, purpose of the experiment was to gather propagation data under a variety of terrains and shadowing conditions using the steered antenna (Berner, 1988a). As is discussed below, data was collected for uncluttered, hill shadowed, vegetatively shadowed, and freeways with overpasses and obstructive vehicles.

The third in the PiFEx series (Tower 2) was performed, once again, at the Wave Propagation Laboratory facility in Erie, Colorado. These experiments were primarily engineering in nature, as before. In addition to the continued evaluation of the performance of the JPL Mechanically Steered Antenna, the performance of a phased array antenna developed by Teledyne Ryan Electronics was tested. A brief description of Tower 2 was published in the MSAT-X Quarterly series (Berner, 1988b).

PiFEx Tower 3, planned for July 1988, will continue to evaluate the performance of the phased array and mechanically steered antennae; of the 8 phase differentially detected, trellis encoded modulation technique (8DPSKTCM); and the 4.8 kilobit speech coders in a full duplex simulated satellite link. Additionally, some aspects of the network protocol will be evaluated.

Satellite 1b, planned for autumn, will concentrate on evaluating propagation effects and the improvement in performance that can be obtained with a directive antenna. Measurements will be made, simultaneously, of the INMARSAT Beacon signal at a fixed site and on the van using two antennas: 1) a drooping dipole (4-5 dBi, omni) and 2) each of the available directive antennas. Measurements will be made over the same terrain and at the same speed for each antenna. These experiments should provide data to enhance the understanding of the propagation effects and the potential system performance.

One of the products of the intensive experiment schedule has been the accumulation of raw data. This raw data has been recorded in several different formats depending upon the maturity of the Data Acquisition System and experiment requirements. In an attempt to make the raw data more accessible to experimenters, we have developed and are implementing an archival file format. This format will not only handle the past experiment data sets, but is extensible so that it will handle future requirements as well (Berner 1988c).

ORIGINAL PAGE IS
OF POOR QUALITY

Satellite 1a

The PiFEx Satellite 1a test was conducted in Santa Barbara, California, from August 9, 1987 to August 19, 1987. The area was selected because the elevation angle to the INMARSAT satellites over the Pacific Ocean is the highest in the Southern California area and because of the proximity to JPL. Initial discussions with INMARSAT had centered around the use of the transponder, providing a signal at +26 dBW EIRP. The transponder was not available for the period selected for the experiment. However, a beacon on the MARISAT satellite was available and was used as the RF source. The beacon level is only +22 dBW EIRP. This, coupled with the lower gain of the antenna at the 13 degree elevation, required that adjustments to the MSAT-X receiver gain profile and antenna control loop parameters be made. A low noise amplifier and bandpass filter were mounted as close to the antenna as practical, between the directional coupler and the rotary joint. (Details of the JPL antenna can be found in Ref. (Emerson et al., 1988).) This added over 30 dB gain and minimized the effects of the losses in the antenna. Additionally, the bandwidth of the loop used to track the satellite azimuth was reduced. This, in turn, limited the turn rate tracking ability. This limitation affected the ratio of open to closed loop data gathered by the experiment. Propagation data gathered by the experiment was not affected.

The tilt of the antenna was also adjusted to maximize the gain of the antenna for the 13 degree elevation of the signal source. No improvement in tracking performance was noted. The impact of this change on propagation has not yet been evaluated.

The path of the experiment is given in Figure 1. Each (+) represents the start of a record of data of approximately 75 seconds. (The legends [e.g. A-5] indicate the name of the data cartridge where the data for that section of the path is stored.)

A section of the path around Santa Barbara has been expanded to show the correlation between the position data collected using Loran-C and a street map (Figure 2). The Loran is sampled every four seconds and no curve fitting was used for the representation of Figure 2. While not perfect, it is still capable of being used to correlate the terrain and shadowing effects with the received signal strength.

A short segment of received signal level data is shown in Figure 3. The data are effectively normalized by receiver limits. A 15 minute segment along the coast was used to determine an average which is then used as the normalized level for the computation of statistics. Data from the in-phase and quadrature outputs of the receiver are sampled 1000 times a second and used to compute the power level. A moving average over 10 ms was used to smooth the data which is shown as the heavier curve in Figure 3. The value of 10 ms was chosen only to verify that the processing program was working correctly. Further work is needed to define how this value should be chosen. Work is also in process to create spectra of the received signal level. This should be useful in evaluating the multipath rejection capability of the antenna.

Two segments of data approximately 15 minutes in length were selected to compute fade statistics. The first of these covered the San Marcos Pass area, a canyon area. The closest hillside was on the same side as the satellite. The second segment was along the coast line with essentially an unobstructed

view of the satellite. There is, however, some vegetative shadowing along this path. Figure 4 shows the fade statistics for these two paths. A fade depth of 0 dB corresponds to the average power in Figure 3. These curves compare favorably with the results of Vogel and Goldhirsh, Butterworth, and others (1988).

Conclusion

The PiFEx series of experiments has been successful in collecting propagation data as well as the engineering performance data. Only preliminary analysis of the propagation data has been done to date. The analysis has been primarily to verify that the processing tools developed so far are useful and correct. These analyses will also guide in the further development of analysis tools.

References

- [1] Emerson, Richard F., Pilot Field Experiments, Proceedings of NAPEX-XI, June 19, 1987, Blacksburg, Virginia.
- [2] Emerson, Richard F., ed., Special Issue of PiFEx Tower-1 Experiments, MSAT-X Quarterly, No. 13, January 1988.
- [3] Parkyn, James, Sla Link Analysis, JPL Internal Document, September 18, 1987.
- [4] Sue, Miles, Preliminary Link Budgets for PiFEx Using the INMARSAT Satellites Over the Pacific Ocean, JPL Internal Document, October 15, 1987.
- [5] Berner, Jeff, The PiFEx Satellite 1a Experiment, MSAT-X Quarterly, No. 15, June 1988.
- [6] Berner, Jeff, The PiFEx Tower-2 Experiment, MSAT-X Quarterly, No. 15, June 1988.
- [7] Goldhirsh, J. and Vogel, W., Attenuation Statistics Due to Shadowing and Multipath from Roadside Trees at UHF and L-Band for Mobile Satellite Systems, JHU/APL S1R88U 004, February 1988.
- [8] Berner, Jeff B., PiFEx Data and Archival Formats, NAPEX-XII, June 10, 1988, Syracuse, NY.

Santa Barbara Experiment (S-1a)

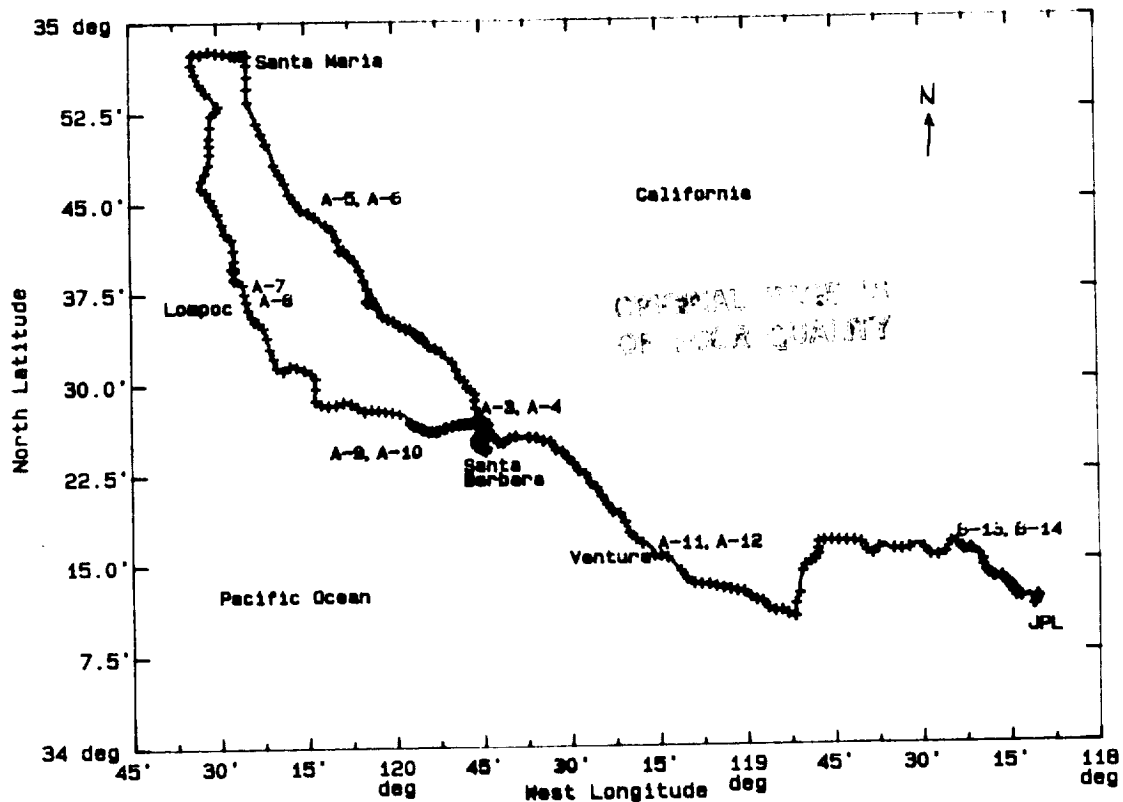


Figure 1 Satellite 1a Experiment Path

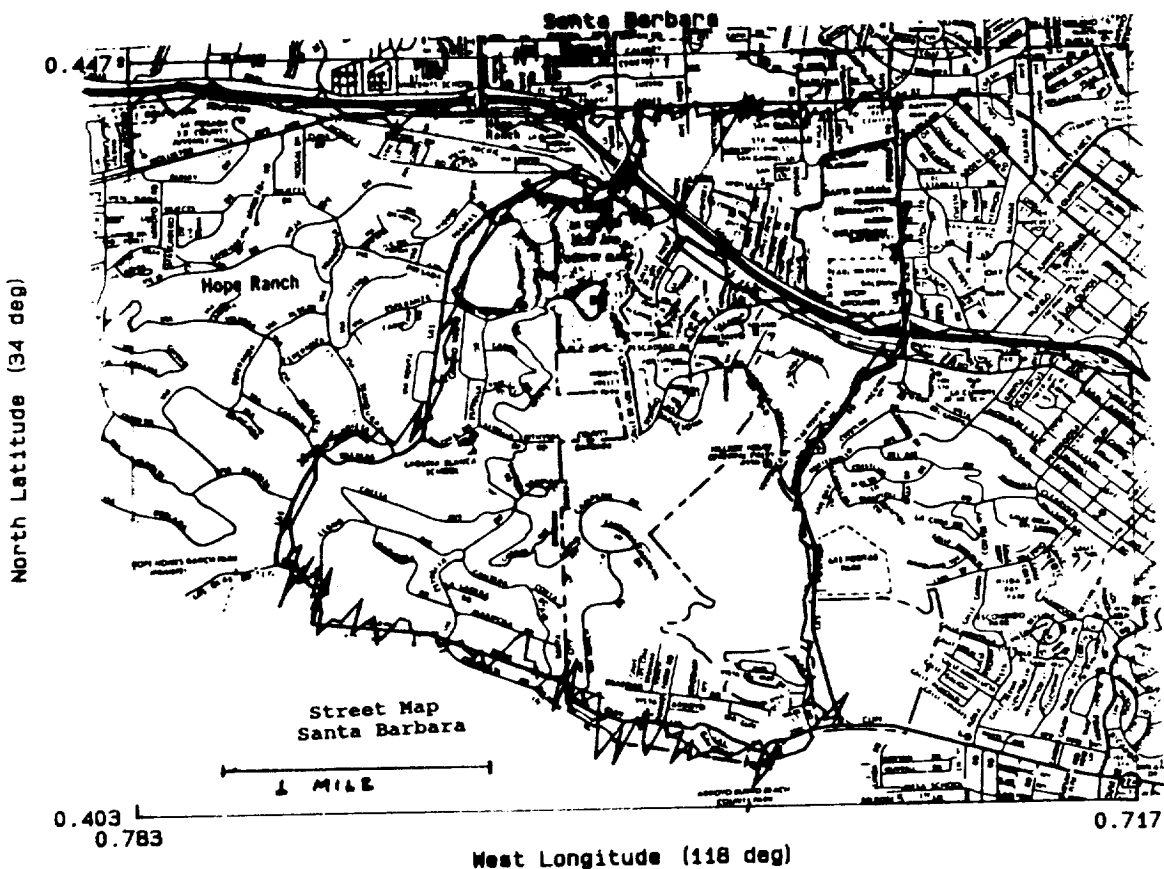


Figure 2 Map and Loran Data Comparison

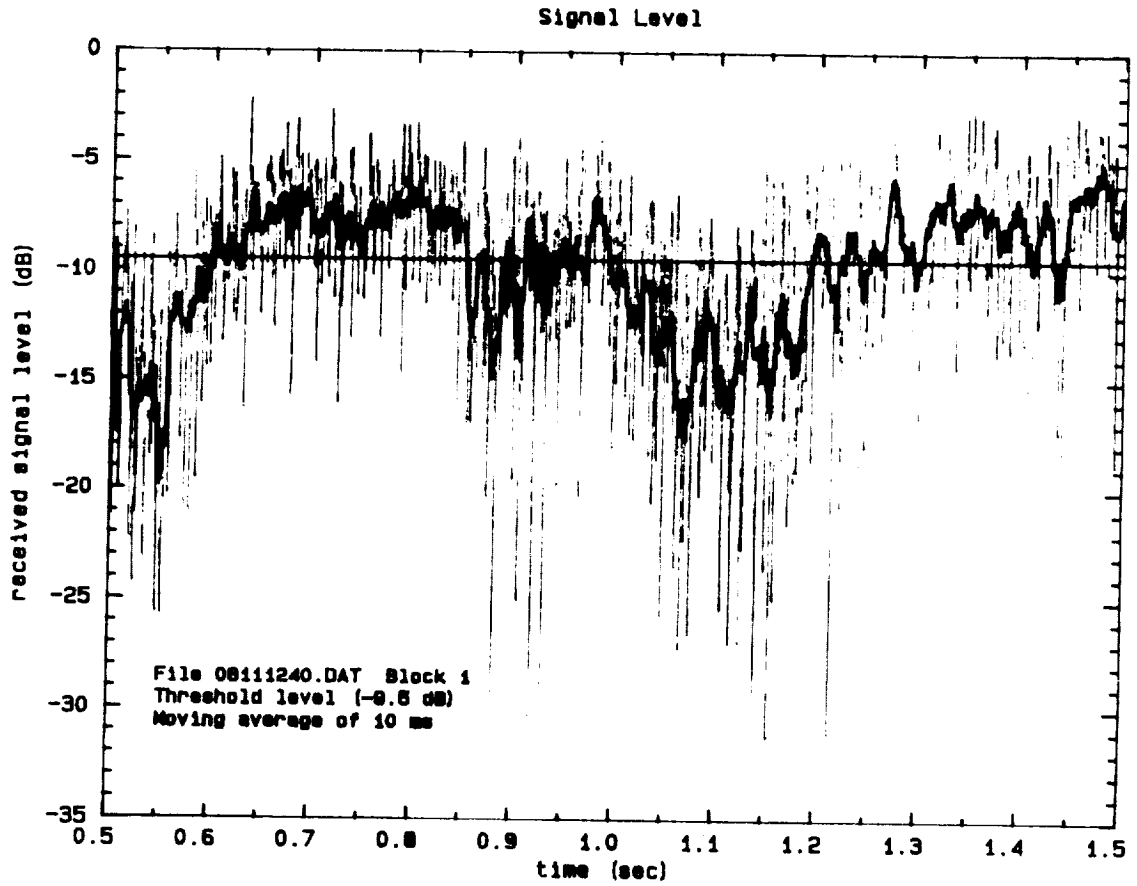


Figure 3 Received Power vs Time

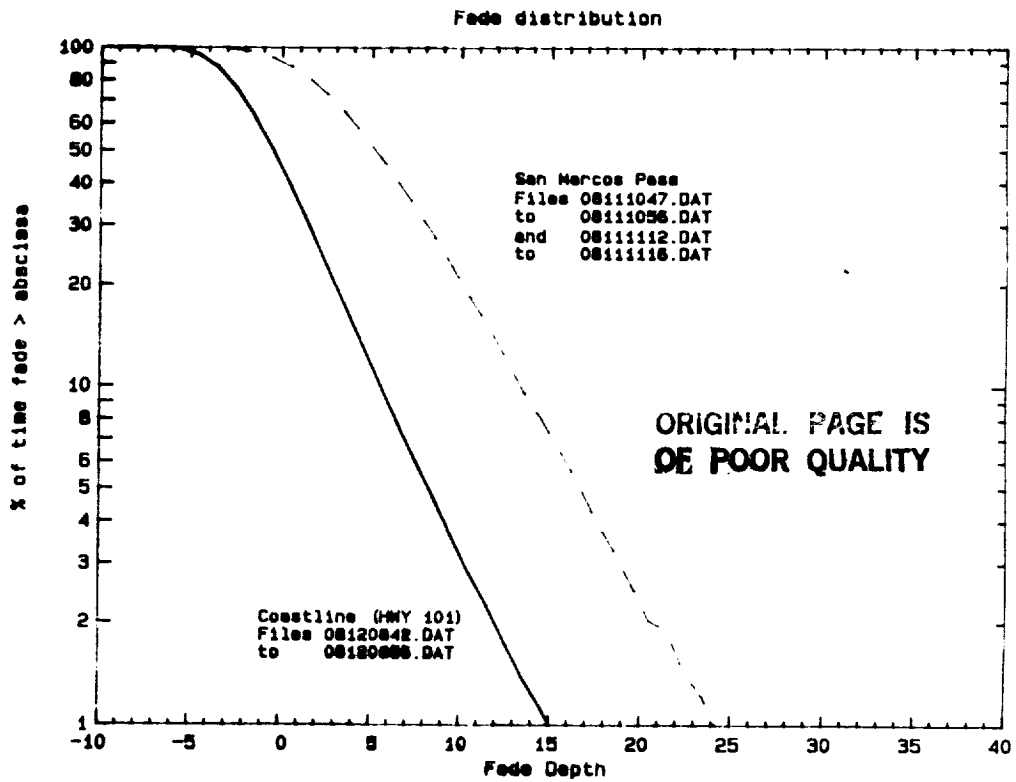


Figure 4 Fade Depth Distribution

ORIGINAL PAGE IS
OF POOR QUALITY

PIFEX DATA AND ARCHIVAL FORMATS

Jeff B. Berner
 Member of the Technical Staff
 California Institute of Technology
 Jet Propulsion Laboratory
 4800 Oak Grove Drive
 Pasadena, California 91109

Introduction

JPL has assembled, as a part of NASA's Mobile Satellite Experiment (MSAT-X), a mobile laboratory for conducting experiments on MSAT-X developed equipment and determining L-band propagation effects. To gather this experimental data, a central data acquisition system (DAS) was built around an IBM PC/AT. A description of the van and the DAS is given in (Emerson, 1987). Up to this point, the mobile laboratory (ML) has been used for three major Pilot Field Experiments (PiFEx): Tower 1, Satellite 1a, and Tower 2 (Berner, 1987, 1988a,b). At least two more are planned: Tower 3 and Satellite 1b. Nearly a gigabyte of data has been collected so far. Each test has introduced new equipment to the ML and new requirements on the DAS. To date, each experiment has resulted in a different file format for storing the raw data, making the subsequent analysis programs experiment dependent. To combat this, JPL has developed an archival format that is experiment independent and expandable for future additions.

Experiment Data File Formats

The starting point for the JPL DAS development was the data acquisition system developed by Dr. Wolfhard Vogel of the University of Texas at Austin (Vogel, 1985). Dr. Vogel's files consist of sixty-three 4120 byte records. Each record consists of a 24 byte header, 1024 samples of the received signal level, and 1024 samples of the signal phase (see Figure 1).

Since MSAT-X was interested in testing equipment along with the propagation investigation, the DAS had to record data from all instruments, not just the receiver. For the first PiFEX experiment, Tower 1, the DAS took data from the antenna subsystem, the MSAT-X receiver, and a reference receiver and stored it in the memory of the IBM. When the memory was full, the DAS stopped taking data and dumped its memory to a Bernoulli Box cartridge disk. This resulted in 2.5 minutes of data taking and 30 seconds of data writing, making the data acquisition non-continuous. Time tagging of the data was provided by the data file's name, MMDDHHMM.DAT (month, date, hour, minute).

The Tower 1 data was written in blocks of like data (see Figure 2). For example, the High Speed Analog group consisted of 150,000 records, with each record consisting of a sample each of the reference receiver inphase channel, the reference quadrature channel, the pilot receiver inphase channel, and the pilot

quadrature channel. These blocks were then stacked sequentially into a named file when the data was written to the cartridge disk (Bernoulli Box). Memory constraints prevent using this method if additional equipment is to be added without decreasing the data acquisition rates of the original equipment.

For Satellite 1a and Tower 2, the data taking method underwent a radical change. First, a Loran receiver was added to the ML configuration. Secondly, the data acquisition became continuous, with the data being written in files containing 75 seconds of data. Each file now consists of 20 blocks, each block containing 3.75 seconds of data (see Figure 3). This removed the memory limitation that prevented expanding the Tower 1 configuration. Each block contains data stacked in a similar manner as the Tower 1 format. Although this method provides continuous data acquisition, the file format now requires an additional block demultiplexing step for data analysis programs.

For the July 1988 Tower 3 experiment, additional equipment has been added to the ML configuration: the JPL terminal processor (adding an additional digital interface) and a data channel signal-to-noise ratio measurement (an HP-IB recording and an analog channel). The overall data format will remain the same, but the absolute location of each data record will change because of the additional data items.

For Satellite 1b this may change again. Thus, we may have at least 4 different file formats. Adding to the problem is the fact that we have run tests on the JPL Antenna Range with the DAS sampling the pilot receiver at a higher rate, resulting in yet another file format to deal with. Obviously, an archival format is required.

Archival Format

The archival format consists of a header, which may list the experiment name and any special conditions; a table of contents, which would list the data set number, the absolute position in the file of the first byte of the set, the number of bytes of data in the set, and a data type description; and finally the data sets (see Figure 4).

The only experiment dependent item required would be a program that translates the data format used for the experiment to the archival format. This translation would be done after the experiment and prior to any data analysis.

The advantages of this method are clear. Using just one byte for the data set numbering provides the ability to store 256 different data sets. Since the table of contents lists the start position and the data length, different sampling rates can be accommodated. Analysis programs would need to read only the table of contents for the location of the data of interest; thus, one version of the program could analyze data for all of the experiments. Specific programs could be written to extract

limited data sets; this would ease the dissemination of data, such as propagation data, to experimenters other than JPL.

Conclusion

A standard archival format has been presented for the JPL MSAT-X PiFEX experiments, which will overcome the deficiencies of the current set-up. This format allows ease of data processing, flexibility for future experiments, and controllable data dissemination to other experimenters.

References:

- Emerson, Richard F. 1987. "Pilot Field Experiments," Proceedings of NAPEX XI, JPL D-4647, August 31, 1987.
- Berner, Jeff B. 1987. "PiFEX Tower 1 Results," Proceedings of NAPEX XI, JPL D-4647, August 31, 1987.
- Berner, Jeff B. 1988a. "The PiFEX Satellite 1a Experiment," MSAT-X Quarterly, Number 15, June 1988.
- Berner, Jeff B. 1988b. "The PiFEX Tower 2 Experiment," MSAT-X Quarterly, Number 15, June 1988.
- Vogel, Wolfhard J. 1985. Personal Communication to Anil V. Kantak, December 3, 1985.

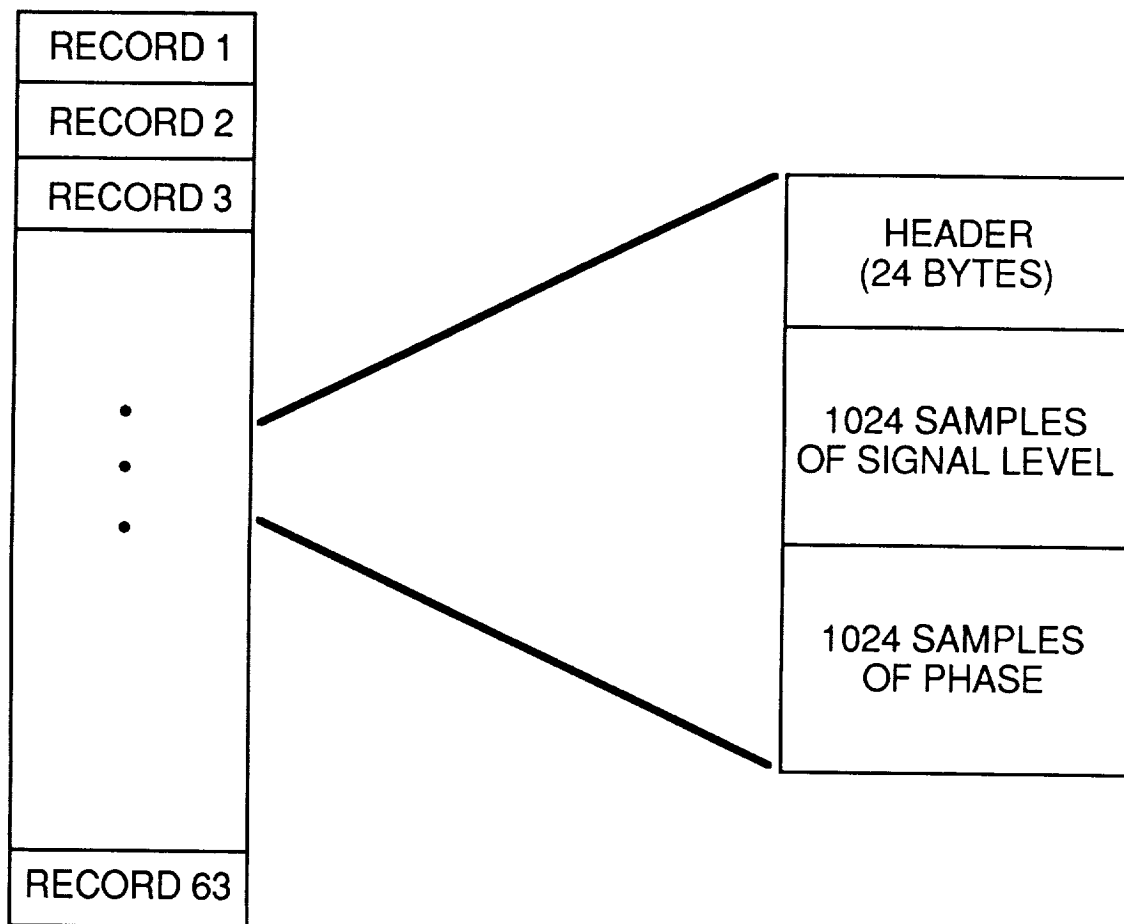


Figure 1
University of Texas Format

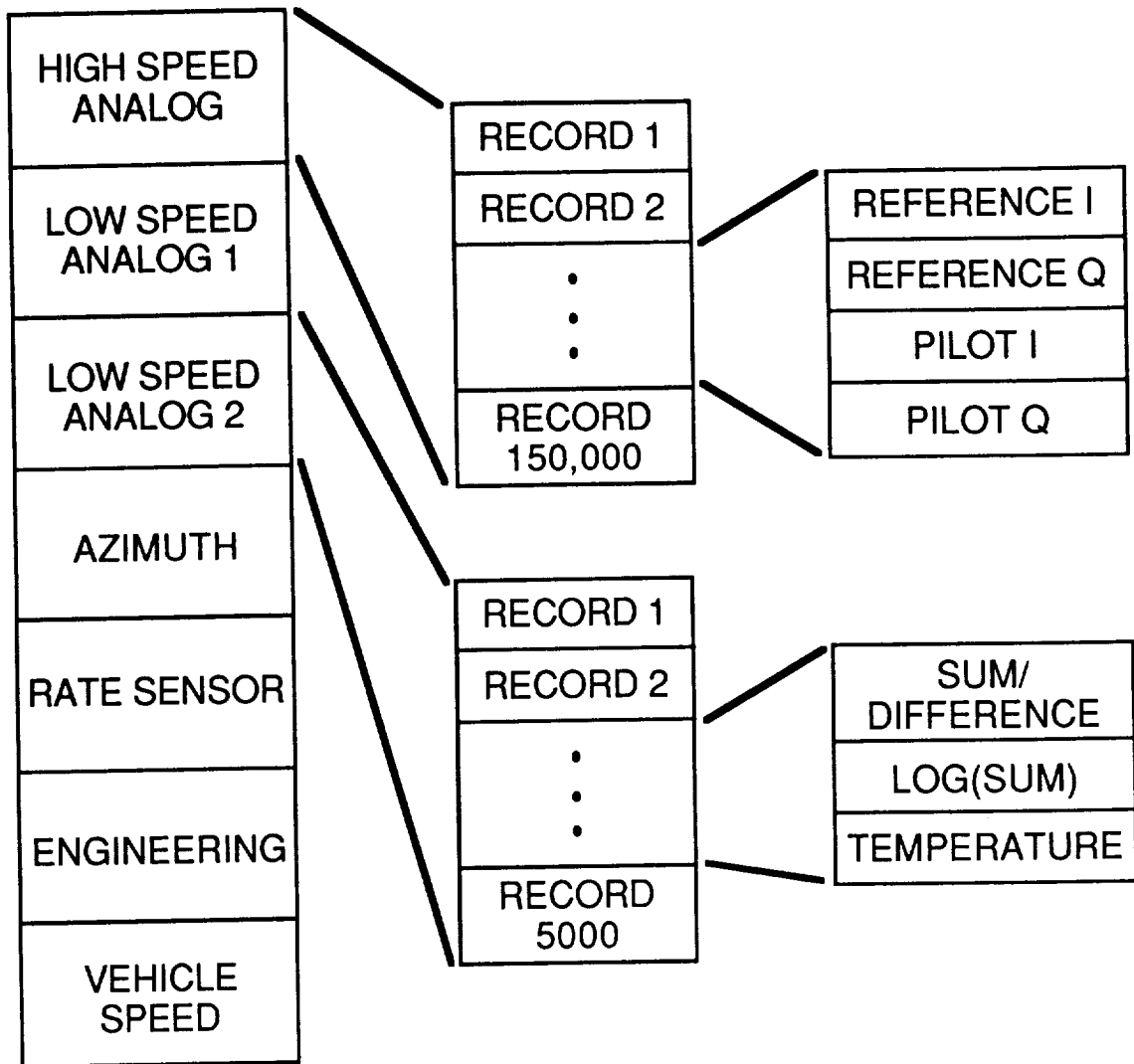


Figure 2
Tower 1 Format

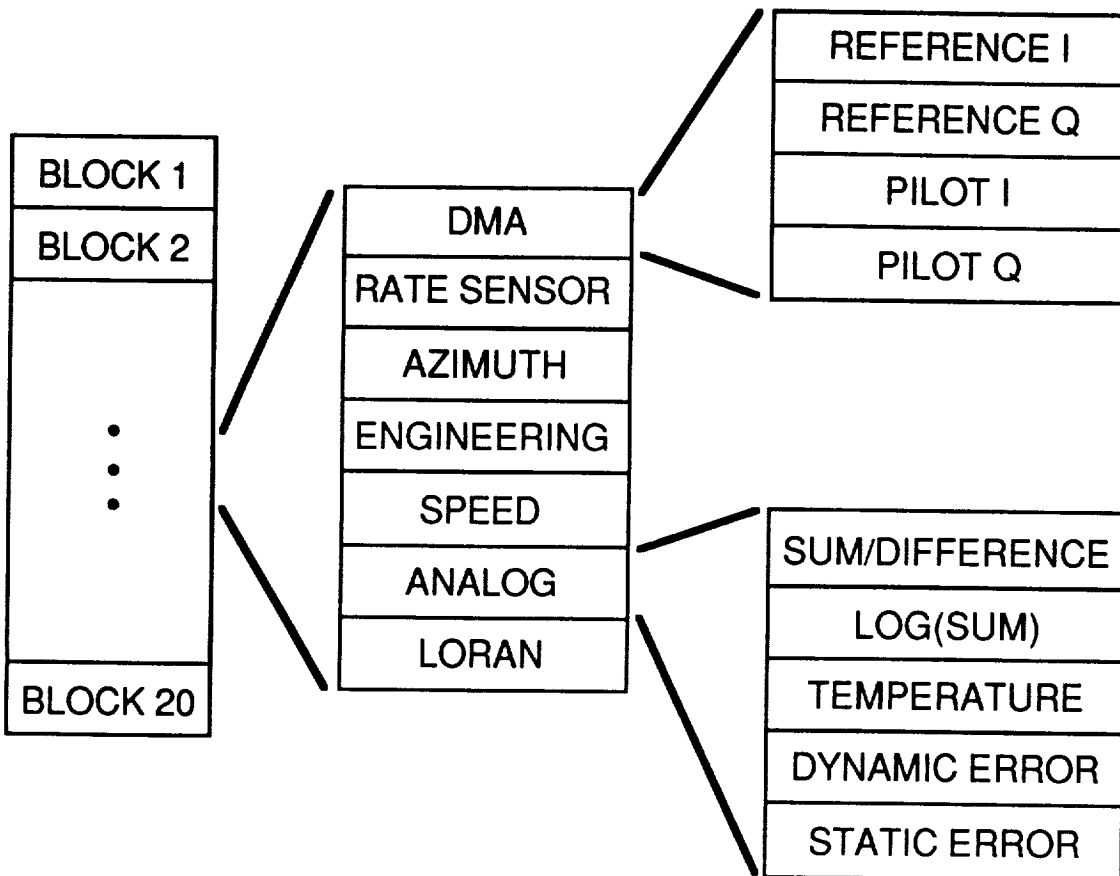


Figure 3
Satellite 1a Format

0167357 N89-11074
thru N89-11094
Unclass

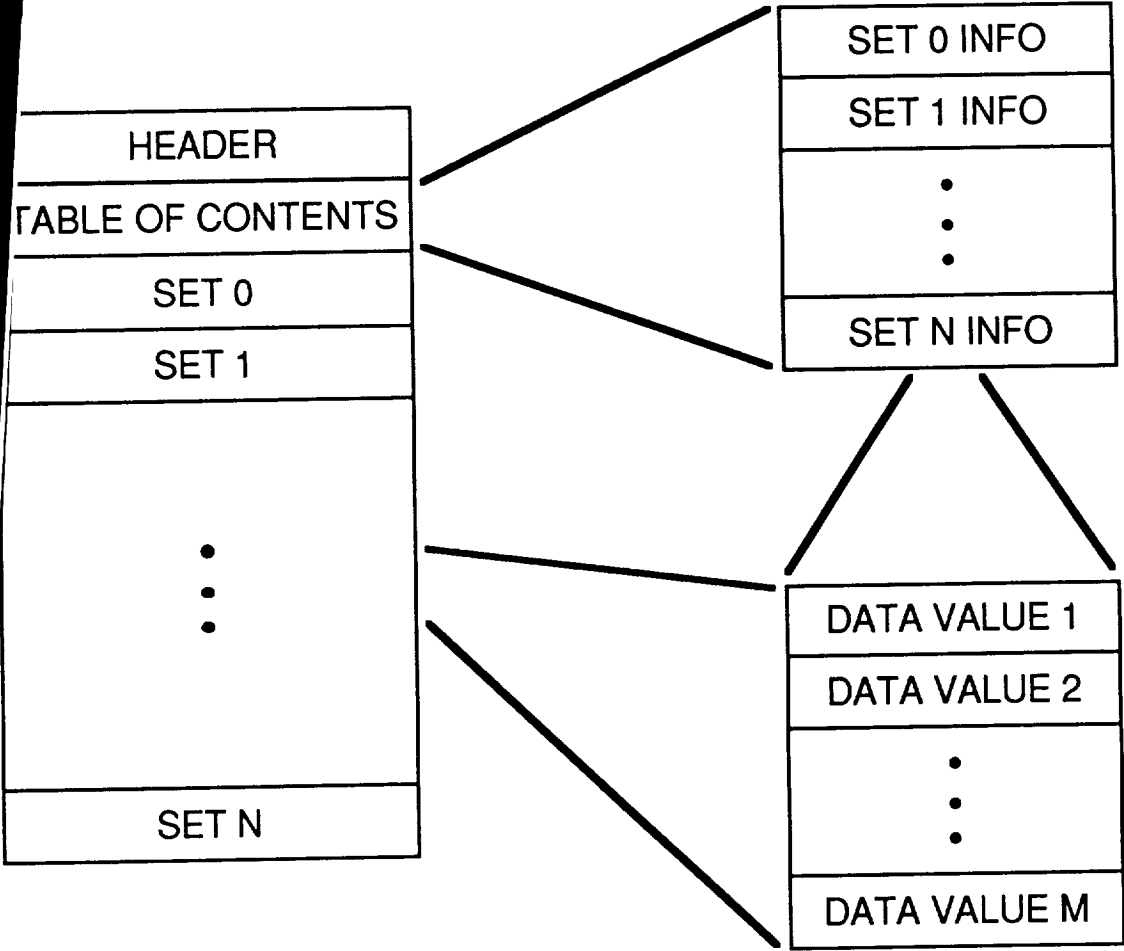


Figure 4
Archival Format

G3
D
32

G3
D
32

RESULTS OF 1987 MSS HELICOPTER PROPAGATION EXPERIMENT
AT UHF AND L BAND IN CENTRAL MARYLAND

Julius Goldhirsh

Applied Physics Laboratory, Johns Hopkins University, Johns Hopkins Road,
Laurel, MD 20707-6099

Wolfhard J. Vogel

Electrical Engineering Research Laboratory, University of Texas at Austin,
Austin, Texas 78758-4497

Abstract

This effort emphasizes several important results pertaining to a mobile satellite system propagation experiment performed in Central Maryland during June 1987. In particular, we examine fade distributions due to multipath and roadside trees at L Band (1.5 GHz) during a period in which the deciduous trees were in full blossom. We compare the multipath statistics for roadside trees with previous multipath measurements made in canyon terrain in North Central Colorado. Also examined is the repeatability of previous UHF measurements made in Central Maryland and the attenuation effects of foliage on trees at UHF. Fade duration for the multipath mode for fade levels of 5 dB and 10 dB is also presented.

1.0 Introduction

Designers of planned mobile satellite systems require information as to the extent of fading caused by shadowing and multipath from roadside trees and terrain. The Applied Physics Laboratory of the Johns Hopkins University and the Electrical Engineering Research Laboratory of the University of Texas at Austin conducted the fifth in a series of mobile satellite system experiments in June of 1987 in Central Maryland [Vogel and Goldhirsh, 1986; 1988, Goldhirsh and Vogel 1987; 1988a; 1988b]. The objectives of the June 1987 test were as follows: (1) Determine roadside tree fade distribution statistics for roadside tree shadowing and multipath geometries. (2) Determine fade distributions for various elevation angles, road types, and for lane of road driven. (3) Assess the variability of fade distribution statistics for combined road cases at the various elevation angles. (4) Express the overall fade distribution due to combined road cases in the form of convenient and accurate functional forms. (5) Obtain a scaling factor describing the ratio of UHF (870 MHz) and L Band (1.5 GHz) fades. (6) Obtain fade duration statistics. (7) Establish repeatability with previous measurements at UHF. (8) Compare L Band multipath measurements for roadside trees and previous canyon measurements. We describe here the results of objectives (5) through (8) as the others were previously presented by Goldhirsh and Vogel [1988a].

2.0 Background

The transmitter platform was a Bell Jet Ranger helicopter which carried L Band and UHF antennas on a steerable mount below the helicopter fuselage. The antennas transmitted right circular polarization and both had nominal beamwidths of 60° . Also located on the mount was a video camera. An observer inside the aircraft viewed the scene on a monitor and pointed (with remote controls) the mount in the direction of the mobile van which carried the receiving antennas and receivers operating at the corresponding frequencies. The receiver antenna gains were approximately omnidirectional in azimuth and the beamwidths (in elevation) were approximately 60° within the interval 15° to 75° . The received signal levels were sampled at a one kHz rate. The receiver gain settings and vehicle speeds were also measured.

Measurements were made along three stretches of roads in Central Maryland. These were: (1) Route 295 north and south between Routes 175 and 450, a distance of 25 km. (2) Route 108 southwest and northeast between Routes 32 and 97, a distance of 15 km. (3) Route 32 north and south between Routes 108 and 70, a distance of 15 km. Route 295 is a popular four lane highway (connecting Baltimore and Washington DC). This road contains pairs of lanes carrying traffic in opposite directions with trees located about 75% of the extreme sides and along 35% of the median. Route 108 is a relatively narrow two lane suburban road containing approximately 55% roadside trees along the stretch examined. Route 32 is a two lane rural road with more sparsely placed trees displaced further away from the sides and containing approximately 30% trees.

Fade measurements due to shadowing were obtained for the geometry in which the helicopter traveled along a trajectory parallel to the van and the propagation path was normal to the line of roadside trees. Such a configuration is considered as a "worst case" for corresponding satellite paths as they give maximum attenuation. Fade measurements due to "multipath" were generated for the geometry in which the helicopter followed the van maintaining a nominal fixed geometry and a visible line of sight. Repeated runs were made for both measurement modes for elevation angles of 30° , 45° , and 60° . The nominal height of the aircraft was 300 m for all cases. The attenuation levels were derived by comparing the shadowed and unshadowed signals.

3.0 Repeatability and Seasonal Effects on Measurements

We address here the following questions: (1) How repeatable were the UHF measurements as compared to those derived in the previous years over the same roads? (2) What are the relative seasonal effects on the distributions for October 1985 which consisted of trees having 80% of full blossom with branches and leaves having low water content, March 1986 in which the deciduous trees were devoid of leaves, and June 1987 corresponding to 100% full blossom with branches and leaves having high water content? In Figure 1 we compare the October 1985, March 1986, and June 1987 UHF fade distributions for Route 295 south, right side of the road driving. The vertical scale represents the percentage of the distance the fade is greater than the abscissa and the abscissa corresponds to the fade

depth in dB. Since the vehicle speeds were nominally constant for the individual runs, the ordinate may also represent the percentage of time the fade is greater than the abscissa value. The abscissa fade depth is taken between -6 dB and 28 dB where the negative fades represent constructive interference due to multipath. Figure 2 depicts the October 1985 and June 1987 distributions for left side of the road driving. The March 1986 distribution is not shown in this figure since no March measurements were implemented for this geometry. We note from Figure 1 that the October 1985 and June 1987 distributions are within 2 dB of each other at the 1% level and are nearly coincident above 2%. Figure 2 shows the October and March distributions to be nearly coincident. Since the dB differences of these two sets of curves give a measure of both the repeatability of the measurements and the relative seasonal effects, we may conclude that: (1) negligible seasonal effects exist between the October and June period, and (2) the repeatability of the measurements is generally smaller than one dB. The March 1986 distribution in Figure 1 (no leaves case) gives fades which are consistently smaller than those for October and June. For example, at the 1% and 10% levels the fades are at most 3 and 1 dB smaller during March. These represent seasonal fade reductions of less than 20%. We may conclude from these results that, on the average, the effects of leaves on trees are small for the dynamically acquired statistics. Stationary fade measurements made on individual trees at UHF gave consistently similar results (e.g., 14% to 40% reduction) [Goldhirsh and Vogel, 1987]. Although the seasonal effects on attenuation have been examined only at UHF, the results are not expected to differ significantly at L Band.

4.0 L Band-UHF Scaling Factor

Figure 3 shows equal percentage values of the ratio of L Band to UHF fades for eight runs at the elevation angle of 30° (solid points). The dashed lines at the individual percentage values represent the +/- rms levels relative to the average for the respective percentage. The runs correspond to Routes 295 north and south for right and left lane driving and Routes 108 and 32 for both directions. The total road length for the combined runs (for each path angle) constitutes approximately 160 km. Shown in this figure are the ratios at the equal percentage values at 1, 2, 5, 10, 20, and 30% levels. Also plotted is the best fit linear line through the set of points. We note that these best fit ratios are approximately independent of percentage in the interval 1 to 30%. Similar results were derived for 45° and 60°. The overall ratio (all elevation angles) of L Band to UHF fade was noted to be

$$R_f = 1.35 \pm 0.1 \text{ (RMS)} \quad (1)$$

or

$$R_f = \left[\frac{f(\text{L Band})}{f(\text{UHF})} \right]^{0.551} \quad (2)$$

5.0 Fade Distributions Due to Multipath Geometries

Fade distributions for multipath geometries in mountainous and canyon terrain were previously measured by Vogel and Goldhirsh [1988]. To insure that the phenomenon examined was fading due to multipath in this previous effort, the helicopter followed the van maintaining an unshadowed line of sight for the propagation paths. In a similar fashion, the multipath interference effects caused by roadside trees were also measured in Central Maryland during the June 1987 period. In Figure 4 are shown comparisons of multipath fade distribution for the roadside tree case (Route 295 S, right lane driving, 45° elevation), and the worst case fade distributions for the canyon terrain (Big Thompson Canyon, into and out of canyon at 45° elevation). The cartoon in the figure depicts the helicopter following the van at the fixed elevation angle. The roadside tree multipath fades at L Band are noted to be approximately 6 dB and 3 dB at the 1% and 10% levels, respectively. Virtually no differences were noted for the multipath distributions for the 30° and 60° elevation cases. We note that at the 1% level the canyon multipath fades flank those due to the roadside tree case by approximately ± 1 dB. On the other hand, at the 10% level the tree fade exceeds both canyon cases by 1.3 dB. We thus observe that no excessive multipath conditions exist in mountainous terrain and that the distributions from roads having roadside trees may even exceed those for mountainous terrain.

6.0 Multipath Versus Shadowing

The dramatic effects of attenuation caused by shadowing at L Band are depicted in Figure 5. Shown is a comparison of the distributions corresponding to multipath and shadowing geometries for Route 295 south (right lane driving) at a path angle of 45° . We note 20 dB and 10 dB fades at the 1% and 10% levels, respectively, for the shadowing case as compared to 6 dB and 3 dB for the multipath roadside tree case. The enhanced attenuation effects caused by shadowing relative to those from multipath have also been measured by other investigators [Jongejans et al, 1986].

7.0 Fade Duration Statistics

Fade durations distributions are presented in Figure 6 and 7. The curves in these figures correspond to the combined results of the eight shadowing runs described above for each of the indicated elevation angles and for 5 dB and 10 dB fade thresholds. In each of these figures two sets of statistics are presented; namely, "faded" (solid) and "unfaded" (dashed). These correspond to durations for which the attenuations are greater and less than the indicated fade thresholds, respectively. The vertical scales represent the percentage of the durations greater than the abscissa values which have been normalized to number of wavelengths; one wavelength at L band being 20 cm. The duration may alternately be expressed in terms of time duration by dividing by the vehicle speed. Hence, for a speed of 88 km/hr (24.4 m/s), the abscissa ranges in values from 8.2×10^{-4} seconds ($.1 \lambda$) to .82 seconds (100λ). Also given in Figure 6 are the fade durations due to multipath at the 5 dB fade threshold. These were derived by combining the three elevation angle runs on Route 295 south (right side of

the road driving). Recall, these data sets correspond to the geometry in which the helicopter followed the van while maintaining a visible line of sight.

Figures 6 and 7 show the distributions to systematically depend on elevation angle. That is, the lower the elevation angle, the greater the fade duration at any fixed percentage. This result is consistent with the fact that lower elevations result in more persistent shadowing. We also note from Figure 6 that a large difference in fade durations exists when comparing multipath with shadowing cases. This is attributed to the different characteristics of randomness of the received signals associated with multipath interference versus those associated with shadowing; i.e., absorption and scattering from trees, branches, and foliage. In comparing Figures 6 and 7, we note that the larger shadowing (10 dB versus 5 dB) thresholds result in smaller fade durations. This is again attributed to the nature of the absorption and scattering phenomena where deep fades of long duration are less likely than less intense fades of long duration. This is also consistent with the fact that there is a smaller dependence of elevation angle on fade duration for the 10 dB threshold than for the 5 dB case.

8.0 Summary

We summarize the salient results of this effort as follows:

(1) Although foliage on trees at UHF produces enhanced fade depths relative to the bare tree case (e.g., nominally 20% increase in attenuation), the dominant attenuation effects are caused by the branches and trunk of the trees. It is believed that similar results should apply at L Band although no measurements at this wavelength have been made to verify this.

(2) Repeatabilities of the measurements at UHF were found to be smaller than 10% in fade at the 1% and greater exceedance levels.

(3) The overall average best fit ratio of L Band to UHF fades (scaling factor) is 1.35 (+/- 0.1 rms), and it is relatively insensitive to the path angle and the exceedance percentage over the interval of 1% to 30%. This ratio is approximately equal to the square root of the ratio of frequencies (equation (1)). The above ratio was derived for an overall average road and driving condition corresponding to 24 runs (comprised of Route 295 right lane and left lane driving for north and south directions, Route 108 northeast and southwest directions, and Route 32 north and south directions for 30°, 45°, and 60° elevations (480 km of road).

(4) Attenuations caused by shadowing of roadside trees far exceed those due to multipath. For example, fading due to multipath at the 1% level was found to be approximately 6 dB as compared to fades as high as 25 dB due to shadowing at a 30° path angle.

(5) Fades due to multipath from roadside trees were found to be comparable and in many cases slightly larger (e.g., 1 to 2 dB) than those obtained in canyon terrain. This may be attributed to the fact that roadside trees are nearby and tall and therefore give rise to more appropriate scattering geometries for the given antenna pattern. The canopy tops of the trees may also represent more of an isotropic scatterer than nearby faceted canyon walls.

(6) Fade durations are elevation angle dependent for the shadowing geometry. For the multipath case, fade durations are dramatically smaller than those for shadowing cases at the same exceedance percentage.

9.0 Acknowledgements

The authors are grateful to J. R. Rowland for his ingenuity in outfitting the helicopter transmitter platform and to G. W. Torrence for the development of the receiver system. Many thanks are also extended to A. J. Walker, Steve Babin, and Jack Miller for assisting the experiment. This work was supported by NASA Headquarters Communications Division under Contract #N00039-87-C-5301 for APL and by the Jet Propulsion Laboratory for the University of Texas under Contract #JPL956520.

10.0 References

- Goldhirsh, J. and W. J. Vogel, "Roadside Tree Attenuation Measurements at UHF for Land-Mobile Satellite Systems," IEEE Trans. on Antennas and Propagat., vol AP-35, pp 589-596, May 1987.
- Goldhirsh, J. and W. J. Vogel, "Propagation Effects by Roadside Trees Measured at UHF and L-Band for Mobile Satellite Systems," Proceeding of the Mobile Satellite Conference, Pasadena, California pp 87 - 94, May 3-5, 1988a (Jet Propulsion Laboratory Publication 88-9, Jet Propulsion Laboratory, Pasadena, California)
- Goldhirsh, J. and W. J. Vogel, "Attenuation Statistics Due to Shadowing and Multipath from Roadside Trees at UHF and L Band for Mobile Satellite Systems," Johns Hopkins University/Applied Physics Laboratory Technical Report SLR88U 004, February, 1988b (Applied Physics Laboratory, Johns Hopkins Road, Laurel MD 20707)
- Jongejans, A. and A. Dissanayake, N. Hart, H. Haugli, C. Lois and R. Rogard, "PROSAT - Phase 1 Report," European Space Agency Technical Report ESA STR-216, May 1986 (European Space Agency, 8-10 rue Mario-Nikis, 75738 Paris Cedex 15, France)
- Vogel, W. J. and J. Goldhirsh, "Tree Attenuation At 869 MHz Derived from Remotely Piloted Aircraft Measurements," IEEE Trans. Antennas and Propagat., vol AP-34, pp 1460-1464, Dec. 1986.
- Vogel, W. J. and J. Goldhirsh, "Fade Measurements at L Band and UHF in Mountainous Terrain for Land Mobile Satellite Systems," IEEE Trans. Antennas and Propagat., vol AP-36, Jan. 1988.

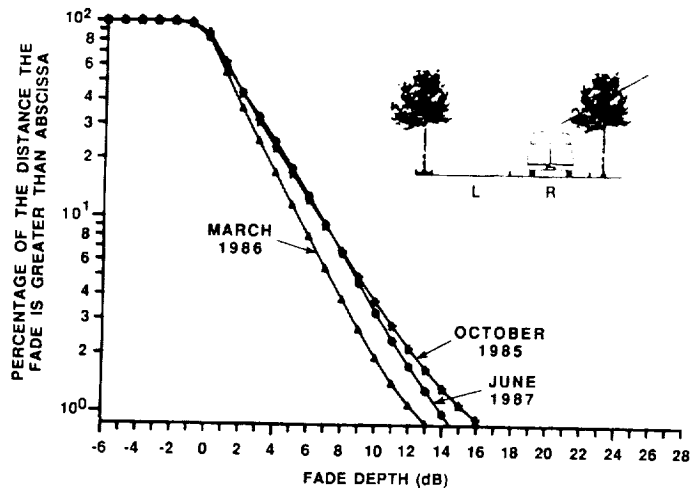


Figure 1 Cumulative fade distributions for various seasons (Route 295 South (RHS) - UHF at 45°)

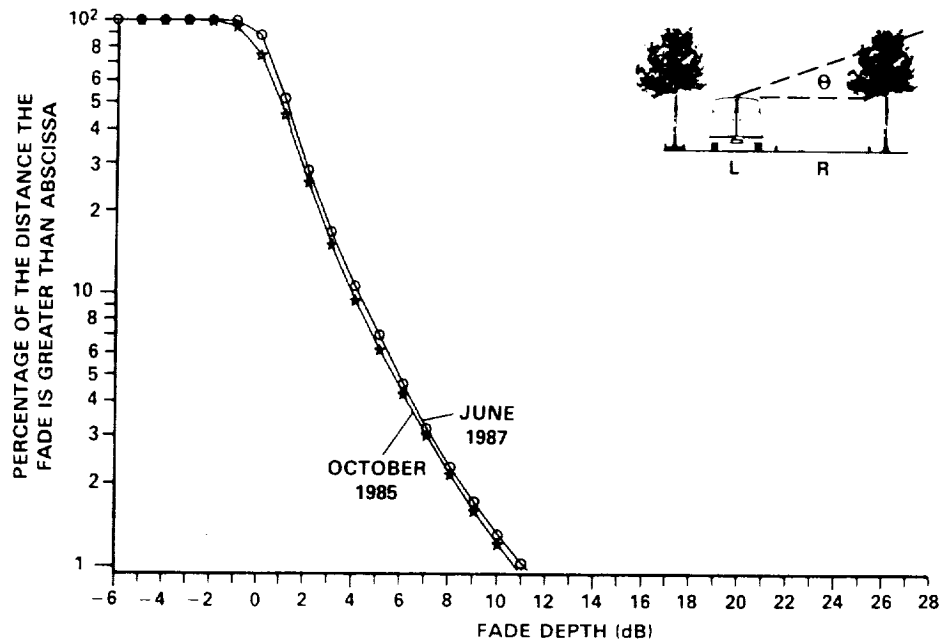


Figure 2 Cumulative distributions for Route 295 South (LHS) for October 1985 and June 1987 at UHF for 45°

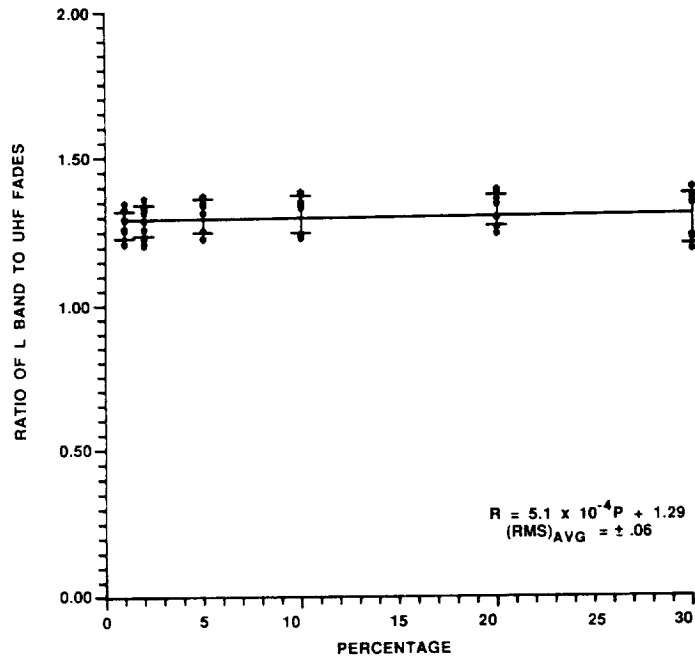


Figure 3 Ratio of L-band to UHF fades at equal percentages versus percentages of distance fade is exceeded (all roads - elevation angle = 30°)

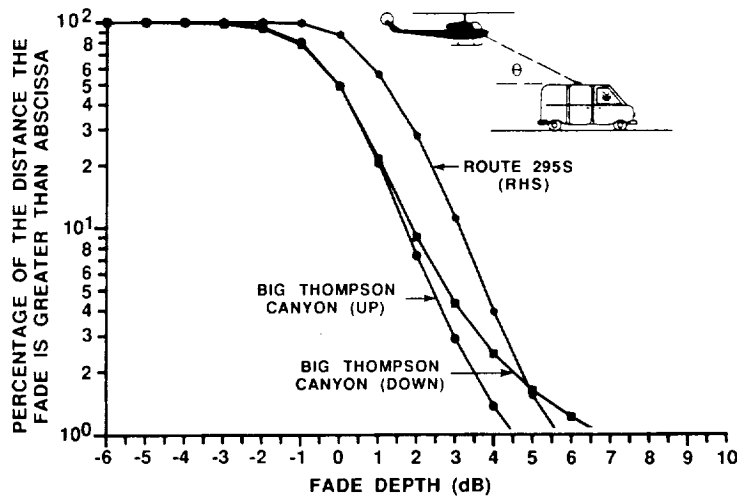


Figure 4 Comparison of cumulative fade distributions due to multipath (helicopter behind) at L-band at 45° for Big Thompson Canyon versus Route 295 South

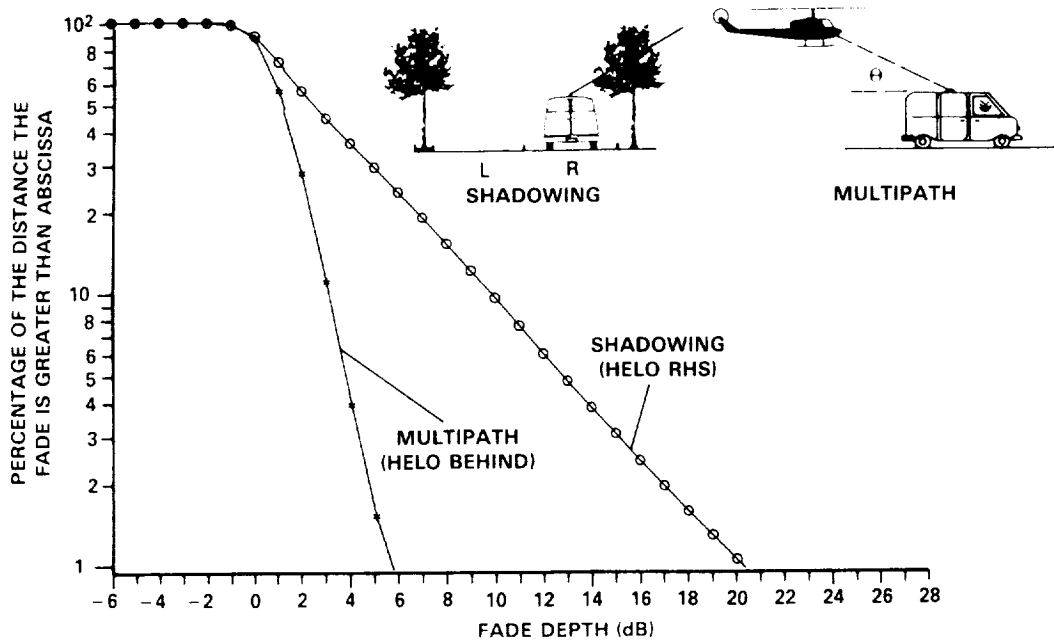


Figure 5 Comparison of cumulative fade distributions due to multipath and shadowing at elevation = 45° at L-band for Route 295 South

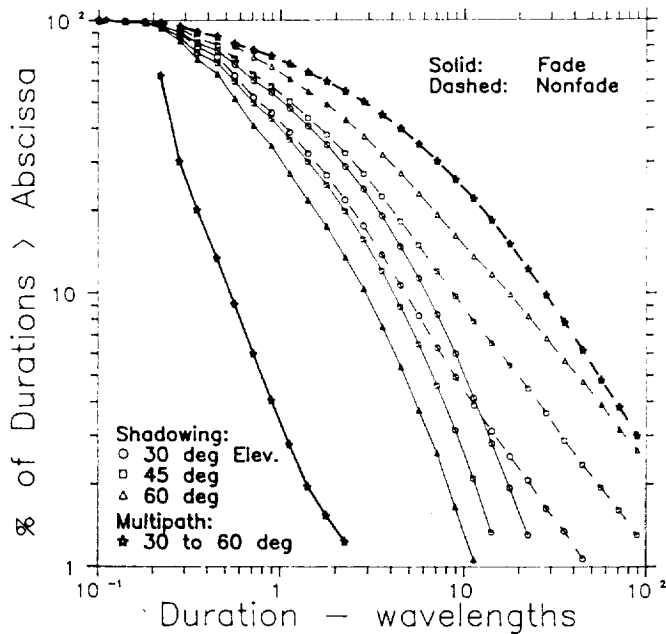


Figure 6 Fade and nonfade durations at L-band for 5 dB fade threshold

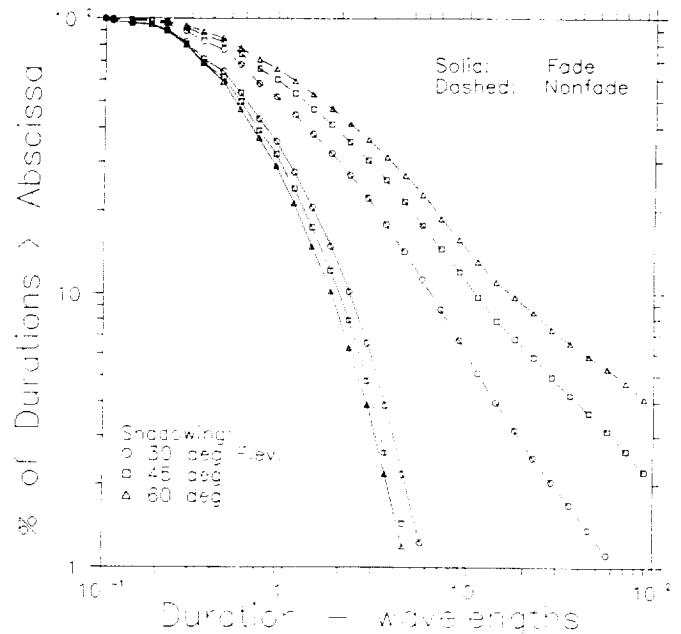


Figure 7 Fade and nonfade durations at L-band for 10 dB fade threshold

LMSS PROPAGATION MODELING

AT VIRGINIA TECH

Warren L. Stutzman, R. Michael Barts,
and Charles W. Bostian

Satellite Communications Group
Bradley Department of Electrical Engineering
Virginia Polytechnic Institute and State University
Blacksburg, VA 24061

Abstract--In this paper recent efforts in the modeling of land mobile satellite systems are reported. These include descriptions of a simple model for prediction of fading statistics, a propagation simulator, and results from studies using the simulator. Predictions are compared to available measured data.

1. Introduction

First generation MSS voice channels are being planned with as little as 3 dB margin. [Rafferty, Dessouky, and Sue, 1988] Small power margins are common for fixed service applications of satellite links. However, mobile satellite service presents special problems. In land mobile the line-of-sight path (LOS) is frequently blocked by trees and structures. For suburban and rural roads tree shadowing is statistically significant. A recent review article by several researchers in the MSS research community summarizes the measurements and modeling work to date for MSS propagation. [Stutzman, 1988]

In this paper we report on MSS propagation modeling activities at Virginia Tech. Because of the low signal margin, it is important to quantify the propagation effects. Experiments offer a direct or quasi-direct means of quantifying propagation effects; however, such experiments are costly. Also, there are many parameters in the MSS environment and not all vehicle travel situations can be measured. Instead, reliable models allow study of system performance for controlled propagation conditions. It is in this context that our modeling program is being developed.

2. Theoretical Background

Model development for MSS propagation is following a course similar to that for (fixed) satellite-to-earth propagation through rain at microwave frequencies. (This is not entirely coincidental because many of the same researchers are also involved in MSS propagation research.) There are several steps that must be taken in proper order. First, as complete a theoretical model as possible which describes the physics of the problem is set up. This is more difficult for vegetatively sha-

dowed propagation in the MSS problem than for microwave propagation through rain. The theoretical model will have several parameter values that are unknown and that can only be obtained by measurement. This is where direct measurement results are necessary. Next, simple models for the propagation environment are developed to drive the theoretical model. Finally, simple models are built that do not require evaluation of complicated theoretical expressions but still include the parameter variations. MSS propagation modeling is developing faster than rain propagation modeling did because data (required to establish model parameter values and to verify models) can be collected much faster. In the rain propagation problem prediction of annual statistics requires years of data collection, whereas data of statistical significance can be collected in a matter of hours with a mobile experimental unit for MSS.

The MSS signal is divided into two components: unshadowed and vegetatively shadowed. Each is treated separately and then the results are combined to form a complete model. The total distribution function for fade level F in a mixed shadowed/unshadowed mobile path is expressed as [Bradley and Stutzman, 1985; Lutz et al., 1986]

$$C(F) = C_u(F) * (1-s) + C_s(F) * s \quad (1)$$

where $C_u(F)$ is the fade distribution for an unshadowed signal, $C_s(F)$ is the fade distribution for a shadowed signal, and s is the fraction of vegetative shadowing along the mobile path. The unshadowed distribution function, $C_u(F)$, arises from an unobstructed line-of-sight component with Rayleigh distributed multipath, resulting in a Rician distribution with one parameter K , which is the carrier-to-multipath ratio. The distribution function associated with pure vegetatively shadowed paths, $C_s(F)$, results from a lognormally distributed LOS signal component with Rayleigh distributed multipath. This distribution function [Loo, 1984] is characterized by a mean, μ , and standard deviation, σ , for the lognormal part and K (ratio of unfaded carrier to multipath) for the Rayleigh portion.

The analytical functions (which are not all in closed form) as described above and combined as in (1) have been coded into a program referred to as LMSSMOD. Statistics from this program have been shown to produce results agreeing with experiments. [Barts and Stutzman, 1987; Barts and Stutzman, 1988]

3. A Simple Empirical Model for Fade Distributions

The rather cumbersome LMSSMOD computer program is required to evaluate (1) directly. To avoid this a simple empirical model has been developed. It uses (1) and the following fitted functions. For an unshadowed signal, the probability that a fade will be greater than F dB is

$$C_u(F) = e^{-(F+U_1)/U_2} \quad (2a)$$

where

$$U_1 = 0.01 * K^2 + 0.378 * K + 3.98$$

$$U_2 = 331.35 * K^{-2.29}$$

K = carrier-to-multipath ratio [dB]

For a vegetatively shadowed signal, the probability that a fade will be greater than F dB is

$$C_S(F) = [(50-F)/V_1]^{V_2} \quad (2b)$$

where

$$V_1 = -0.275 * \bar{K} + 0.723 * \mu + 0.336 * \sigma + 56.153$$

$$V_2 = [-0.006 * \bar{K} - 0.008 * \mu + 0.013 * \sigma + 0.103]^{-1}$$

\bar{K} = carrier-to-multipath ratio [dB]
 μ = mean of lognormal signal [dB]
 σ = standard deviation of lognormal signal [dB]

Then the percent of distance of travel for which the fade exceeds F dB is

$$P = 100 * C(F) \quad (3)$$

The empirical model of (1) with (2) and (3) was developed by first finding parameter values of K, μ, σ, \bar{K} , and s which lead to LMSSMOD fade distributions that fit to measured data supplied by W. Vogel for balloon and helicopter experiments [Stutzman, 1988]. Then the fit coefficients in (2) were adjusted to obtain a fit of the empirical model to the data. An example is shown in Fig. 1. The typical ranges of parameter values over which the model is valid are:

$$13 \text{ dB} < K < 22 \text{ dB}$$

$$12 \text{ dB} < \bar{K} < 18 \text{ dB} \quad (4)$$

$$-1 \text{ dB} < \mu < -10 \text{ dB}$$

$$0.5 \text{ dB} < \sigma < 3.5 \text{ dB}$$

4. The Propagation Simulator

A software propagation simulator originally developed by Schmier [1986] simulates MSS signals and predicts primary and secondary fade statistics. A block diagram of the simulator is shown in Fig. 2. This simulator is unique because instead of generating the simulated signal from random number generators, it is generated using universal data sets, derived from experimental data supplied by Vogel, with known statistical properties. By processing Vogel's experimental data, data sets for each signal component having the proper statistical properties can be created. These data sets are scaled to have the proper statistical distribution and recombined to form a composite signal. The output of the simulator simulates a time sequence signal that can be used to produce secondary statistics of average fade duration and of level crossing rate. The simulator output is normalized to produce samples every 0.1 wavelength traveled in order to remove the effect of vehicle speed from the simulation.

The data sets are generated by first separating the experimental data into shadowed and unshadowed data points using a 2

dB below LOS criterion for shadowing. Then the running mean of the data is calculated using a 20 wavelength sliding window. For the shadowed data, this running mean has been found to be lognormally distributed. Subtracting the running mean from the shadowed data on a point by point basis generates a database which has been found to be Rayleigh distributed.

In Schmier's original simulator the unshadowed Rayleigh data set had a uniform phase distribution while the shadowed Rayleigh data set had a bimodal phase distribution centered around 0 and 180 degrees. The current version uses a shadowed Rayleigh data set with a uniform phase. Figure 3 shows that the fade distributions predicted by the analytical model and the simulator are in good agreement.

5. Using the Propagation Simulator

A major aspect associated with theoretical, empirical, or simulation modeling is knowledge of the input parameters. The only known work on this portion of the modeling problem is the deterministic path model (DPM) of Smith and Stutzman [1986]. The DPM uses the CCIR Modified Exponential Decay Model (MED) for calculating the attenuation of a signal propagating through foliage. For MSS modeling, roadside foliage is modeled as a semi-infinite block of a known height and setback from the vehicle. Given the elevation angle to the satellite and the bearing angle with respect to the vehicle, simple geometry can be used to calculate the path length through foliage. From the path length, the attenuation of the signal is calculated using the MED. The Deterministic Path Model assumes that the vegetation height and setback are uniformly distributed variables with a minimum and maximum value. The DPM yields the mean and standard deviation of the attenuation, which are estimates of the log normal mean, μ , and standard deviation, σ . These values can be used as inputs to drive the simulator. Results of using the DPM to estimate the lognormal mean and standard deviation have shown good agreement with experimental data. Figure 4 shows a fade distribution for data measured by Vogel and Goldhirsh on RT 295 between Baltimore and Washington and the output of the propagation simulator using the DPM to estimate the lognormal mean and standard deviation. Measurements were made for elevation angles of 30, 45, and 60 degrees along the same section of road on both UHF and L-Band. The DPM was used to estimate the lognormal mean and standard deviation for each case with the results used to drive the simulator. The results of the simulator showed good agreement in all cases.

The propagation simulator (as indicated in Fig. 2) also is used to drive the channel simulator developed at Virginia Tech. The channel simulator is used to determine bit error rates of MSS channels for various modulation and coding formats in the presence of propagation effects.

References

- Barts, R. M., W. L. Stutzman, W. T. Smith, R. S. Schmier, and C. W. Bostian, "Land Mobile Satellite Propagation Modeling," Proceedings of the 1987 IEEE Antennas and Propagation Society International Symposium, vol. I, pp. 20-23, 1987.
- Barts, R. M. and W. L. Stutzman, "Propagation Modeling for Land Mobile Satellite Systems," Proceedings of the Mobile Satellite Conference, pp. 95-100, May 1988.
- Bradley, W. S., and W. L. Stutzman, "Propagation Modeling for Land Mobile Satellite Communications," Virginia Tech Report 85-3 submitted to JPL under NASA Contract 956512, August 1985.
- Goldhirsh, J., and W. J. Vogel, "Propagation Effects by Roadside Trees Measured at UHF and L-band for Mobile Satellite Systems," Proceedings of the Mobile Satellite Conference, pp. 87-94 May 1988.
- Loo, C. "A Statistical Model for a Land Mobile Satellite Link," Proceedings of the 1984 IEEE International Communications Conference, pp. 588-594, 1984.
- Lutz, E., W. Papke, and E. Plochinger, "Land Mobile Satellite Communications-Channel Modeling, Modulation, and Error Control," Proceedings of the 7th Inter. Conf. on Digital Satellite Communications, Munich, Germany, May 1986.
- Rafferty, William, Khaled Dessouky, and Miles Sue, "NASA's Mobile Satellite Development Program," Proceedings of the Mobile Satellite Conference, pp. 11-20, May 1988.
- Schmier, R. G., and C. W. Bostian, "Fade Durations in Satellite-Path Mobile Radio Propagation," Virginia Tech Report No. 86-5 submitted to NASA/JPL under NASA Contract 956512, 1986.
- Smith, W. T., and W. L. Stutzman, "Statistical Modeling for Land Mobile Satellite Communications," Virginia Tech Report No. 86-3 submitted to NASA/JPL under NASA Contract 956512, August 1986.
- Stutzman, W. L., editor, "Mobile Satellite Propagation Measurements and Modeling: A Review of Results for Systems Engineers," Proceedings of the Mobile Satellite Conference, pp. 107-117, May 1988.

P = 92.5% K = 21.5 DB \bar{K} = 9.9 DB
MU = -4.8 DB SIGMA = 1.7DB

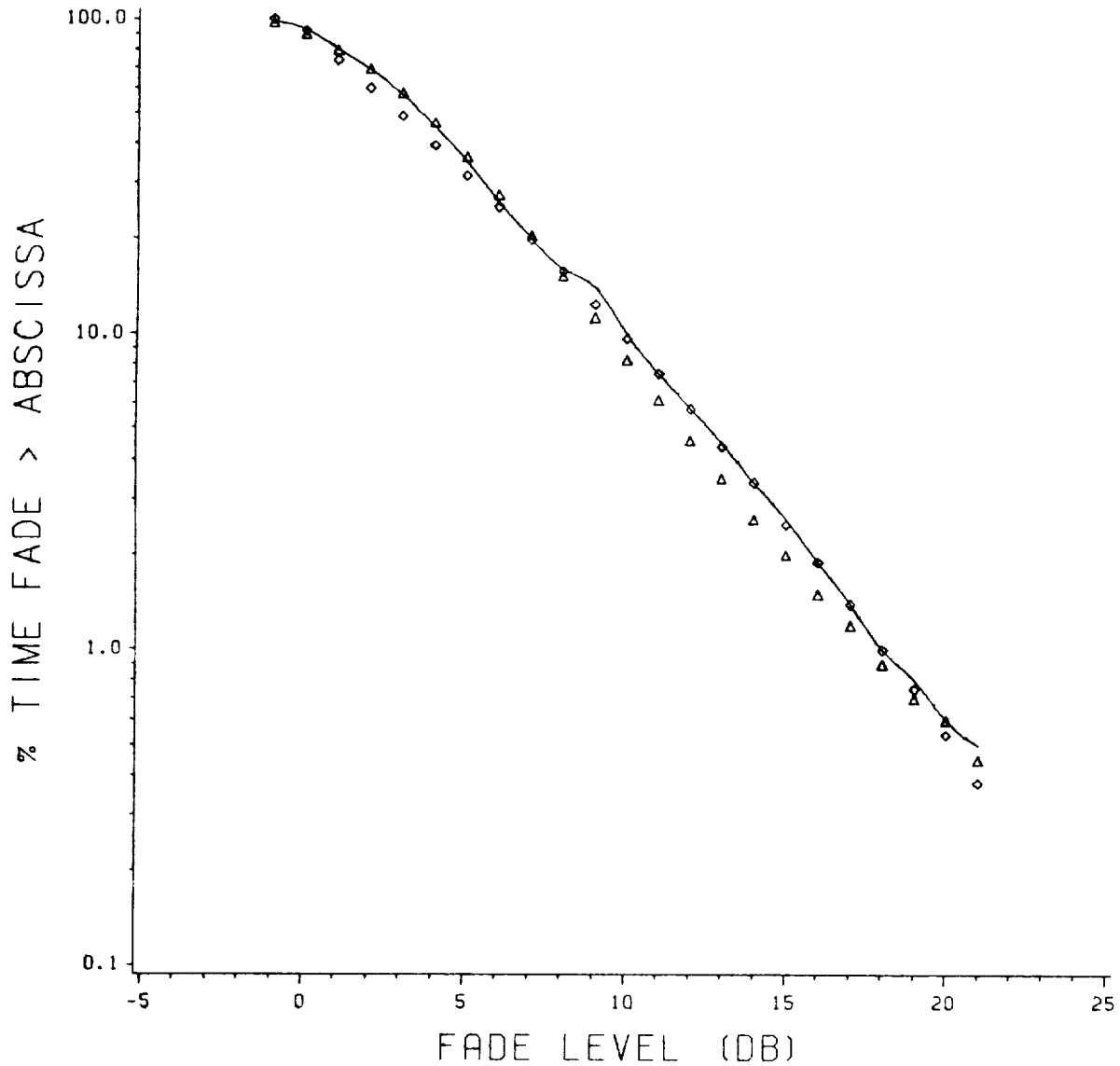


Figure 1. Fade distributions Vogel's 1985 helicopter data [Schmier and Bostian, 1985] (solid curve) compared to predictions of LMSSMOD using (1) (triangles) and to the simple empirical model of (2) (diamonds).

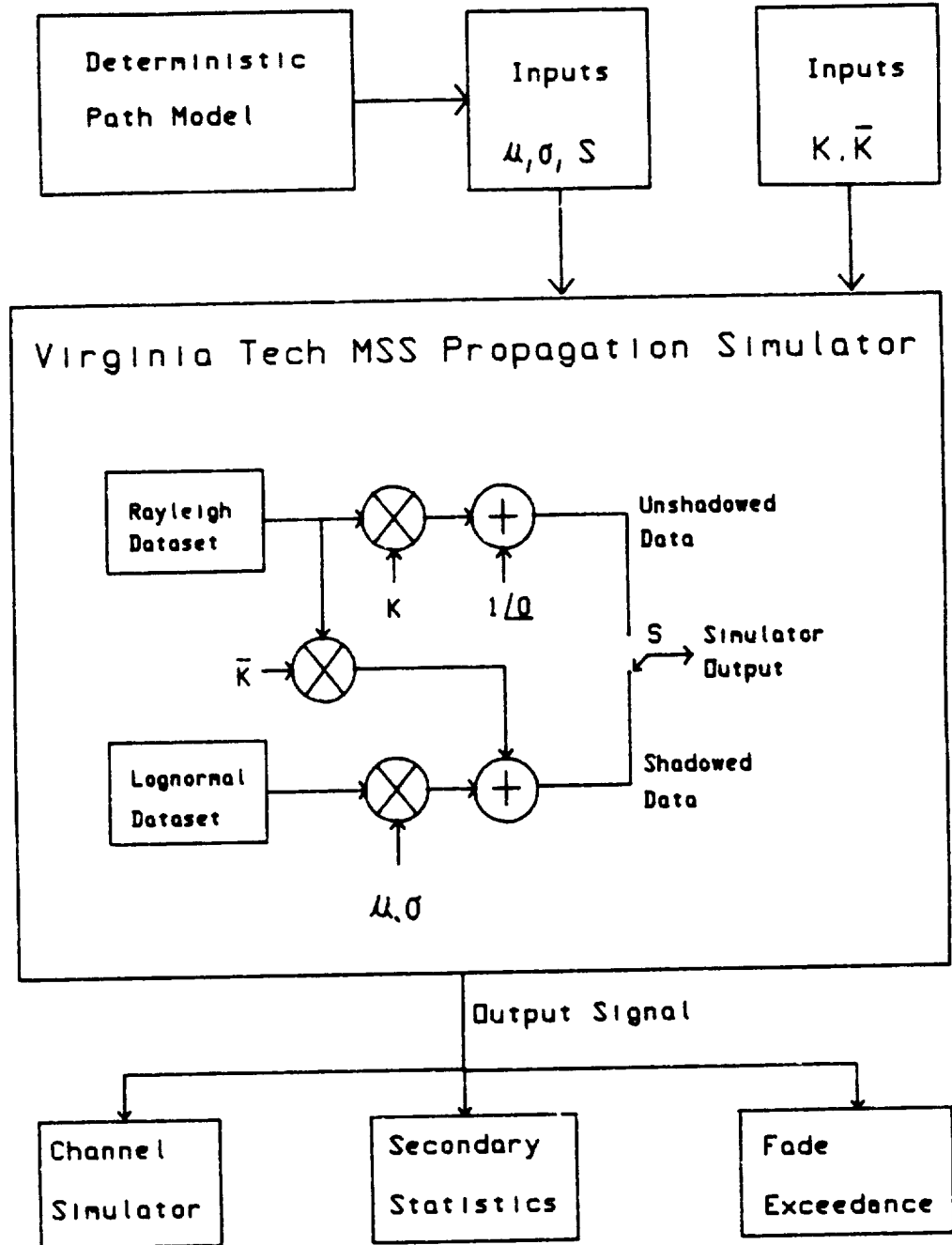


Figure 2. A block diagram of the propagation simulator.

P = 92.5% K = 21.5 DB $\bar{K} = 9.9$ DB
MU = -4.8 DB SIGMA = 1.708

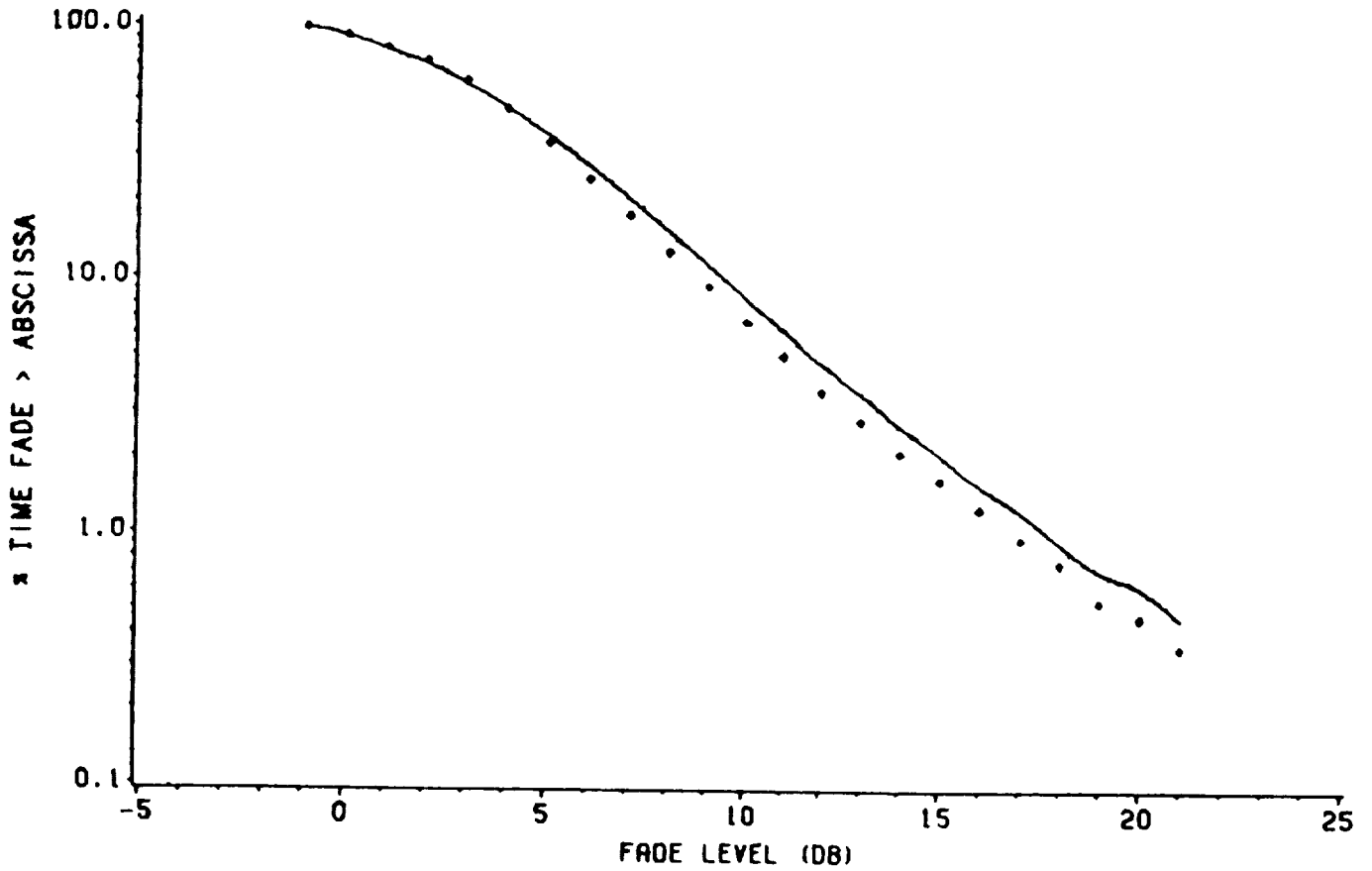


Figure 3. Fade distributions from LMSSMOD using (1) (solid curve) and the propagation simulator (diamonds).

VOGEL/MARYLAND DATA - RT 2959
L-BAND 30 DEG EL - MEASURED VS SIM2

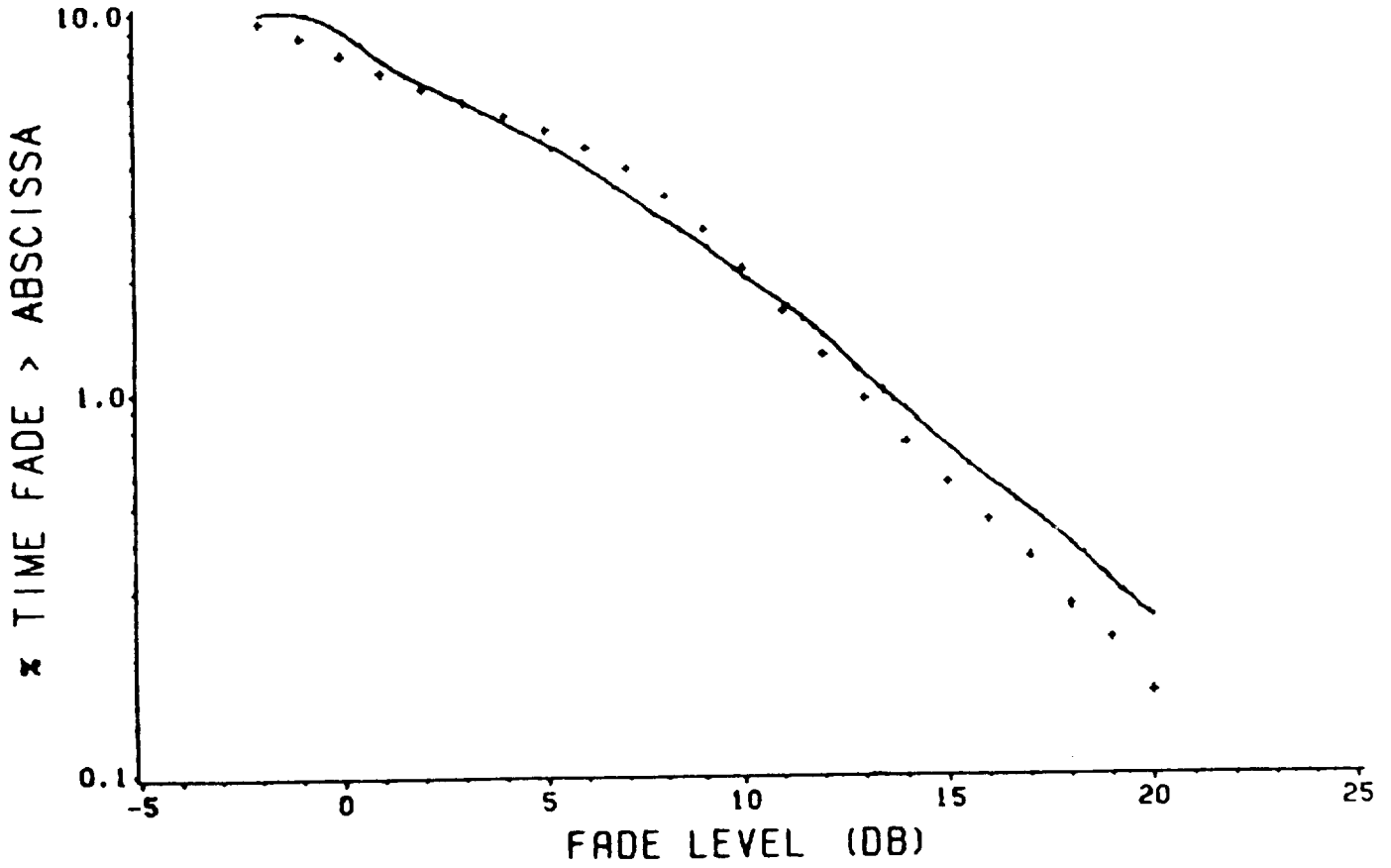


Figure 4. Comparisons between measured helicopter data at L-band [Goldhirsh and Vogel, 1988] (solid curve) and predictions for 30 degrees elevation angle from the propagation simulator using the Deterministic Path Model (crosses).

**PRELIMINARY RESULTS OF MARECS-A MEASUREMENTS IN CENTRAL MARYLAND
AND PLANS FOR 1988 MSS EXPERIMENT IN AUSTRALIA**

Wolfhard J. Vogel

Electrical Engineering Research Laboratory, The University of
Texas at Austin, Austin, Texas 78758-4497

Julius Goldhirsh

Applied Physics Laboratory, Johns Hopkins University, Johns
Hopkins Road, Laurel, MD 20707-6099

Abstract--Past and future efforts are described, using L Band (1.5 GHz) satellite signals for MSS propagation measurements. Preliminary results from the December 1987 campaign in Central Maryland with the Atlantic Ocean MARECS satellite are given. The fade level statistics from this 22 degree elevation source are consistent with helicopter measurements made along the same roads and presented in a companion paper. The day to day repeatability of the fade probabilities is shown to usually be better than about 20 percent. An experiment plan is presented for measurements using ETS-V's southern beam. These measurements will be made in Australia in collaboration with AUSSAT during the July/August 1988 time-frame.

1.0 Introduction

In early December of 1987, the Electrical Engineering Research Laboratory of The University of Texas and the Applied Research Laboratory of Johns Hopkins University jointly performed a further test of LMSS propagation, part of a series of systematic experiments, starting with balloon measurements in 1983, and then also using remotely piloted vehicles and helicopters as source platforms until June 1987. References describing these experiments can be found in a companion paper in this issue of the NAPEX proceedings. The new aspect of the last measurement was that a satellite signal was received. The opportunity to do this arose, because the Atlantic Ocean satellite operated by INMARSAT (MARECS-A) was being used by the European Space Agency (ESA) for land mobile propagation measurements in Europe. Through the cooperation of ESA, we were informed of the experiment schedule, allowing us to make low elevation angle measurements in Central Maryland along the same roads where a number of helicopter measurements were performed previously.

Another opportunity for satellite beacon measurements of LMSS propagation effects arises with the launch of ETS-V by Japan. This satellite's southern beam illuminates all of the Australian continent. AUSSAT, Australia's National Satellite System, has entered into an agreement with Japan, allowing them to use the

satellite transponder for LMSS measurements in Australia. We have been invited by AUSSAT to come to Australia at the end of July 1988 with our receiving van and perform propagation measurements there. AUSSAT is contributing payment for the shipping and travel expenses of this trip and supplies the uplink, NASA is contributing the receiving van and the experimenters and supports the analysis and Japan contributes the use of the satellite. All parties will have access to the results of these measurements. This experiment will allow us to obtain satellite data at higher elevation angles than was possible before. Previous measurements have shown that the behavior of the communication link most strongly depends on scatterers and obstacles in the close vicinity of the vehicle. It is therefore possible to apply the results obtained at any location to any other one, as long as similarity exists in the general close environment. The results obtained in Australia can be applied to the US (or Japan), as long as similar percentages of shadowing by roadside trees or scattering by roadside objects are assumed.

2.0 The MARECS-A Experiment

The elevation angle to the satellite along the East Coast of the US was about 22 degrees, lower than angles measured with the helicopter, but within the range of operational angles for a real system covering the US. The satellite transmitted a carrier at a frequency of 1541.35 MHz with right hand circular polarization and an EIRP of 28 dBW. This resulted in a signal-to-noise ratio of better than 25 dB in a bandwidth of 100 Hz, using an azimuthally omni-directional crossed drooping dipole antenna mounted on the roof of the vehicle.

The fade distributions for the three roads along which measurements were made (Rt. 295, Rt. 108 and Rt. 32) are given in Figures 1 through 4. In order to demonstrate the repeatability of the measurements, data were collected on two consecutive days along the same roads. The results of each day are shown, for each particular direction of driving and, on Rt. 295, each lane selected. The abscissa shows the percentage of the distance driven, for which the fade exceeded the value along the ordinate. Negative values along the ordinate represent signal enhancements due to constructive interference.

At the 10 percent level, along Rt. 295, the attenuation ranged from 12 to 19 dB, depending upon the driving geometry. The satellite was to the east. Therefore the best performance was obtained when the van drove south in the right lane. The worst performance was found for driving north, in the shadow cast by the trees immediately to the right. Surprisingly, driving north in the left hand lane seemed to produce fades about 1 dB higher than those obtained when driving in the right hand lane. Along the two lane roads, the corresponding spread was narrower, about 1 dB for each road.

The day-to-day repeatability of the measurements is demonstrated in Fig. 5. The repeat error is defined as the percentage difference of the measured probability for each particular fade depth. The differences are less than about ± 20 percent for Rt. 295. For instance, going south on Rt. 295 in the left lane resulted in a 1.72% probability of the fades exceeding 20 dB on the first day and a 2.15% probability on the second one, which results in a $[(1.72-2.15)/2.15*100=]$ 20% repeat error. The error is larger for Rts. 108N and 32W, for which at fades above about 18 dB the error exceeds 50% and appears to be systematic.

The variability of the fade distribution function has been plotted in Fig. 6 for Rt. 295, in Fig. 7 for Rt. 108, in Fig. 8 for Rt. 32 and in Fig. 9 for the three roads combined. In these figures the axes have been reversed from the previous ones. The fade depth is plotted on the ordinate and the percentage of distance that a fade level exceeded the ordinate value is plotted on the abscissa. There are three curves in each plot. They were derived by first calculating the fade distribution function for consecutive 90 second intervals and then by finding the 90th, 50th and 10th percentile fade level of these distributions at the 1, 2, 5, 10 and 20 percent 90 second distribution value. From Fig. 9, for instance, one can see that there was a 90% chance that 10% of the distance the fades within a 90 second period exceeded 6 dB, a 50% chance that 10% of the distance the fades within a 90 second period exceeded 15 dB and a 10% chance that 10% of the distance fades within a 90 second period exceeded 20 dB.

It is expected that a typical voice call over the satellite link will last about 90 seconds. The overall fade distributions of Figs. 1 to 4 give information about the fade margin required for many callers in one particular area. The fade statistics are not stationary however, and within one general area one can, in a 90 second interval, encounter situations with much or little shadowing by roadside trees. Therefore information about the variability of the fade distributions is needed, if one wants to estimate the success of a particular call.

3.0 The ETS-V Experiment

3.1 Objectives

This experiment is to evaluate the fading probabilities of land mobile satellite communication systems at elevation angles between 42 and 57 degrees. The experiment will be performed at a frequency between 1540.5 to 1548 MHz, where the ETS-V satellite can transmit 27.2 dBW (EIRP) in its southern beam, illuminating all of Australia. The results will be fade distributions and their statistical variation as well as fade and no-fade duration data for a variety of environments, ranging from urban to rural to desert, with flat, rolling and mountainous terrain. Fades in LMSS channels are either due to (1) multipath reflections from

roadside scatterers or (2) shadowing/scattering from roadside trees or (3) a combination of both. Using a satellite as a signal source will allow one to make systematic measurements of these effects by varying the driving direction along selected roads. Using a satellite source will also enable one to obtain a large amount of data in a relatively short time.

The data acquired will allow us to determine fade distribution statistics for shadowing and multipath geometries, for a variety of road types and lanes of road driven, in different environments and over a range of elevation angles from about 40 to 60 degrees. Fig. 10 indicates the vegetation zones of Australia along with the angle of elevation. We also will assess the variability of fade distributions as a function of location and elevation angle and express the results in functional form. We also will derive fade duration statistics from the measurements. Measurements will be performed at selected spots along the general route shown in Fig. 11, where we can vary the driving direction with respect to the satellite.

3.2 Logistics

The van with its receivers, data acquisition hardware and power generator has been consigned to a shipper in Houston on June 9th, 1988. It will sail to Sydney June 20th and is scheduled to arrive July 13th. It will be taken through customs in Sydney by AUSSAT upon arrival. At the conclusion of the measurements, the van will be shipped back to Houston.

3.3 Schedule in Australia

During the three weeks of the campaign, 15 days of measurements have been planned, with approximately 4 hours of data acquisition per measurement day. In order to be able to use both the video camera for recording the environment, as well as the sky brightness detector for assessing the shadowing percentages, all measurements will be performed during daylight hours. This schedule will result in about 1,500 MBytes of data recorded over a total distance of about 3000 km. The table below is a preliminary schedule for the experiment:

Table I
Campaign Schedule for ETS-V MSS Measurements

Measurement Day	Location	Elevation (deg)	Environment
1	Sydney	51	urban, sub-urban
2	Sydney	51	urban, sub-urban
3	Sydney to Canberra	51..48	rural, mountains
4	Canberra to Albury	48..46	mountains
5	Albury to Melbourne	46..42	hilly
6	Melbourne to Cobram	42..46	hilly, flat
7	Cobram to Dubbo	46..51	rolling
8	Dubbo to Armidale	51..53	mountains
9	Armidale to Brisbane	53..57	mountains
10	Brisbane	57	urban, sub-urban
11	Brisbane environs	57	rural, sub-urban
12	Brisbane to Grafton	57..55	flat, rural
13	Grafton to Port Mac	55..53	flat, rural
14	Port Mac to Sydney	53..51	flat, rural
15	Sydney	51	urban, sub-urban

Depending on road, traffic, weather or driver conditions, this schedule may be subject to real-time adaptive optimization.

3.4 Data Analysis

The data obtained in this experiment will be analyzed during the Sept. 1988 to Sept. 1989 time frame. Both these authors and AUSSAT will be involved in this phase, which will lead to a joint paper in a peer-review journal.

4.0 Acknowledgements

We very much would like to acknowledge the cooperation we received from Dr. Gert Brussaard of ESA in conducting the MARECS-A experiment. We also appreciate the initiative taken by Dr. Kim Dinh of AUSSAT, enabling us to significantly add to our data base. We also thank G. W. Torrence of EERL for continually improving the receiver van and for helping to carry out the experiment.

5.0 References

See: Goldhirsh and Vogel, Results of 1987 MSS Helicopter Propagation Experiment at UHF and L Band in Central Maryland, in this issue of the NAPEX proceedings.

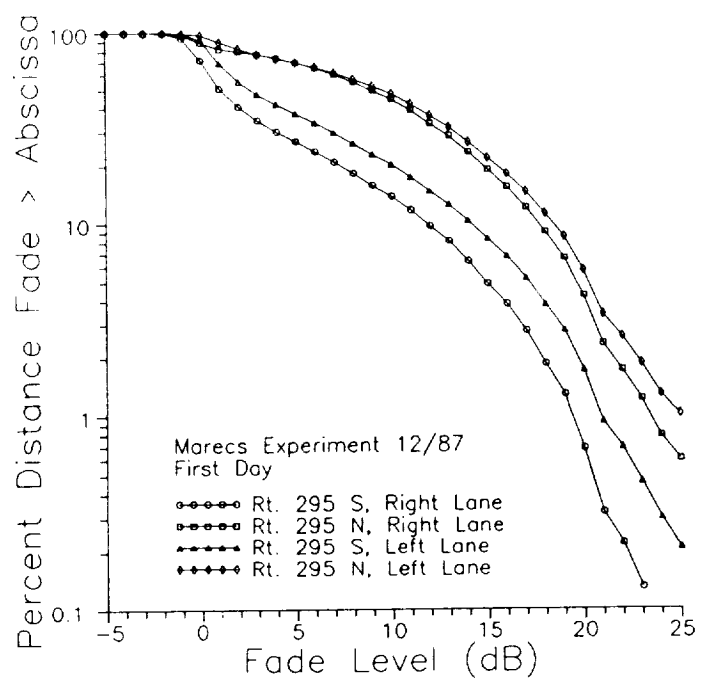


Figure 1 Cumulative fade distribution for Rt. 295 measured on the first day of the experiment.

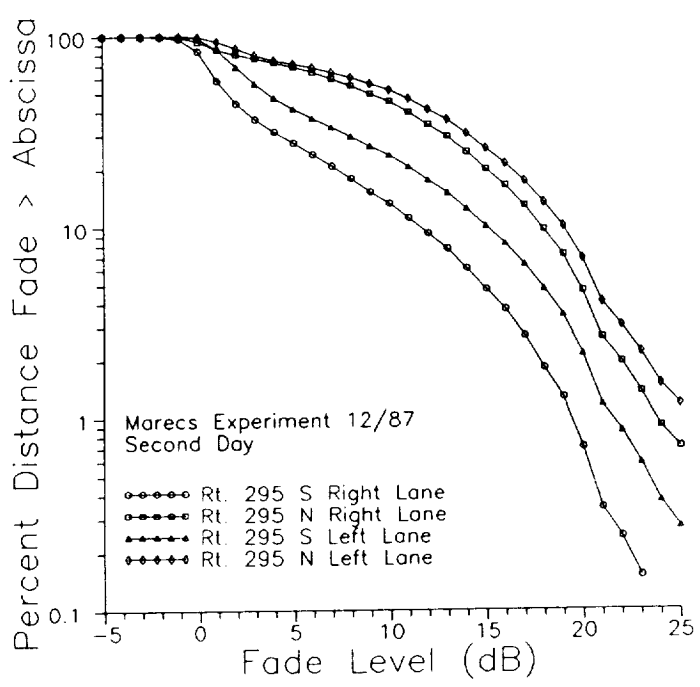


Figure 2 Cumulative fade distribution for Rt. 295 measured on the second day of the experiment.

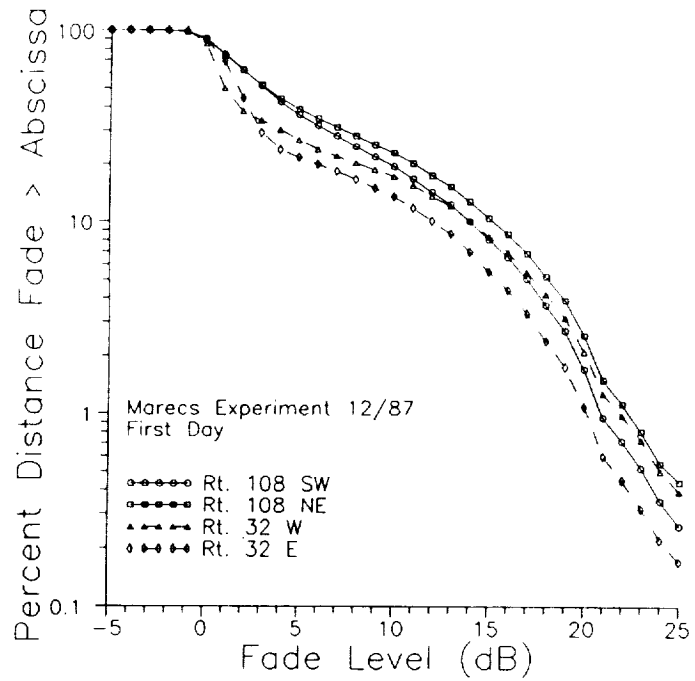


Figure 3 Cumulative fade distribution for Rts. 108 and 32 measured on the first day of the experiment.

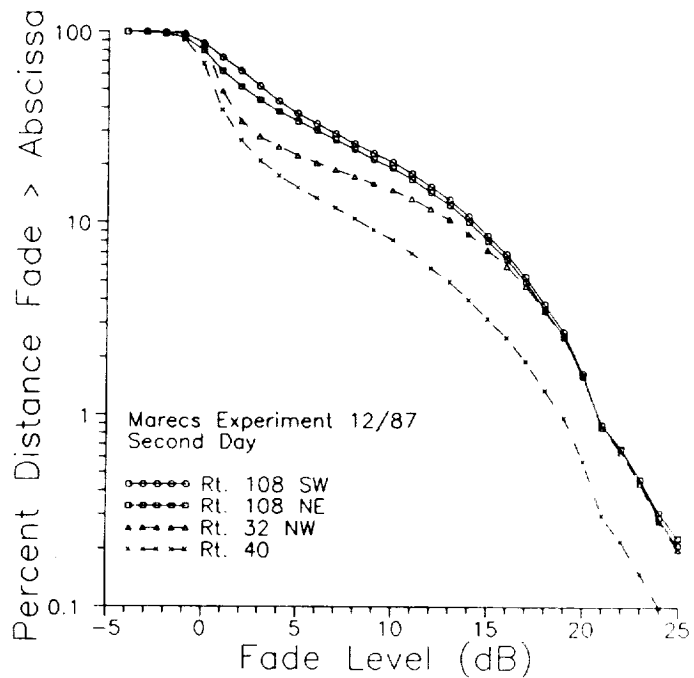


Figure 4 Cumulative fade distribution for Rts. 108, 32 and 40 measured on the second day of the experiment.

ORIGINAL PAGE IS
OF POOR QUALITY

ORIGINAL PAGE IS
OF POOR QUALITY

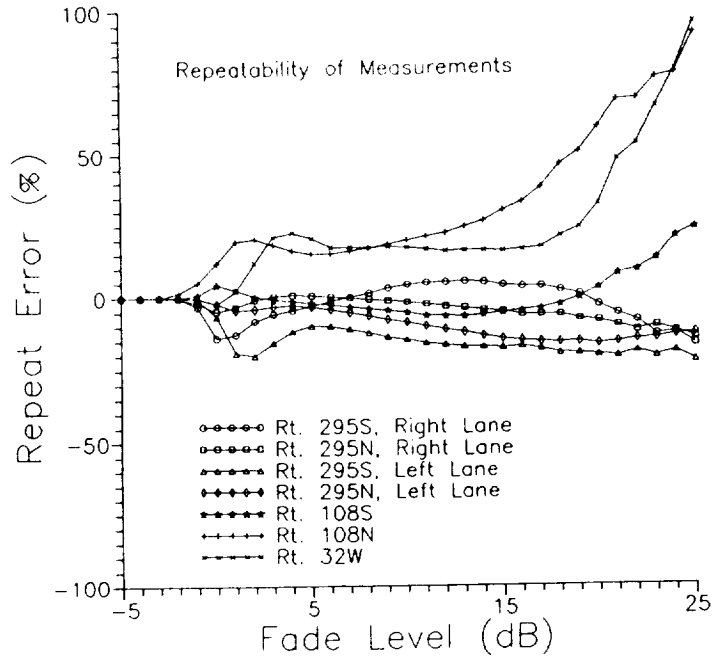


Figure 5

Repeatability of the distribution curves expressed as the % change at each fade level.

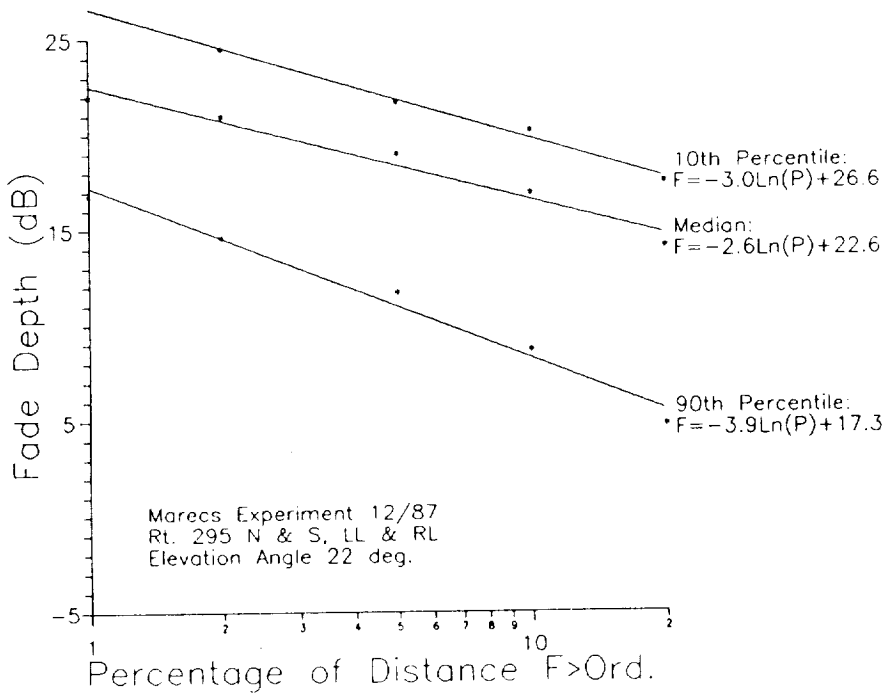


Figure 6

Measured 10th, 50th and 90th percentiles of the fade cumulative distributions taken over 90 seconds duration for Rt. 295.

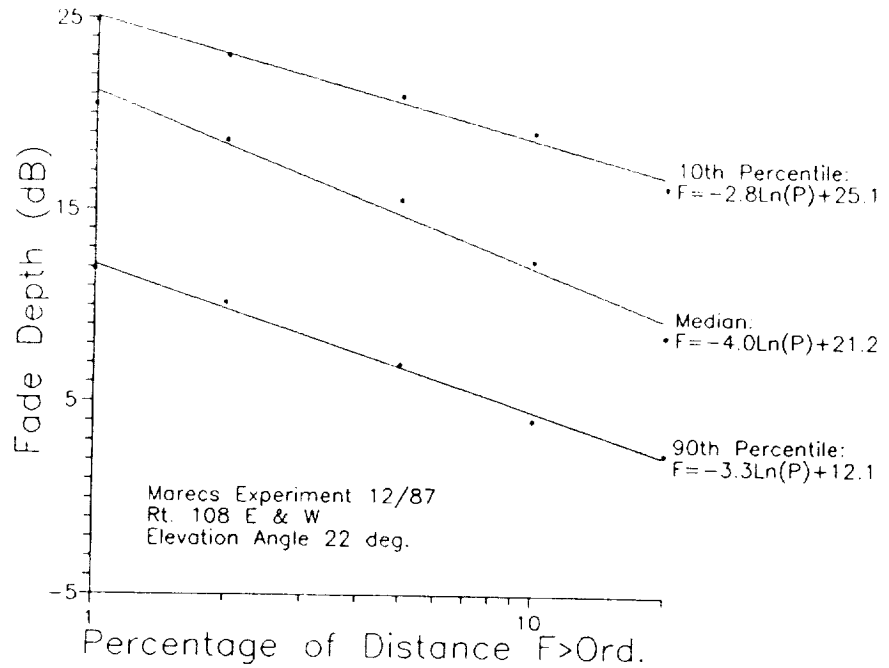


Figure 7 Measured 10th, 50th and 90th percentiles of the fade cumulative distributions taken over 90 seconds duration for Rt. 108.

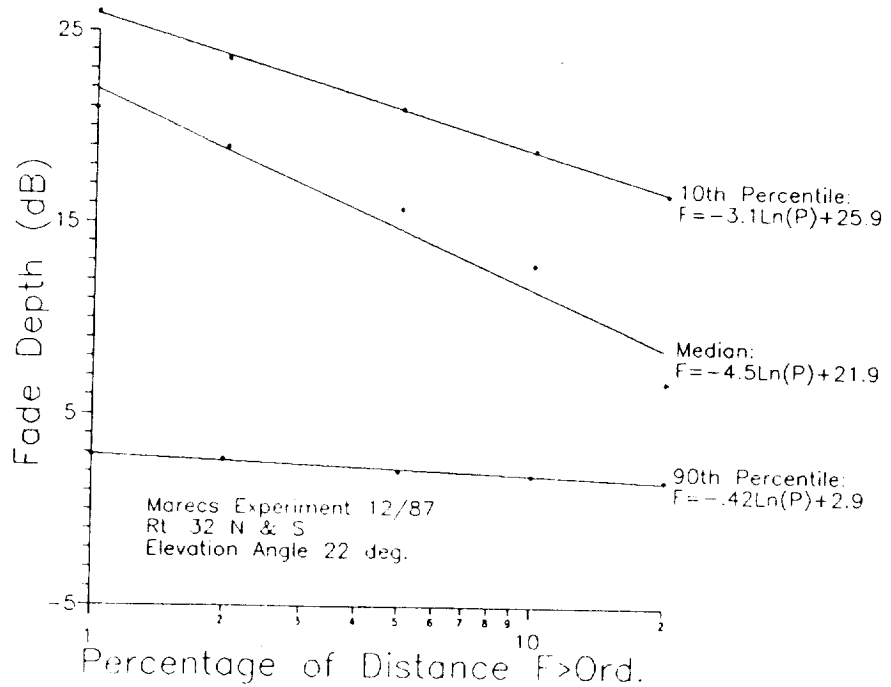


Figure 8 Measured 10th, 50th and 90th percentiles of the fade cumulative distributions taken over 90 seconds duration for Rt. 32.

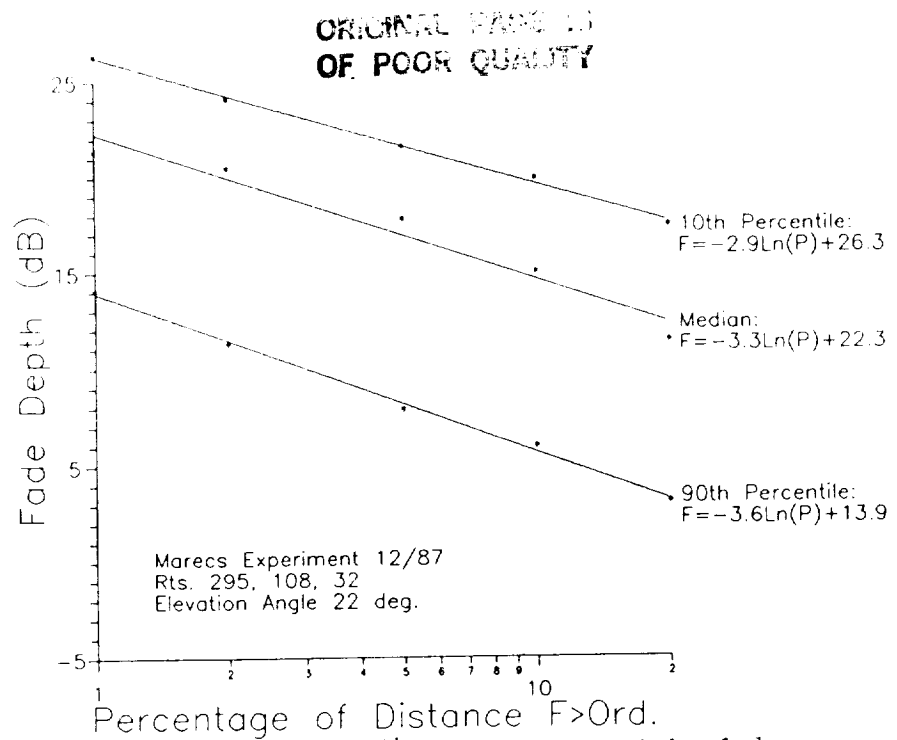


Figure 9 Measured 10th, 50th and 90th percentiles of the fade cumulative distributions taken over 90 seconds duration for the combined roads.

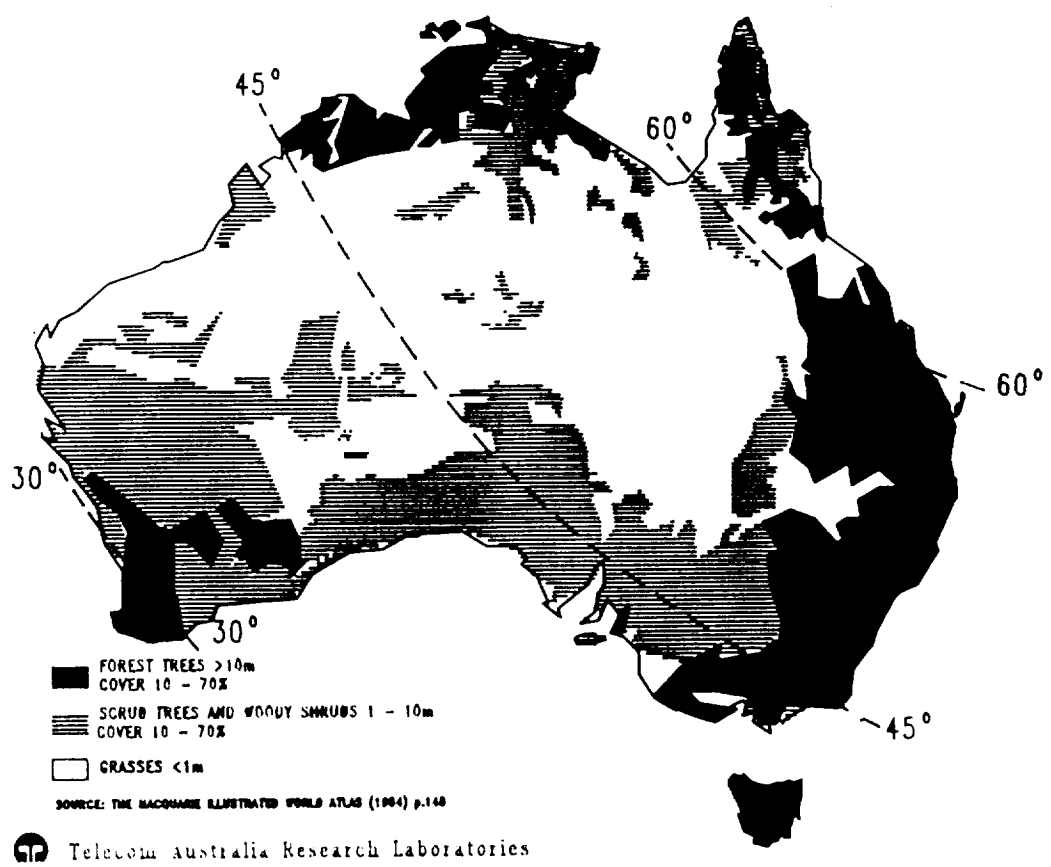


Figure 10 Vegetation zones of Australia

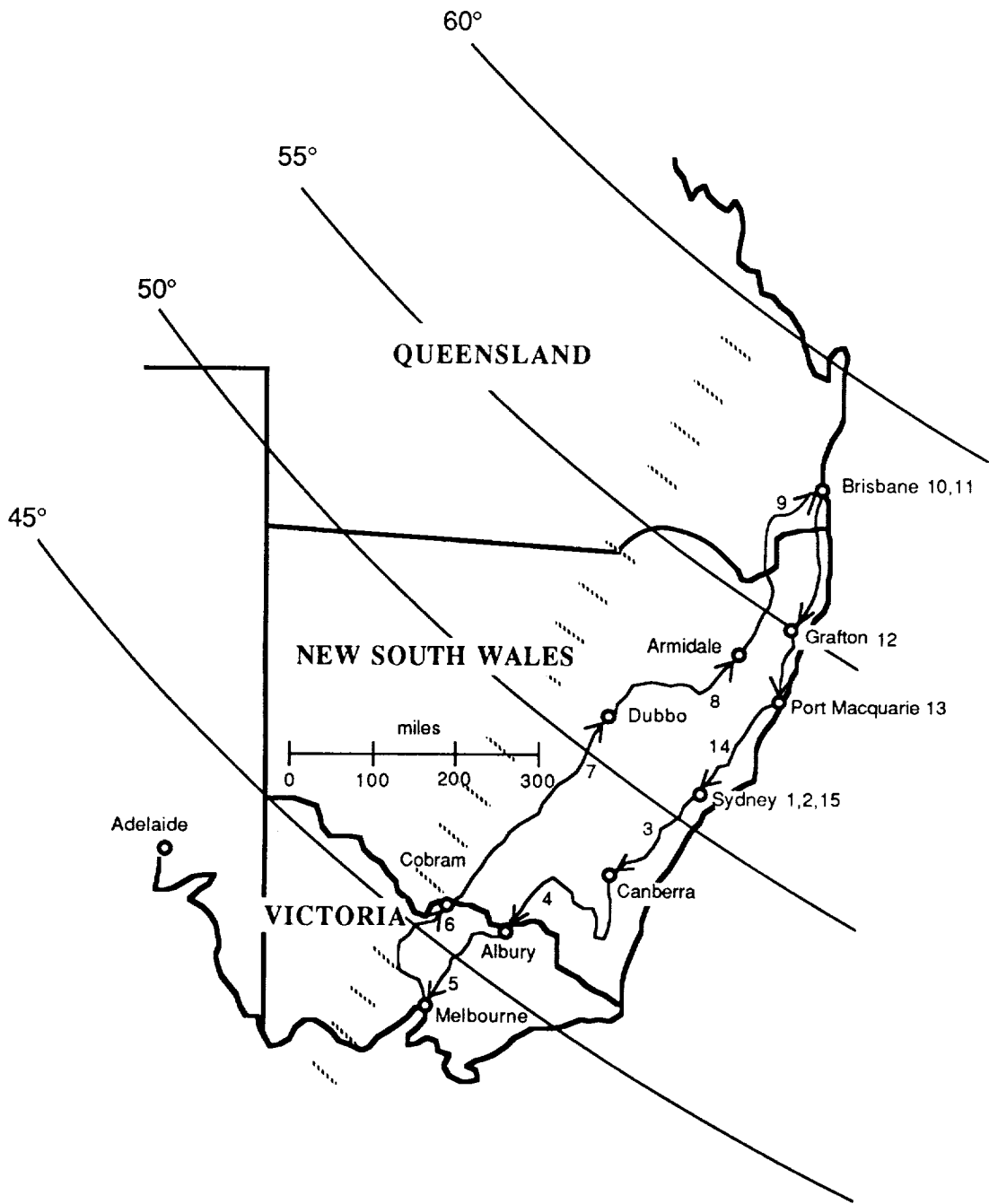


Figure 11 Preliminary itinerary for 15 days of measurements in southeastern Australia, covering a variety of vegetation zones and landscapes.

ETS-V PROPAGATION EXPERIMENTS IN JAPAN

Shingo Ohmori
 Kashima Space Research Center
 Communications Research Laboratory
 Ministry of Posts and Telecommunications
 Kashima, 314 Japan

Abstract-- Propagation experiments on ship, aircraft, and land mobile earth stations have been carried out using Engineering Test Satellite V (ETS-V), which was launched in August, 1987. The propagation experiments are one of missions of an Experimental Mobile Satellite System (EMSS). The project of EMSS is aimed for establishing basic technologies for future mobile satellite communications systems. This paper shows initial experimental results of ETS-V/EMSS on propagations using ship, aircraft and land mobiles with the ETS-V.

1. Introduction

Ministry of Posts and Telecommunications (MPT) of Japan has promoted Experiments on Mobile Satellite Communications using an Engineering Test Satellite V (ETS-V), which experimental system is called an Experimental Mobile Satellite System (EMSS) (Hase et al, 1987). The EMSS consists of the ETS-V, a feeder link earth station (Kashima Space Research Center) and several kinds of mobile earth stations including a ship, an aircraft, land mobiles and a hand carrying terminal. The ETS-V was launched on August 27 in 1987 by an H-1 rocket to a geostationary orbit over the Pacific Ocean (150 E).

Communications Research Laboratory (CRL) is leading the EMSS experiments, and Nippon Telegraph and Telephone Co. (NTT) (Shindo et al, 1987) and Kokusai Denshin Denwa Co. (KDD) are participating in the experiments to establish basic technologies of future mobile satellite communication systems. This paper describes initial experimental results on propagation problems.

2. Ship earth station

2.1 Outline of experiments

On board experiments were carried out in the South Pacific Ocean from Oct. 20 to Dec. 24 in 1987 by using a fish training ship of Hokkaido University (about 1400 tons). A ship earth station (SES) consists of an antenna system (15 dBi in gain) with a mechanical stabilizer and experimental terminals with several kinds of MODEMs and CODECs. The antenna system has a function to reduce effects of sea reflection fading, which can not be neglected in low elevation areas to the satellite (Ohmori et al, 1983)

2.2 Sea reflection fading

Before the launch of ETS-V, several experimental and theoretical analyses of sea reflection fading were carried out by CRL (Ohmori et al, 1985) and KDD (Karasawa et al, 1984), especially in the case of low elevation angles. Figure 1 shows the data of wave height and received signal level, which were measured during 180 seconds. The wave height was measured by a wave height detector mounted on the head of a ship, which measures wave motion by using microwave doppler effects. Sea wave condition shown in Fig. 1 was very rough, however, a

range of fading was as small as about 2 dB, because elevation angles to the satellite were so high as to vary from 20 to 55 degrees. As shown in Fig.2, spectra of wave height, ship motion and antenna motion were analyzed to evaluate sea conditions and a satellite tracking capability of the antenna system. Fig.2 shows clearly that ship moves according to wave motions and the antenna moves according to ship motions; it means that the antenna system has enough capability to track the satellite.

2.3 Blocking effect of above deck structures

The antenna system is installed on the deck near a mast in order to evaluate blocking effect to received signal level from the satellite. Figure 3 shows overlook of the antenna and the mast, on which sets of radars are installed as shown by a dotted circle. By scattering effects due to the mast, received signals consists not only of co-polarized component but of cross-polarized component. Figure 4 shows co- and x-polarized components of received signals under the blocking conditions. Accumulative distributions of co- and x-components are shown in Fig. 5. Co-component and X-component are found to fit to Ricean and Gaussian distribution, respectively.

3. Aircraft earth station

3.1 Outline of experiments

In flight experiments were carried out using a Boeing 747 jet cargo (JAL) between Tokyo and Anchorage. At Anchorage, an elevation angle to the ETS-V is 5 degrees, in such low elevation areas multipath fading caused by sea reflection is expected to be observed. Newly developed phased array antenna is adopted as an airborne antenna and its gain varies from about 12 to 15 dBi within beam coverage area. The antenna is mounted on the top of fuselage. Flight routes are shown in Fig. 6 with those of a ship.

3.2 Fading effects by a main wing

As shown in Fig. 7(a), fading effects by sea reflection was so small as to be neglected even in low elevation areas near Anchorage. The reasons may be that the antenna is installed on the top of the aircraft body, so reflected signals by sea surface were blocked by main wings and fuselage. However, slow speed fading effects were observed as shown in Fig. 7(b). The deviation of received signals was about 3 dB. The reason of this phenomenon is consider to be the scattering of signals due to a main wing and its edge, because in these experimental conditions the beam direction was correspond to the direction of a right side main wing.

4. Land Mobile Earth Station

CRL has already developed several kind of land mobile earth stations using such modulation techniques as ACSSB, MSK and SS (spread spectrum). However, propagation experiments on land mobiles with ETS-V have just started and there are only basic data. Figure 8(a) and (b) show propagation data measured in city area (down town Tokyo) and in open area (Kashima Space center), respectively. An antenna for measurements is an one-element microstrip patch and its gain is about 7 dBi.

5. Conclusion

The ETS-V propagation experiments on an initial stage were reported. The experiments have now been on progress and a large amount of data are now analyzed. Main topics of experiments in the initial stage on aircraft and on a ship are scattering by main wings and blocking effects by above deck structures such as masts and radars, respectively. In 1988, CRL has a plan to perform 2-on board experiments in North and South Pacific Ocean, 14-in flight experiments between Tokyo and Anchorage and Land mobile experiments in many kinds of terrains. NTT and KDD have also many schedules to carry out propagation experiments using ships, aircraft and land vehicles.

References

- Hase, Y. et al, "Experimental Mobile Satellite System (EMSS) Using ETS-V," IEEE Denshi Tokyo, No. 25, 1986.
- Shindo, S. et al, "A Multi-beam Mobile Satellite Communications System in Japan," International Workshop on Digital Communications, Tirrenia, Italy, 1987.
- Ohmori, S. et al, "A Fading Reduction Method for Maritime satellite Communications," IEEE Trans. on Ant. and Prop., vol.AP-31, No.1, Jan. 1983.
- Ohmori, S et al, "Characteristics of Sea reflection Fading in Maritime Satellite Communications," IEEE Trans. on Ant. and Prop., vol.AP-33, No.8, August 1985.
- Karasawa, Y et al, "Characteristics of L-band multipath fading due to sea surface reflection", IEEE, Trans. on Ant. and Prop., vol.AP-32, No.6 1984.

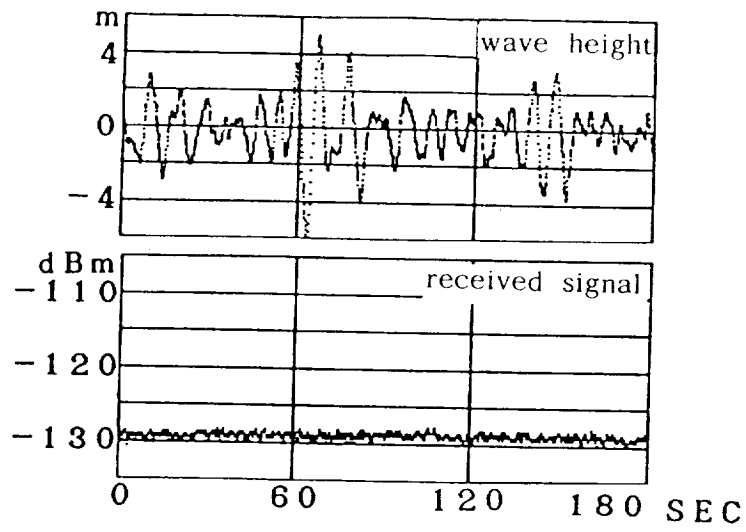
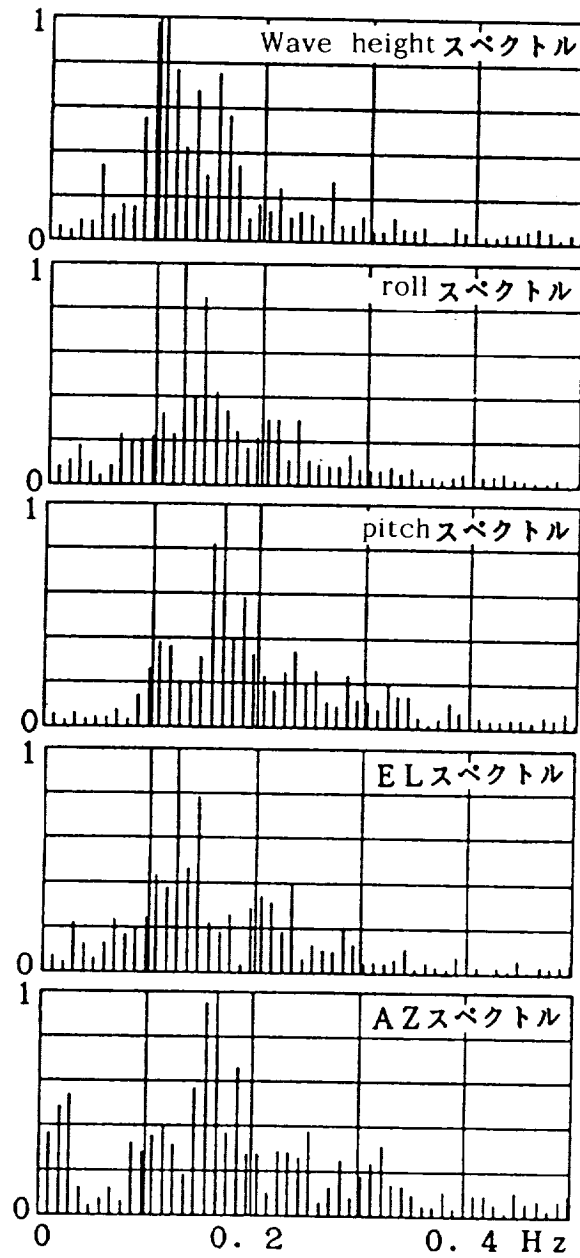


Fig.1 Wave height and received signal level.



ORIGINAL QUALITY
OF POOR QUALITY

Fig.2 Spectra of wave height, ship motion (roll & pitch) and antenna motion (Az & El).

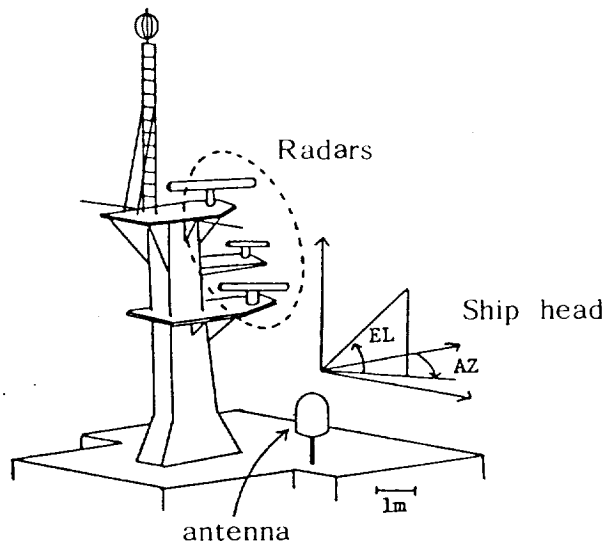


Fig.3 Overlook of the antenna and above deck structures.

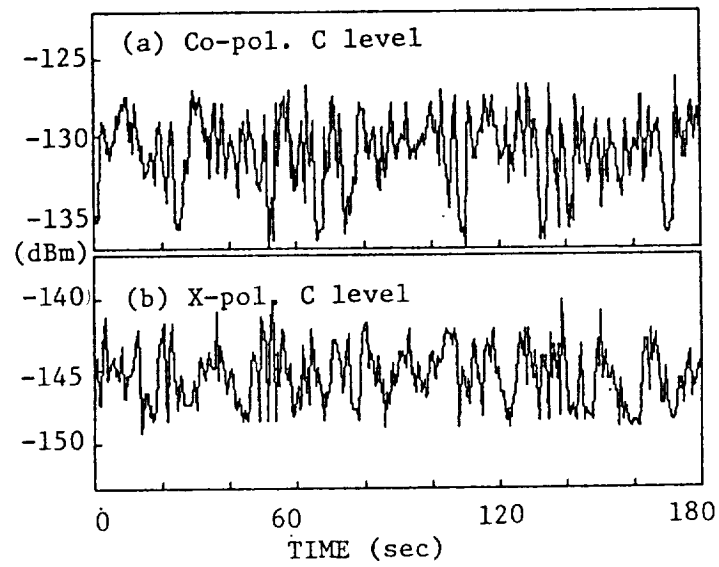


Fig.4 Co- and X-polarized received signals under the blocking conditions.

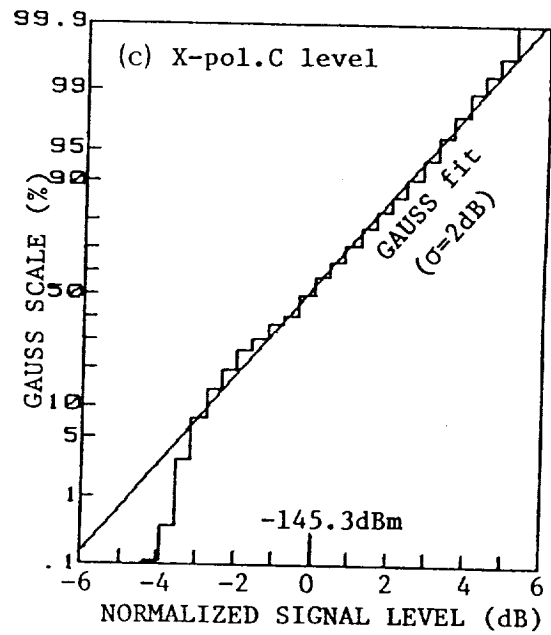
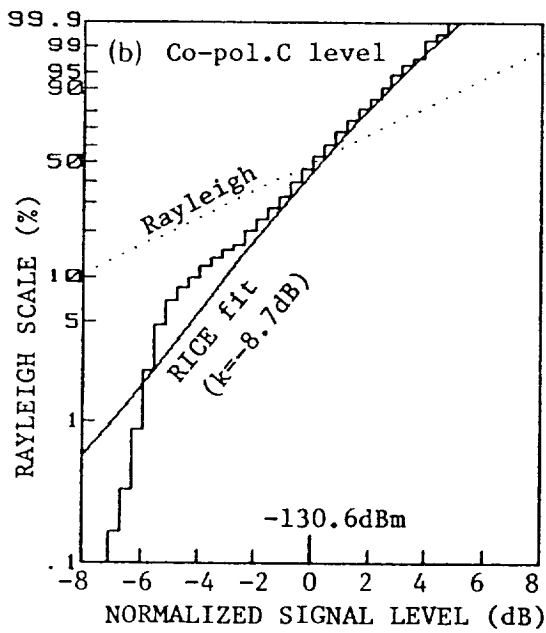
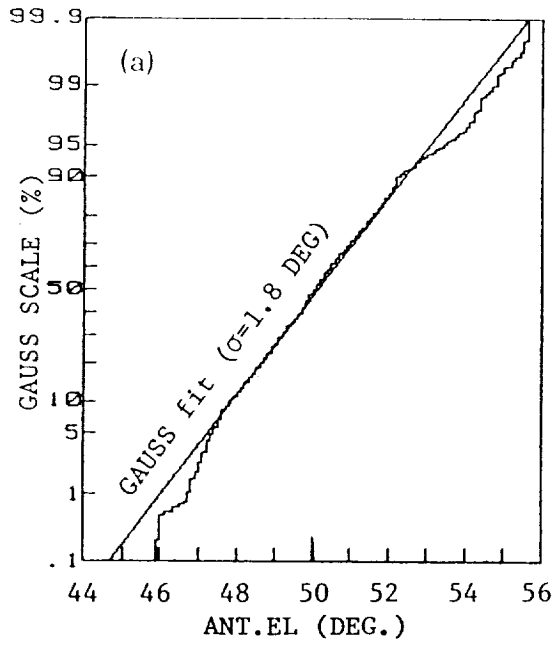


Fig.5 Accumulative distributions of antenna motion (a), co- (b) and X-polarized signal levels (c).

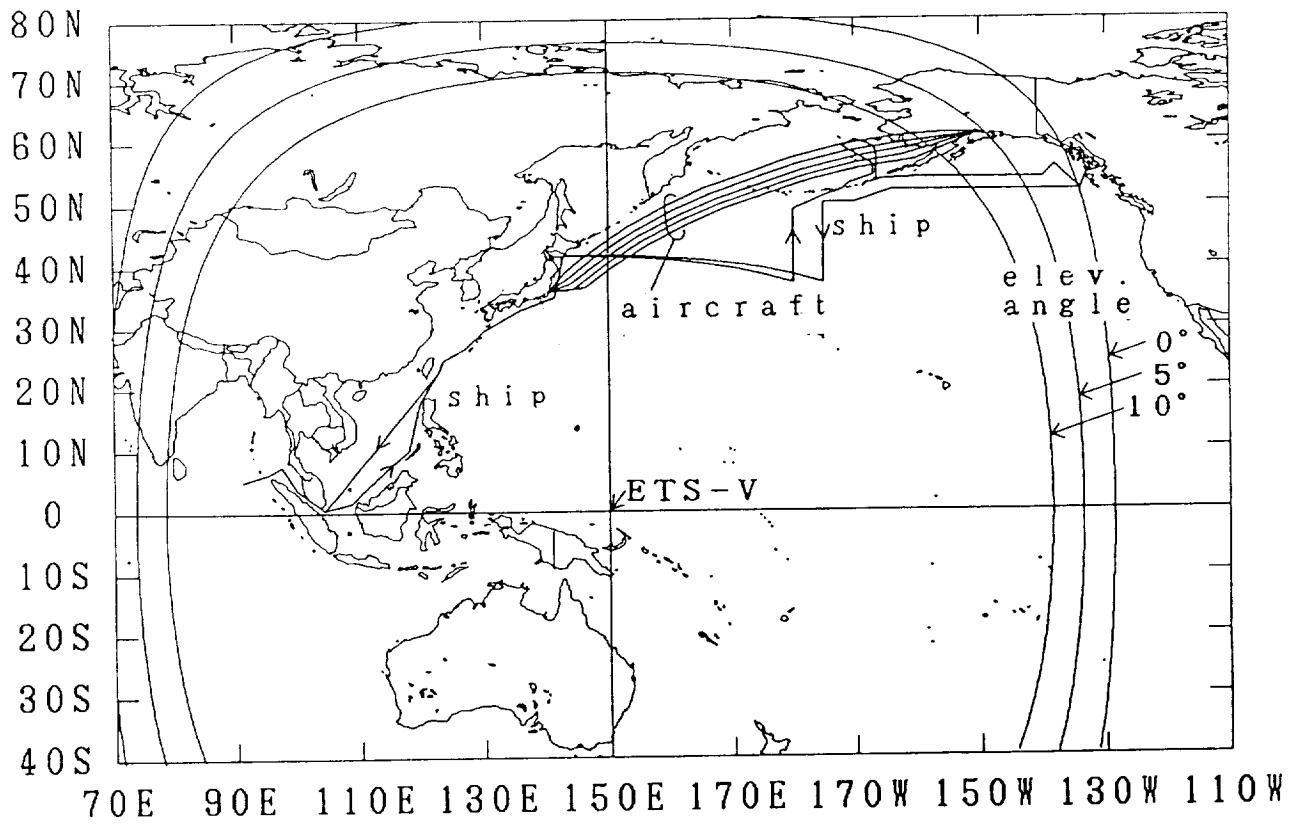


Fig.6 Flight and cruising routes of the aircraft and the ship.

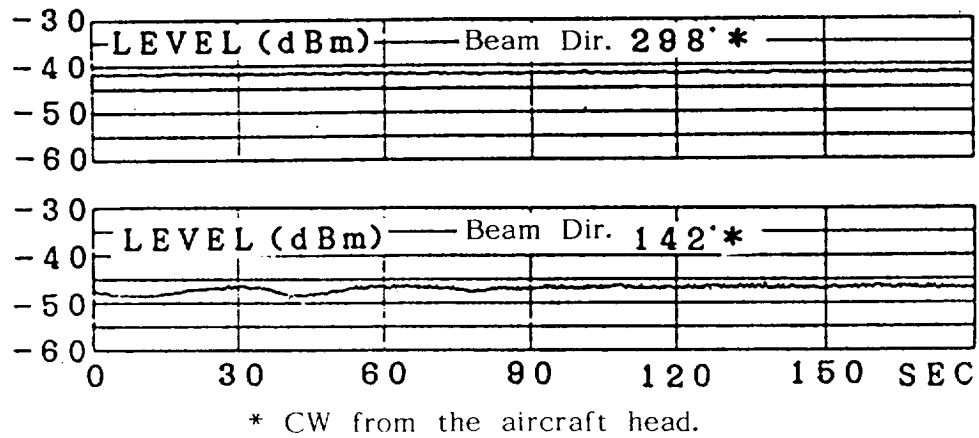
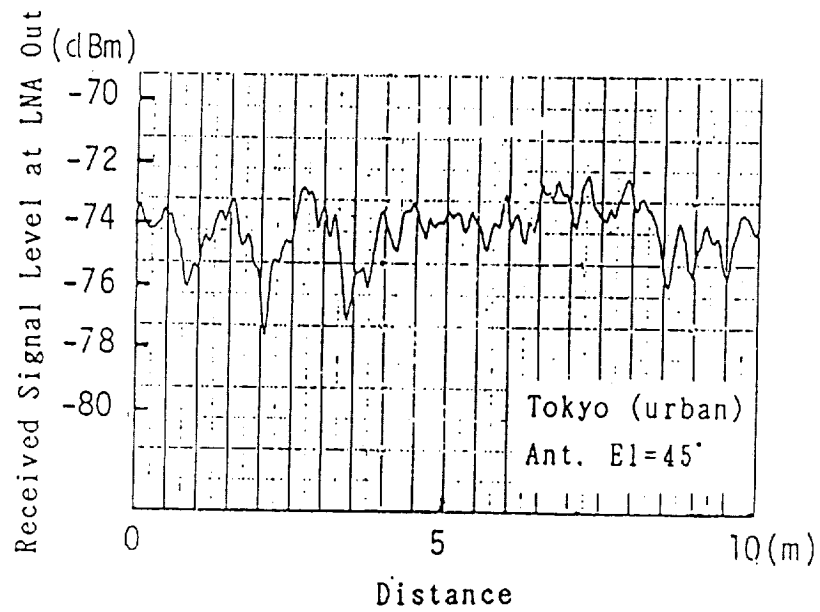
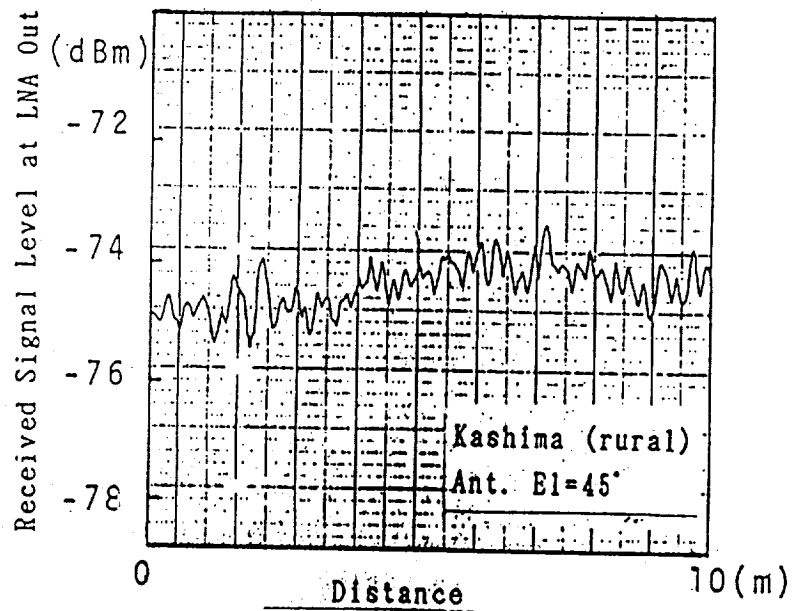


Fig.7 Received signal levels measured on the aircraft.



Received Signal at Moving Trolley



Received Signal at Moving Trolley

Fig.8 Received signal levels measured on the land mobile.
(a) Urban area (b) Rural area.

ORIGINAL COPY IS
OF POOR QUALITY

MOBILE SATELLITE PROPAGATION MEASUREMENTS AND MODELING:
A REVIEW OF RESULTS FOR SYSTEMS ENGINEERS

Editor:

W. L. Stutzman Virginia Tech

Contributors:

R. M. Barts	Virginia Tech
C. W. Bostian	Virginia Tech
J. S. Butterworth	CRC, Canada
R. Campbell	Michigan Tech
J. Goldhirsh	Applied Physics Lab./JHU
W. L. Stutzman	Virginia Tech
W. J. Vogel	U. of Texas

VIRGINIA TECH

Satellite Communications Group
Bradley Department of Electrical Engineering
627 Whittemore Hall
Blacksburg, VA 24061

ABSTRACT

This overview of Mobile Satellite System (MSS) propagation measurements and modeling is intended as a summary of current results. While such research is on going, the simple models presented here should be useful to system engineers. A complete summary of MSS propagation experiments with literature references is also included.

INTRODUCTION

This paper is a collective effort by a group of researchers in the U. S. and Canada in the area of Land Mobile Satellite propagation. It concerns the propagation effects of the natural environment as encountered under highway conditions at UHF and L-Band frequencies. It presents results, experimental and theoretical, that are applicable to future operational Mobile Satellite Systems (MSS). Our understanding of MSS propagation is by no means complete. Much needs to be done both in measurement and in theory. This review is essentially a summary of the current state of knowledge.

This paper emphasizes results, not the details of how experiments were performed or the theoretical background of the models developed. A comprehensive list of MSS related propagation experiments is presented (see Table 1); literature references for these experiments as well as for key theory and modeling works are given.

CHARACTERISTICS OF MSS PROPAGATION EFFECTS

MSS communications system design presents new problems. Mobile terminals do not have the fixed-terminal advantage of placing antennas with a clear line of sight view to the satellite. Instead, a mobile with a roof mounted antenna will encounter several propagation effects that will influence the system margin, reliability, and modulation format selection. These may be classified as follows:

- (a) Tree shadowing of the direct wave
- (b) Blockage from natural terrain and structures like overpasses
- (c) Multipath scattering from terrain, and from simple scatterers like utility poles

Specular reflection is not significant above 15 degrees elevation with circularly polarized antennas [5] and therefore, we have not listed it as a propagation problem. Blockage from structures such as overpasses has been noted by Vogel during his balloon experiments [9]. They are obviously serious short term blockage problems but are not statistically significant. This paper does not include structure blockage effects, but concentrates on vegetative blockage and multipath scattering.

MSS PROPAGATION RESEARCH LITERATURE

Overview

The MSS propagation problem is attacked on three fronts: experimental, basic EM theory, and modeling. The most important of these is the establishment of an experimental data base. Satellite, helicopter, balloon, remotely piloted aircraft and tower platforms have been used, and most results appear to be applicable to satellite-to-earth mobile systems. This data base serves

two purposes. First, it may be used for system planning if data of the proper frequency, elevation angle, etc. are available or can be scaled. Second, experimental data are used in verifying theoretical models and to drive software simulators.

Complete analytical solutions from electromagnetic theory are not available due to the complexity of the propagation environment, but partial analytical and empirical statistical models of MSS propagation have been developed [14, 20, 21, 22]. These offer considerable insight into the physics of slant path propagation.

The mobile aspect of MSS propagation complicates the problem. Theoretical models do not provide complete information on the variation of the parameters in terms of highway and system constraints. Simple empirical models can be developed to give fade statistics for simple relationships with the highway and system parameters as inputs.

Experiments

Mobile satellite propagation experiments have been conducted since 1978. Table 1 presents a chronology of slant path propagation experiments in the UHF and L-bands. Most of the experiments produced fade depth and duration statistics for various mobile travel conditions. Some results from these are given in following sections.

Some experiments also collected phase data. The peak-to-peak variations of the phase, ϕ , as a function of peak-to-peak signal level fluctuations in dB, L , can be expressed by [14]

$$\phi = c * L \quad \text{[degrees]} \quad (1)$$

where

c = 6.0	analytical value for unshadowed multipath
7.6	90th percentile) measured, includes
3.9	median) shadowing for fades up
2.1	10th percentile) to about 15 dB

The signal arriving at an MSS receiver has two components: a direct path component which can experience shadowing, and a diffuse component that is the sum of signals reflected from nearby objects. Campbell has performed experiments focusing on characterization of the diffuse component, which is quantified by the power level relative to the unattenuated direct signal power, \bar{K} , and the spatial distribution of arrival angles for the diffuse power. The measurements were made at 1300 MHz at

several elevation angles near 10 degrees along a section of a hardwood tree lined road in upper Michigan. The average total diffuse signal power is 17 dB below the unattenuated direct path signal. The diffuse signal has a rather even angular distribution, except for trees within about 100 m of the receiver which have significant contributions. The diffuse component is relatively unaffected by instantaneous blockage of the direct component; therefore, during deep fading the diffuse component will dominate.

FADE DISTRIBUTIONS

Form Of The Fade Distribution

Both experimental observations and basic theory indicate that the fade statistics measured over a large distance become Rician at low fade levels because of the dominant multipath effects. For high fade levels a number of experiments indicate that they become lognormal when vegetative shadowing dominates. Thus, MSS fading is modeled by a Rician distribution, described by the carrier-to-multipath ratio K , to predict fading when there is no blockage of the signal. When tree blockage is present, the fading is modeled by the sum of a lognormal distribution, described by the mean, μ , and standard deviation, σ , and a Rayleigh distribution, described by \bar{K} , the carrier-to-multipath ratio. Bradley and Stutzman [20] showed how these distributions can be combined for an arbitrary percentage of shadowing along the travel route; apparently Lutz et al. [11] found this independently.

Experimental Results

Representative experimental results are plotted in Fig. 1. Shown are cumulative fade distributions over typically tens of km of road distance [18]. The distributions depend strongly on the elevation angle when shadowing by roadside trees dominates. A four-lane divided freeway lined with trees (Fig. 1a) can produce larger fades than a two-lane road lined with utility poles and trees (Fig. 1b). In comparison, a road with a wider cleared easement, even though tree lined (RT. 32), will have smaller probabilities. Measurements obtained at UHF on a road for various growing seasons (Leafless, March 1986; Fall Foliage, October 1985; Full Blossom,

June 1986) show only a small increase in attenuation due to leaves (Fig. 1c).

To scale UHF data to L-Band, the relationship

$$F_L = (1.35 + 0.1) * F_U \quad (3)$$

can be used where F_L and F_U are the L-Band and UHF fades in dB, respectively [18]. A comparison of distributions obtained in differing geographic areas (Fig. 1d) emphasizes the dependence of the distribution on the dominating environmental parameters, from heavy tree shadowing (Curve A) to pure multipath (Curve G).

Simple Model

A simple model for predicting the probability that the fades will be less than a certain amount F is given by [23]

$$C(F) = C_U(F) * (1-s) + C_S(F) * s \quad (2)$$

where

F = fade level with respect to LOS in dB
 s = fraction of time vegetative shadowing occurs along travel route

and where

$$C_U(F) = e^{-(F+U_1)/U_2}$$

= fade distribution for an unshadowed signal

$$U_1 = 0.01 * K^2 - .378 * K + 53.98$$

$$U_2 = 331.25 * K^{-2.29}$$

$$K = \text{carrier-to-multipath ratio [dB]}$$

and where

$$C_S(F) = [(50-F)/V_1]^{V_2}$$

$$V_1 = -0.275 * \bar{K} + 0.723 * \mu + 0.336 * \sigma + 56.153$$

$$V_2 = [-0.006 * \bar{K} - 0.008 * \mu + 0.013 * \sigma + 0.103]^{-1}$$

$$\bar{K} = \text{carrier-to-multipath ratio [dB]}$$

$$\mu = \text{mean of lognormal signal [dB]}$$

σ = standard deviation of lognormal signal [dB]

The percent time that the fade F is exceeded is then found from (2) simply as $P=100*C(F)$.

This simple model is valid for typical ranges of the propagation parameters. Typical values for each of the parameters are as follows:

$$\begin{aligned} 13 \text{ dB} < \bar{K} < 22 \text{ dB} \\ 12 \text{ dB} < \bar{K} < 18 \text{ dB} \\ -1 \text{ dB} < \mu < -10 \text{ dB} \\ 0.5 \text{ dB} < \sigma < 3.5 \text{ dB} \end{aligned}$$

Behavior Of Statistical Parameters With Time

Cumulative fade distributions give information about the average link performance for a large number of transmissions for particular environmental conditions. A typical telephone call has a shorter duration (about 90 seconds) and therefore covers a shorter distance than the one on which Fig. 1 is based. When cumulative fade distributions are determined for successive 90 second intervals, they will vary, depending upon the short term variation of the shadowing parameter statistics. At percentage levels of main interest, from 1% to 20%, the 10th, 50th and 90th percentiles of the 90 second fade levels have been calculated and are given in Fig. 2 for elevation angles of 30, 45 and 60 degrees. The curve labeled median represents the median cumulative fade distribution and the upper and lower curves give the bounds into which 80% of the measured distributions fall. The curves can be fit by the relationship:

$$F(n,P) = A(n)*\ln(P) + B(n) \quad (4)$$

where

$F(n,P)$ = Fade at nth percentile for P percent of time fade is exceeded

$A(n)$, $B(n)$ = fit coefficients (see Table 2)

Hence, these experimental results indicate that over the limited percentage interval a simple logarithmic relationship holds.

FADE DURATIONS

Measured fade durations for a 5 dB threshold are

given in Fig. 3. The curves correspond to the combined results of repeated runs along several roads at the indicated elevation angles, both under predominantly shadowing or under multipath conditions. Two sets of statistics are provided, "fade durations": the duration the signal is below the threshold and "nonfade durations": the duration the signal is greater than the threshold. The duration is expressed as spatial variable in wavelengths (0.2m) to gain independence from the vehicle speed. The durations are seen to systematically depend upon the elevation angle for the shadowing data. The lower the elevation, the longer the fades and the shorter the nonfades. Multipath durations are independent of the elevation angle, having very short fades and long nonfades.

The distribution of fade durations cannot in general be predicted analytically. Schmier and Bostian have reported a software simulator [24] which they claim will accurately predict the fade duration statistics of a signal whose cumulative fade distribution is known. The simulator operation is based on scaling values from a universal data set. Its predictions of the total number of fades exceeding specified thresholds agree well with experiment, but unpublished work by Barts indicates that it may not predict average fade durations well. Barts' work indicates that Schmier and Bostian's simulator works correctly, but its universal data set may have been incorrectly derived. Each side can make an effective case for the correctness of its results, and at the time this paper was written the issue was still unsettled.

REFERENCES

1. G. C. Hess, "Land Mobile Satellite Path Loss Measurements," Third Year ATS-6 Experiment Final Report, Motorola Inc., Schaumburg, IL, Sept. 6, 1978.
2. G. C. Hess, "Land mobile satellite excess path loss measurements," IEEE Trans. on Vehicular Technology, vol. VT-29, pp. 290-297, May 1980.
3. R. E. Anderson, R. L. Frey, and J. R. Lewis, "Satellite-Aided Mobile Communications Limited Operational Test in the Trucking Industry," Final Report for NASA Contract NAS5-24365 (N81-20338), June 1979.
4. R. E. Anderson, R. L. Frey, J. R. Lewis, and R. T. Milton, "Satellite-aided mobile communications: Experiments, applications, and prospects," IEEE Trans. on Vehicular Technology, vol. VT-30, no. 2, pp. 54-61, May 1981.
5. J. S. Butterworth, "Propagation Measurements for Land-Mobile Satellite Services in the 800 MHz Band," Communications Research Centre Technical Note No. 724, Department of Communications, Canada, Aug. 1984.
6. J. S. Butterworth, "Propagation data for land-mobile satellite systems," Proceedings of NAPEX VIII, Vancouver, B.C., Canada, Aug. 1985.
7. J. S. Butterworth, "Propagation Measurements for Land Mobile Satellite Systems at 1542 MHz," Communications Research Centre Technical Note No. 723, Department of Communications, Canada, Aug. 1984.
8. W. J. Vogel and G. W. Torrence, "Measurement Results From A Balloon Experiment Simulating Land Mobile Satellite Transmissions," MSAT-X Report No. 101, NASA-JPL, Pasadena, CA, April 1984.
9. W. J. Vogel, "Land Mobile Satellite Transmission Measurements at 869 MHz," MSAT-X Report No. 106, NASA-JPL, Pasadena, CA, April 12, 1985.
10. R. J. C. Bultitude, "Measured characteristics of 800/900 MHz fading radio channels with high angle propagation through moderately dense foliage," IEEE Journal on Selected Areas in Communications, vol. SAC-5, No. 2, Feb. 1987.
11. E. Lutz, W. Papke, and E. Plochinger, "Land mobile satellite communications - channel modeling, modulation and error control," Proceedings of 7th International Conference on Digital Satellite Communications, Munich, Germany, May 1986.
12. W. J. Vogel, and J. Goldhirsh, "Tree attenuation at

- 869 MHz derived from remotely piloted aircraft measurements," IEEE Trans. on Antennas and Propagation, vol. AP-34, No. 12, Dec. 1986.
13. J. Goldhirsh, and W. J. Vogel, "Roadside tree attenuation measurements at UHF for land mobile satellite systems," IEEE Trans. on Antennas and Propagation, vol. AP-35, No. 5, May 1987.
 14. W. J. Vogel, and U. Hong, "Measurement and modeling of land mobile satellite propagation at UHF and L-Band," IEEE Trans. on Ant. and Prop., vol. AP-36, May 1988.
 15. W. J. Vogel, and J. Goldhirsh, "Fade measurements at L-Band and UHF in mountainous terrain for land mobile satellite systems," IEEE Transactions on Antennas and Propagation, vol. AP-36, Jan, 1988.
 16. J. B. Berner, "PiFEX Tower 1 Results," Proceedings of NAPEX XI, NASA-JPL, Pasadena, CA, Aug. 31, 1987.
 17. Special Issue on PiFEX Tower 1 Experiments, MSAT-X Quarterly, JPL, No. 13, Jan. 1988.
 18. J. Goldhirsh and W. J. Vogel, "Attenuation Statistics Due to Shadowing and Multipath from Roadside Trees at UHF and L-Band for Mobile Satellite Systems," Johns Hopkins University/APL Report No. S1R-88-U004, Feb. 1988.
 19. W.J. Vogel and J. Goldhirsh, "A Comparison of Mobile Satellite Fade Statistics Obtained with a Helicopter and a Geosynchronous Satellite," manuscript in preparation.
 20. W. S. Bradley, and W. L. Stutzman, "Propagation Modeling for Land Mobile Satellite Communications," Technical Report submitted to JPL under NASA Contract 956512, August 1985.
 21. W. T. Smith, and W. L. Stutzman, "Statistical Modeling for Land Mobile Satellite Communications," Technical Report submitted to JPL under NASA Contract 956512, August 1986.
 22. C. H. Loo, "A statistical model for the land mobile satellite link," Proceedings of the IEEE International Communications Conference, pp. 588-594, 1984.
 23. R. M. Barts, W. L. Stutzman, W. T. Smith, R. S. Schmier, and C. W. Bostian, "Land mobile satellite propagation modeling," Proceedings of 1987 IEEE Antennas and Propagation Society International Symposium, Blacksburg, VA, June 1987.
 24. R. G. Schmier and C. W. Bostian, "Fade durations in satellite path mobile radio propagation," IEEE Transactions on Vehicular Technology, Nov. 1987.

25. A. Jongejans, et al., "PROSAT Phase I Report,"
European Space Agency Report ESA STR-216, May 1986.

**CUMULATIVE DISTRIBUTIONS FOR ROUTE 295 SOUTH (RHS)
COMPARISON FOR DIFFERENT ELEVATION ANGLES AT L-BAND**

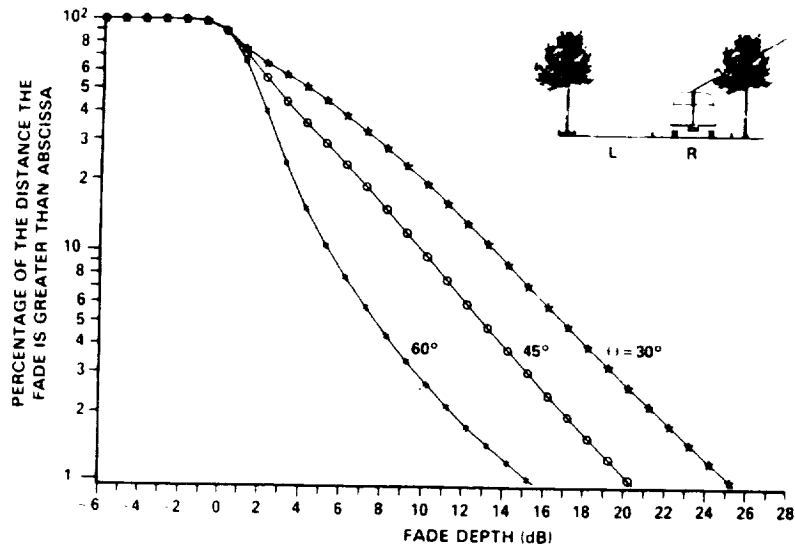


Figure 1a

**COMPARISON OF CUMULATIVE FADE DISTRIBUTIONS
FOR VARIOUS ROADS AT AN ELEVATION ANGLE OF
45° FOR L-BAND**

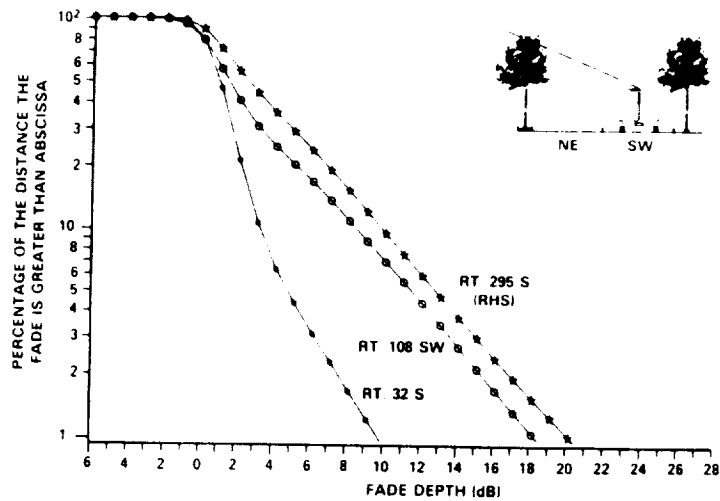


Figure 1b

**CUMULATIVE FADE DISTRIBUTIONS FOR
VARIOUS SEASONS
ROUTE 295 SOUTH (RHS) - UHF AT 45°**

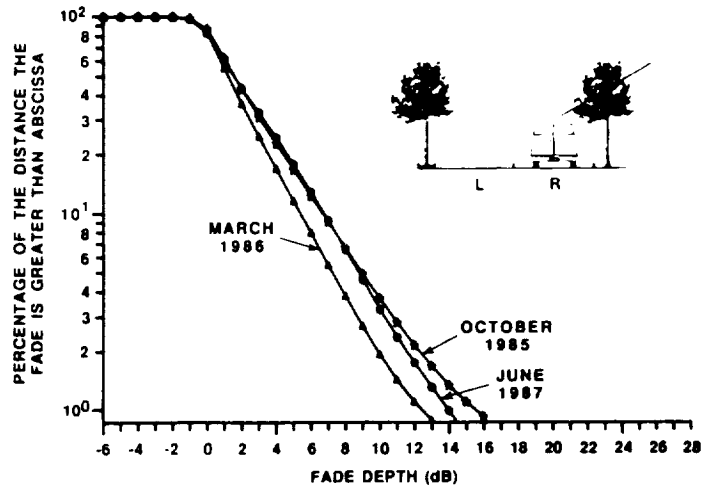


Figure 1c

**COMPARISON OF L BAND FADE DISTRIBUTIONS
FOR VARIOUS MSS INVESTIGATIONS**

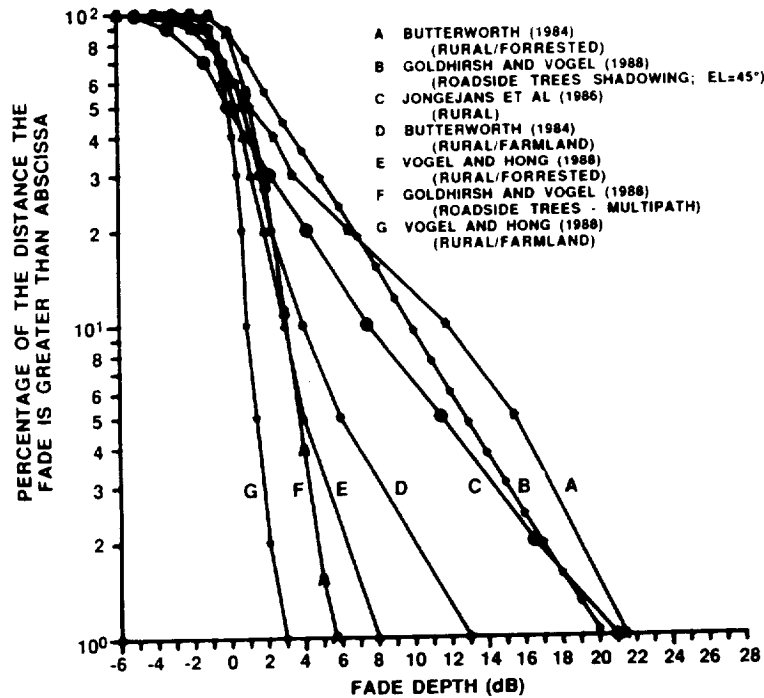


Figure 1d

BEST FIT CUMULATIVE MEDIAN FADE DISTRIBUTION
WITH 10 AND 90 PERCENTILE BOUNDS
(ELEVATION ANGLE = 30°)

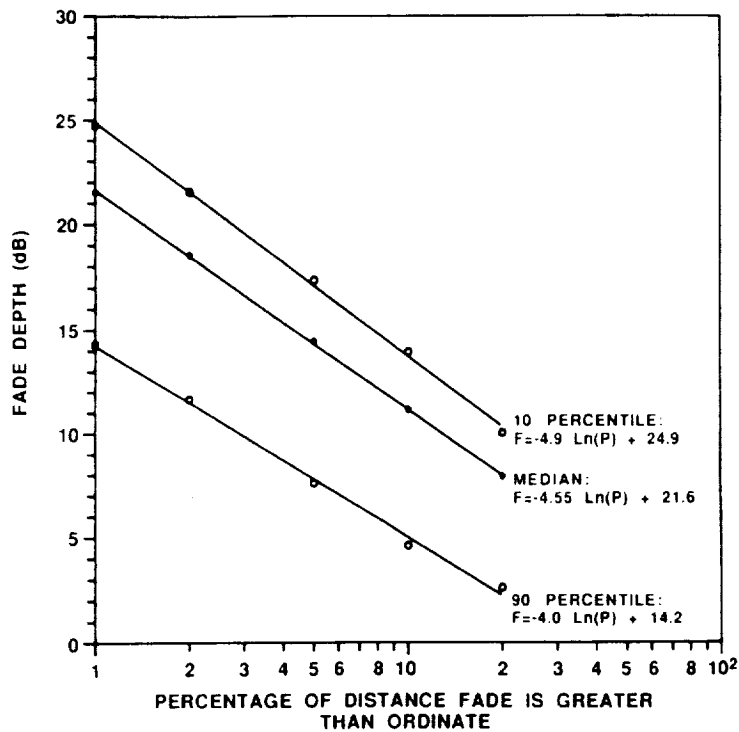


Figure 2a

BEST FIT CUMULATIVE MEDIAN FADE DISTRIBUTION
WITH 10 AND 90 PERCENTILE BOUNDS
ELEVATION ANGLE = 45°

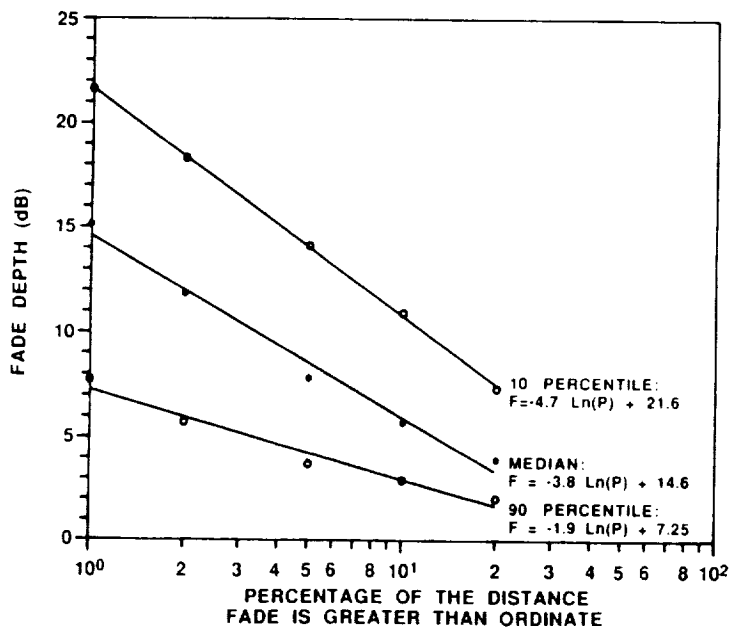


Figure 2b

BEST FIT CUMULATIVE MEDIAN FADE DISTRIBUTION
WITH 10 AND 90 PERCENTILE BOUNDS
ELEVATION ANGLE = 60°

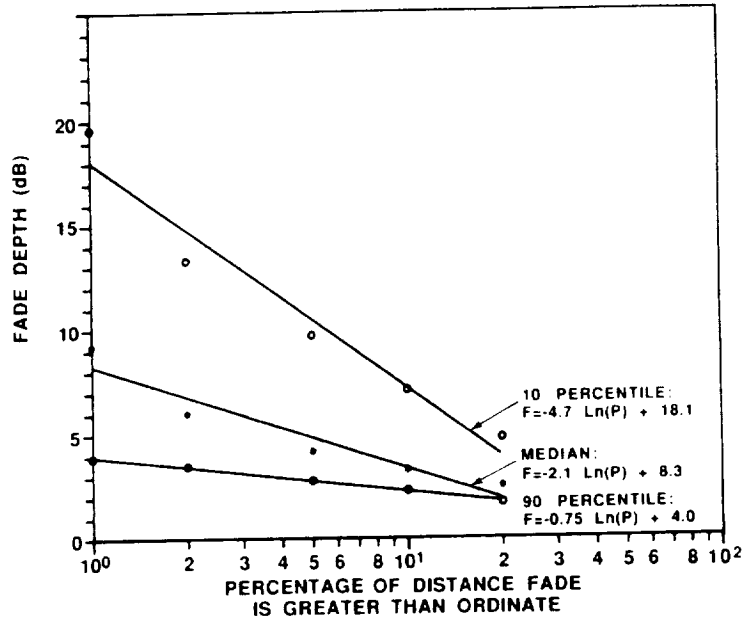


Figure 2c

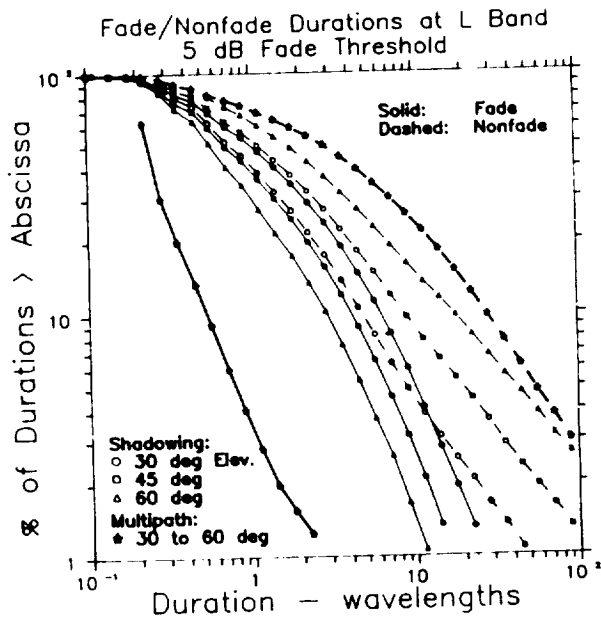


Figure 3

Table 1

Summary of Slant Path UHF/L-Band Land Mobile
Propagation Experiments

Entry No.	Investigators	Date	Freq		Comments
			Source	(MHz)	
1	Hess [1,2] (Motorola)	3/78	ATS-6	860 1550	Mostly cities: Chicago to San Francisco; whip antenna for receive; found shadowing more important than multipath
2	Anderson [3,4] (GE)	78	ATS-6	1550	Voice to trucks; CP; low elevation angles; concluded works well in non-urban areas but vegetation causes dropouts; multipath not a problem
3	Butterworth [5] (CRC)	4-11/81	Tower	840	Static tests
4	" [5]	82	Tethered Balloon	840	
5	" [5]	9/82	Helicopter	870	15o elevation
6	" [6]	6/83	Helicopter	870	5o,15o,20o elevation
7	" [7]	11/82	MARECS A	1542	19o elevation, no leaves
8	" [6]	6/83	MARECS A	1542	19o elevation, with leaves
9	Vogel [8] (Univ. Texas)	10/83 1/84	Balloon	869	Pooled; 10 to 35o elevation; also processed by elevation angle interval; frequent tree shadowing
10	Vogel [9]	11/84	Balloon	869 1501	
11	Bultitude [10] (CRC)	85	Tower	800 900	Spread spectrum measurements
12	Lutz, et al. [11] (DFVLR)	83-84	MARECS	1540	Germany measurements
13	Jongejans, et al. [25] (ESTEC)	1/84-7/84	MARECS	1540	Measurements made in Europe
14	Vogel/Goldhirsh [12]	6/85	RPV	869	Single trees; Wallops Island; van stationary
15	Goldhirsh/Vogel [13]	10/85 3/86	Helicopter	870	80% leaf shadowing No leaves
16	Vogel/Hong [14]	7/86	Balloon	870 1502	Open land; 20 to 59o el, 35o el typical; 2 to 8 o'clock azimuth; 9% level= 3 dB
17	Vogel/Goldhirsh [15]	8/86	Helicopter	870 1502	Canyons and mountains in CO; multipath
18	Pifex [16,17] (JPL)	3/87	Tower	870	No propagation data avail.
19	Goldhirsh/Vogel [18]	6/87	Helicopter	870 1502	Full leaf; 30o,45o,60o fixed elevation runs
20	Vogel/Goldhirsh [19]	12/87	MARECS A	1541	21o elevation angle

Table 2
Fit Coefficients for Equation (4)

nth Percentile	Elevation Angle (deg)					
	30		45		60	
	A(n)	B(n)	A(n)	B(n)	A(n)	B(n)
10	-4.9	24.9	-4.7	21.6	-4.7	18.1
50	-4.6	21.6	-3.8	14.6	-2.1	8.3
90	-4.0	14.2	-1.9	7.3	-.8	4.0

PROPAGATION HANDBOOK, FREQUENCIES
ABOVE 10 GHz

Louis J. Ippolito
Westinghouse Electric Corporation
Electronics Systems Center
Baltimore, Maryland 21203

Abstract-- The National Aeronautics and Space Administration (NASA) has been involved for nearly a decade in the development and updating of propagation handbooks to document the results of NASA Propagation Program efforts and other related measurements, studies and programs involving earth-space propagation. This paper describes the progress and accomplishments in the development of the Fourth Edition of the NASA Propagation Effects Handbook for Satellite Systems Design, for frequencies from 10 to 100 GHz, NASA Reference Publication 1082(04), dated May 1988, prepared by Westinghouse Electric Corporation for the Jet Propulsion Laboratory, JPL (Ippolito, 1988).

1. Introduction

The NASA Propagation Effects Handbook for Satellite Systems Design was first published in March 1980, and the document has been updated several times. The NASA handbook was conceived as an evolving document and has continually strived to provide relevant information for both the propagation specialist and the satellite systems designer/planner.

The first edition, published as a contractor report (ORI Inc., Technical Report 1905, March 1980), was updated the following year by ORI and published as NASA Reference Publication 1082 (Ippolito, Kaul, and Wallace, 1981). Two years later, the Third Edition was developed for NASA Headquarters by ORI and published as NASA Reference Publication 1082(03), (Ippolito, Kaul and Wallace, 1983). All of the above documents focused on propagation impairments on earth-space links operating in the 10 to 100 GHz frequency bands. A companion handbook, Propagation Effects on Satellite Systems at Frequencies Below 10 GHz (Flock, 1983) was also developed for the lower frequency bands. A Second Edition of that handbook has been published recently (Flock, 1987).

Several hundred copies of the Propagation Handbooks have been distributed by NASA Headquarters, and they have been referenced extensively in numerous government and civil projects. Comments back to the authors indicate that the earlier editions of the Handbook have served as a useful resource to the system designer and planner in the evaluation of propagation impairments on satellite links operating in the frequency bands above 10 GHz.

In the five years since the Third Edition was published, there have been many new developments in the analysis and evaluation of propagation effects on space communications, as well as continuing growth of developmental and operational systems in the K_u , K_a , and EHF frequency bands, for civil, government and international applications. The objective of the development of the Fourth Edition was to document these new developments and incorporate the new technology areas into the Handbook to keep the document up to date and relevant in the rapidly expanding area of communications above 10 GHz.

2. Development of the Fourth Edition

Updating of the Handbook was initiated in January 1988 by a compilation of new reference material and discussions with several of the major propagation experimenters and space communications organizations. Updated reference lists and descriptions of recent work were received from several organizations, including VPI & SU, the U. of Texas, and COMSAT. Their cooperation and help in the development of the Fourth Edition is greatly appreciated.

Since a camera ready copy or an electronic copy of the Third Edition was not available, the first step in the development of the new edition was accomplished by optically scanning clean copies of the earlier edition, utilizing a Kurzweil 4000 optical character reader. An electronic copy of the document was then generated using the Xerox Star 8010 System. This allowed for easier editing as the document revisions were developed.

Major revisions were generated in all seven chapters, with over one hundred and twenty pages of new text and figures produced, in addition to re-writes and text revisions.

The final draft copy of the Fourth Edition was

submitted to JPL on April 29, 1988. Completion of the camera ready copy, originally planned for June 1988, has been deferred pending completion of the draft review by JPL reviewers.

3. Major Revisions and Additions

The handbook is arranged in two parts to facilitate efficient reference and application of the information. Chapters II through V comprise the descriptive part, which describes the propagation effects, prediction models, and available experimental data bases. Chapters VI and VII make up the system design portion of the handbook. In Chapter VI design techniques and prediction methods available for evaluating propagation effects on Earth-space communications systems are presented. Chapter VII addresses the system design process and how the effects of propagation on system design and performance should be considered. Chapter VII also covers several mitigation techniques, such as site diversity and adaptive forward error correction (FEC), useful for overcoming adverse propagation impairments. Figure 1 presents a summary of the major contents of each chapter of the Fourth Edition of the handbook.

Major revisions and additions to Chapters I through VI of the Fourth Edition include:

- o updated versions of CCIR prediction models for gaseous attenuation, rain attenuation statistics, and depolarization (CCIR, 1986),
- o addition of a new fog attenuation prediction procedure (Altshuler, 1984),
- o replacement of the VPI&SU Piecewise Uniform Rain Rate Model with the Simple Attenuation Model (SAM), (Stutzman and Yon, 1986),
- o new information on fade duration statistics, low elevation angle effects, and ice depolarization,
- o new data measurements and propagation statistics for rain rate, rain attenuation, fade statistics, and rain/ice depolarization, and
- o updating of the reference lists through early 1988.

Chapter VII contains extensive new material on new applications, including SS/TDMA, on-board processing satellites, and VSAT systems. Descriptive material on several representative advance satellite systems have been added, including: ACTS, INTELSAT VI, FLTSATCOM, DSCS III, OLYMPUS, ITALSAT, and ATRSS. New information on rain fade mitigation techniques has been added, including orbit diversity, power control, and adaptive FEC.

Extensive sample calculations and examples are included throughout the handbook to highlight key analysis and prediction procedures. Table 1 summarizes the propagation calculation examples provided in Chapter VI, and Table 2 lists the example system analysis procedures provided in Chapter VII.

Figures 2 through 9 present examples of some of the new material included in the handbook.

4. Summary

The final draft of the Fourth Edition of NASA's Propagation Effects Handbook for Satellite Systems Design, 10 to 100 GHz, has been completed and is now under final review by JPL. This paper has reviewed the development process for the new edition and presented a summary of the major additions and revisions included in the handbook.

Copies of the Fourth Edition will be available through NASA Headquarters, Communications and Information Processing Division, Washington, D.C., at the completion of the review and reproduction process, currently anticipated for the fall of 1988.

References

- Altshuler, E.A. (1984), "A Simple Expression for Estimating Attenuation by Fog at Millimeter Wavelengths," IEEE Trans. Ant. & Prop., Vol. AP-32, No. 7, pp. 757-758.
- CCIR (1986), "Propagation Data and Prediction Methods Required for Earth-Space Telecommunications Systems, Report 564-3, in Volume V, Recommendations and Reports of the CCIR - 1986, International Telecommunications Union, Geneva.

- Flock, Warren L. (1987), "Propagation Effects on Satellite Systems at Frequencies Below 10 GHz, A Handbook for Satellite Systems Design," Second Edition, NASA Reference Publication 1108(02), NASA Headquarters, Washington, D.C., December 1987.
- Flock, Warren L. (1983), "Propagation Effects on Satellite Systems at Frequencies Below 10 GHz, A Handbook for Satellite Systems Design," NASA Reference Publication 1108, NASA Headquarters, Washington, D.C., December 1983.
- Ippolito, Louis J. (1988), "Propagation Effects Handbook for Satellite Systems Design, A summary of Propagation Impairments on 10 to 100 GHz Satellite Links with Techniques for System Design," Fourth Edition, NASA Reference Publication 1082(04), NASA Headquarters, Washington, D.C., draft, June 1988.
- Ippolito, Louis J., R.D. Kaul, and R.G. Wallace, (1983), "Propagation Effects Handbook for Satellite Systems Design, A summary of Propagation Impairments on 10 to 100 GHz Satellite Links with Techniques for System Design," Third Edition, NASA Reference Publication 1082(03), NASA Headquarters, Washington, D.C., December 1983.
- Ippolito, Louis J., R.D. Kaul, and R.G. Wallace, (1981), "Propagation Effects Handbook for Satellite Systems Design, A summary of Propagation Impairments on 10 to 100 GHz Satellite Links with Techniques for System Design," Third Edition, NASA Reference Publication 1082, NASA Headquarters, Washington, D.C., December 1981.
- Stutzman, W.L., and K.M. Yon, (1986), "A Simple Rain Attenuation Model for Earth-space Radio Links Operating at 10-35 GHz," Radio Science, Vol. 21, No. 1, pp. 65-72.

CONTENTS OF FOURTH EDITION



- CHAPTER I INTRODUCTION**
 - Overview of Propagation Effects

- CHAPTER II CHARACTERISTICS OF RAIN ATTENUATION**
 - Types and Spatial Distributions of Rain
 - Specific Rain Attenuation
 - Rainfall Data

- CHAPTER III RAIN AND RAIN ATTENUATION MODELS**
 - Rice-Holmberg Model
 - Dutton-Dougherty Model
 - Global Model
 - Two-Component Model
 - CCIR Model
 - Ln Model
 - Simple Attenuation Model (SAM)

- Chapter IV DEPOLARIZATION ON EARTH-SPACE PATHS**
 - Classical Formulation
 - Rain Induced Depolarization
 - Ice Polarization

- CHAPTER V PROPAGATION DATA BASES**
 - Cumulative Attenuation Statistics
 - Temporal Distribution of Fades
 - Fade Duration
 - Depolarization Statistics
 - Phase and Amplitude Dispersion

- CHAPTER VI PREDICTION TECHNIQUES**
 - Gaseous Attenuation
 - Cumulative Rain Attenuation Statistics
 - Cloud, Fog, Sand and Dust Attenuation
 - Signal Fluctuations and Low-Angle Fading
 - Rain and Ice Depolarization
 - Bandwidth Coherence
 - Sky Noise

- CHAPTER VII APPLICATION OF PROPAGATION PREDICTIONS TO EARTH-SPACE TELECOMMUNICATIONS SYSTEMS DESIGN**
 - System Performance Criteria
 - Recent Satellite Technology
 - Representative Systems
 - Design Procedures
 - Rain Fade Mitigation Techniques

Figure 1 Contents of the Fourth Edition

Paragraph Number	Description	Page Number
6.2.4	Relative humidity to water vapor density conversion	6-15
6.2.5	Gaseous attenuation calculation	6-15
6.3.2.2	Analytic estimate of cumulative rain attenuation distribution (Global Model)	6-28
6.3.2.4	Analytic estimate of cumulative rain attenuation distribution (CCIR Model)	6-34
6.3.3.2	Estimate of cumulative rain attenuation distribution by distribution extension	6-40
6.3.5.1	Estimates of duration and return periods of fades and intense rain events	6-49
6.4.3.3	Estimation of fog attenuation	6-71
6.5.6.1	Estimate of variance of signal amplitude fluctuation due to tropospheric turbulence	6-99
6.5.6.2	Estimates of variance of phase and angle-of-arrival fluctuations due to tropospheric turbulence	6-101
6.5.6.3	Estimate of average received signal gain reduction due to tropospheric turbulence	6-101
6.7.2.1.1	Calculation of theoretical frequency dependence of rain attenuation	6-123
6.7.3.2	Calculation of theoretical frequency dependence of ionospheric phase delay	6-127

Table 1 Guide to Propagation Examples in Chapter VI

Paragraph Number	Description	Page Number
7.3.4	Performance specification of digital and analog systems	7-39
7.3.5	Analog and digital system synthesis and tradeoffs	7-42
7.3.6	Analog and digital system propagation analysis and link budgets	7-51
7.3.7	Calculation of composite margin	7-66
7.4.2.1.3	Estimates of parameters required for empirical diversity model	7-89
7.4.2.1.4	Analytic estimate of site diversity gain	7-98

Table 2 Guide to Systems Analysis Procedures in Chapter VII

ORIGINAL PAGE IS
OF POOR QUALITY

Model	Inputs	Outputs	Comments
Rice-Homberg	Climate or Site-Specific Mean Annual Rainfall plus Ratio of Thunderstorm-to-Total Rain.	Cumulative Time Distribution of Rainfall.	Two Rain Modes Considered: Thunderstorm & Uniform Rains. Probability of Rain Rate Exceedance for Either or Both Modes is Available.
Dutton-Dougherty	Same as Rice-Homberg and Link Parameters (e.g., Frequency, Elevation Angle)	Rain or Gaseous Attenuation Associated with a Given Exceedance Time Percentage.	Utilizes Modified Rice-Holmberg Rain Model. Provides Confidence Limits, Given Two Additional Rain Rate Distributions.
Global	Location and Link Parameters.	Rain Attenuation Associated with a Given Exceedance Time Percentage.	All Rain Attenuation Parameter Values are Self-contained. Globally Applicable.
Two-Component	Same as Global.	Exceedance Time Percentage Associated with a Given Rain Attenuation.	Same Rain Model (& Comments) as for Global Model. Two Rain Modes Considered: Convective Cell and Debris Rains.
CCIR	Same as Global.	Rain Attenuation Associated with a Given Exceedance Time Percentage.	All Rain Attenuation Parameter Values are Self-contained. Globally Applicable.
Lin	Five Minute Rain Rate and Link Parameters.	Attenuation Associated with a Given Rain Rate.	Simple Extension of Terrestrial Path Rain Attenuation Model.
Simple Attenuation (SAM)	Rain Statistics and Link Parameters.	Attenuation Associated with a Given Rain Rate.	Assumes Exponential Shaped Rain Profile.

Figure 2 Summary of Rain and Rain Attenuation Prediction Models described in Chapter III

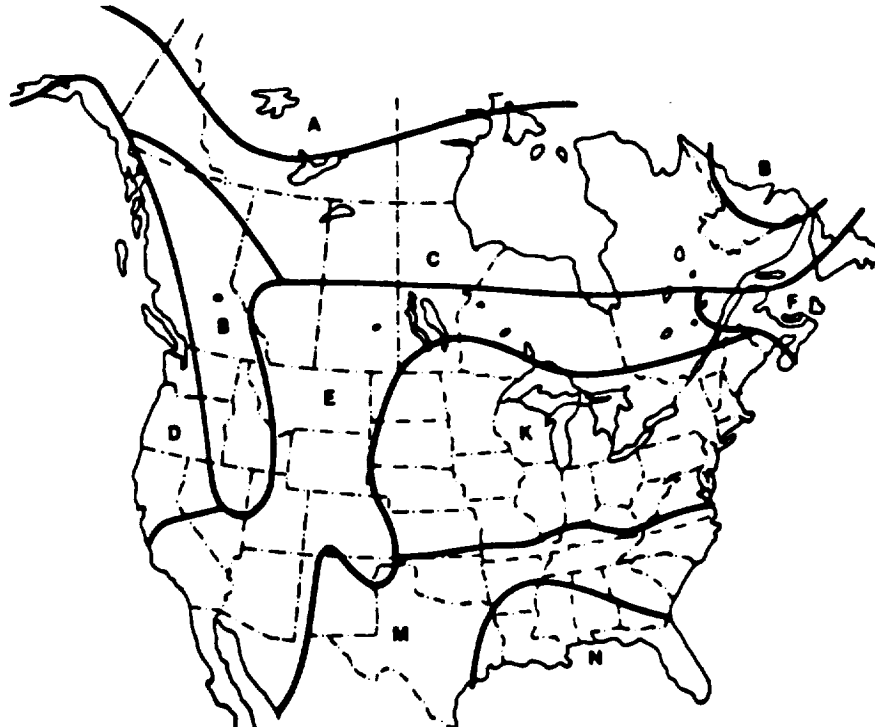


Figure 3 Expanded CCIR Rain Zone Map (Sec. 3.6)

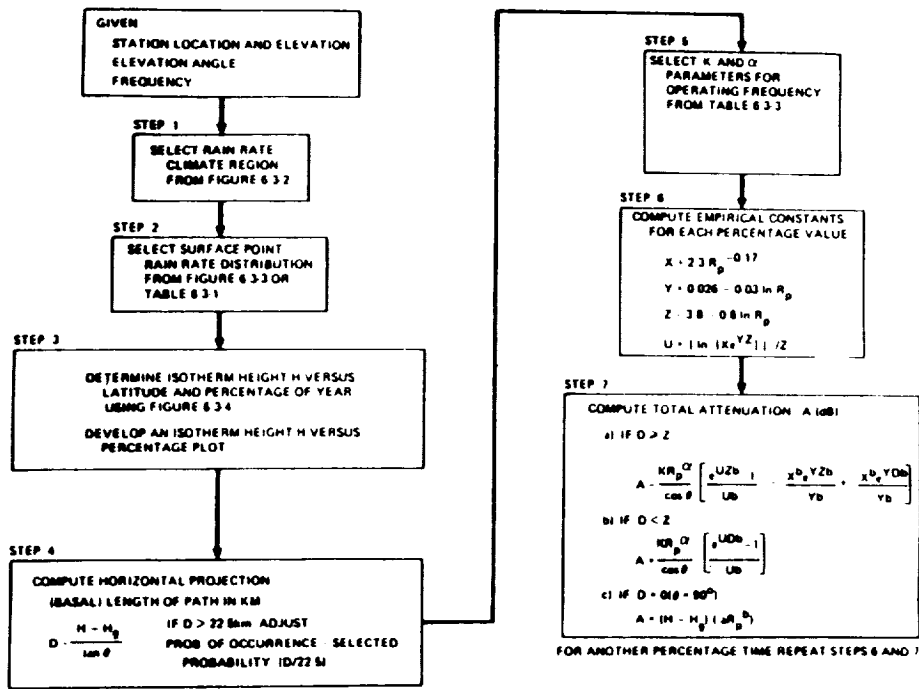


Figure 4 Estimation Procedure Flow Chart for Global Model (Sec. 6.3)

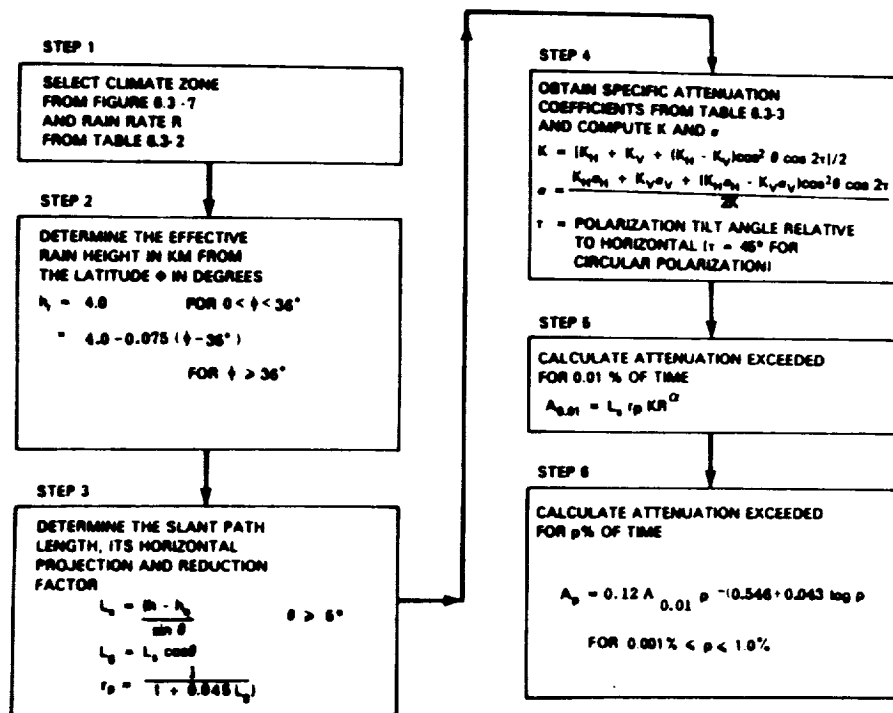


Figure 5 Estimation Procedure Flow Chart for the CCIR Model for Rain Attenuation Statistics (Sec. 6.3)

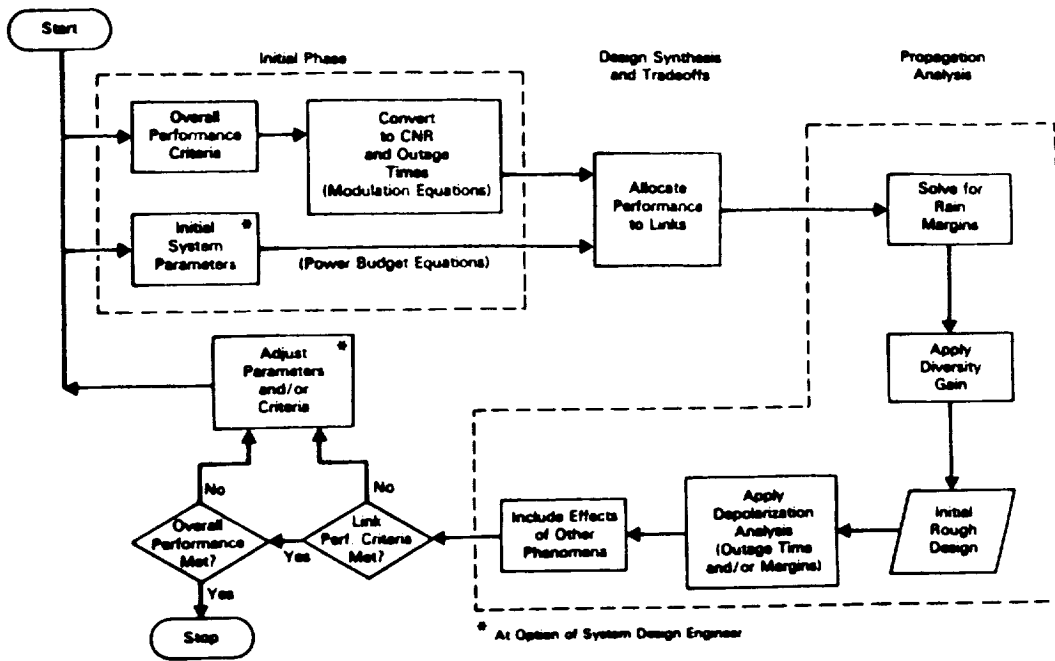


Figure 6 System Design Process described in Chapter VII

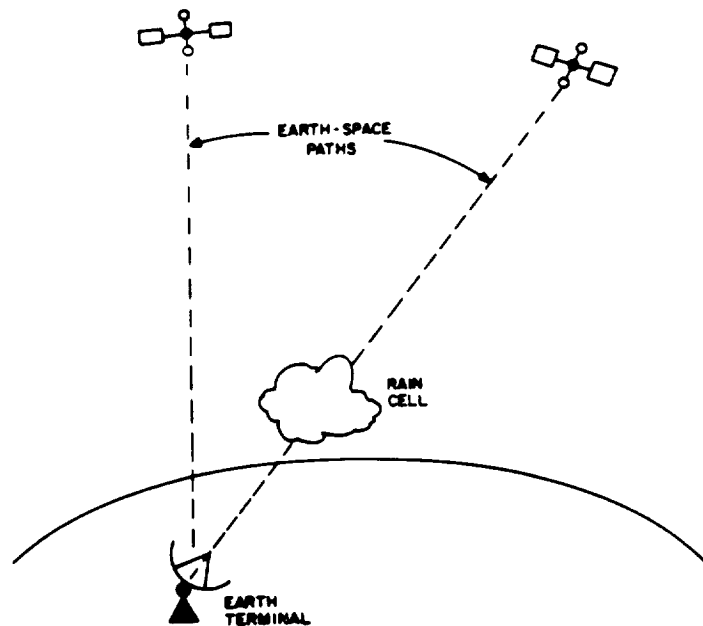


Figure 7 Orbital Diversity Configuration described in Chapter VII

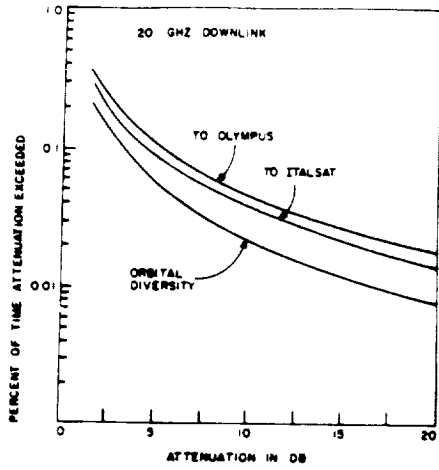


Figure 7.4-13.

Predicted Orbit Diversity Performance at Spino d'Adda, Italy

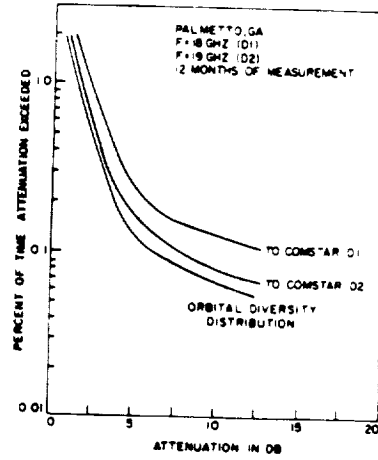


Figure 7.4-14.

Orbital diversity measurements at Palmetto, GA

Figure 8 Orbital Diversity Measurements presented in Chapter VII

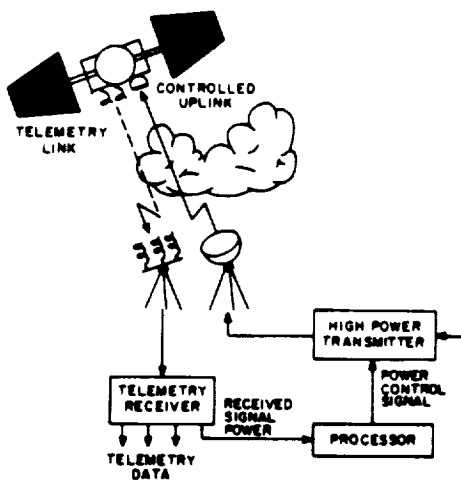


Figure 7.4-15. Closed loop uplink power control

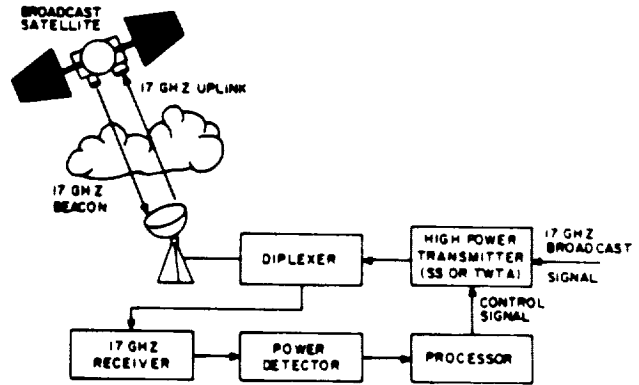


Figure 7.4-16. Open loop uplink power control

Figure 9 Power Control Techniques described in Chapter VII

c-2

RESULTS OF APL RAIN GAUGE NETWORK MEASUREMENTS IN MID-ATLANTIC
COAST REGION AND COMPARISONS OF DISTRIBUTIONS WITH CCIR MODELS

Julius Goldhirsh, Norman Gebo, and John Rowland

Applied Physics Laboratory, The Johns Hopkins University
Laurel, Maryland, 20707-6099

Abstract

In this effort are described cumulative rain rate distributions for a network of nine tipping bucket rain gauge systems located in the mid-Atlantic coast region in the vicinity of the NASA Wallops Flight Facility, Wallops Island, Virginia. The rain gauges are situated within a gridded region of dimensions 47 km east-west by 70 km north-south. Distributions are presented for the individual site measurements and the network average for the year period June 1, 1986 through May 31, 1987. A previous six year average distribution derived from measurements at one of the site locations is also presented. Comparisons are given of the network average, the CCIR climatic zone, and the CCIR functional model distributions, the latter of which approximates a log normal at the lower rain rate and a gamma function at the higher rates.

1.0 Introduction

Earth-satellite telecommunications may be seriously degraded by rain attenuation at frequencies above 10 GHz. In order to account for realistic fade margins, design engineers require information as to the expected number of hours per year given fade levels are exceeded. This information can be derived employing direct attenuation measurements, or it may be inferred from rain attenuation models using rain rate statistics of the type described in this effort [CCIR, 1986].

We address here the following specific questions for the mid-Atlantic Coast region: (1) What are the variabilities in rain rate statistics due to microclimate effects? (2) How do short term spatially averaged rain distributions compare with longer term temporally averaged statistics? (3) What are appropriate functional forms for describing rain rate distributions? (4) How does the network rain rate distribution compare with the CCIR model distributions? A comprehensive description of this effort is described by Goldhirsh et al [1988].

2.0 Experimental Aspects

The gauges employed are of the tipping bucket type and are calibrated such that with each 0.25 mm of rainfall, a bucket tip occurs resulting in a 100 millisecond switch closure interval. Each rain gauge is connected to a Commodore 64 computer. The time of each bucket tip is stored within the computer to a 1 millisecond resolution. The individual tipping times are transferred from computer memory and recorded on a 5-1/4 inch floppy disk at two hour intervals. Also recorded are such items as file number, Julian Day, time the file written to disk, and total rainfall in mm.

Ten rain gauges of the type described above were located within a radial range of 60 km from the SPANDAR facility. The site locations (labeled #1 - #10) are depicted in the map of Figure 1. Only the results of nine gauges are reported here because of the close proximity of two of them (Sites #4 and #5). The individual rain gauge systems are located at the home grounds of staff working at the NASA Wallops Flight Facility. The staff calibrates and maintains these systems on a continual basis. Calibrations are performed at least several times per week. The floppy disks are removed on a weekly basis for subsequent reduction and analysis.

3.0 Cumulative Distributions of Rain Rate

3.1 Spatial Variability of Rain Rate Distributions

In Figure 2 is shown a composite of individual rain rate distributions for each of nine sites. The vertical scale represents the percentage of the year the abscissa value of the rain rate is exceeded. Each curve is labeled with the corresponding site number both at the higher and lower percentage values. Since the rain rate statistics below .001% of the year (5.25 minutes) are noted to be noisy, we characterize the results only down to this percentage level. We observe that at the .001% level the rain rates vary between 85 mm/hr (Site #6) and 125 mm/hr (Site #10). The distance between these sites is only 15 km. This relatively large variation (47% change relative to the smaller value) in the statistics for such a short separation is attributed to the micro-climate effects caused by Site #6 being located closer to the ocean (on Chincoteague Island). The ocean has a tendency to dampen the more intense convective rain rates which originate over land and are sustained by ground heating, as for example, air mass type showers. At the 0.1% level (8.8 hours), the rain rates vary between 15 mm/hr (Site #9) and 25 mm/hr (Site #2), a 67% increase relative to the smaller value. The distance between these sites are noted to be approximately 57 km.

3.2 Network Average Cumulative Rain Rate Distribution

In Figure 3 is presented the combined average network rain rate distribution (circled data points). These were obtained by averaging the percentages at each rain rate level. We note the statistical noise in the vicinity of the .001% range is mitigated significantly as compared to the distributions for individual sites. This is attributed to the statistical smoothing in the averaging process. Also plotted is the 6 year average cumulative rain rate distribution measured at the SPANDAR location (Site #10) during the period 1977-1983 [Goldhirsh, 1983a; 1983b]. This distribution was taken only up to 100 mm/hr since the smallest clock time resolution for these previous measurements was one second resulting in discernible quantization uncertainties at the higher rain rates. It is interesting to note that the network average and the time average distributions practically overlap. It has yet to be established whether it is fortuitous that the spatial average of distributions is equivalent to the long term temporal average for the region under investigation as suggested by the results.

3.3 Best Fit Rain Rate Distributions

It has been suggested that the rain rate distribution can be represented by a log normal functional form in the approximate interval 2 - 50 mm/hr although the rain rate interval of validity is dependent on the climatic region [CCIR, 1986]. Segal [1980], employing measurements made in Canada, demonstrated that a power law relationship satisfactorily approximates the entire cumulative rain rate distribution for rain rates exceeding 5 mm/hr. More recent analysis suggests that rain rate distribution may be also approximated by the log-normal distribution for the lower rain rates and a gamma distribution at the higher rates [Moupfouma, 1985].

3.3.1 Log Normal Distribution

In Figure 4 is shown the average rain rate distribution for the rain gauge network (circled points) plotted vis a vis a Gaussian ordinate (percentage) and a logarithmic abscissa (rain rate). A log normal distribution for this representation is indicated by points which lie along a straight line. We note that the data points (circled points) practically overlap with the fitted log normal distribution (straight solid line) in the rain rate interval 3 to 40 mm/hr. Thereafter, the data points deviate considerably from the log normal. This deviation is considered real as it is consistent with previous multi-year rain gauge measurements made at Wallops Island, Virginia (Figure 3) [Goldhirsh, 1983]. The distribution is consistent with

$$M = \langle \text{Log}_{10} R \rangle = -1.725 \quad (1)$$

$$\sigma^2 = \langle (\log_{10} R - M)^2 \rangle = 0.912 \quad (2)$$

where M and σ are the mean and standard deviation of $\text{Log}_{10} R$, respectively, associated with the log normal.

3.3.2 Power Distribution

Although the log normal distribution has physical ramifications as pointed out by Lin [1975], it represents an awkward functional form for computational purposes. For this reason, we examine here other more convenient functional representations. In Figure 5 is plotted the network rain rate distribution in the 3 to 30 mm/hr interval and the associated least squares power fit. This is given by

$$P(r > R) = A R^{-B} \quad (3)$$

where

$$A = 6.132 \quad (4)$$

$$B = -1.469 \quad (5)$$

and where (3) is directly given in terms of percentage. We note that the power curve fit in Figure 5 agrees with the rain rate values to within a small fraction of 1 mm/hr for any given percentage within the interval 3 to 30 mm/hr. It has a functional form which is significantly easier to handle computationally than the log normal.

3.3.3 Exponential Fit

In Figure 6 is plotted the network distribution in the rain rate interval 30 to 140 mm/hr. Also plotted is the least square exponential (solid line) given by the form

$$P(r > R) = \alpha \exp[- \beta R] \quad (6)$$

where

$$\alpha = 0.1488 \quad (7)$$

$$\beta = 0.04615 \quad (8)$$

and where (6) is also expressed in terms of percentage. The exponential fit describes the rain rate distribution over the higher rain rate interval (30 - 140 mm/hr) with excellent accuracy. At 140 mm/hr we observe only a maximum error of less than 3% in rain rate.

4.0 Comparison with CCIR Model Distributions

We examine here two rain rate distribution models which have been suggested by the CCIR (1986) for use with earth-satellite and terrestrial rain attenuation predictions.

4.1 Climatic Zone Distributions

The climatic zone model divides the world into 14 climatic regions notated A through P (Figure 7). Each zone has associated with it a unique rain rate distribution based on averages of measured distributions. The general location of the rain gauge network (circled area) is in climatic zone K along the mid-Atlantic coast in proximity to region M. The rain rate distributions for the rain gauge network and for regions E, F, K, and M are given in Figure 8. We note that the mid-Atlantic coast network distribution lies between those for regions M and K. This is consistent with the fact the network lies in region K but close to M. Since an abrupt change in the rain rate distribution is obviously non-physical at the region borders, one should expect the network distribution to lie between the distributions for the two climatic zones as indicated.

4.2 Distribution Based On .01% Rain Rate

A model distribution has been proposed by Moupfouma [1985] which approximates a log-normal function at the lower rain rates and a gamma function at the higher rain rates [CCIR, 1986]. This model function is given by

$$P(r > R) = \frac{a \exp (- u R)}{R^b} \quad (9)$$

where

$$a = 10^{-4} (R_{.01})^b \exp (u R_{.01}) \quad (10)$$

$$b = 8.22 (R_{.01})^{-.584} \quad (11)$$

The probability (9) should be multiplied by 100 for conversion to percentage, and $R_{.01}$ represents the measured rain rate at the .01 percent probability. Equating $R_{.01} = 58$ mm/hr (the rain gauge network rain rate at the .01% level), the corresponding rain rate distribution was calculated and plotted in Figure 9. Also shown plotted is the measured rain gauge network distribution. The model rain rate distribution is noted to overestimate the rain rate by approximately 18% at the .001% probability (107 versus 126 mm/hr), and underestimate the rain rate by 21% at the .1% probability (16.5 versus 13.1 mm/hr).

5.0 Conclusions

The results of the network measurements demonstrate that an extreme range of rain rate statistics may exist over short distance intervals; especially near coastal areas. One means in which to smooth out these statistics is to average the distributions for a network of such measurements. Previous multi-year averaging of individual rain rate statistics has been found to have similar smoothing effects and result in a distribution which agreed closely with the short term network average.

In characterizing rain rate statistics in the above described mid-Atlantic coast region, it is suggested that the cumulative distributions be described with a power curve fit at the smaller rain rate interval (3 - 30 mm/hr) and with an exponential fit at the larger rain rates (30 - 140 mm/hr). The log normal distribution provides a good fit over the smaller interval, but is difficult to use computationally. The CCIR model distribution of Moupfouma [1985] is adequate if a 20% rain rate error is acceptable.

6.0 Acknowledgements

The authors are grateful to those individuals in whose homes the rain gauges were located and cared for. In alphabetical order the names are as follows: Lester Atkinson, Albert Barnes, Norris Beasley, Martin Eby, Charles Ethridge, Norman Gebo, Steve Jones, Eugene Ward, and Sam West. The authors are also grateful to Karen Melvin for typing this manuscript. This work was supported jointly by NASA Headquarters, Communications Division, and NASA Goddard Space Flight Center under Contract N00039-87-C-5301.

7.0 References

CCIR (International Radio Consultative Committee), "Recommendations and Reports of the CCIR, 1986", XVith Plenary Assembly, 5, Dubrovnik (Propagation in Non-Ionized Media), 1986.

Goldhirsh, J., N. E. Gebo, and J. R. Rowland, "Rain Rate Statistics From A Rain Gauge Network in a Mid-Atlantic Coast Region", JHU/APL Technical Report, S1R88U--014, April 1988.

Goldhirsh, J., "Yearly Variations of Rain-Rate Statistics at Wallops Island and Their Impact on Modeled Slant Path Attenuation Distributions", IEEE Trans. on Antennas & Propagation, AP-32, No. 6, pp. 918-921, November, 1983.

Goldhirsh, J., "Yearly and Monthly Rain Rate Statistics at Wallops Island, Virginia Over a Six Year Period", JHU/APL Technical Report S1R83U-039, December, 1983 (Johns Hopkins University/Applied Physics Laboratory, Johns Hopkins Road, Laurel, Maryland 20707).

Lin, S.H., "A Method for Calculating Rain Attenuation Distribution on Microwave Paths", Bell System Technical Journal, 54, July-August, 1975.

Moupfouma, F, "Model of Rainfall Rate Distribution for Radio System Design," IEE Proc., Vol 132, Pt H, 1, pp. 39-43, Feb. 1985.

Segal, B., "An Analytical Examination of Mathematic Models for the Rainfall Rate Distribution Function," Ann. des. Telecomm., Vol 35, pp. 434-438, 1980.

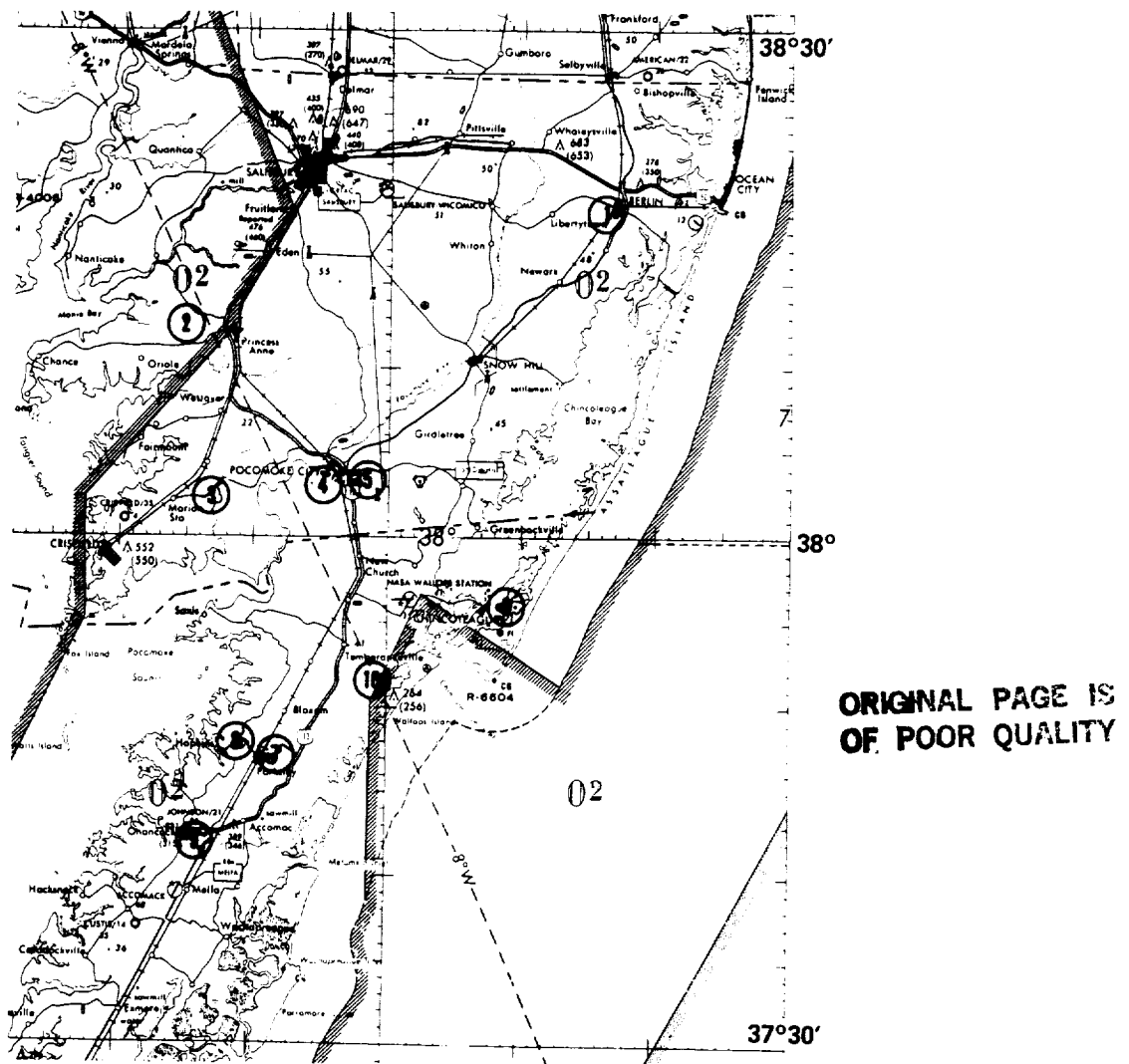


Figure 1 Map showing rain gauge site locations in vicinity of Wallops Island, Virginia

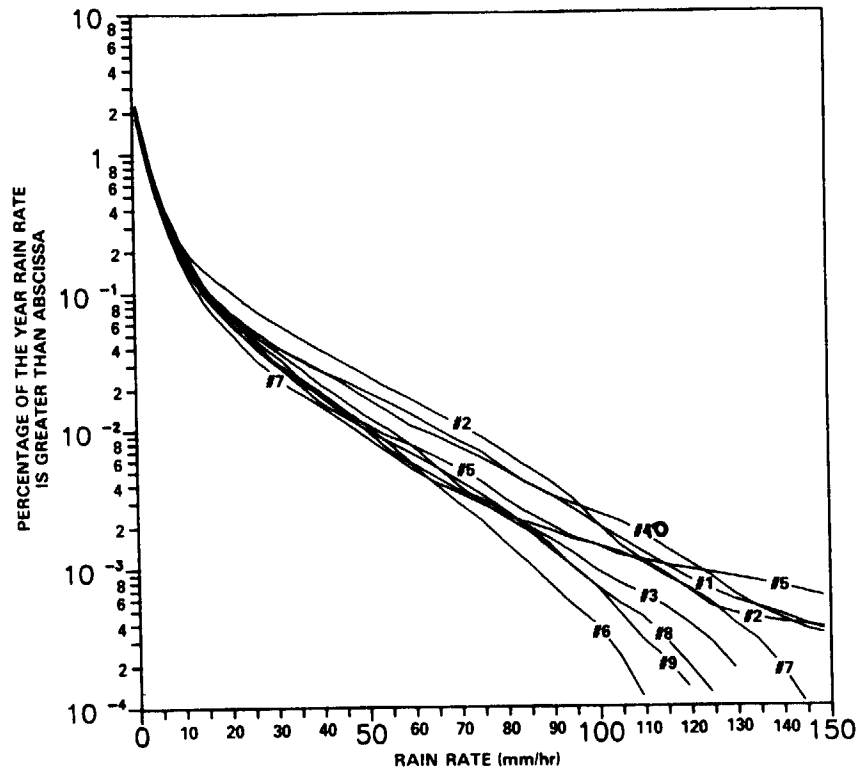


Figure 2 Composite of yearly cumulative rain rate distributions for each of nine site locations in vicinity of Wallops Island, Virginia (June 1986 - May 1987)

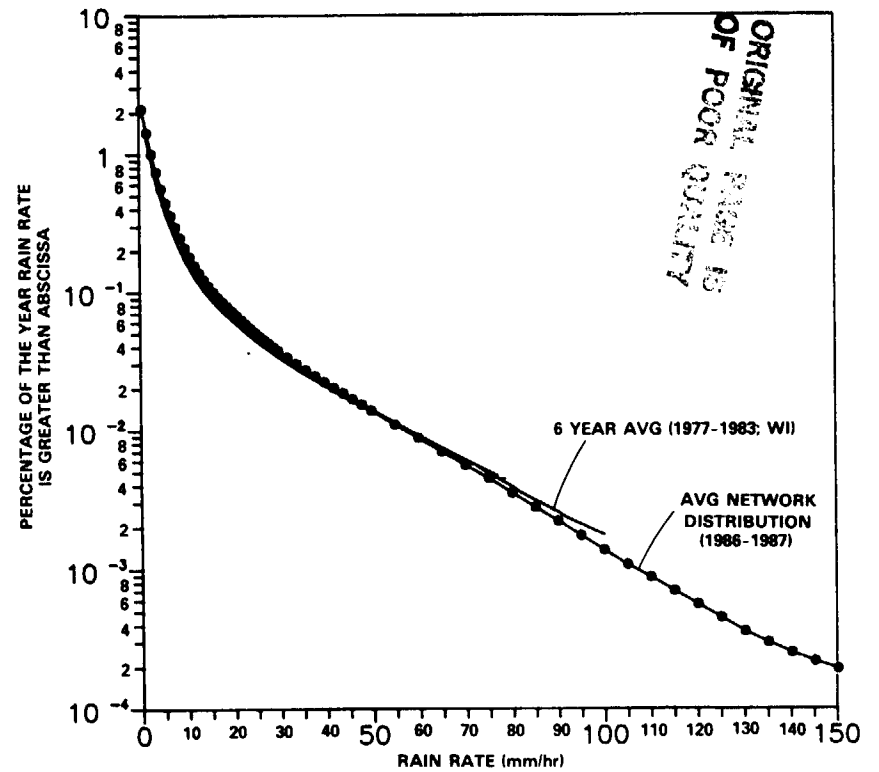


Figure 3 Combined average network yearly cumulative rain rate distribution (June 1986 - May 1987) and comparison with previous 6 year average rain rate distribution at Wallops Island, Virginia

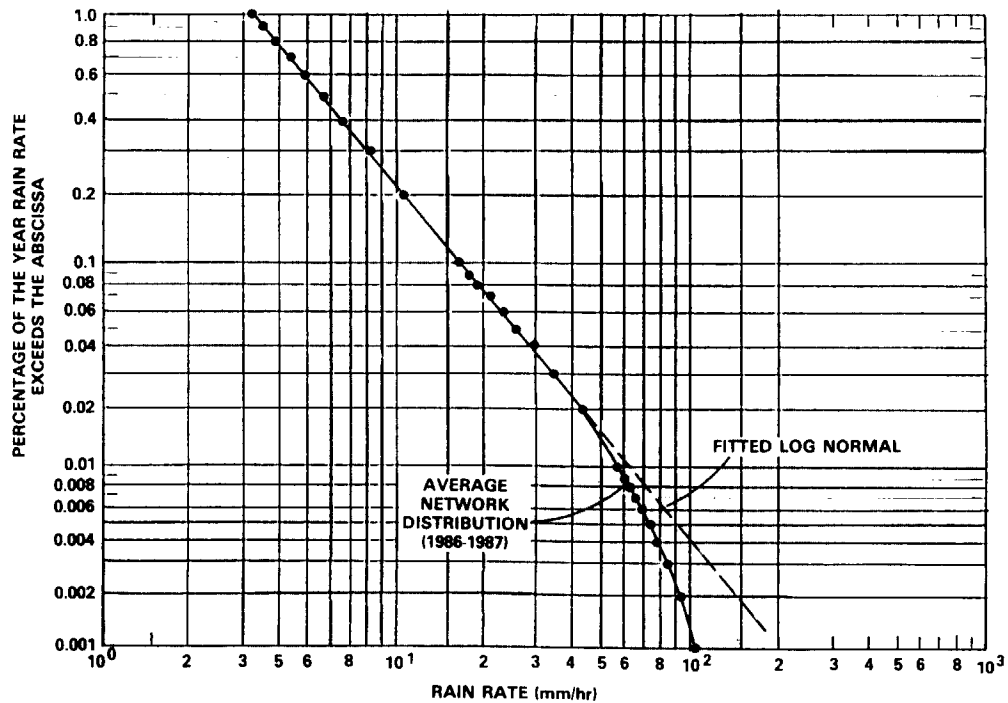


Figure 4 Combined average cumulative rain rate distribution for 12 month period and corresponding log normal fit (solid line).

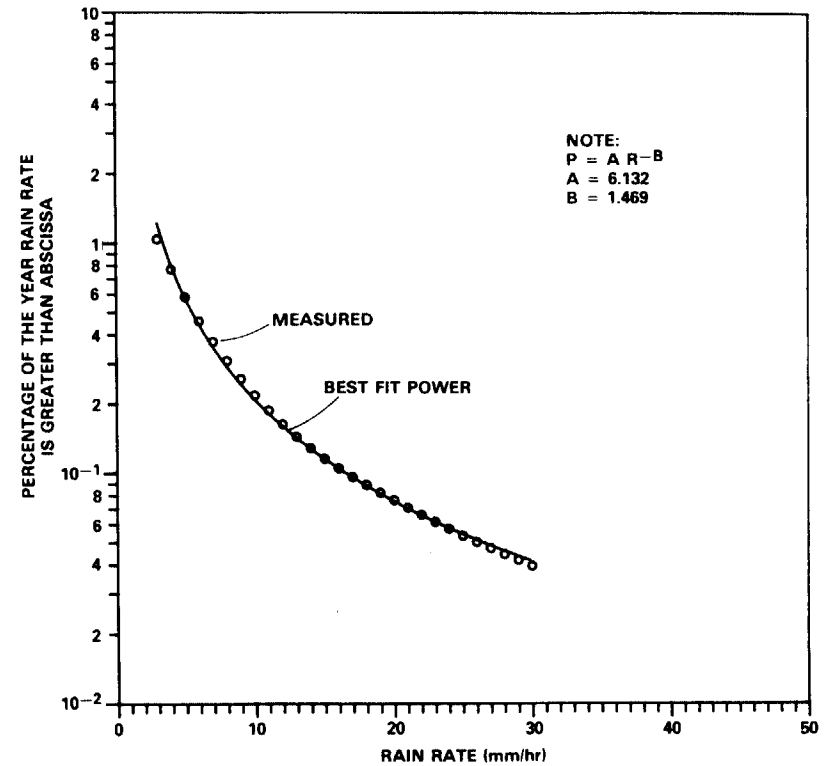


Figure 5 Average network yearly cumulative rain rate distribution and best fit power distribution (3-30 mm/hr).

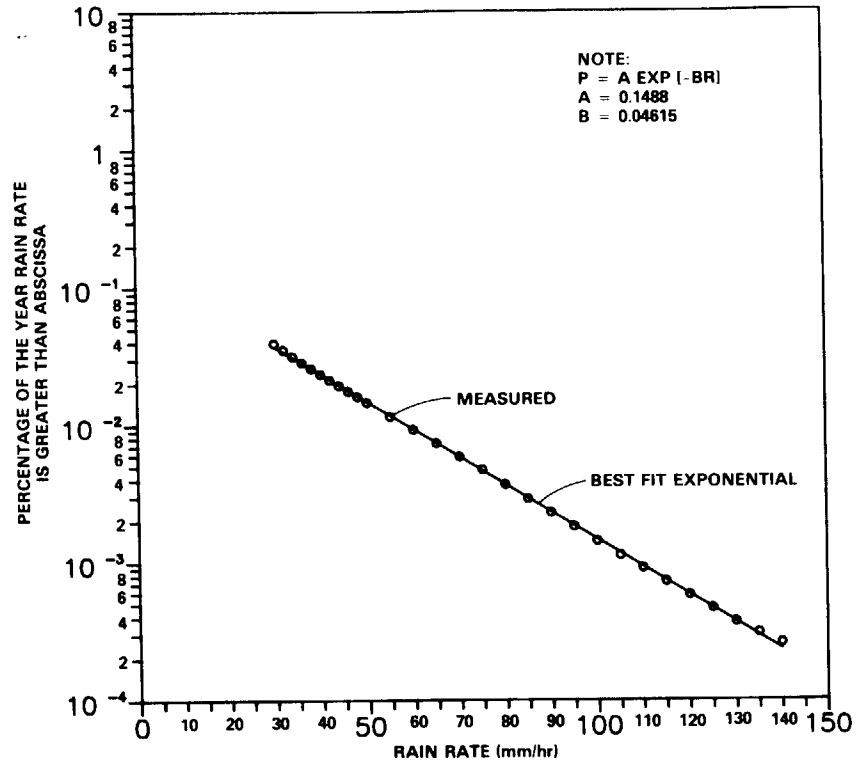


Figure 6 Average network yearly cumulative rain rate distribution and best fit exponential (30-140 mm/hr)

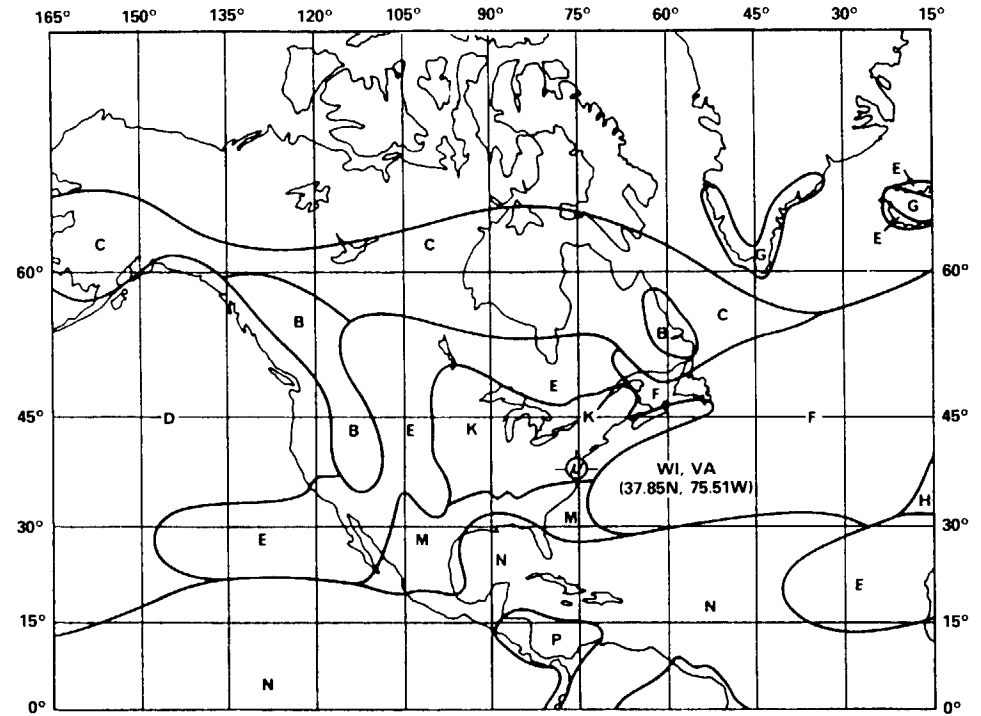


Figure 7 Map showing CCIR climatic zones with designated rain rate distributions (CCIR Report 563-3).

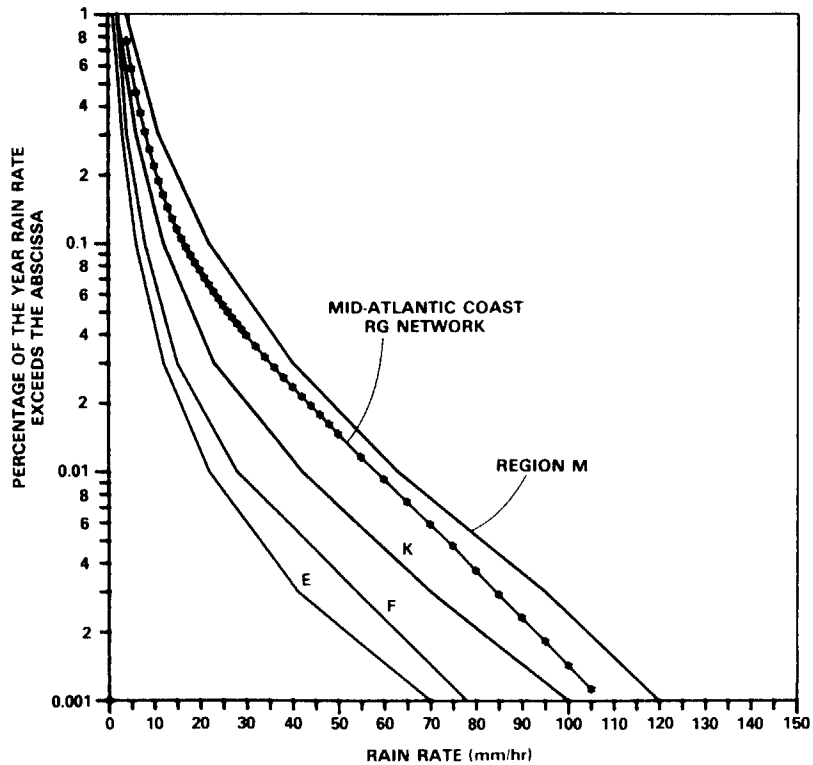


Figure 8 Comparison of rain gauge network rain rate distribution for mid-Atlantic coast and CCIR climatic zone rain rate distributions (CCIR Report 563-3).

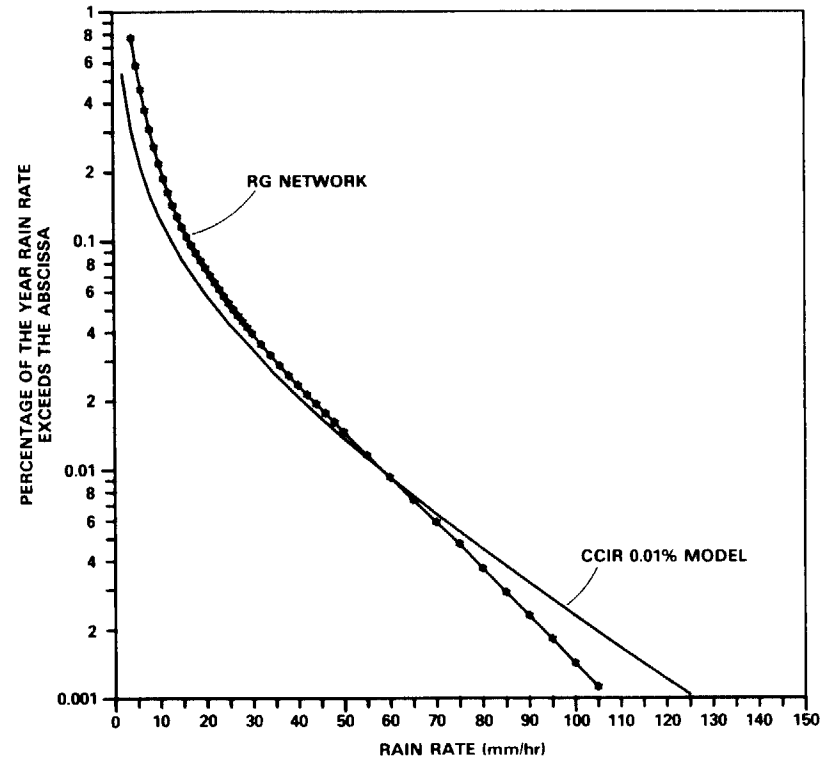


Figure 9 Comparison of rain rate distribution for mid-Atlantic coast rain gauge network and CCIR model distribution based on .01% rain rate (CCIR Report 563-3).

Interference by Rain Scatter

Robert K. Crane
Thayer School of Engineering
Dartmouth College

Introduction.

Rain scatter has long been recognized as a mechanism for the generation of co-channel interference between microwave systems operating at the same frequency. Based on the results of the NASA Virginia Precipitation Scatter Experiment [Crane, 1973], the international radio regulations were modified in the early 70's to force a consideration of the potential for interference by rain scatter as a part of the frequency assignment process (coordination). At the time the rain coordination procedure was introduced, the inadequacy of our knowledge of the statistics of the spatial structure of precipitation was recognized and only a preliminary, ad hoc model for the extension of the coordination procedures to attenuating frequencies could be included to complete the model for the radio regulations [Crane, 1974]. Since that time, a number of equally poor model modifications have been introduced by the International Radio Consultative Committee (CCIR) to cover the acknowledged problem of extension to higher frequencies. In this study for the NASA Propagation Program, we are employing data from a measurement program by the Thayer School of Engineering, Dartmouth College and the U. S. Air Force, Rome Air Development Center (RADC) to supplement a simulation study for the development of an improved model for the prediction of interference level fields at attenuating frequencies.

Frequency allocations personnel in European countries have complained about the rain coordination procedure ever since it was incorporated into the radio regulations. The often heard complaint is that rain scatter does not exist. No occurrences of interference by rain scatter have ever been documented. The problem, however, is not the existence of rain scatter but the recognition of an occurrence of interference by rain scatter at the fraction of a year for which such interference is allowed. As shown in Figure 1, scattering by rain exists and the observations are in close agreement with model predictions at non-attenuating frequencies. The measured reflectivities at a 3 km height (10K-Eastville and 10K-Ft. Lee) are within one dB (the measurement system uncertainty) of the values predicted on the basis of rain rate measurements made at the surface under the scattering volume (Rain Gauge). The bistatic reflectivity factor observations were 3 dB below the values predicted for the Virginia rain climate (Global climate D2 [Crane, 1985a]). In this case, the discrepancy is due to a difference between the observed and predicted surface rain rates but not to the prediction model when surface rain rate measurements are used. Sakagami [1980] made observations of rain scatter over a two year period at a frequency of 6.72 GHz on a 55.2 km forward scatter path near Tokyo and reported good agreement between the observed reflectivities at a height of 2.3 km and equiprobable reflectivity values estimated from surface rain rate measurements. In this experiment adjustments were made for attenuation by rain on the forward scatter path from line-of-sight attenuation measurements to an elevated antenna.

The Virginia Precipitation Scatter Experiment (Figure 1) employed simulated terrestrial and earth-space communications paths. The common volumes for rain scatter coupling between the simulated communications links were located at heights of 10K feet (3 km) and 20K feet (6 km). Terrestrial paths from two separated transmitter locations, Eastville and Ft. Lee, VA, were used to illuminate the scattering volumes along the slant path to the receiver site at the NASA Langley Research Center. Distances from the antennas to the common volume ranged from 13 to 78 km. For the simulated communications links, a transmission loss in

excess of 162 dB would have been required to prevent interference. This transmission loss corresponds approximately to an equivalent reflectivity factor of 22 dBZ_e. For the data displayed in the figure and the communication link parameters assumed for the simulation, interference would have been recorded each time rain with an equivalent rate in excess of 0.5 mm/h occurred within the common volume. From these data it is evident that rain scatter does occur and has the potential for causing interference.

The intervals with interference caused by rain would be brief, corresponding to the occurrences of hydrometeors within the scattering volume at the fractions of a year indicated in Figure 1. Because the procedures in the radio regulations now guard against interference at the percentages of the year corresponding to most of the data in the figure (the assumptions used for the interference simulation were not valid after the 1971 World Administrative Radio Conference which adopted the coordination procedures for rain), the only time a report of excessive interference might be brought to the attention of the frequency allocations community is for rain events with rates significantly in excess of the values corresponding to annual percentages ranging from 0.05 to 0.001 %. Such rains occur with very brief durations and probably would go unnoticed in comparison with the much longer duration interference events that occur due to failures in the CCIR duct propagation prediction model. The interference events, although unnoticed from a practical point of view, still produce a sufficient disruption in service to affect link reliability.

Extension to Higher Frequencies.

The CCIR models for the extension of interference prediction and rain coordination procedures to higher frequencies have varied with time. In the early 70's, a conservative model (favoring the current assignees) was recommended. It considered only attenuation by rain within the scattering volume common to the intersecting antenna beams (the common volume) and ignored any attenuating hydrometeors outside the scattering volume [Crane, 1974]. More recently a series of models have been recommended by the CCIR that try to include statistically the simultaneous occurrences of rain inside the common volume and along the paths from the common volume to the transmitters and receivers. These procedures have tended to be less conservative. Unfortunately, little experimental work on rain scatter interference at the higher frequencies has been reported since the Virginia Precipitation Scatter Experiment. One set of long term observations is now available from Japan at 14 GHz [Awaka et al., 1984].

When it was realized that the original interference estimation bound was too conservative, CCIR Study Group 5's were revised to model the inclusion of an attenuation estimate. The model now predicts too high a transmission loss; the model is now not conservative enough. Awaka [1984] correctly placed the cause for the failure of the model on an inadequate treatment of the statistical relationship between the scattering process in the common volume of the antenna patterns of the potentially interfering systems and the attenuation along the paths between the common volume and the antennas. He suggested the use of a joint log-normal statistical model for predicting the transmission loss when both the scattering and attenuation processes were important.

The problem arises from the competing effects of scattering and attenuation. Figure 2 displays the predictions of the two-component rain model [Crane, 1982] after modification to estimate the expected received power when rain is present in the common volume and attenuation is present along the paths from the antennas to the common volume. It is for the scattering geometry of the Kashima-Inubo and Kashima-Hiraiso measurements reported by Awaka et al. [1984]. Simultaneous bistatic scattering observations from a scattering volume at

a height of 2 km were made at Inubo and Hiraiso. The reflectivity factor for scattering in the absence of attenuation is given by the curves labeled "Rain Gauge" for simultaneous surface rain rate measurements at the transmitter site and "Climate D1" for estimates based on the Global rain climate model [Crane, 1985a]. For this location, the climate model closely approximated the gauge measurements.

The two-component predictions are for the backscatter and forward scatter geometries [Crane, 1974] and the D1 climate rain rate model. The effect of attenuation is evident in the figure. The backscatter geometry models (Back H for Hiraiso and Back I for Inubo) most closely reproduce the observations. Attenuation in the debris component of the two-component rain model causes the plateau in the forward scatter curve at 0.03 % of the year. The nearly 125° and 86° scattering angles for the Hiraiso and Inubo paths were best modeled by backscatter.

Excellent agreement is evident between the two-component model predictions and the 14.3 GHz observations over the 0.0001 to 1 % of the year range. A small discrepancy is evident at higher percentages when the surface rain rate observations depart from the climate model predictions. If the actual surface rain rate values had been used, this discrepancy would disappear. The model adequately handles the simultaneous occurrences of scattering and attenuation for attenuation values up to about 8 dB. No long term observations are available in the literature to test the model over a wider range of attenuations.

Awaka et al [1983] reported bistatic scatter measurements at 34.8 GHz for the summer season for the Hiraiso-Kashima path. These limited duration measurements are displayed in Figure 3 along with the forward and backscatter two-component model predictions for the D1 climate region. The forward scatter model includes sufficient attenuation to suppress the debris component scattering while the cell component rises to within a few dB of the observations at percentages less than 0.01%. The backscatter model again works best and is within 2 dB for less than 0.3% of the summer months. In this case the scattering angle was 19° which, by the CCIR model, should classify the path as forward scatter instead of backscatter.

The Two-Component Rain Scatter Model.

The two-component rain model has been found useful for the prediction of attenuation on terrestrial and slant paths [Crane, 1985a,b]. We now apply it to the problem for which it was originally developed. The model breaks the rain occurrence problem into two parts, the occurrence of cells (isolated) and of widespread rain (debris). The occurrence of either is assumed to be independent of the other. The attenuation prediction model calculates the rain rate needed to produce the desired value of attenuation by each process then sums the probability of the occurrence of cells or debris with the appropriate rain rate anywhere on the path. For application to rain scatter we start with an equivalent rain rate within a cell or debris region (width) located randomly within the common volume created by the intersection of the antenna patterns. We know the probability for the occurrence of that rain rate for either the cell or debris process. We next calculate the attenuation that would occur on the adjacent segments of the propagation path using the cell and debris extent (width) values. If we have a backscatter geometry the attenuation within the common volume is not included but is incorporated in the manner described by Crane [1974].

The probability density for the occurrence of specified values of equivalent reflectivity (or of transmission loss) is then calculated from the probability density for rain rate. The final cumulative probability distribution is then found by integrating the density. The use of

probability densities is required because the relationship between rain rate in the common volume and transmission loss is not monotonic. For the forward scatter case, the cell or debris with or the total path length, whichever is smaller is used for the calculation of attenuation. In the backscatter case, the random locations of the cell or debris structures along the path are used to vary the attenuation in the calculation of the probability density values for the effective reflectivity factor. The inclusion of attenuation as a random process in the backscatter case makes it applicable for all the scattering geometries except those very close to a purely forward scatter case (scattering angle $< 5^\circ$ say).

The Forward Scatter Case.

The Prospect Hill to Mt. Tug troposcatter path used by RADC and Dartmouth for communications studies is a transhorizon propagation path with a scattering angle of 2° . In the context of the two-component rain scatter model, it qualifies as a forward scatter path. In this case, the effect of attenuation is maximized relative to the effect of scattering. Model predictions are given in Figure 4. Attenuation is of little consequence at 5 GHz but is extremely important at 16 GHz. The Ku-band (15.73 GHz) predictions show the plateau produced by debris component attenuation. For rain, the Ku-band received power should not exceed -84 dBm except for very brief intervals when it will increase to -83 dBm. Simultaneous measurements at C-Band should show signal level variations from -84 to -73 dBm over the 0.01 to 0.3 % range when the Ku band signal saturates at -84 dBm. These predictions apply to the cumulative distribution of received signal levels, not to the instantaneous received signal time series.

Figure 5 depicts the cumulative distributions for 49 hours of observations during the spring and summer of 1987. The distributions are for a) clear weather (troposcatter) conditions (11 hrs.), b) all observations (49 hrs.), c) all observations with rain (34 hrs) and d) observations with light rain (24 hrs.). The troposcatter only curves (a) are in close agreement with predictions based on clear air scattering by atmospheric turbulence (not using the CCIR models which do not correctly estimate troposcatter field strengths at frequencies above about 10 GHz). The all rain data (c) show a upper level of -84 dBm at Ku-band (dashed curves in Figures 5 through 7) in apparent agreement with the two-component model predictions but this interpretation is not supported by the C-band (5 GHz) data. If the Ku-band observations are about -84 dBm, the simultaneously occurring C-band measurements should be above -84 dBm. However, the C-band observations are all less than -90 dBm.

Figure 6 depicts a) the cumulative distribution, b) the received power time series, c) the power spectrum for received power variations (in dB) and d) the instantaneous differences between Ku and C band measurements. The power spectra (a) display the $k^{-5/3}$ behavior typical of rain when averaged over spatial scales greater than ~10 km. The time series (b) and (d) show variations in received power typical of light rain (C-band levels are for reflectivities less than 16 dBZ peak). At ku-band, the signal levels exceed those predicted for rain even if no attenuation occurs along the path. These results suggest that more must be involved in the modeling of scattering by rain in the forward direction (and perhaps other directions, the success of the model as shown in Figures 2 and 3 notwithstanding).

Figure 7 displays simultaneous observations at C- and Ku-band for occurrences of light rain. In this case (September), the observations are consistent with a rain scatter interpretation with reflectivities less than 23 dBZ as observed at C-band.

Conclusions.

The data from Japan and the US (the Virginia Precipitation Scatter Experiment) show excellent agreement between the two-component rain scatter model predictions and bistatic scatter measurements. In employing the model, all the scattering geometries should be classified as "backscattering" as defined by Crane [1974]. The forward scatter model should only be used for great circle paths with both antennas pointed at the horizon and at each other in a typical troposcatter communication system geometry. The forward scatter model can also be used for main-lobe, side-lobe coupling when one antenna is pointed toward the other along the great circle path.

The forward scatter observations made over the Prospect Hill - Mt Tug path show that the two-component model is incomplete. Much stronger signals were observed at Ku-band than expected based on simultaneous C-band measurements. The discrepancies may be due to: 1) scattering by ice/snow at height (possible in April (Figure 6) at the 1 km height of the scattering volume), 2) the coherent effects of turbulent fluctuations in the hydrometeor number densities and 3) errors in the modeling of the statistical relationship between attenuation along the path and scattering in the common volume.

References.

- Awaka, J. [1984]: A prediction method for the received power from rain scatter, *Radio Science*, **19**, 643-651.
- Awaka, J., T. Kozu, K. Nakamura, and H. Inomata [1984]: Experimental Results on Bistatic Rain Scattering at 14.3 GHz, *IEEE Trans. Antennas and Propagation*, **AP-32**, 1345-1350.
- Awaka, J., K. Nakamura, and H. Inomata [1983]: Bistatic Rain-Scatter Experiment at 34.8 GHz, *IEEE Trans. on Antenna and Propagation*, **AP-31**, 693-698.
- Crane, R. K. [1985a]: Comparative evaluation of several rain rate attenuation prediction models, *Radio Science*, **20**, 843-863.
- Crane, R. K. [1985b]: Evaluation of global and CCIR models for estimation of rain rate statistics, *Radio Science*, **20**, 865-879.
- Crane, R. K. [1982]: A two-component rain model for the prediction of attenuation statistics, *Radio Science*, **17**, 1371-1387.
- Crane, R. K. [1974]: Bistatic Scatter from Rain, *IEEE Trans. Antennas and Propagation*, **AP-22**, 312-320.
- Crane, R. K. [1973]: Virginia Precipitation Scatter Experiment - Data Analysis, NASA/GSFC X-750-73-55, Goddard Space Flight Center.
- Sakagami, S. [1980]: Some Experimental Results on Bistatic Scatter from Rain, *IEEE Trans. Antennas and Propagation*, **AP-28**, 161-165.

Bistatic Scatter by Rain at 3.7 GHz

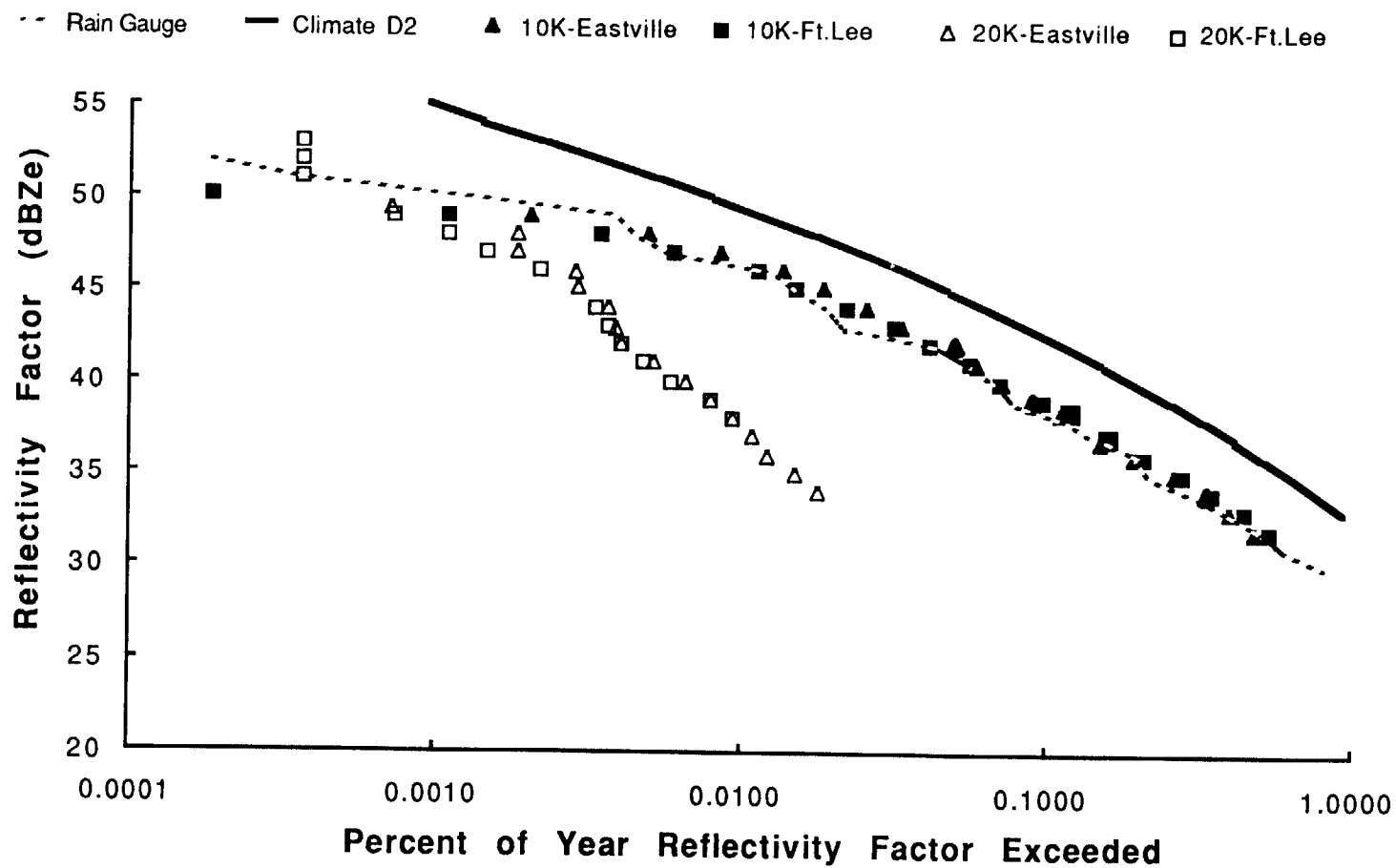


Figure 1 Bistatic scatter measurements October 3, 1970 - October 2, 1971
 Virginia Precipitation Scatter Experiment [Crane, 1973].

Bistatic Scatter From Rain at 14.3 GHz

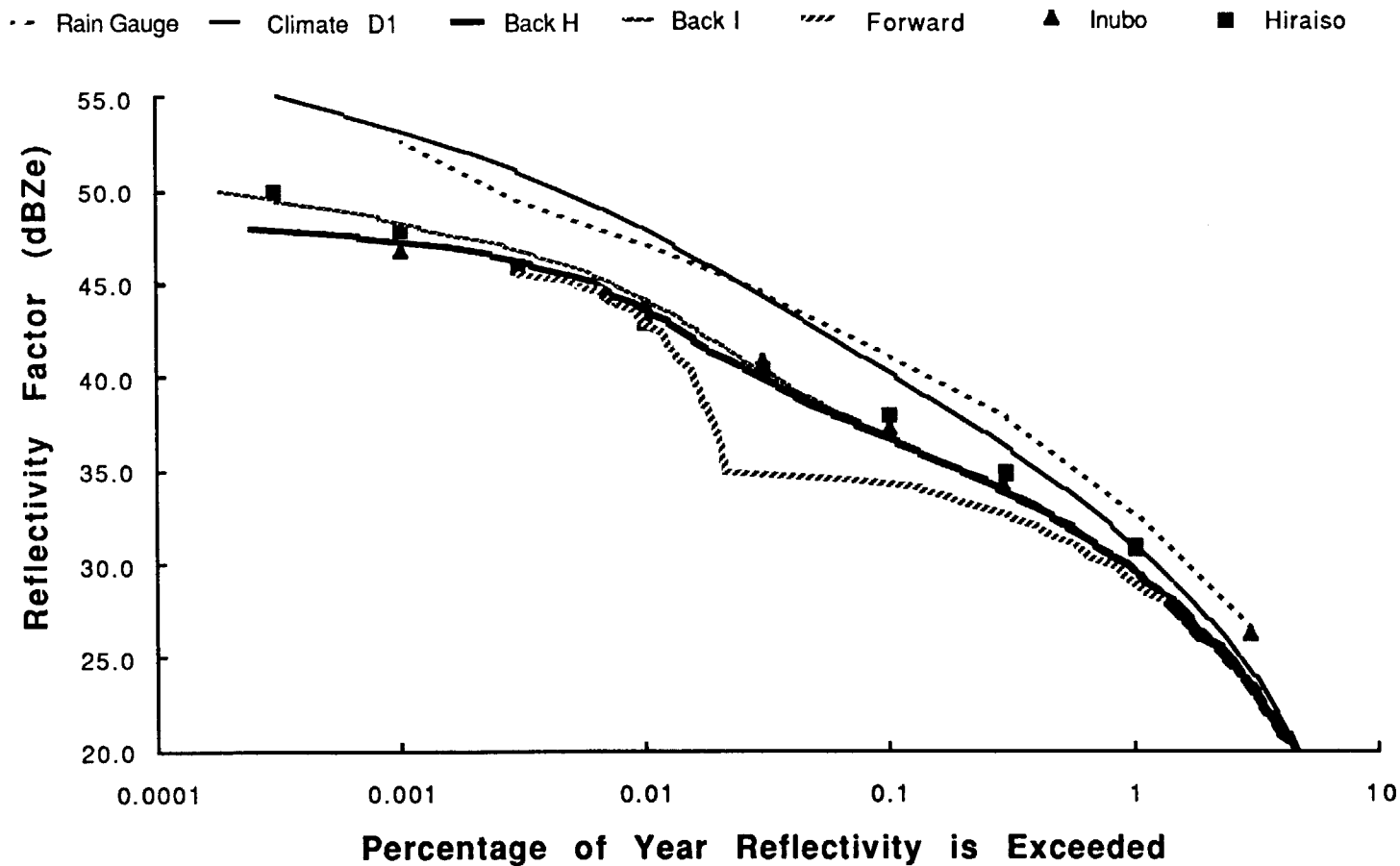


Figure 2 Bistatic scatter measurements May 9, 1981 - May 8, 1982
Kashima, Japan [Awaka et al., 1984].

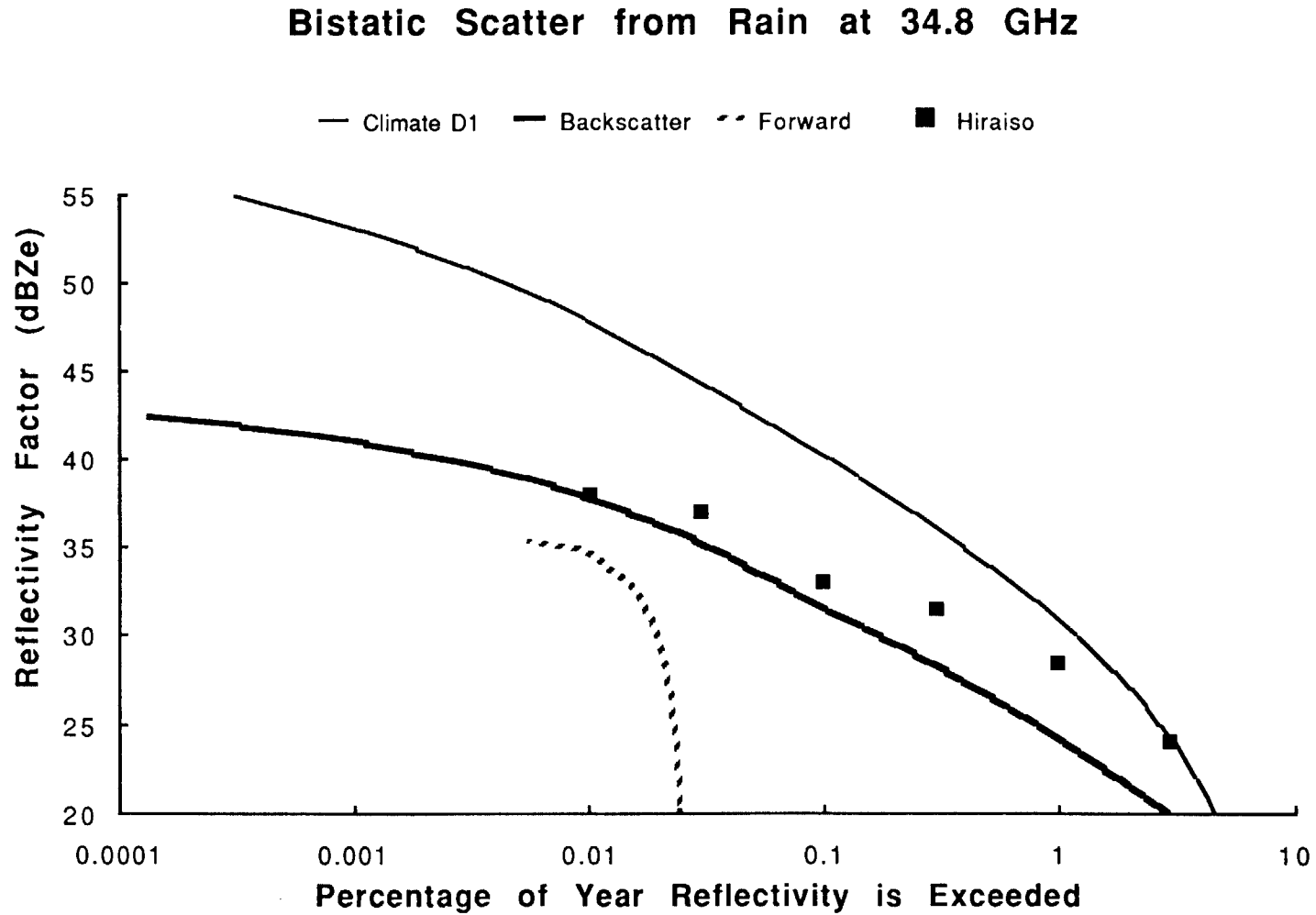


Figure 3 Bistatic scatter measurements June 9 - September 26, 1980
Kashima, Japan [Awaka et al., 1983].

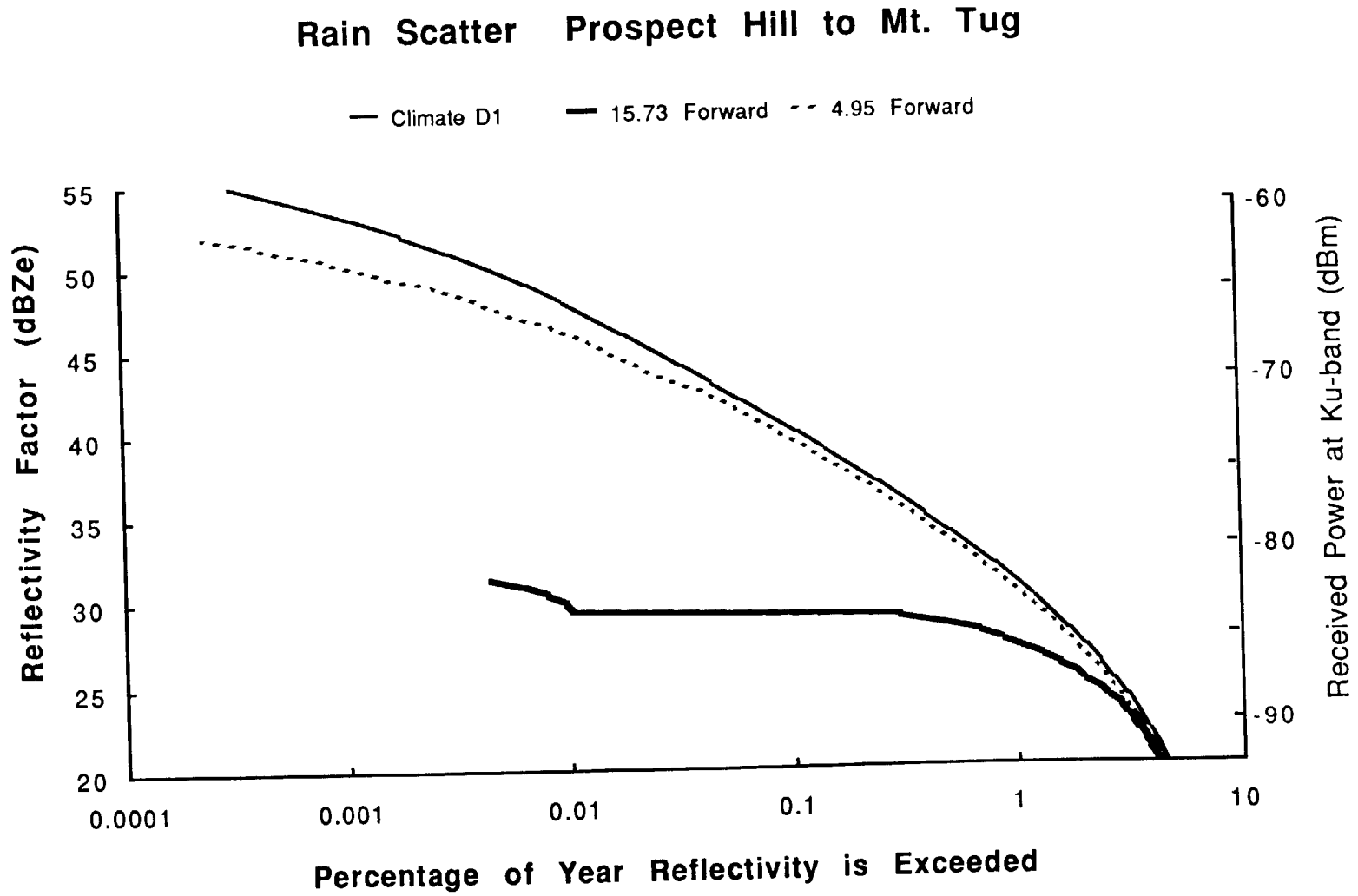


Figure 4 Model predictions for the Prospect Hill - Mt. Tug path

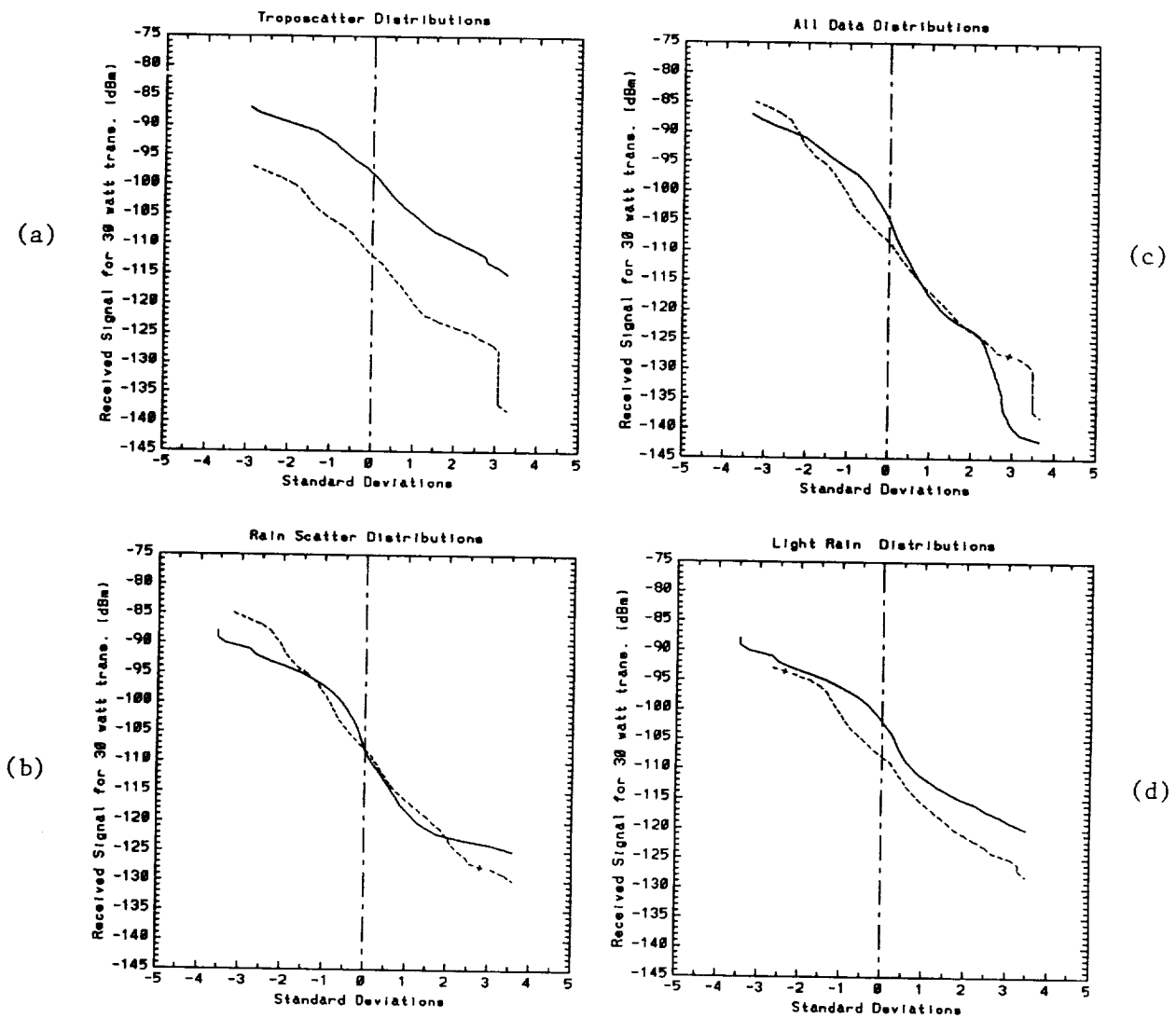


Figure 5. Cumulative Distribution for 49 hours of observations on the the Prospect Hill to Mt. Tug troposcatter path. (Solid curves for C-band and dashed curves for Ku-band).

ORIGINAL PAGE IS
OF POOR QUALITY

ORIGINAL PAGE IS
OF POOR QUALITY

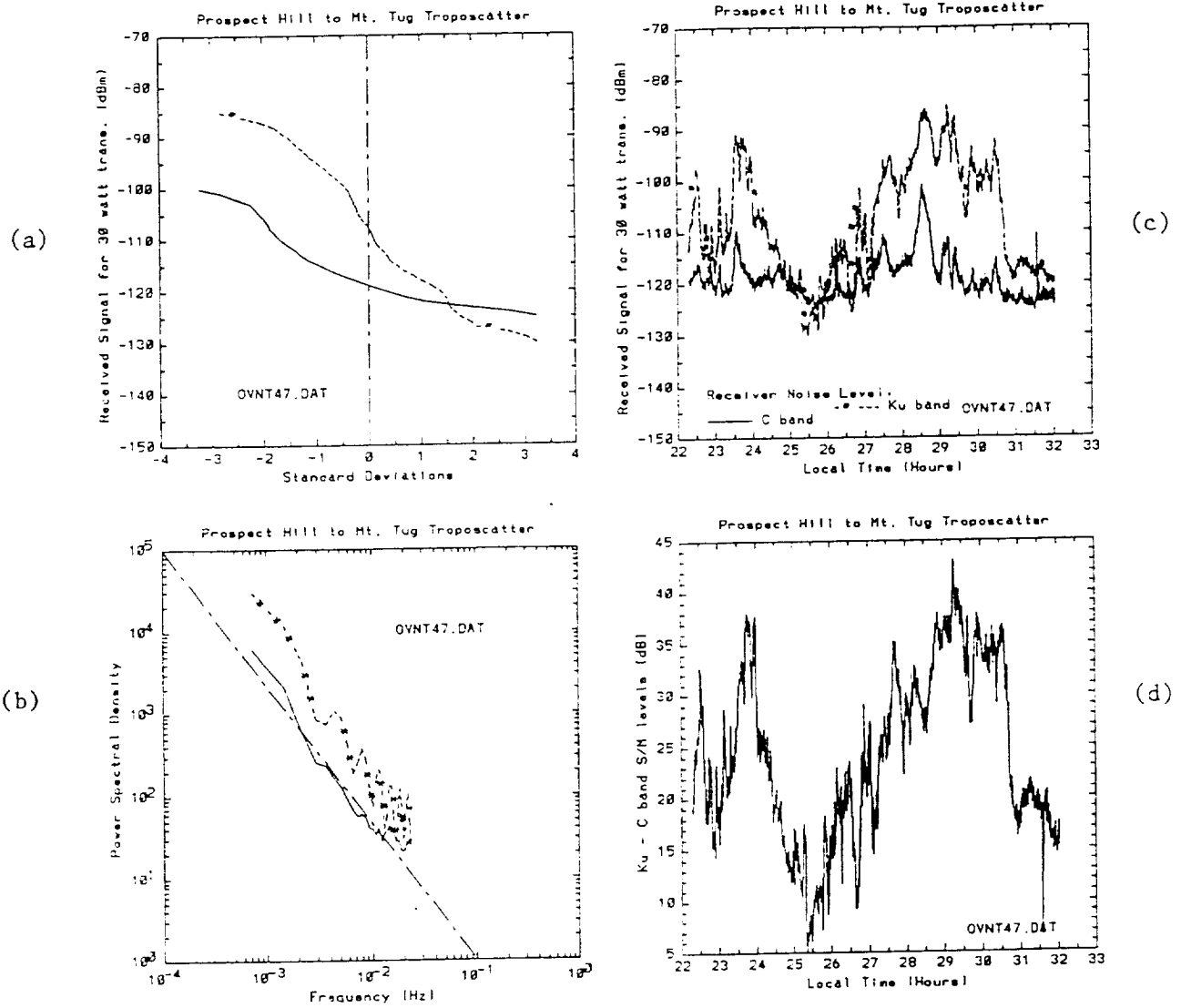


Figure 6. Observations in rain, April 6 and 7, 1987.

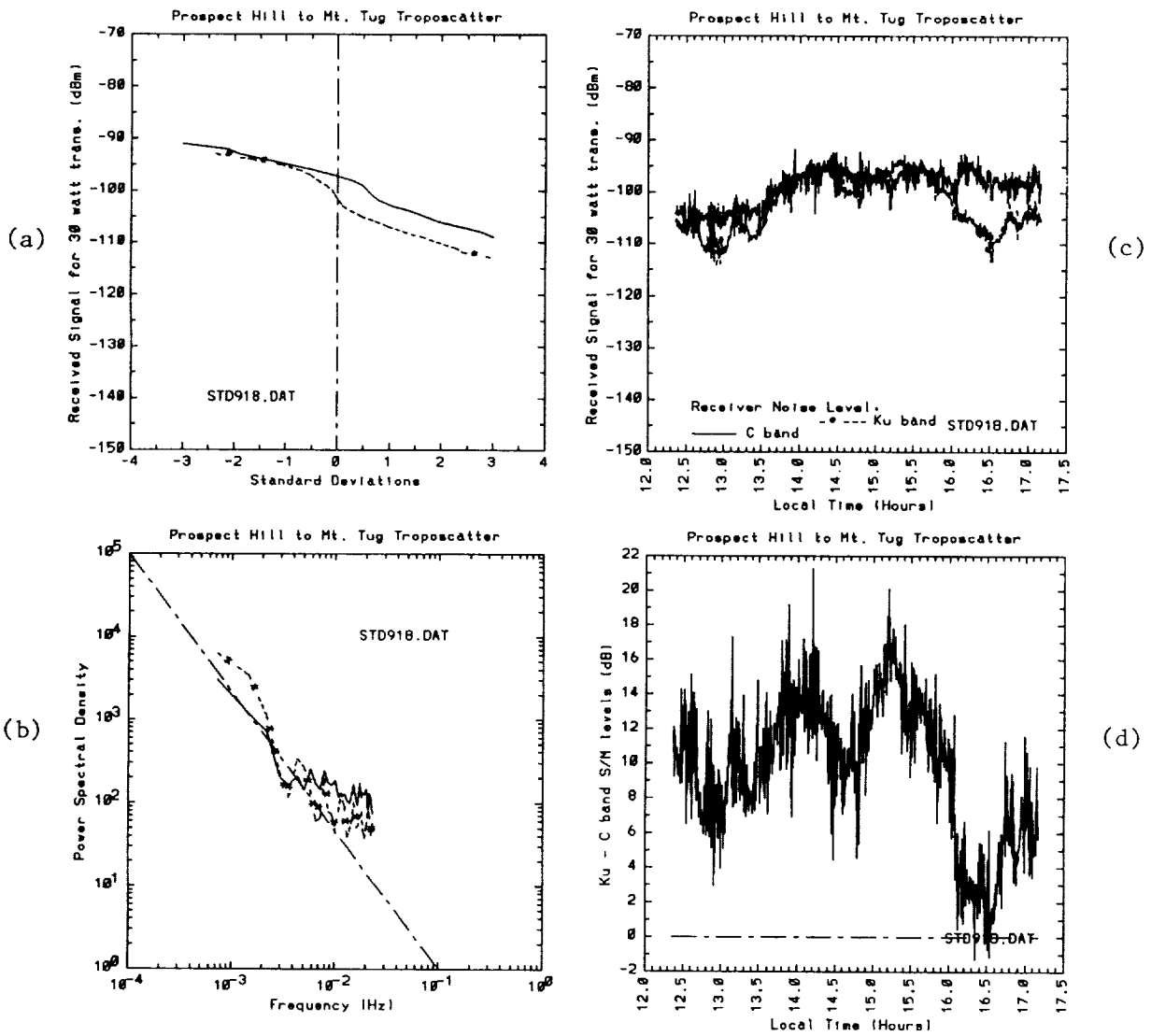


Figure 7. Observations in light rain, September 18, 1987.

ORIGINAL PAGE IS
OF POOR QUALITY

MILLIMETER-WAVE STUDIES

Kenneth C. Allen
U.S. Department of Commerce
National Telecommunications and Information Administration
Institute for Telecommunication Sciences
325 Broadway
Boulder, CO 80303 USA

Abstract - Progress on millimeter-wave propagation experiments in Hawaii is reported. A short path for measuring attenuation in rain at 9.6, 28.8, 57.6, and 96.1 GHz is in operation. A slant path from Hilo to the top of Mauna Kea is scheduled. On this path, scattering from rain and clouds that may cause interference for satellites closely spaced in geosynchronous orbit will be measured at 28.8 and 96.1 GHz. In addition the full transmission matrix will be measured at the same frequencies on the slant path. The technique and equipment used to measure the transmission matrix are described.

1. Introduction

It is well-known that high rates of attenuation in rain will limit the availability of millimeter-wave telecommunication links. Fortunately, on Earth-satellite paths only a short segment of the path (depending on elevation angle and altitude of the ground station) is in the lower atmosphere where liquid water droplets occur. For this reason, millimeter waves may prove to be economically viable for a number of applications involving earth-space communications. To accurately predict the limitations that rain (and clouds) will place on such systems, a great deal more knowledge is needed about the interaction of millimeter waves and naturally occurring atmospheric hydro-meteors.

A three-stage experiment measuring the effect of rain on some millimeter-wave propagation parameters is under way in Hawaii. The first stage of the experiment, to measure the dependence of the attenuation rate (dB/km) on rain rate (mm/h) at 9.6, 28.8, 57.6, and 96.1 GHz using a 1-km path on General Lyman Field in Hilo, Hawaii, is in progress. In the second stage, a slant path from the airfield to the top of Mauna Kea will be used to measure scattering from rain and clouds that may cause interference for satellites closely spaced in geosynchronous orbit. In the third stage, measurements of the complex transmission matrix at 28.8 and 96.1 GHz will be made on the same slant path.

The Hawaiian location was chosen because of the availability of a slant path from sea level to 4,205 m altitude, which would approximate the lower atmospheric portion of an earth-satellite path, on which rainfall is frequent (approximately 300 inches per year near mid-path).

The paths and equipment are described in the remainder of this report. The third stage (transmission matrix measurements) will be described before the second stage (interference measurements) to allow a more concise description of the equipment.

2. Short-Path Experiment

The purpose of the short path is to measure the attenuation rate (dB/km) in rain as a function of rain rate (mm/h) in the Hawaiian climate. Measurements have been made in the past in California, Colorado, and Alabama. This experiment extends the study of the climate dependence of attenuation in rain to Hawaii.

The short path has been in operation since February 23, 1988. The receivers at 9.6, 28.8, 57.6, and 96.1 GHz are located about 15 m above ground level in the old control tower on General Lyman Field in Hilo, Hawaii. The transmitters are located approximately 4 m above ground level on top of two standard scaffolding sections about 1 km south on the Shop and Yard grounds of the Hawaii Water Department. A tipping bucket and a laser rain rate gauge along with air and rain temperature measuring instruments are mounted on top of the old control tower. Hourly accumulated rainfalls measured with a tipping bucket are also available from the National Weather Service office located in the base of the tower. The radio frequency equipment has been described previously (Espeland et al., 1986).

The movement of most rain showers is north to south along the propagation path. The showers typically last for less than 30 minutes.

The data will be analyzed and reported in Fiscal Year 1989.

3. Transmission Matrix Measurements

Measurements of attenuation in rain are often made. However, rain has polarization dependent effects. More than attenuation measurements at a single polarization are needed to understand these effects. A more complete description of the propagation effects is provided by the transmission matrix.

3.1 Transmission Matrix

A transmitted, polarized wave can be represented by a complex valued, two element vector, E_t , the elements of which represent the phase and amplitude of two orthogonal polarization components of the wave, e.g., vertical and horizontal. When the wave is altered during propagation, a new vector, E_r , represents it at the receiver. The altered wave at the receiver can be related to the original using a 2x2, complex valued matrix, T , by

$$E_r = TE_t. \quad (1)$$

The matrix T is called the transmission matrix and provides the desired description of the propagation characteristics of the path. See Figure 1.

3.2 Experiment

The planned experiment described here is to measure the transmission matrix at 28.8 and 96.1 GHz on a simulated earth-satellite path. This path from the old control tower on General Lyman Field, in Hilo, Hawaii to the top of Mauna Kea has an elevation angle of 5° and is 45.6 km long. The path profile is shown in Figure 2. When measuring the transmission matrix, it is

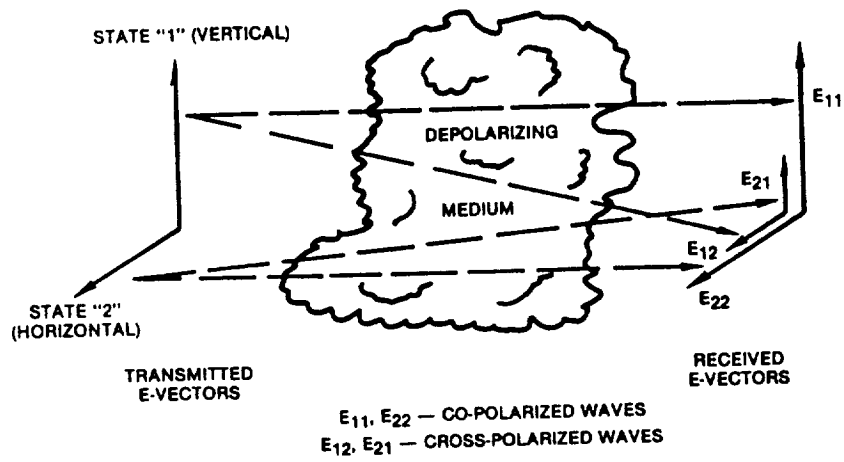


Figure 1. Depolarization (Ippolito et al., 1981).

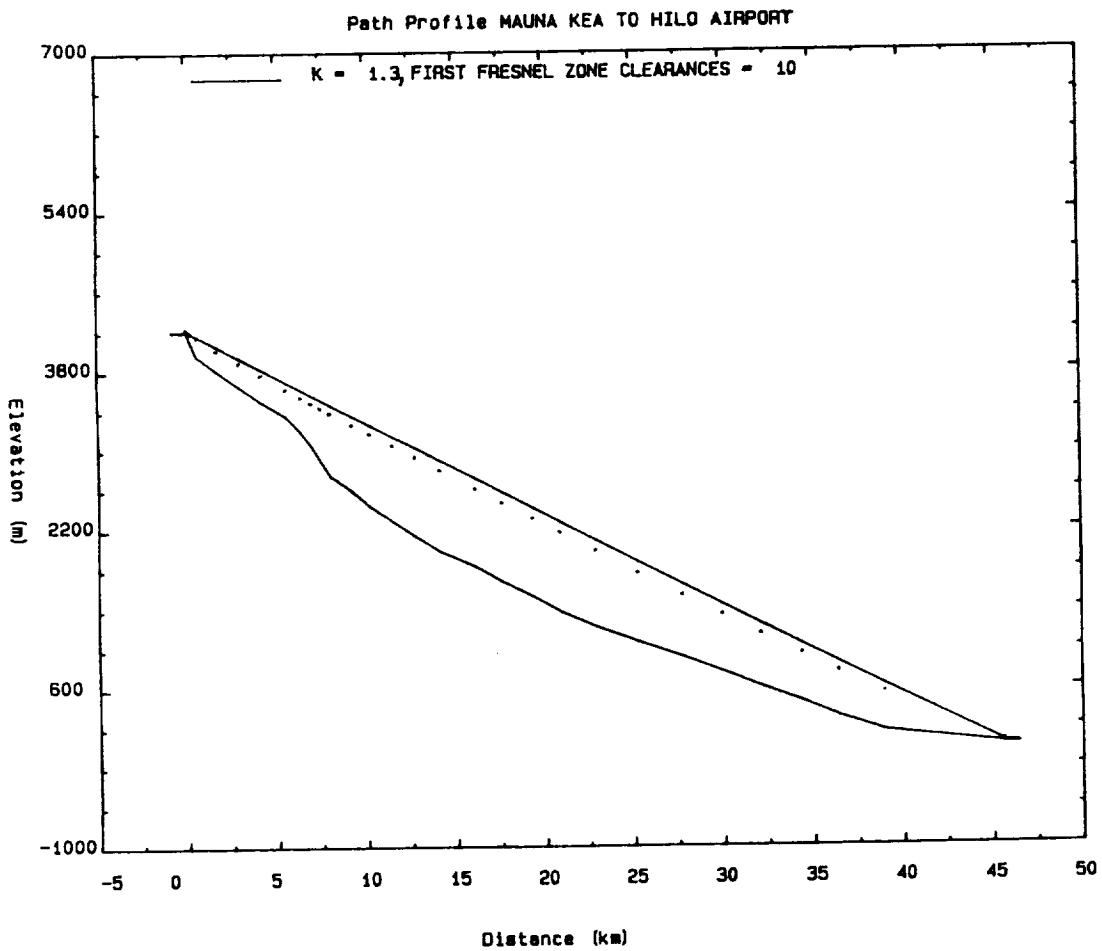


Figure 2. Path profile from the top of Mauna Kea to Hilo airport.

important to account for the effects of equipment that can be represented by additional matrices in (1). These effects will not be discussed here, but the reader can find a complete discussion in Marvira (1986).

The transmission matrix will be measured by transmitting vertically and horizontally polarized waves at slightly different frequencies. This allows the original polarization of the wave to be identified at the receiver. At the receiver, horizontal and vertical components will be received separately. There will be four IF's at the receiver corresponding to the waves transmitted vertically and received vertically, VV, transmitted vertically and received horizontally, VH, transmitted horizontally and received vertically, HV, and transmitted horizontally and received horizontally, HH. The phase and amplitude of these four IF's give the phase and amplitude of each of the elements in the transmission matrix.

Typically, transmission matrix measurements have been made by switching polarization devices at the transmitter and receiver. The technique described here has the advantages of allowing simultaneous measurements of phase at each polarization with a frequency response well in excess of 1 MHz μ s.

3.3 Transmitters and Receivers

The phase of three of the transmission matrix elements can be measured with respect to the remaining one, usually one of the copolarization elements. However, the equipment for this experiment has been designed so that the phase delays of all four matrix elements at 28.8 and 96.1 GHz are measured with respect to the phase delay of the 9.6 GHz signal. This gives the additional information of the relative phase delays on the path of the different frequencies. The absolute phase delays could be measured, but variations in the absolute delay would make the measurements of the relative delays between the transmission matrix elements more difficult.

In Figure 3, a block diagram of the transmitters is presented. The 9.6-GHz signal serves as a phase reference for the receiver local oscillator. The 28.8 (vertical), 28.815 GHz (horizontal), 96.1 (vertical), and 96.15 GHz (horizontal) transmitted signals are all phase coherent with the 9.6 GHz signal, being derived from the same transmitter local oscillator (LO).

In Figure 4, a block diagram of the 9.6-GHz receiver and the reconstruction of the transmitter LO are shown. The 9.6-GHz received signal has a phase of

$$\theta_s = 19200\theta_{TLO} + 9.6\tau \quad (2)$$

in wavelengths at 9.6 GHz where $200\theta_{TLO}$ is the phase of the 100-MHz transmitter LO and τ is the propagation delay of the 9.6-GHz wave in nanoseconds. All constant phase delays are neglected in this analysis.

The reference oscillator is phase locked to the received signal through Phase Lock Loop 1. The phase locking electronics (PLE) control the reference oscillator so that its phase and the phase of the IF output of the mixer are the same. This results in the reference oscillator frequency of

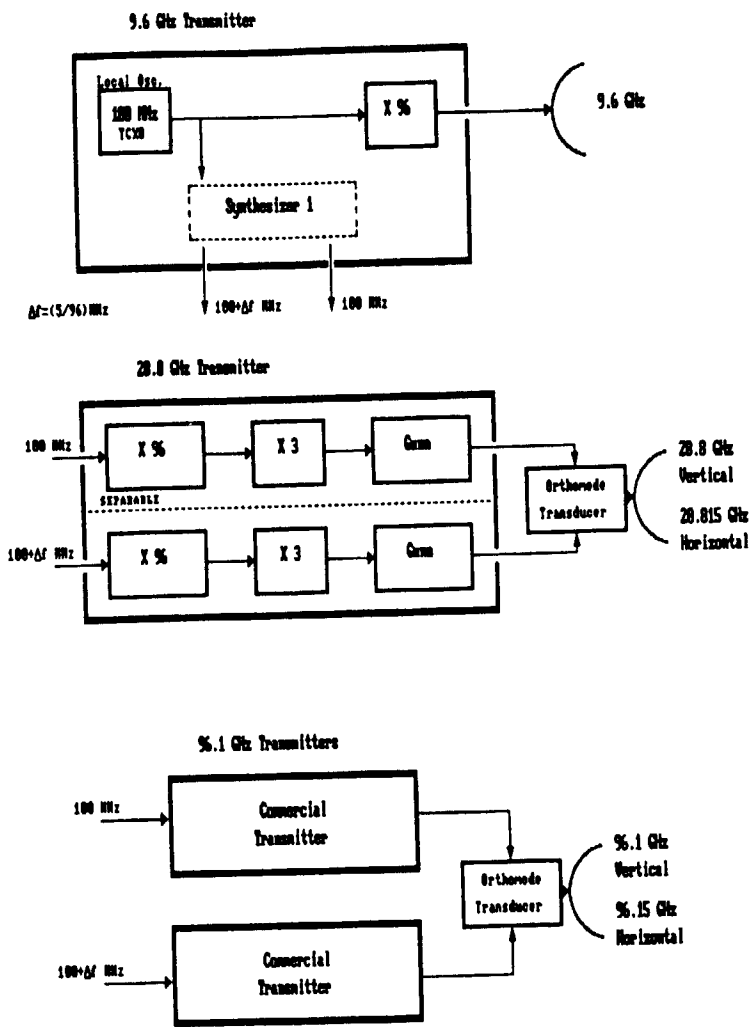


Figure 3. Block diagram of transmitters.

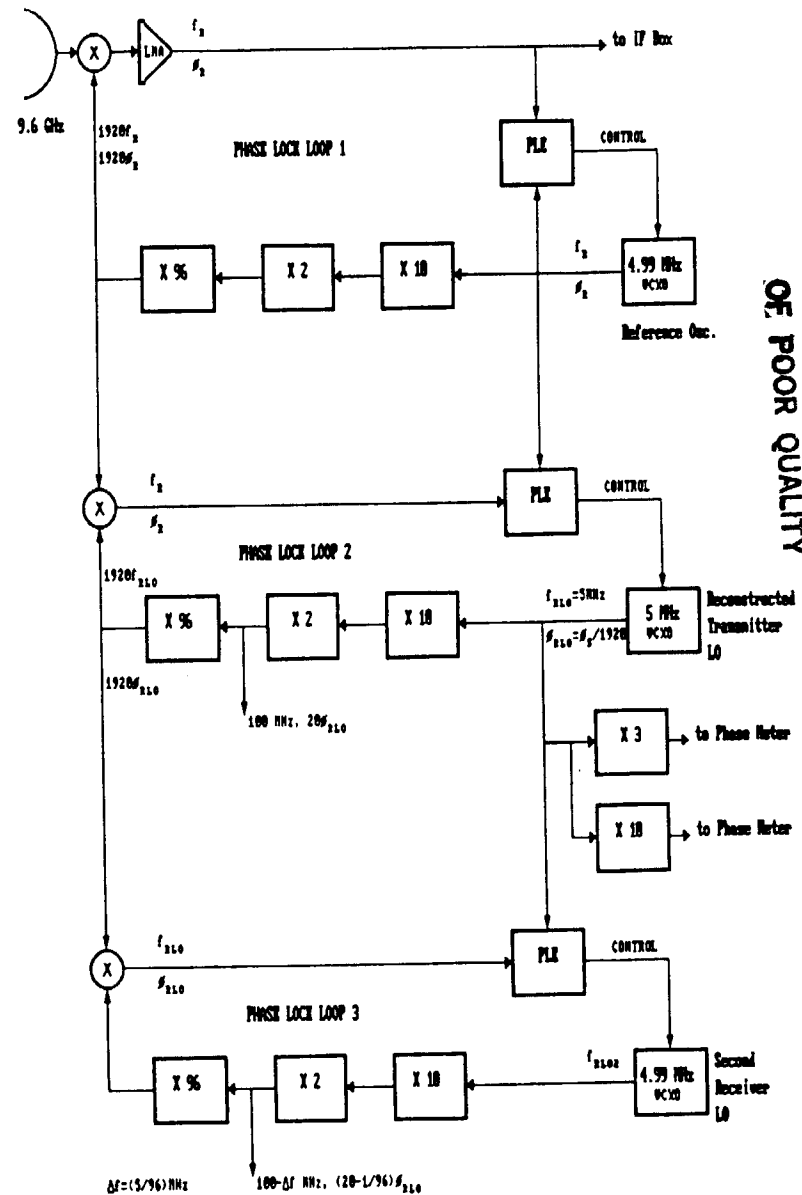


Figure 4. Block diagram of 9.6 GHz receiver and reconstruction of transmitter LO.

$$f_R = 9.6 \text{ GHz}/1921 = 5 \text{ MHz} \cdot 1920/1921 \quad (3)$$

and the phase of

$$\theta_R = \theta_S/1921. \quad (4)$$

In Phase Lock Loop 2 the reference oscillator signal is removed and the transmitter LO is reconstructed. In this second loop, the PLE controls the receiver LO so that the IF output of the mixer has the same phase as the reference oscillator. This results in the receiver LO frequency of

$$f_{RLO} = f_R \cdot 1921/1920 = 9.6 \text{ GHz}/1920 = 5 \text{ MHz} \quad (5)$$

and phase of

$$\theta_{RLO} = \theta_R \cdot 1921/1920 = \theta/1920 = \theta_{TLO} + 9.6\tau/1920. \quad (6)$$

Thus, the 5 MHz receiver LO is phase coherent with the phase of the 100 MHz transmitter LO plus the 9.6 GHz propagation delay phase divided by 1920. The 100 MHz signal with phase

$$20\theta_{RLO} = 20\theta_{TLO} + 9.6\tau/96 \quad (7)$$

is used in the 96-GHz receivers.

The purpose of Phase Lock Loop 3 is to generate a phase coherent LO signal at $100-\Delta f$ MHz for the other receivers. The PLE controls the second receiver LO so that the IF output of the mixer is the same as the receiver LO. Thus, the oscillator frequency is

$$f_{RLO2} = f_{RLO} \cdot 1919/1920 \quad (8)$$

so that when multiplied by 1920, it is 9.595 GHz or 5 MHz below the 9.6-GHz signal. In a similar fashion it results in proportional IF frequencies when used as the LO for 28.8 GHz of 15 MHz and for 96.1 GHz of 50 MHz. The $(100-\Delta f)$ -MHz signal has a phase of $(20 - 1/96)\theta_{RLO}$.

In Figure 5, a conceptual block diagram of the receivers is presented. Each IF is sent to an IF processing box. There the IF's are amplified and filtered and fed into logarithmic amplifiers. The log amplifiers have limited outputs of the IF signal and analog outputs proportional to the logarithm of the IF amplitude. The analog outputs of signal amplitude are sent to an analog-to-digital (A/D) converter and recorded in a computer. The limited outputs are sent to phase meters. The analog outputs of the phase meters are sent to the A/D converter to be recorded in the computer.

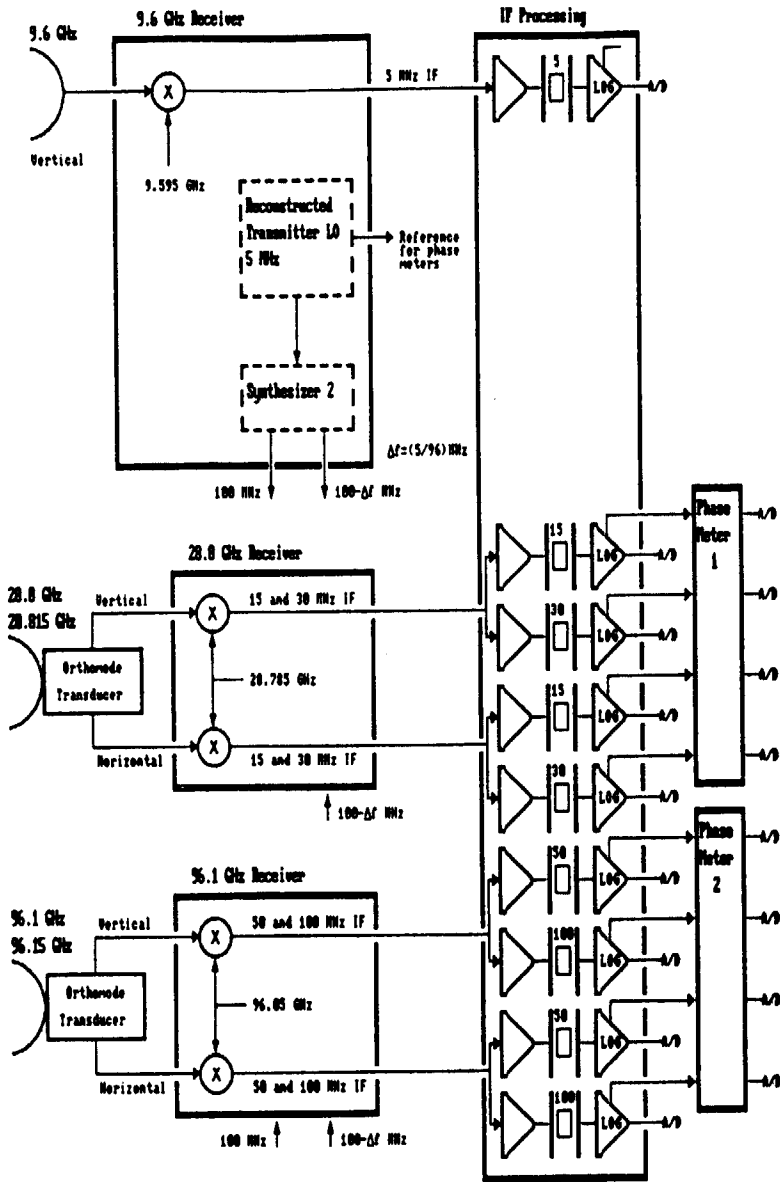


Figure 5. Block diagram of receivers.

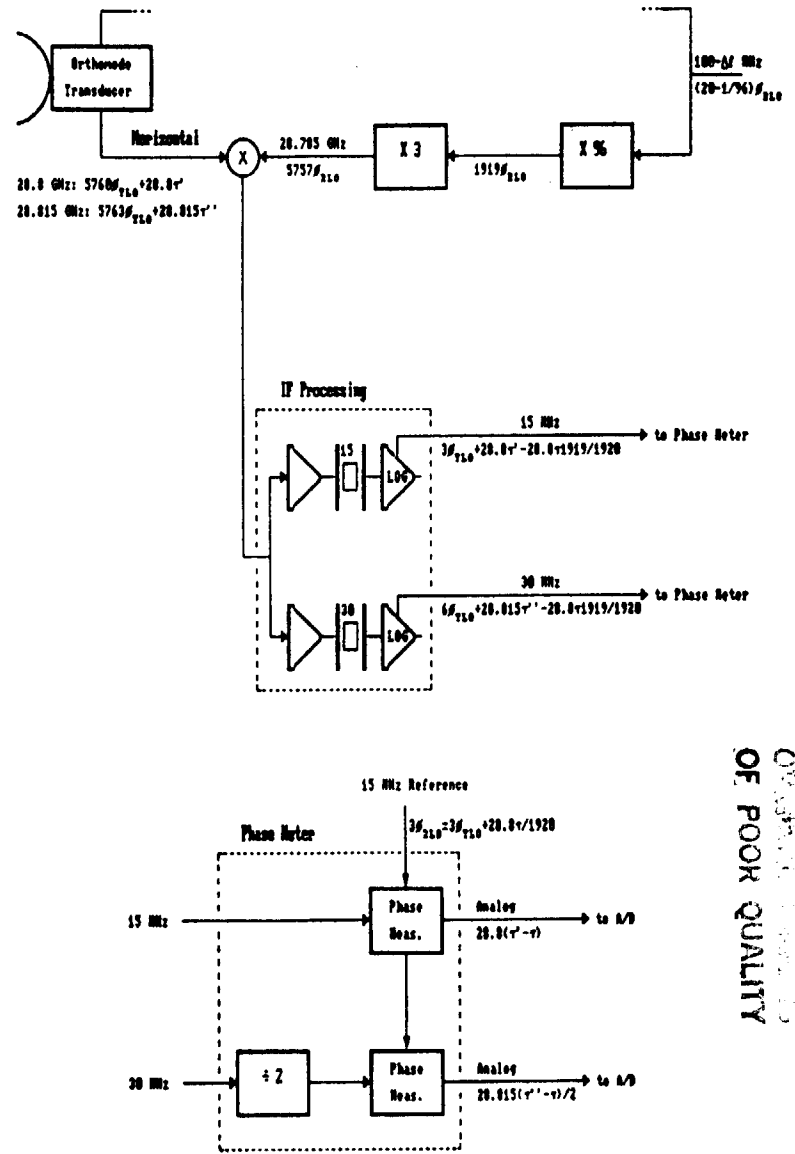


Figure 6. Example of phase analysis of 28.8 GHz receiver.

OF POOR QUALITY

In Figure 6 an example of phase analysis is shown for the 28.8 GHz receiver. The phase of the 28.8-GHz VH signal (transmitted with vertical polarization and received with horizontal polarization) is $5760 \theta_{TLO} + 28.8\tau'$ where τ' is the delay time of this signal in nanoseconds. The phase of the 28.815-GHz HH signal is $5760 \theta_{TLO} + 28.815\tau''$ where τ'' is the delay time of this signal. These two signals are mixed with the 28.785-GHz LO signal with phase $5757 \theta_{RLO}$. The resultant IF's and their phases are shown in the figure. The output of the phase meter for the 15 MHz-VH IF is the propagation delay time at 28.8-GHz VH minus the propagation delay time at 9.6 GHz in 28.8-GHz wavelengths. The output for the 30 MHz HH IF is the propagation delay time at 28.815-GHz HH minus the delay time at 9.6 GHz in 28.815-GHz wavelengths. The results for the VV and HV signals follow similarly.

3.4. Phase Locking Electronics

The phase locking electronics (PLE) used in the transmitter and receiver are of a uniform design shown in Figure 7. Each signal is amplified to TTL levels and a digital phase comparison is done. The phase detector used is also a frequency detector so that even if the signals differ in frequency the control voltage will tune the VCXO until the frequencies are equal and then will lock the phase. Thus, phase lock is always achieved avoiding the problem with many phase lock loops in achieving or re-achieving lock. The frequency response of the phase detector and loop filter allow the tracking of phase shifts as rapid as 25 kHz.

3.5 Phase Meters

The phase meters were also designed to have fast response times. A block diagram of the phase meters is shown in Figure 8. The input signals can be as high as 100 MHz. Each input is amplified to ECL levels. These digital signals are then fed through a binary frequency divider capable of dividing by from 1 to 256. The dividing factor determines the scale of the analog output so that rapid folding over can be avoided. It also allows some flexibility in matching input and reference frequencies.

The phase measuring electronics can respond to phase shifts as rapid as one-half the frequency fed to it. The accuracy is about 2 to 3 degrees of the phase of the input to the measuring circuit so that the overall accuracy is scaled up by the dividing factor. The output is filtered before being fed to the A/D converter. Cutoff frequencies for these low-pass filters of 5 kHz are to be used initially.

4. Interference Measurements

The purpose of the interference measurements is to determine the potential of scattering from rain and clouds to cause interference on earth-satellite paths. One possible interference scenario is presented in Figure 9. Ground station B causes interference to satellite A receiving ground station A because energy from ground station B's beam directed at satellite B is scattered from the cloud toward satellite A. The geometry is the same for satellite A to interfere with ground station B receiving satellite B.

Phase Locking Electronics (PLE)

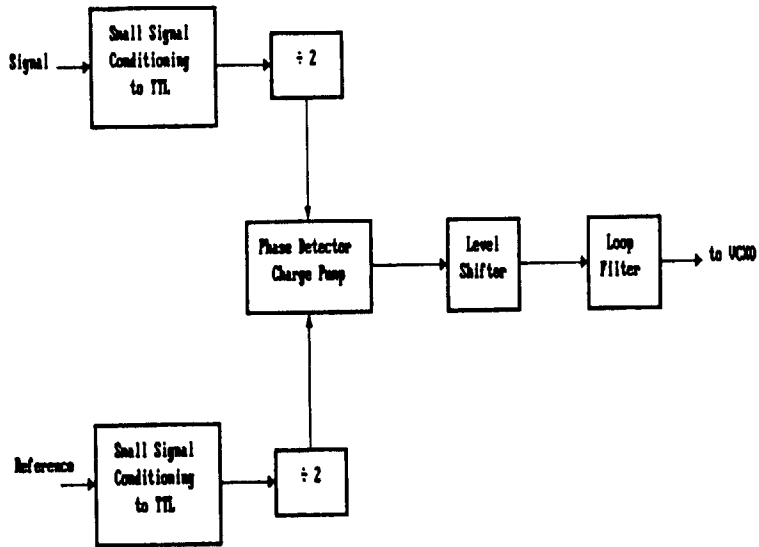


Figure 7. Block diagram of phase locking electronics.

Phase Meter

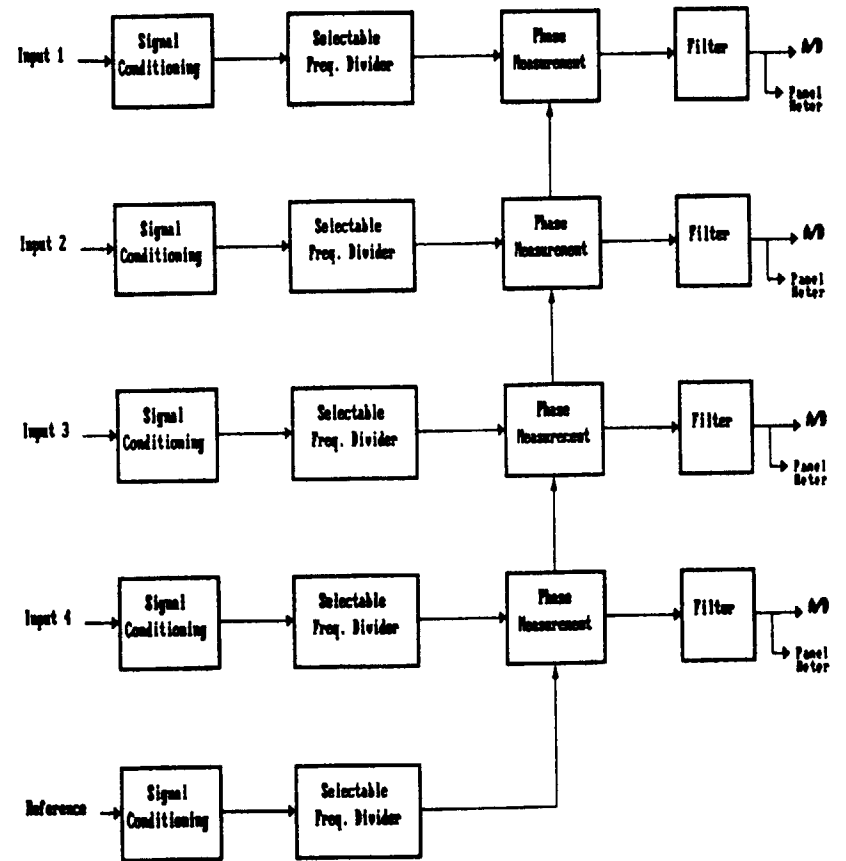
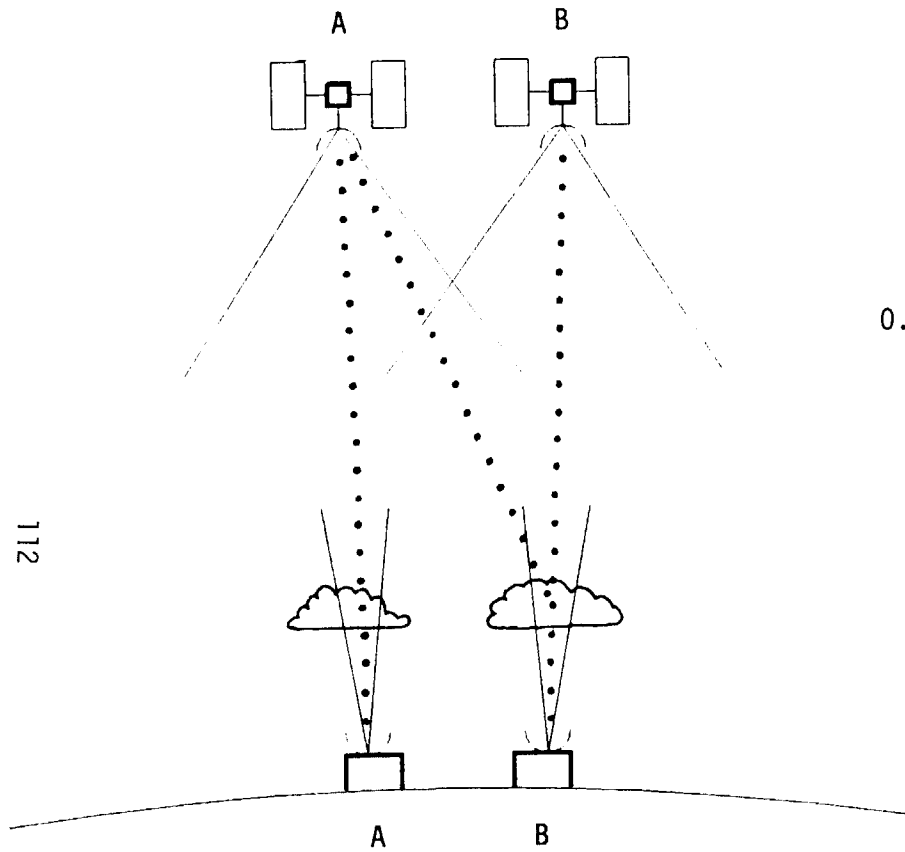


Figure 8. Block diagram of phase meters.

INTERFERENCE SCENARIO



112

Figure 9. Geometry of earth-satellite path interference by scattering from rain and cloud.

SCATTERING MEASUREMENTS

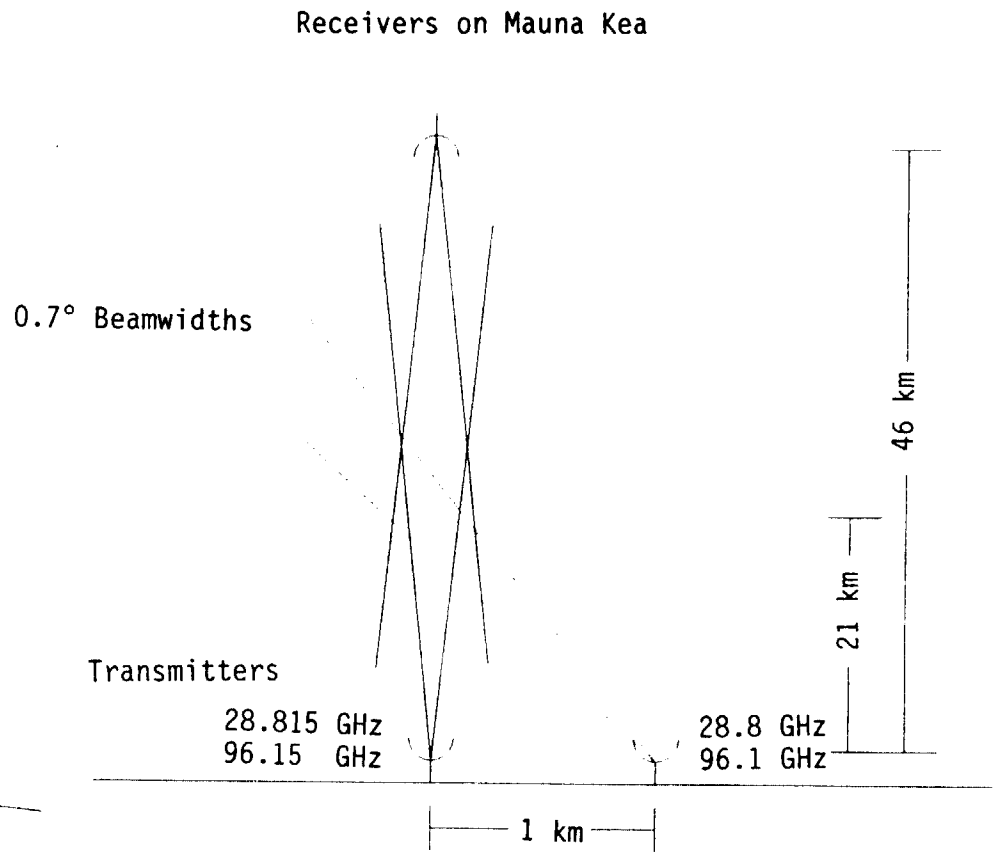


Figure 10. Geometry of slant path interference measurements.

This interference scenario will be simulated as shown in Figure 10 employing the same equipment used for the transmission matrix measurements. The receivers at 9.6, 28.8, 28.815, 96.1, and 96.15 GHz will be located on top of Mauna Kea. The transmitters at 9.6, 28.815 and 96.15 GHz will be located in the old control tower but the transmitters at 28.8 and 96.1 GHz will be located on the scaffolding 1 km south of the old control tower. This will result in a separation of 1.2° degrees between the two transmitters as seen from the mountain top receivers. The receiving antennas will be pointed at the 28.8 and 96.1-GHz transmitters. Because of the narrow beamwidths and the shortness of the path, the other transmitters and the clouds above them are outside the receiving antenna beam. Therefore, the 28.815- and 96.15-GHz transmitting antennas will need to be pointed toward the clouds lying in the desired link. The scattering angles are still nearly forward as in the interference scenario being simulated.

The isolation between the desired transmitters and the interfering transmitters should be high (> 60 dB). Both signal levels will be monitored to measure how much this isolation is degraded by scattering from rain and clouds.

5. Summary

A description of a three-stage experiment has been presented. The first stage, measuring the specific attenuation in rain at 9.6, 28.8, 57.6, and 96.1 GHz in a tropical marine environment, is in progress in Hilo, Hawaii. The second stage will measure scattering from rain and clouds on a slant path from Hilo to the top of Mauna Kea. The third stage will measure the transmission matrix at 28.8 and 96.1 GHz on the same slant path.

The results of the experiments should be reported next fiscal year.

References

- Espeland, R. H., E. J. Violette and K. C. Allen, "Rain attenuation measurements at 28.8, 57.6, and 96.1 GHz on a 1-km path," NTIA Report 86-190, 1986.
- Ippolito, L. J., R. D. Kaul, and R. G. Wallace, "Propagation Effects Handbook for Satellite Systems Design," second ed., NASA Reference Publication 1082, December 1981.
- Marvira, A., ed., Olympus Propagation Experiment Handbook for Data Preprocessing, Part 1: Theory and Basic Information, Issue 1, European Space Research and Technology Center, Noorduyk, The Netherlands, OPEX-11, Sept. 1986.

GROUND-BASED RADIOMETRIC OBSERVATIONS OF EMISSION AND
ATTENUATION AT 20.6, 31.65, AND 90.0 GHz

Ed R. Westwater, Jack B. Snider, and Michael J. Falls

NOAA/ERL/Wave Propagation Laboratory
Boulder, Colorado 80303

Abstract--During 1987, ground-based zenith-viewing observations of atmospheric thermal emission were made at frequencies of 20.6, 31.65, and 90.0 GHz. At the locations of the experiments, San Nicolas Island, California, and Denver, Colorado, radiosonde observations of temperature and humidity were also available. The data, after conversion to attenuation using the mean radiating temperature approximation, are processed to derive attenuation statistics. In addition, both clear and cloudy attenuation characteristics are examined and compared with the most recent theories. Finally, the predictability and interdependence of the three separate channels are examined.

1. Introduction

Over the past decade, the Wave Propagation Laboratory (WPL) has designed, constructed, and field-tested several ground-based microwave radiometers to observe the atmosphere (Hogg et al., 1983; Westwater and Snider, 1987). In particular, extensive experience has been gained by using both zenith-viewing and steerable dual-frequency instruments operating at 20.6 and 31.65 GHz. These instruments continue to provide unique and meteorologically useful observations of precipitable water vapor (PWV) and integrated cloud liquid. Perhaps equally as useful, but certainly not as well studied, are the microwave attenuation characteristics that these devices can easily provide. Within the last year, WPL extended its radiometric capabilities by adding a channel at 90.0 GHz to the steerable and transportable radiometer. All three channels have equal beamwidths of 2.5 degrees, point in the same direction from the same location, and hence, are capable of simultaneously measuring emission and attenuation from the same volume of air. We present here examples of some of the data taken with the new system; from these data, several statistical and physical quantities, relevant to radio propagation studies, are derived and compared with theory.

2. Description of Experiments

2.1 San Nicolas Island, California, July 1987 (SNI)

In July 1987, WPL participated in an investigation of the characteristics of marine stratocumulus clouds at San Nicolas Island (SNI), located approximately 50 nautical miles west of Los Angeles. Observations of zenith brightness temperatures were made continuously by the WPL mobile, microwave radiometer operating at 20.6, 31.65 and 90.0 GHz. Although the primary purpose of the SNI observations was to study cloud properties, a secondary goal was the acquisition of statistics on attenuation by cloud liquid water, especially at 90.0 GHz. Supporting data for the attenuation measurements at SNI consisted of radiosondes launched up to several times daily and standard surface meteorological observations.

Clouds were persistent during the three week measurement period, being present for 76 percent of the time. Precipitable water vapor (PWV) was variable ranging from about 0.9 to 3.1 cm with a mean value of 1.9 cm.

2.2 Denver, Colorado, December 1987 (DEN)

The mobile three-channel radiometer was installed at the Denver (DEN) National Weather Service Forecasting Office (NWSFO) in December 1987, where it operated alongside the WPL six-channel radiometer (PROFILER) which measures PWV, cloud liquid, and temperature profiles. At Denver, supporting data were provided by the PROFILER, by the daily radiosondes released at standard times of 00 and 12 GMT, and by surface meteorological data. Denver weather in December is characterized by relative dry periods (PWV \leq 0.5 cm) with occasional periods of snow. Clouds containing supercooled liquid water are common, especially prior to the onset of and during precipitation.

In contrast to SNI, clouds were present only 15 percent of the time. The PWV was low, ranging from 0.1 to 1.0 cm with a mean value of 0.5 cm.

2.3 General

Radiometers are calibrated using the "tipping curve" or elevation scan method in which absolute absorption at each operating frequency is calculated from the slope of the relative absorption versus relative path length (air mass) measured as the radiometer antenna is scanned in elevation (Hogg et al., 1983). Tipping curve calibrations are performed only during clear weather. The radiometer output at each operating frequency is related to the atmospheric brightness temperature calculated from the absolute absorption (in nepers) by

$$T_b = 2.75 e^{-\tau} + (1 - e^{-\tau})T_{mr} \quad (1)$$

where T_{mr} is a mean radiating temperature of the atmosphere and 2.75 is the cosmic background brightness (both in K). T_{mr} is normally calculated from climatological radiosonde data and was done so for DEN. For SNI, however, T_{mr} was computed from the 69 soundings recorded during July, 1987. The absorptions discussed in parts 4 to 6 are presented in dB which have been computed from the measured brightness temperatures by

$$\tau(\text{dB}) = 4.343 \ln \frac{T_{mr} - 2.75}{T_{mr} - T_b} \quad (2)$$

where the variables are defined in (1).

It should be noted that different humidity sensors were employed by the radiosondes at SNI and DEN. Soundings at SNI were made using Vaisala RS80 radiosondes with HUMICAP humidity sensors. At DEN standard VIZ radiosondes with "yellow element" humidity sensors were employed. Accuracies of 2 percent are claimed by both manufacturers. However, to the authors' knowledge, a rigorous intercomparison of the two units has not been made.

Representative brightness temperatures measured simultaneously at each operating frequency are shown in the time series of Fig. 1 for SNI and DEN. The maxima and higher scintillation rates are associated with liquid-bearing

clouds. Note the relative increase in 90 GHz brightness temperature as clouds pass through the radiometer antenna beam.

3. Attenuation Statistics

The time series of the data was edited in several ways before statistics were computed. First, 24-hr time series of all data were plotted and then visually inspected for the presence of outliers or questionable points. For Denver data, measurements at 20.6 and 31.65 GHz were also available from an adjacent radiometer; these also were used in visual editing. After the preliminary editing was completed, computer screening, based on approximately known physical relationships between the frequencies, was performed. This additional screening eliminated, for example, a segment of data in which snow on the antenna adversely affected the 90.0 GHz channel. After these stringent procedures were applied, there remained a total of 4805 5-min average data for SNI (about 400 hr) and 14181 2-min average data for DEN (about 473 hr). The cumulative probability distributions for the two data sets are shown in Figs. 2 and 3. At all frequencies, the mean attenuation at SNI is about a factor of 2 to 3 higher than at DEN. Several climatic factors are responsible for the differences between the two locations. First, the sea level altitude of SNI results in the dry attenuation always being greater than that at DEN. Second, the mean absolute humidity in SNI is a factor of three higher than at DEN, resulting in a much higher vapor absorption. Finally, the marine stratocumulus clouds of SNI contained measureable liquid 76 percent of the time and were only rarely present at temperatures below 0.0 degrees Celsius; the winter clouds at DEN contained measurable liquid about 15 percent of the time and were frequently supercooled. We are anticipating a completely different set of statistics when we operate at Denver during summer 1988.

4. Clear Air Absorption: Modeling Versus Experiment

The dominant microwave absorption from atmospheric gases in the troposphere arises from water vapor and oxygen, and the modeling of this absorption over the frequency range of 1 to 1000 GHz has been extensively studied by Liebe (1985). For water vapor, Liebe's model uses the known properties of all H₂O spectral lines below 1000 GHz and a Van Vleck-Weisskopf line shape to calculate the absorption. In addition, a "continuum" term, that accounts for contributions from lines above 1000 GHz, as well as from possible dimer contributions, is added to the line contribution. We used data from a recent publication of Liebe and Layton (1987) to model H₂O absorption, as a function of pressure, temperature, and water vapor pressure. Oxygen absorption was modeled using Liebe's formulas and computer software, but with an updated version of O₂ interference coefficients given by Rosenkranz (1988). Our experience has been that the wing absorption at 20.6, 31.65, and 90.0 GHz is sensitive to the value of the O₂ interference coefficients. For example, the constants given by Liebe and Layton gave rise to calculated brightness temperatures at 90.0 GHz that differed from our measurements (and from calculations based on Rosenkranz's values) by about 5 degrees. However, Liebe's and Layton's constants gave slightly better agreement at 20.6 and 31.65 GHz. Thus, for very precise calculations, such as are required in remote sensing, further study may be necessary.

We calculated brightness temperature from radiosonde soundings of temperature, pressure, and water vapor pressure as a function of height.

Since radiosondes do not measure cloud liquid, only data taken under clear conditions can be used for comparison. Tables 1 and 2 show mean and rms differences of measured and calculated brightness temperatures at SNI and DEN.

It is apparent from these tables that the agreement between theory and experiment in calculating clear air brightness temperatures is not completely satisfactory. Fairly substantial differences in the mean brightness temperature are present. However, the low standard deviations of the measurements suggest that the differences may be due to modeling the almost constant dry term. When comparing radiometer measurements with parameters derived from radiosondes, it should always be kept in mind that there are differences in the volumes of air sampled between the two instruments, and that the radiosonde itself is not a perfect instrument. Nevertheless, it seems that the mean differences between theory and experiment are significant, and that minor adjustments in parameters may be necessary.

5. Observations of Attenuation from Clouds

When attempting to verify calculations of microwave emission and attenuation from clouds, a limitation has been that conventional radiosondes do not measure cloud liquid. Even if they did, the highly variable temporal and spatial characteristics of clouds would make comparisons difficult. With our radiometer design of equal beamwidths at all three channels, emission from a common volume can be observed simultaneously. The problem then is to remove oxygen and water vapor emission when clouds are present, and then study the relative cloud effects between the three channels. The procedure that we use is straightforward and seemingly effective. We first establish a lower cloud liquid threshold L_t for the presence of clouds using the 20.6 and 31.65 GHz channels. In the past, this threshold has proven to be effective in separating clear and cloudy conditions. Next, we derive the precipitable water vapor V from the dual-channel measurements. This determination of V has been extensively verified by comparison with radiosondes, and, indeed, is of the same order of accuracy as the radiosonde. For data, whose inferred cloud liquid L is less than L_t , the "clear" set, we derive a regression relation between the measured absorption τ_{clr} and V :

$$\tau_{clr} = A + BV. \quad (3)$$

The frequency dependent coefficients A and B in (3) have the physical significance of dry attenuation and mass absorption coefficient. Finally, for the data set whose inferred L is greater than L_t , the "cloudy" set, we determine the cloud attenuation τ_{cld} by

$$\begin{aligned} \tau_{cld} &= \tau - \tau_{clr} \\ &= \tau - A - BV \\ &= C + DL. \end{aligned} \quad (4)$$

The coefficient D has the physical significance of the mass-absorption coefficient for cloud liquid, while if the procedure of subtracting clear from cloud attenuation were perfect, C would be zero. It should be understood that V in (3) has been derived from the measured 20.6 and 31.65 absorptions in cloudy conditions. We also derive L , but of course the accuracy of this determination has not been experimentally established, although theoretical estimates yield an accuracy of 0.0033 cm rms (Ciotti et al., 1987). Our

results on the relationships between attenuation at the various frequencies will be shown in Section 6; here, in Tables 3 and 4, we will present the results of our regression analyses to determine A, B, C, and D.

The calculations presented in these tables show that there is reasonable agreement between modeling and experiment, but also that, at Denver, in December, where the surface pressure is around 830 mb and the surface temperatures are frequently below zero, perhaps additional refinements are necessary. Since cloud liquid attenuation is sensitive to temperature, perhaps the disagreement between measurements and calculations at 90.0 GHz is significant. We intend to study this as more data become available.

6. Predictability of Attenuation Between Various Frequencies

There exists a fairly extensive amount of brightness temperature data at 20.6 and 31.65 GHz. Since data at 90.0 GHz are not plentiful, and certainly, simultaneous measurements at all three frequencies are scarce, it is of interest to examine their between-channel predictability. Such considerations are of importance when trying to estimate attenuation at various locations, but also for multi-frequency remote sensing, when the consideration of dependent channels is of utmost importance. We determined regression relations between the various channels for clear, cloudy, and all conditions. The form of the linear regression is

$$\tau \text{ (dependent)} = c_0 + c_1 \tau_1 \text{ (independent)} + c_2 \tau_2 \text{ (independent)}.$$

The results of the regression analyses are shown in Tables 5 and 6.

It is clear from Tables 5 and 6 that there is a high degree of predictability between the channels, and that if care is taken to distinguish between clear and cloudy conditions, the correlation coefficients are greater than about 0.90 for the linear regression equations.

7. Conclusions

Atmospheric attenuation at 20.6, 31.65, and 90.0 GHz has been derived from ground-based zenith-viewing microwave radiometers. These radiometers have equal beamwidths at all frequencies and simultaneously view the same common volume of atmospheric emitters. Calibration procedures for these radiometers utilize the "tipping-curve" method, and are independent for each channel. Measurements at two climatically different locations and months, San Nicolas Island, California, July 1987, and Denver, Colorado, December, 1987, have shown reasonable consistency between theory and experiment, both in clear air and during cloudy conditions. During clear conditions, comparisons between measured brightness temperatures and those calculated from on-site radiosondes, have average differences less than 2.9 K and standard deviations less than 1.2 K. The average differences may be due to uncertainties in calculating the wing contribution to absorption from the 60 GHz molecular band of oxygen. We used the most recent absorption models of Liebe and Layton (1987) and Rosenkranz (1988) when calculating absorption and emission from radiosondes. The ratios of cloudy attenuation values are reasonably consistent between the two locations. Probability distributions for attenuation were derived for the two climatologies, and as expected, San Nicolas Island had higher attenuation at all three frequencies than Denver.

Finally, we examined the inter-frequency predictability of the data and demonstrated that any two of the channels could significantly predict the remaining one (correlation coefficients greater than 0.90). This predictability was based on stratifying the data sets into clear and cloudy samples and then using linear regression analysis.

References

- Hogg, D.C., F.O. Guiraud, J.B. Snider, M.T. Decker and E.R. Westwater, "A Steerable Dual-Channel Microwave Radiometer for Measurement of Water Vapor and Liquid in the Troposphere," *J. Appl. Meteor.*, vol. 22, pp. 789-806, May 1983.
- Liebe, H.J., "An Updated Model for Millimeter Wave Propagation in Moist Air," *Radio Sci.*, vol. 20, pp. 1069-1089, Sept.-Oct. 1985.
- Liebe, H.J. and D. H. Layton, "Millimeter-Wave Properties of the Atmosphere: Laboratory Studies and Propagation Modeling," NTIA Report 87-24, pp. 1-80, October 1987.
- Rosenkranz, P.W., "Interference Coefficients for Overlapping Oxygen Lines in Air," *J. Quant. Spectrosc. Radiat. Transfer*, vol. 39, pp. 287-297, 1988.
- Westwater, E.R. and J.B. Snider, "Microwave Radiometer Facilities at the Wave Propagation Laboratory," *Proceedings of NAPEX XI*, JPL D-4647, pp. 24-27, Aug. 1987 (JPL internal document).

Table 1. Comparison between measurements and calculations of brightness temperature. San Nicolas Island, California, July 1987, Sample size = 14

	20.6 GHz	31.65 GHz	90.0 GHz
mean difference (K)	2.88	1.80	1.39
standard deviation (K)	0.65	0.32	1.16

Table 2. Comparison between measurements and calculations of brightness temperature. Denver, Colorado December 1987, Sample size = 22

	20.6 GHz	31.65 GHz	90.0 GHz
mean difference (K)	1.68	1.08	0.46
standard deviation (K)	0.72	0.33	0.97

Table 3. Regression relationships between zenith absorption (dB), precipitable water vapor V (cm), and integrated cloud liquid L (cm). San Nicolas Island, California, July 1987

	20.6 GHz	31.65 GHz	90.0 GHz
clear conditions (L < 0.0033 cm) (N = 3417)			
A (dB)	0.0494	0.1281	0.2392
B (dB/cm)	0.1974	0.0787	0.3328
corr. coef.	0.9995	0.9811	0.9705
clear conditions (calculated from 14 radiosondes)			
A (dB)	0.0812	0.1333	0.2387
B (dB)	0.1759	0.0782	0.3488
corr. coef.	0.9797	0.9595	0.9518
cloudy conditions (L > 0.0033 cm) (N = 14168)			
C (dB)	0.0055	0.0073	0.0183
D (dB/cm)	3.5582	8.1057	45.2292
corr. coef.	0.9338	0.9662	0.9926

Table 4. Regression relationships between zenith absorption (dB), precipitable water vapor V (cm), and integrated cloud liquid L (cm). Denver, Colorado, December, 1987

clear conditions (L < 0.0033 cm) (N = 12015)			
	20.6 GHz	31.65 GHz	90.0 GHz
A (dB)	0.0499	0.1073	0.1881
B (dB/cm)	0.1894	0.0547	0.2575
corr. coef.	0.9967	0.8419	0.7681
clear conditions (calculated from 937 a priori radiosondes)			
A (dB)	0.0373	0.0821	0.1355
B (dB)	0.1811	0.0643	0.3244
corr. coef.	0.9717	0.8205	0.9732
cloudy conditions (L > 0.0033 cm) (N = 2166)			
C (dB)	-0.0030	-0.0065	0.0136
D (dB/cm)	4.5601	10.3796	38.9128
corr. coef.	0.9999	0.9999	0.9728
cloudy conditions (calculated from 500 a priori radiosondes; cloud liquid determined from a cloud model)			
C (dB)	0.0028	0.0074	-0.0812
D (dB/cm)	4.5166	10.1190	52.9839
corr. coef.	0.9922	0.9951	0.9954

Table 5. Regression relations between absorption (dB) at 20.6, 31.65, and 90.0 GHz. San Nicolas Island, California, July 1987. Values in parentheses following the equations are standard error of estimate, the correlation coefficient, and 100 x standard error of estimate/mean, respectively.

clear conditions

(N = 3417)

$$\tau(20.6) = -0.271 - 0.055 \tau(90.0) + 0.266 \tau(31.65), (0.011, 0.986, 3.5)$$

$$\tau(31.65) = 0.086 + 0.141 \tau(90.0) + 0.162 \tau(20.6), (.003, 0.995, 1.1)$$

$$\tau(90.0) = -0.332 - 0.107 \tau(20.6) + 4.50 \tau(31.65), (0.015, 0.991, 2.2)$$

cloudy conditions

(L > 0.0025 cm)

(N = 14162)

$$\tau(20.6) = -0.044 - 0.890 \tau(90.0) + 5.72 \tau(31.65), (0.041, 0.933, 6.3)$$

$$\tau(31.65) = 0.093 + 0.172 \tau(90.0) + 0.089 \tau(20.6), (0.005, 0.999, 1.4)$$

$$\tau(90.0) = -0.539 - 0.460 \tau(20.6) + 5.73 \tau(31.65), (0.029, 0.998, 2.1)$$

all data

(N = 24129)

$$\tau(20.6) = -0.385 - 0.849 \tau(90.0) + 5.43 \tau(31.65), (0.039, 0.939, 9.7)$$

$$\tau(31.65) = 0.087 + 0.175 \tau(90.0) + 0.092 \tau(20.6), (0.005, 0.999, 1.6)$$

$$\tau(90.0) = -0.499 - 0.463 \tau(20.6) + 5.64 \tau(31.65), (0.029, 0.998, 2.5)$$

Table 6. Regression relations between absorption (dB) at 20.6, 31.65, and 90.0 GHz. Denver, Colorado, December, 1987. The numbers in parentheses following the equations are the standard error of estimate, the correlation coefficient, and 100 x standard error of estimate/mean, respectively.

clear conditions

(N = 12105)

$$\tau(20.6) = -0.272 - 0.203 \tau(90.0) + 3.57 \tau(31.65), (0.024, 0.889, 16.1)$$

$$\tau(31.65) = 0.076 + 0.136 \tau(90.0) + 0.108 \tau(20.6), (0.004, 0.972, 3.0)$$

$$\tau(90.0) = -0.396 - 0.252 \tau(20.6) + 5.57 \tau(31.65), (0.026, 0.958, 8.2)$$

cloudy conditions

(L > 0.0033 cm)

(N = 2166)

$$\tau(20.6) = 0.055 + 0.047 \tau(90.0) + 0.443 \tau(31.65), (0.028, 0.956, 12.6)$$

$$\tau(31.65) = 0.019 + 0.178 \tau(90.0) + 0.455 \tau(20.6), (0.028, 0.981, 10.0)$$

$$\tau(90.0) = -0.207 + 0.892 \tau(20.6) + 3.27 \tau(31.65), (0.122, 0.958, 13.3)$$

all data

(N = 14181)

$$\tau(20.6) = 0.084 + 0.139 \tau(90.0) + 0.107 \tau(31.65), (0.040, 0.802, 25.2)$$

$$\tau(31.65) = 0.056 + 0.242 \tau(90.0) + 0.014 \tau(20.6), (0.014, 0.984, 9.0)$$

$$\tau(90.0) = -0.229 + 0.279 \tau(20.6) + 3.78 \tau(31.65), (0.056, 0.985, 13.7)$$

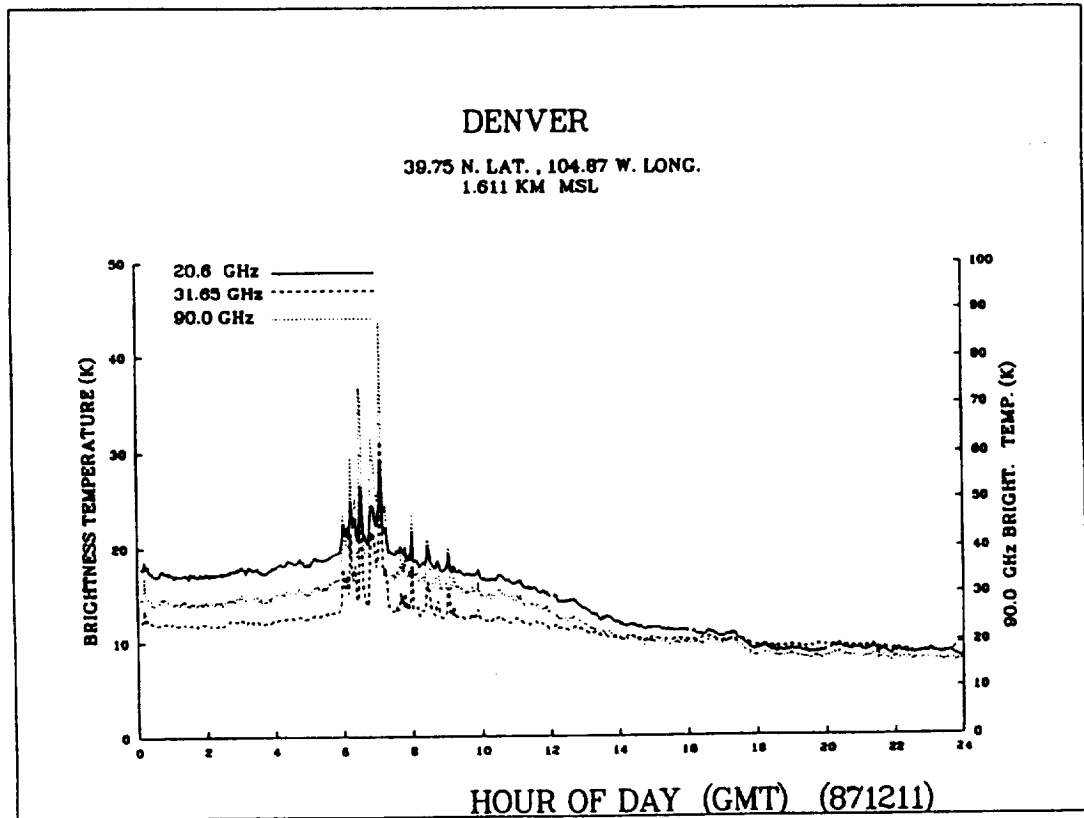
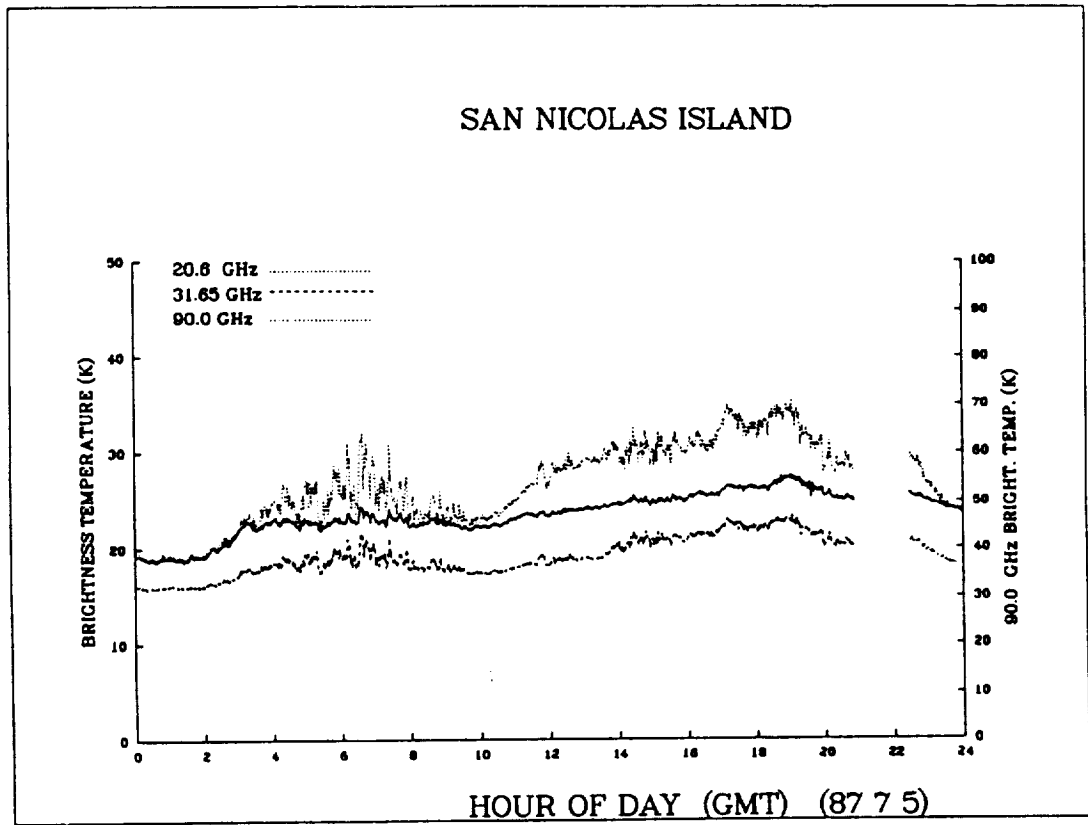


Fig. 1. Time series of brightness temperatures measured by 3 channel radiometer at San Nicolas Island and Denver.

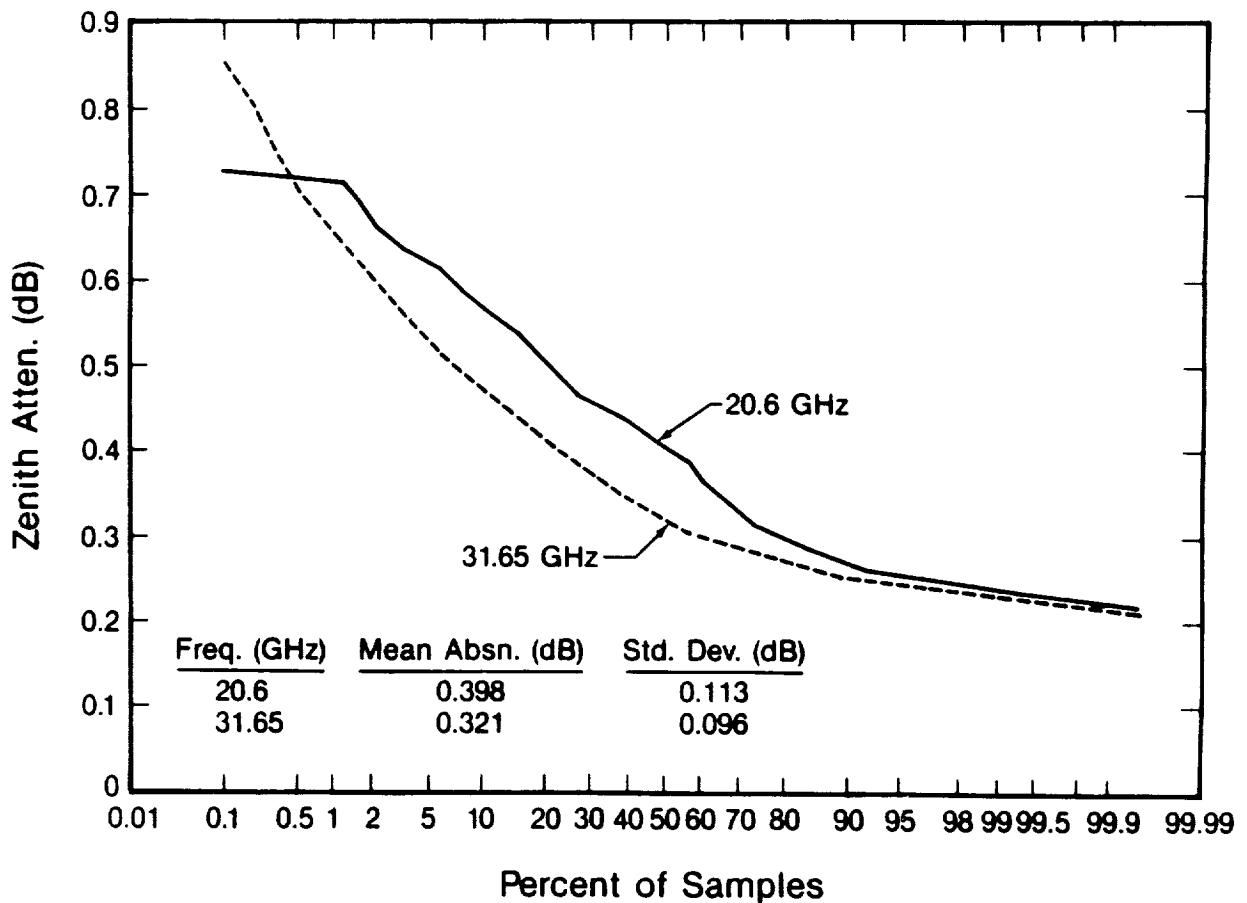
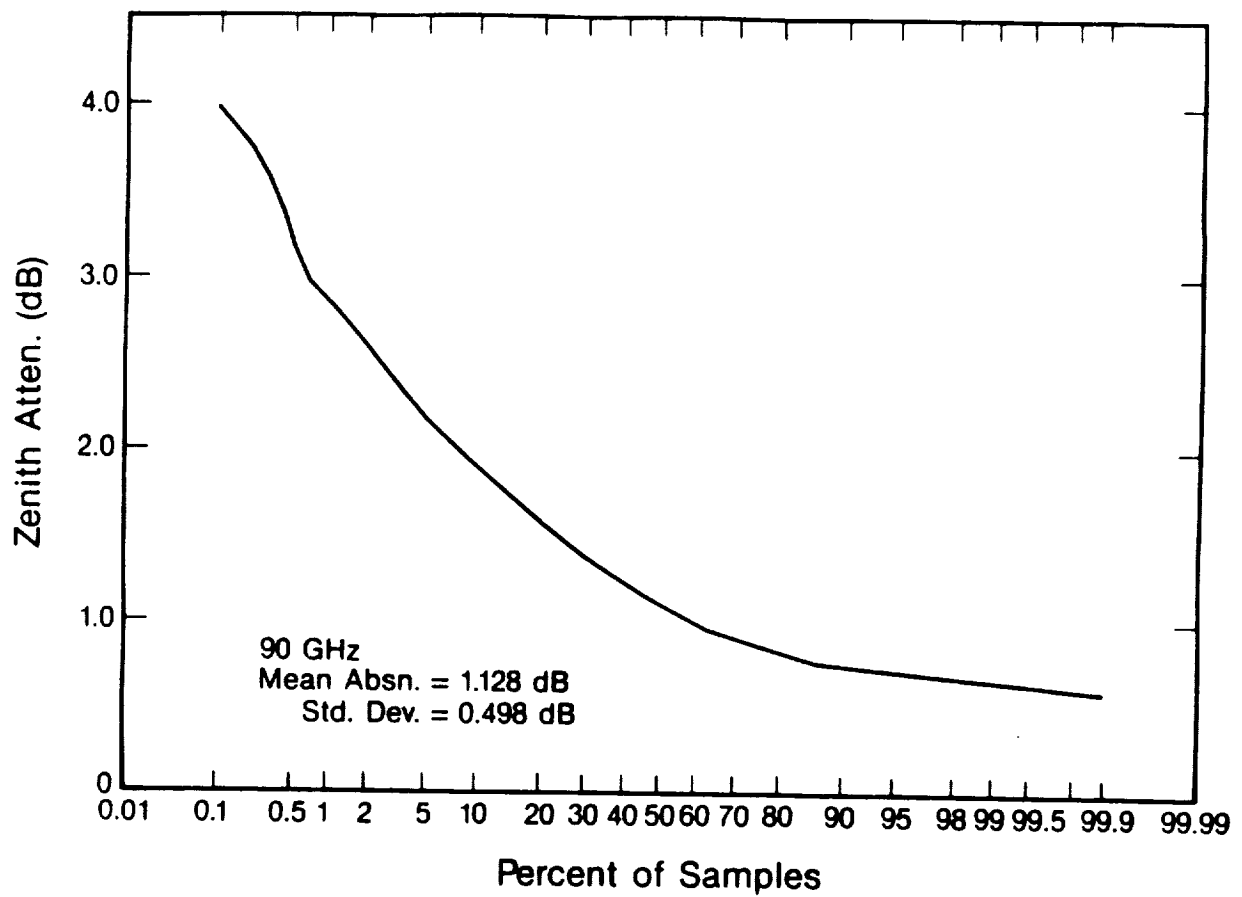


Fig. 2. Cumulative distribution of zenith attenuation measured by 3 channel radiometer at San Nicolas Island, July 1987. 4805 five-minute averages.

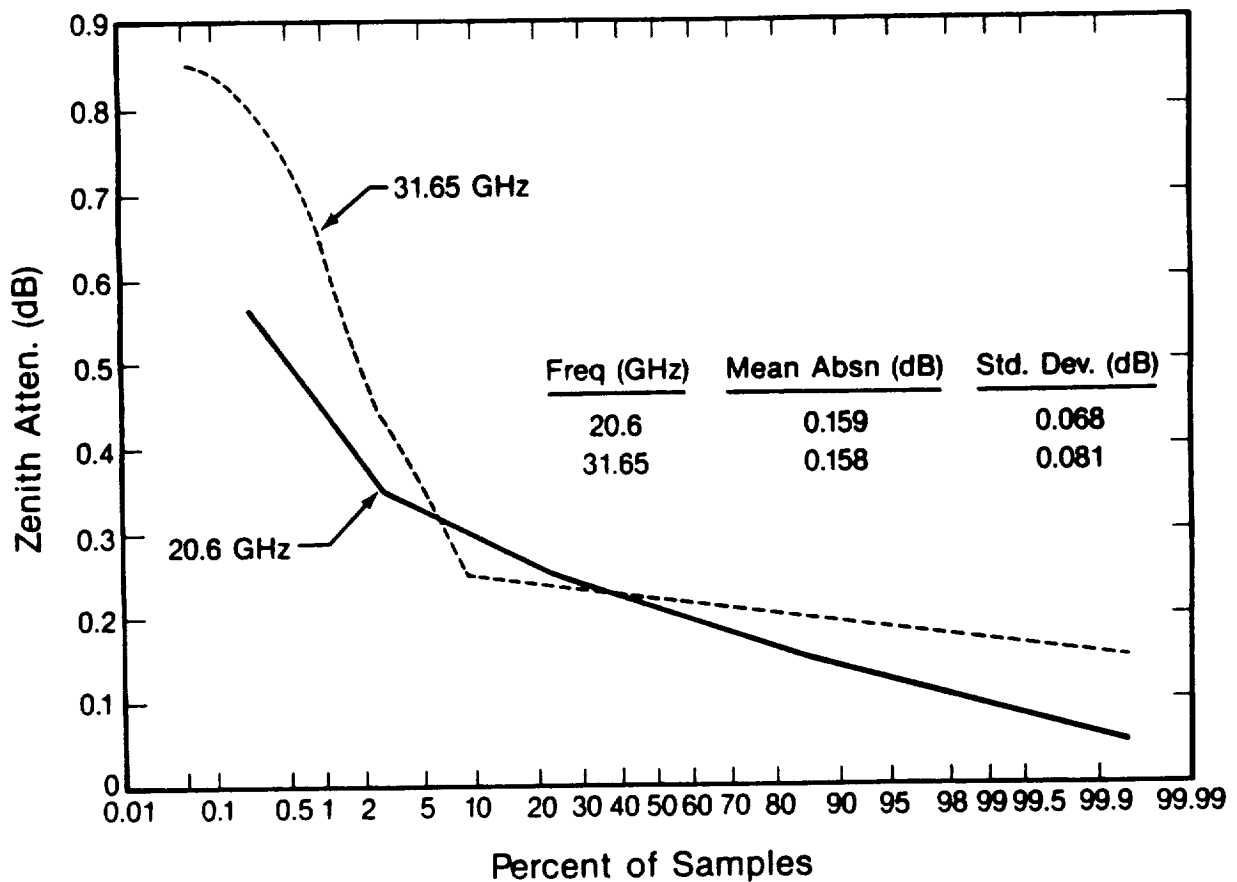
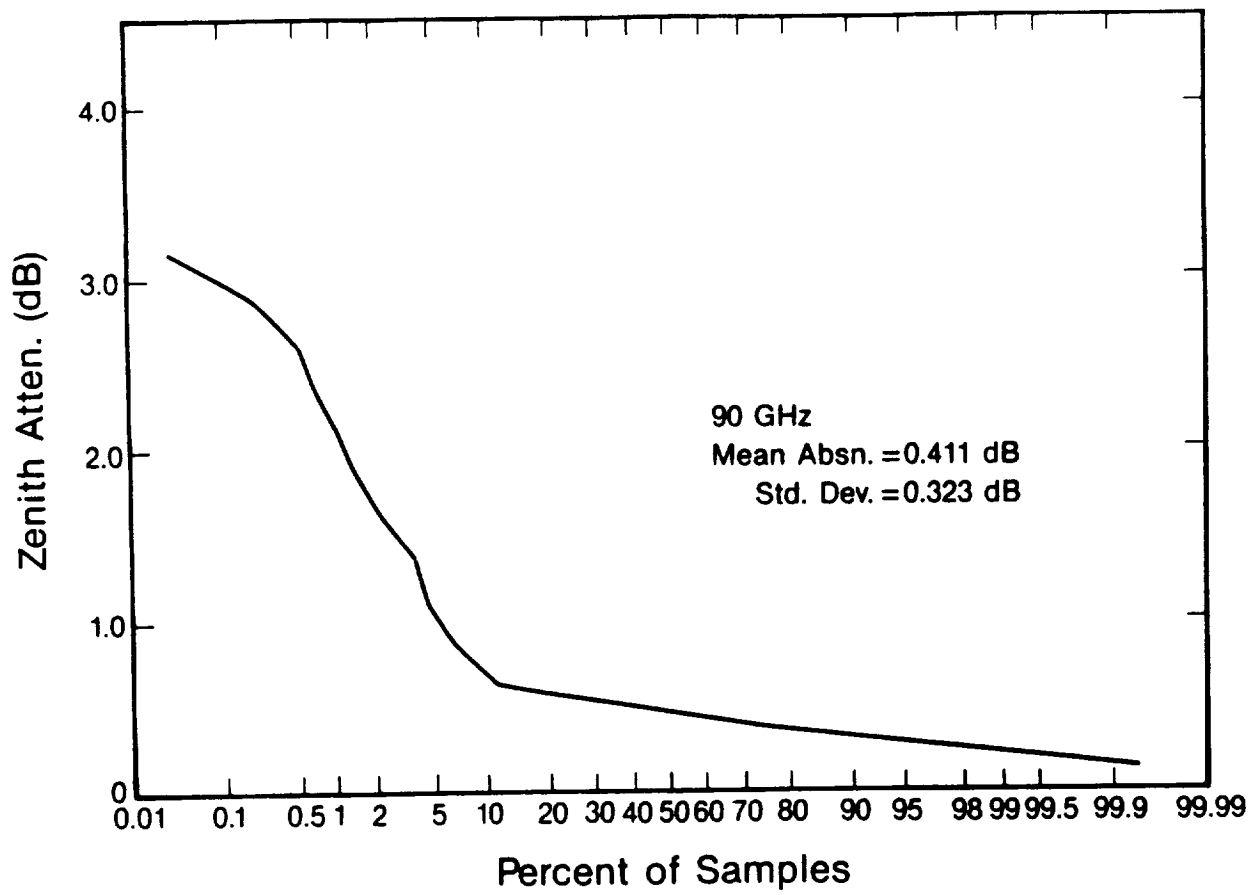


Fig. 3. Cumulative distribution of zenith attenuation measured by 3 channel radiometer at Denver, Colorado, December 1987. 14181 two-minute averages.

Laser Communications Through the Atmosphere

Kamran Shaik

Jet Propulsion Laboratory
California Institute of Technology
Pasadena, California 91109

J. H. Churnside

National Oceanic and Atmospheric Administration
Environmental Research Laboratories
Boulder, Colorado 80303

Abstract

Atmospheric properties affecting laser propagation with reference to optical communications are reviewed. Some of the optical space network configurations and various diversity techniques that may need be utilized to develop robust bi-directional space-earth laser communication links are explored.

1. Introduction

The interest in laser optical communications follows a dominant trend in communications systems research. Communications systems with higher carrier frequencies are inherently capable of operating at higher antenna gain and modulation bandwidth. Optical frequencies ($\approx 10^{14}$ Hz) are several orders of magnitude higher than the operating carrier frequencies of the conventional radio frequency (RF) communication systems ($\approx 10^{10}$ Hz) in use today. The promise of large antenna gain and enormous modulation bandwidth, which become available at optical frequencies, provide basic reasons for the compelling interest shown by commercial, civilian, and military establishments in the development of optical communication systems.

For similar modulation depths, the gain in the available bandwidth will be about 10^4 -fold for optical communication systems. Also, for a given transmitter antenna size, the angular beamwidth is inversely proportional to the carrier frequency and the spatial power density at the receiver corresponds to the square of the frequency. This implies, for example, that the power density at the receiving aperture will be 10^6 times larger for an optical system with a 0.1 m antenna operating at 10^{14} Hz than for a system with 10 m antenna operating at 10^9 Hz. Optical systems with bit rates higher than a Gbit/s without multiplexing have been achieved; with various types of multiplexing 10^5 Gbit/s data rate is possible [1].

Optical systems also promise to be smaller in size and weight and have lower power consumption as compared to RF systems with similar performance characteristics. A decrease in the equipment size is very desirable as it will result in lower costs to put communication satellites in space. In the case of other space missions, the advantage of size and weight will leave more room for scientific payloads and allow for more flexibility in spacecraft design.

Since optical transmitters experience relatively much lower diffractive spreading, optical communications provide excellent means for the design of secure systems with low probability of intercept and, intentional or unintentional, jamming. Tight laser beams also provide extensive opportunities for frequency reuse.

In short, laser communication technology has the potential to provide (i) an enormous data bandwidth

for significantly improved channel performance, (ii) a significant advantage in weight, size, and power consumption over RF systems, and (iii) non-interacting multiple access link geometries that are amenable to extensive frequency reuse, and secure systems with low probability of interception and jamming.

The commercial interest in laser communications is focused on the development of a high quality multiplexed voice, video, and data transmission network. The commercial sector envisions a network of satellites and ground stations to move information efficiently on a global scale. However, there is strong competition from the relatively mature fiber optic technology for point-to-point communications. Since the terrestrial and under-sea fiber links between the continents are being under-utilized at present, the commercial sector, at least for the short term, has lost some of its enthusiasm for the development of a global satellite communications network.

The civilian interests are based on the need to develop high throughput real time data transfer mechanisms for remote sensing or earth resource satellites in low earth orbits. The data from low earth orbiting satellites will, perhaps, be first transmitted to strategically placed geosynchronous satellites for subsequent transfer to appropriate ground station. Other applications include communication links to science probes in deep space for planetary and extra-planetary exploration.

2. Optical Communications in Atmosphere

The atmospheric channel for optical communication is characterized by (i) attenuation due to scattering and absorption by molecules and other particulate matter, (ii) diffractive and turbulent beam spreading, (iii) log-normal fading due to scintillation, (iv) a coherence bandwidth of 10^{10} Hz or greater, (v) a long coherence time (~ 1 msec), (vi) a significant wavefront distortion, which, among other things, limits the power collecting capability of a diffraction limited receiver, and (vii) background noise from stellar and earth-based light sources [1-4].

Shapiro and Harney [5] have developed an expression for the received power, $P_R(t)$, in terms of the transmitted power, $P_T(t)$, and relevant atmospheric propagation effects. Neglecting the propagation delay and background noise effects, we have

$$P_R(t) = P_T(t) (D_R^2 / \pi \theta_T^2 Z^2) \epsilon \exp[-\tau] \exp[2u(t)], \quad (2.1)$$

where $(D_R^2 / \pi \theta_T^2 Z^2)$ represents free space propagation loss in terms of receiver diameter D_R , transmitter beam divergence θ_T , and path length Z . ϵ is the efficiency of the optical system, τ is the optical depth for the propagation path due to scattering and absorption, and $u(t)$ is the time varying aperture-averaged log-amplitude fluctuation due to turbulence. $\exp[2u(t)]$ is, then, the time varying aperture-averaged irradiance fluctuation at the receiver.

The only noticeable effect of scattering and absorption due to gas molecules, aerosols, and other particulate matter in the atmosphere is signal attenuation. The optical depth τ in eq. (2.1) expresses this attenuation loss (Bouguer's law). If $\gamma_t(z)$ at position z is the total scattering and absorption coefficient due to various atmospheric constituents, the optical depth is given by

$$\tau = \int_0^Z \gamma_t(z) dz, \quad (2.2)$$

where Z is the distance over which the laser light travels through the atmosphere.

Eq.(2.1) disregards the effect of fluctuations in the angle of arrival at the receiver. In heterodyne systems this leads to a loss in the mixing efficiency. For direct detection schemes, the focused signal moves randomly in the image plane affecting energy collection capabilities of the system at the detector. It has been shown that incorporation of tilt correction techniques into the receiver system can result in improvements as high as 8 dB [6].

Scintillation and loss of communication link due to opaque clouds are two of the most important problems, and will be discussed in the following paragraphs. We will also look at some of the possible optical space network (OSN) configurations and explore various diversity techniques.

2.1 Scintillation

Scintillation causes fades and surges in received signal power. These fades may be as long as 10 msec, which is long enough to wipe out an entire message packet. The fade level, F in dB, is defined as [7]

$$F = -10 \log[I(t)/I_m], \quad (2.3)$$

where I_m is the mean and $I(t)$ is the instantaneous irradiance observed. Yura and McKinley [7] have developed various results to compute the fraction of time that a fade exceeds some given value. For the worst case scintillation, fades exceeding 3 dB occur more than 50% of the time and fades exceeding 10 dB occur more than 10% of the time. For more reasonable values of scintillation strength, fades exceeding 10 dB occur only 1% of the time.

An obvious strategy to counter scintillation effects is to incorporate sufficient excess margin into the optical link. With this approach for an earth-space link, a margin of 20 dB will be necessary for the system to work properly 99.9% of the time under worst case scintillation. However, this costly solution to the problem can be avoided by employing temporal diversity. These methods include simple repetition of the message, coding, and interleaving. If coding is used, a careful matching of coding schemes to the channel can provide substantial improvement in performance [8].

2.2 Opaque Clouds

Another aspect of the problem that is not readily apparent from eq.(2.1) is the non-zero probability of opaque cloud cover. Presence of thick clouds, in general, will have a catastrophic effect on the availability of an optical communication link. Though scattered laser light is available for communication, the system has to be designed to have (i) a wide field of view to collect enough power, which greatly increases the background noise and (ii) a low data rate to avoid inter-symbol interference due to pulse spreading. Also, polarization coding of the signal can not be used as the scattered light is depolarized. An optical communication system designed to employ the scattered beam, then, quickly loses its advantages over the conventional systems.

An OSN for optical communications can be designed to avoid the clouds by employing spatial and temporal diversity. We need to identify sites for the installation of optical receiver/transmitter stations where the clouds have a low probability of occurrence. Several such sites with uncorrelated weather patterns may need be operated simultaneously to obtain desired link availability.

Cloud cover exhibits a number of cycles, nocturnal, diurnal, seasonal, and long range. A large number of databases, statistical studies, and computer models are available in the literature which describe and simulate cloud behavior. However, it is not clear how much of it is useful or relevant to optical communications. A concrete view of the OSN is essential to help identify available information that may be worthwhile for our purposes. We will discuss two representative configurations of an OSN and see how spatial diversity can be employed to develop robust communication links.

2.2.1 Dispersed Direct Link

The network may be designed to have 6-9 receiving stations roughly equidistant from each other, and placed around the globe near the equatorial region. The inter-station distance would be roughly 5000 km and

the individual sites will be chosen for their high probability of having clear weather. Since the characteristic scale of a weather pattern or a climatic zone is of the order of a few hundred kilometers, the adjacent stations would lie in different climatic regions and thus have uncorrelated cloud cover statistics. For satellite-earth links with tight laser beams, the pointing capability of the spacecraft telescope may be employed to hand-off the communication channel to appropriate ground station. We will need to work out joint cloud cover statistics for two or more consecutive sites for link availability. In cases where the spacecraft is several light-hours away, it would be necessary to develop models with the ability to predict future cloud cover statistics. The probability of an outage for this configuration will be low because (i) several stations are monitoring the signal jointly or the spacecraft has the ability to point to one of several stations by choosing the optimum site for cloud-free optical communication, and (ii) the stations lie in different climatic zones and hence their weather patterns are uncorrelated. Since the receiving sites are far apart, there is no initial need to obtain high resolution data on cloud cover. Later, to examine and validate a short list of likely sites high resolution site specific data will be required. The temporal resolution of the data has to be high to compute short-term outage statistics accurately. For validation purposes we will need to do a cloud-free line of sight (CFLOS) and cloud-free arc (CFARC) analysis to compute outage probabilities for single sites as well as jointly for two or more sites. (discussed below).

2.2.2 Clustered Direct Link

For economical, geophysical, or geo-political reasons, the OSN may consist of only 3-4 locations around the globe, chosen for their optimally cloud-free skies. In this configuration, one may build a cluster of two or more autonomous receiving stations on each of these locations. Note that this geometry also includes the case where a single geosynchronous satellite, which accepts messages from other satellites, planes, and ground stations, is linked to a single cluster of receiving stations. Let us consider an extreme situation where the receiving stations are only a few tens of kilometers apart from each other at each of the selected regions. For a major portion of the time the spacecraft can point to only one of these clusters, handing-off the signal beam to the next cluster as it rises above the horizon.

We will need to do most of the studies listed in the preceding section to determine the suitability of sites for ground stations. However, spatial resolution on sky cover in this case needs to be very high (about an order of magnitude better than the distance between the ground sites). The stations would all be in the same climatic zone, and hence their weather patterns will be correlated. An ultra-high temporal resolution may be necessary to extract meaningful statistics. The outage times when all the ground stations are unable to receive will happen more often, and will be of longer duration when compared to the dispersed configuration discussed in sec. 2.2.1 above for the same number of receivers on ground.

2.3 Weather Models and Simulations

Almost all data and statistics currently available on cloud cover is not readily amenable to the study of optical communications through the atmosphere. The next best thing to do is to use available weather data, which is incomplete and insufficient, as a guide to develop computer models and simulations that mimic real time dynamic behavior of clouds. An early model for cloud cover was developed by scientists at SRI International. Work at AFGL, which is based on the SRI model, has produced considerably sophisticated computer simulations of cloud dynamics. The computer programs developed by AFGL may be used to compute cloud-free line of sight (CFLOS) or cloud-free arc (CFARC) probabilities for any site. It is also possible to compute joint CFLOS and CFARC probabilities for two or more sites. These statistics, needless to say, are of great importance to the development of an OSN.

Shaik [9] has proposed a preliminary weather model that may be used to compute link availability statistics. The model may be used to predict joint probability for the percentage time for which weather

is such that the extinction loss through the atmosphere is less than some threshold for at least one of the ground stations. If $\omega_n(\tau)$ is the cumulative distribution function (CDF) giving percentage weather for n sites for which at least one of the sites has an optical depth of the atmosphere less than or equal to τ , then the model states that

$$\omega_n(\tau) = 1 - [q \exp [-b(\tau - \tau_0)]]^n, \quad (\tau \geq \tau_0), \quad (2.4)$$

where τ_0 is an empirical constant representing the minimum possible optical depth of the atmosphere associated with an average clear day, b is a site-dependent parameter to model the slope of the CDF curve, and q is the probability of non-clear skies and is assumed, for simplicity, to be the same for all sites. The probability of non-clear skies, for example, in the southwestern US are less than 0.4 and the worst case value for the parameter b is 0.03 [10]. Hence, for a single site in the southwestern U.S. with $q = 0.4$, $\tau_0 = 0.6$, and $b = 0.03$, the probability that the optical depth $\tau \leq 1.0$ (-4.3 dB) is $\omega_1(\tau = 1) = 0.61$. If there are three such independent and identically distributed sites, we have $\omega_3(\tau = 1) = 0.94$. In other words, if a system is designed to absorb extinction loss of 4.3 dB, a three-site receiving network will be functional 94% of the time. However, it is not very clear how the independence of weather patterns at various sites can be insured. It is known, as noted earlier, that the scale size of weather patterns is of the order of a few hundred kilometers, and this measure may be used to find sites with uncorrelated weather. Joint observation of weather parameters for the probable sites will be necessary to make a more accurate determination.

2.4 Other Diversity Techniques

We have discussed path or site diversity in some detail in the sec. 2.3 as it appears to be one of the most important techniques for the design of robust optical communication links. We have also touched on temporal diversity to overcome short-term turbulence induced fades. Brandinger [11] and Engelbrecht [12] have suggested a number of other diversity techniques. Some of these are (i) frequency diversity, (ii) transmitter power diversity, and (iii) transmission delay or temporary data storage diversity.

Apart from strong molecular scattering and absorption lines, the effect of the atmosphere on optical frequencies does not change much over the entire range. For example, the refractive index of the atmosphere changes by 10% and the effect of changing humidity is quite small for all optical frequencies. It may be concluded that the use of frequency diversity can not provide acceptable engineering gain in system design.

The use of transmitter power diversity can be a feasible solution to counter the loss through the atmosphere, especially for the uplink configuration. The power output of ground lasers may be adjusted so as to maintain a constant power level at the spacecraft receiver. However, the transmitter configurations on spacecraft at present must use maximum attainable laser power leaving little room for the use of power diversity.

Temporary storage diversity is an attractive alternative, but only when real time operation is not necessary.

3. Conclusion

We have discussed some of the pressing problems that need to be investigated in depth to acquire necessary know-how for the development and design of an optical communication link through the atmosphere.

Scattering and absorption attenuate the signal. It is therefore necessary to use higher transmitter power to maintain a given irradiance level at the receiver when the laser beam must travel through the atmosphere rather than free space.

Refractive turbulence causes log-normal fading of the signal. This problem can be handled by increased signal power or by the use of temporal diversity. Refractive turbulence also degrades spatial phase front

of the signal. Coherent detection methods, which depend on the integrity of the phase front, are relatively more sensitive to this type of degradation than the direct detection systems. Other effects of atmospheric turbulence like pulse broadening and signal depolarization are quite small and can be neglected.

The most effective strategy to counter the problem of opaque clouds is to employ spatial diversity. For three well-chosen sites it is possible to get 94% link availability. However, we note that there is a dearth of quantitative results and directly applicable data in the field. Development of reliable weather models is contingent upon the acquisition of useful data and site-specific statistics.

4. References

1. Kerr, J.P. et al, "Atmospheric Optical Communications Systems", Proc. IEEE, vol.58, no.10, pp.1691-1709, 1970.
2. Brookner, E., "Atmosphere Propagation and Communication Model for Laser Wavelengths", IEEE Trans. Com., vol. COM-18, no. 4, pp.396-416, 1970.
3. Lawrence, R.S. and Strohbehn, J.W., "A Survey of Clear-Air Propagation Effects Relevant to Optical Communications", Proc. IEEE, vol.58, no.10, pp.1523-1545, 1970.
4. Shapiro, J.H., "Imaging and optical communication through atmospheric turbulence" in Topics in Applied Physics, Vol. 25, Springer-Verlag, NY, 1978.
5. Shapiro, J.H. and Harney, R.C., "Simple algorithms for calculating optical communication performance through turbulence", Proc. SPIE, vol. 295, pp. 41-54, 1981.
6. Fante, R.L., "Electromagnetic Beam Propagation in Turbulent Media: An Update", Proc. IEEE, vol.68, no.11, pp.1424-1443, 1980.
7. Yura, H.T. and McKinley, W.G., "Optical Scintillation Statistics for IR Ground-to-Space Laser Communication Systems", Appl. Opt., vol.22, no.21, pp.3353-3358, 1983.
8. Chan, V.W.S., "Coding for the Turbulent Atmospheric Optical Channel", IEEE Trans. Com., vol.COM-30, no.1, 1982.
9. Shaik, K.S., "A preliminary weather model for optical communications through the atmosphere", TDA progress report, Jet Propulsion Laboratory, to be published.
10. Wylie, D.P. and Menzel, W.P., "Cloud cover statistics using VAS", SPIE's OE-LASE '88 Symposium on Innovative Science and Technology, Los Angeles, CA, 10-15 Jan., 1988.
11. Brandinger, P., "Propagation requirements for 30/20 GHz systems design", Spring USRI Meeting, Washington, D.C., 1978.
12. Englebrecht, R.S., "The effect of rain on satellite communications above 10 GHz", RCA Review, vol. 40, p. 191, 1979.

PLAN OF PROPAGATION AND COMMUNICATION EXPERIMENTS USING ETS-VI

Shingo Ohmori
 Kashima Space Research Center
 Communications Research Laboratory
 Ministry of Posts and Telecommunications
 Kashima, 314 Japan

Abstract--In 1992, an Engineering Test Satellite VI is scheduled to be launched by an H-II rocket. The missions of ETS-VI are to establish basic technologies of inter-satellite communications using millimeter waves and optical beams and fix satellite communications using multibeam antenna on board the satellite. Several kinds of frequency bands will be used for the communications missions, however, these frequencies can be used for propagation experiments.

1. Introduction

An Engineering Test Satellite VI (ETS-VI) is a 2-ton class, three axis stabilized satellite, which is scheduled to be launched in August 1992 by an H-II rocket. One of main missions of the ETS-VI is to develop basic technologies for advanced satellite communication systems in the future. Almost all experiments will be focused on subjects such as millimeter waves, inter-satellite and optical communications, however, propagation experiments will be carried out using 2.5GHz, 25GHz and 40 GHz frequency bands.

2. Experimental system

The ETS-VI has basic missions to establish advanced satellite technologies such as inter-satellite communications, mobile satellite communications and fix satellite communications (Shiomi et al; 1988) (Nakagawa et al; 1988). CRL has three missions as shown in Fig.1, and these are summarized as follows.

(1) S-band inter-satellite communications

Communications Research Laboratory (CRL) develops S-band multiple access data relay and tracking system (2.3/2.1 GHz) with 19-element phased array antenna in cooperation with NASDA. Data relay and tracking experiments between ETS-VI and low orbit satellites are planned. Figure 2 shows a concept of a S-band and optical inter-satellite communication system.

(2) Millimeter wave inter-satellite and personal satellite communications

CRL develops millimeter wave (43/38 GHz) transponder on the basis of research through the ETS-II (1977) and ECS (1979) satellite programs. The objectives of millimeter wave mission are to develop high data rate inter-satellite communication technology and to study the feasibility of personal satellite communication system. Figure 3 shows a concept of this mission.

(3) Optical inter-satellite communications

CRL develops optical communication system with a telescope of 75 mm in diameter, which has a beam pointing/tracking mechanism with a gimbal mirror. The onboard system has fundamental optical communication functions with a laser diode transmitter of wave length 0.83 micron, laser beam point-ahead mechanism, a receiver of wavelength 0.51 micron, modulation/demodulation subsystems, and so on. Figure 4 shows the concept of this mission.

3. Frequency bands for propagation experiments

The following frequency bands, which are used for corresponding missions, can be used for propagation experiments.

2.3/2.1 GHz	S-band inter-satellite communications
2.6/2.5 GHz	Mobile satellite communications
30/20 GHz	Feeder links for the ETS-VI
32/23 GHz	Ka-band inter-satellite communications
43/38 GHz	Millimeter wave communications

4. Conclusion

Experiments on advanced satellite communications will start in 1992 using an ETS-VI satellite. Propagation experiments are scheduled to carry out with several frequency bands such as 2 GHz, 20 GHz and 40 GHz.

References

- Shiomi, T. et al; "Plan of Advanced Satellite Communications Experiment Using ETS-VI," International Symposium on Space Technology and Science (ISTS), Sapporo, May 1988.
- Nakagawa, K. et al; "Fixed and Mobile Multibeam Communications Experiment Payload for ETS-VI," ISTS, Sapporo, May 1988.

ORIGINAL PAGE IS
OF POOR QUALITY

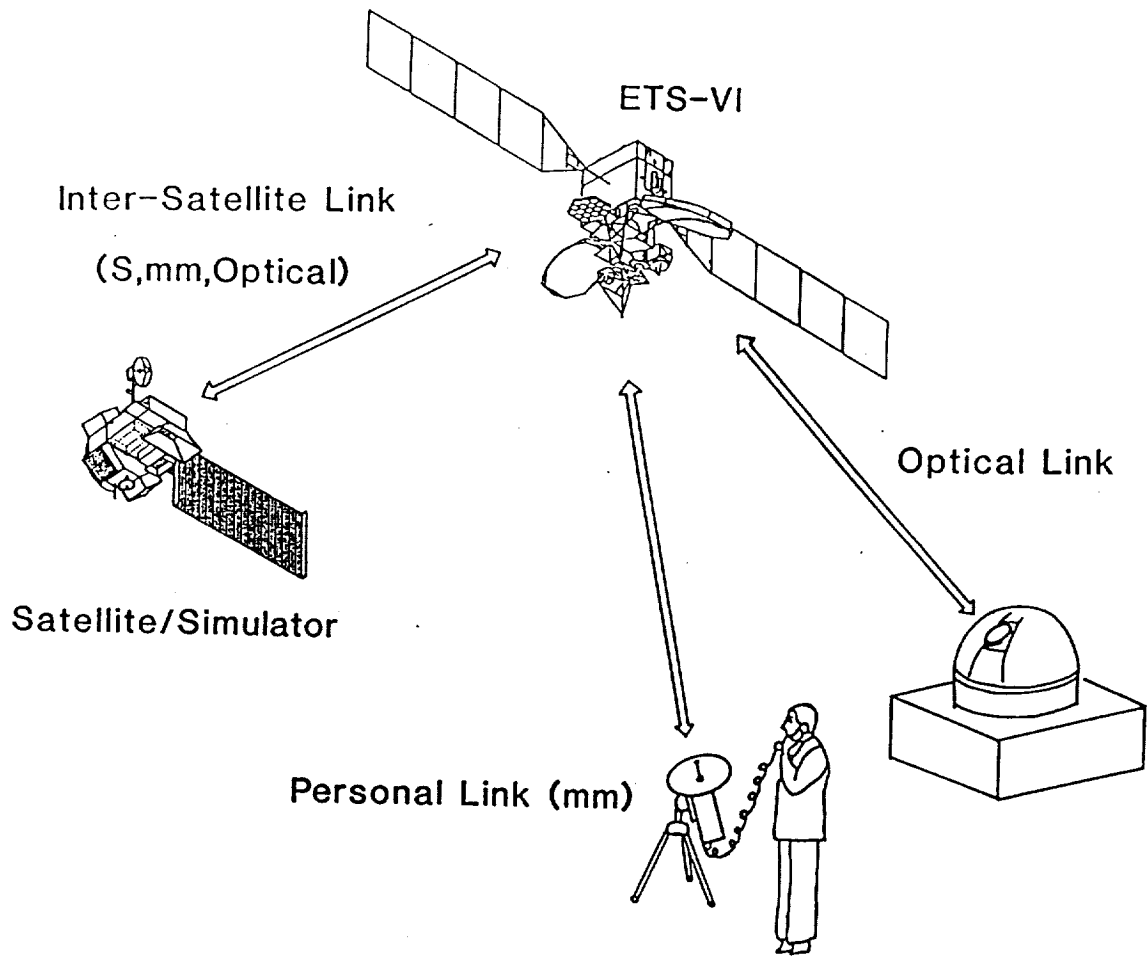


Fig.1 Advanced Satellite Communications Experiment

(CRL)

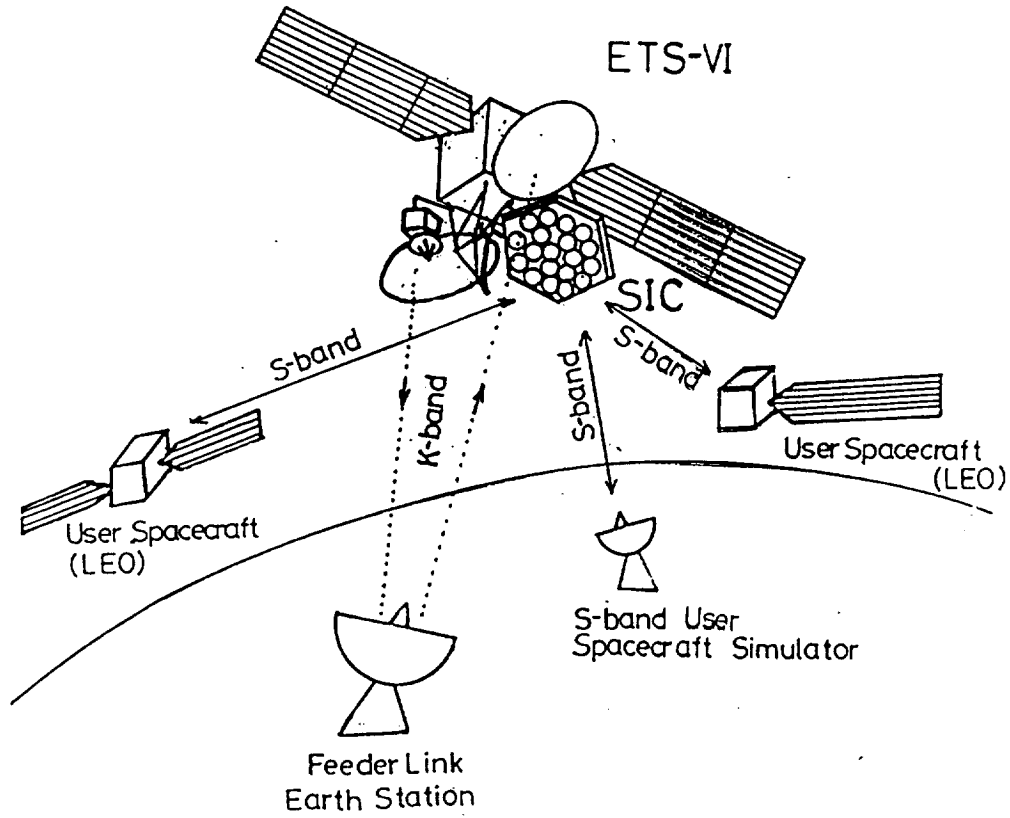


Fig.2 S-band Tracking and Data Relay

ORIGINAL PAGE IS
OF POOR QUALITY

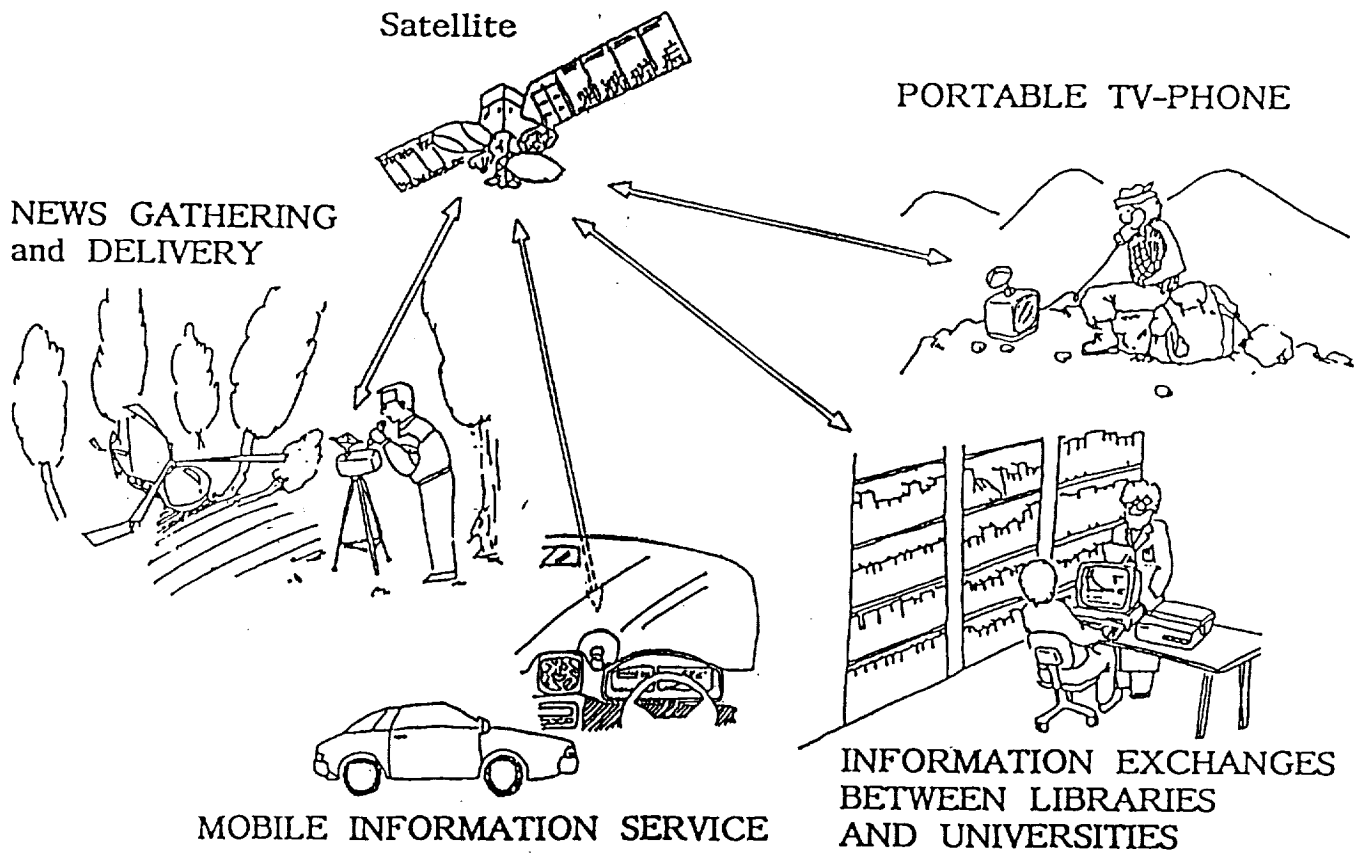


Fig.3 Millimeter-wave Personal Satellite Communications System

ORIGINAL PAGE IS
OF POOR QUALITY.

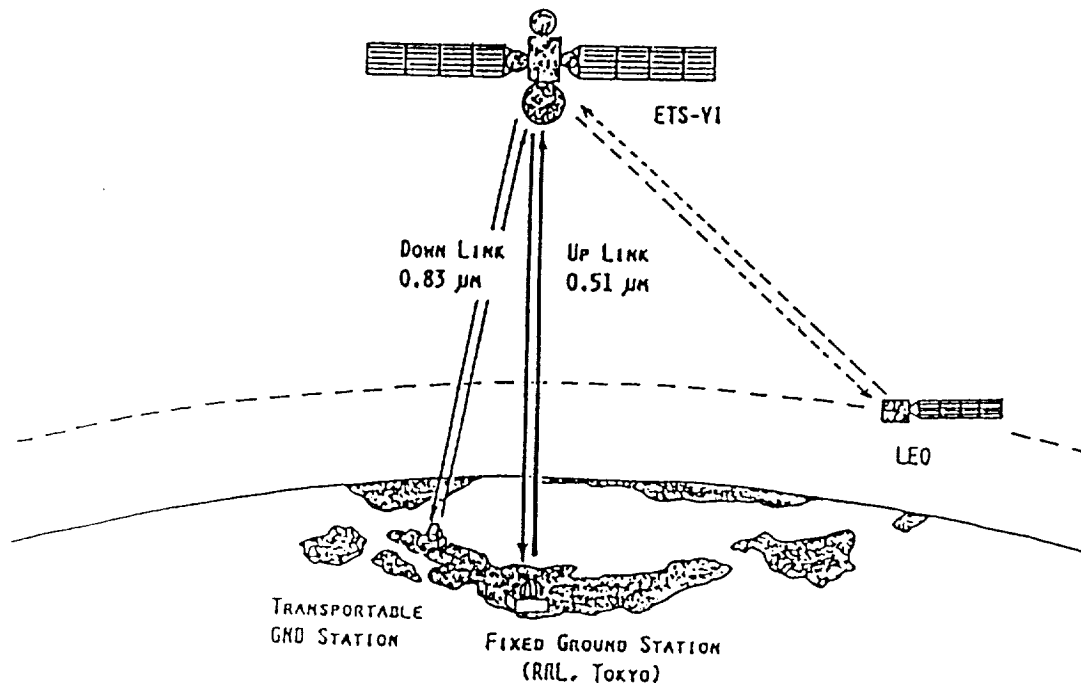


Fig.4 Optical Satellite Communication

Plan of Advanced Satellite Communications Experiment Using ETS-VI

Tadashi Shiomi
Space Systems Section, Space Communications Division
Communications Research Laboratory
Ministry of Posts and Telecommunications

4-2-1 Nukuikita-Machi, Koganei-Shi, Tokyo 184, Japan
Phone : 0423-21-1211
Telefax: 0423-24-8966

Communications Research Laboratory (CRL, Ministry of Posts and Telecommunications, Japan) has been engaged in development of three advanced satellite communication payloads aiming at experiments by Japan's 2-ton class Engineering Test Satellite VI (ETS-VI) which is to be launched in H-II rocket by NASDA in August 1992.

CRL's three experimental systems are:

(1) S-band inter-satellite communications

CRL develops S-band multiple access data relay and tracking system with 19-elements phased array antenna in cooperation with NASDA. Data relay and tracking experiments between ETS-VI and low altitude earth orbiting satellites such as ADEOS (Advanced Earth Observing Satellite to be launched by NASDA in 1993) are planned. A user satellite simulator on the ground will also be used for fundamental and applied experiments. The system has capability of data relay at less than several Mbps, and is designed to keep inter-operability with SMA(S-band Multiple Access) system of NASA TDRSS.

(2) Millimeter-wave inter-satellite and personal-satellite communications

CRL develops millimeter-wave (43/38 GHz) transponder to use high frequency bands in satellite communications on the basis of research through ETS-II(1977) and Japan's ECS(1979) projects. The objective of the millimeter-wave mission is twofold. The first is to develop high data

rate inter-satellite communication technology and the second is to investigate personal satellite communication systems. The onboard system has 40 cm dish antenna and is installed on a gimbal platform of ETS-VI. A solid state power amplifier of 0.5 w output power is under development for the transponder. A possible user spacecraft for inter-satellite link is Japanese Experimental Module of the Space Station. Personal communication terminals with 30 cm-class antennas can communicate each other at the data rate of about 16 kbps. Ground stations with antennas of various sizes will also be prepared for experiments to demonstrate a personal communications concept.

(3) Optical inter-satellite communications

CRL develops experimental optical communication system with telescope of 75 mm diameter which has gimbal mirror beam pointing/tracking mechanism. The onboard system has fundamental optical communication functions with laser diode transmitter of wavelength 0.83 micron, laser beam point-ahead mechanism, receiver of wavelength 0.51 micron, modulation/demodulation subsystem, and so on. Various basic experiments simulating inter-satellite link are planned. In the experiments two optical ground stations are used, one is a fixed station with 1.5 m telescope and the other is a transportable station.

OPEX - Olympus Propagation Experiment

by Gert Brussaard, Dr. Ir.

European Space Technology Centre
Noordwijk, the Netherlands

The Olympus propagation mission

The Olympus-1 satellite carries four distinct payloads for experimental utilisation and research in the field of satellite communications:

- the Direct Broadcasting Service (DBS) Payload
- the Specialised Services Payload
- the 20/30 GHz Advanced Communications Payload
- the Propagation Payload.

Experimental utilisation of the first three payloads involves ground transmissions to the satellite and hence sharing of available satellite time among experimenters. This is coordinated through the Olympus Utilisation Programme.

The Beacon Payload consists of three microwave transmitters that produce three unmodulated CW (Continuous-Wave) signals through three individual horn antennas. The beacon signals are designated B0, B1 and B2, respectively. B0 is at 12.5 GHz and provides 10 dBW of radiated power (EIRP) over the entire visible earth. The horn antennas for B1 and B2 are designed to cover W. Europe with an EIRP of 24 dBW. High EIRP, and hence high flux density on the ground allow the use of relatively small earth stations, with antenna diameters ranging from 1 to 6 meters. The beacon frequencies are all derived from a common oscillator through multiplication chains. This allows coherent detection of all three beacons, providing possibilities for special experiments and several alternatives for earth station design. An interesting feature of the coverage of the 20 and 30 GHz (B1 and B2) beacons is that reception from the U.S. and Canadian East coast is not excluded, albeit with reduced signal power and stability (see Proceedings of NAPEX XI).

The Propagation Payload allows reception on ground by all participants simultaneously and is available continuously. Its utilisation therefore is not a matter of scheduling. Instead, the high level of interest in utilising this payload shown by many research institutes has led to a programme of intensive cooperation in preparing for the propagation experiments with Olympus. This voluntary cooperation project is coordinated by ESA/ESTEC under the acronym OPEX (Olympus Propagation Experiment).

History of European cooperation

In the period July 1976 - October 1977 the NASA satellite ATS-6 was placed at 35 deg E longitude and the European scientific community was given the opportunity to carry out propagation experiments using the beacon facilities of the satellite. These included the so-called millimeter-wave (MMW) experiment using stable on-board beacons at 20 and 30 GHz and the COMSAT experiment using a transponder arrangement allowing 13 and 18 GHz uplink measurements. Unfortunately, these experiments could only be carried out during certain hours of the day (or rather, the night). The rather complicated arrangements that were necessary for participation included dissemination of schedules, loan of transmit equipment and centralised processing of the uplink measurements. ESA was asked to coordinate the European participation in the experiments and represent experimenters vis a vis NASA and COMSAT. This led to the establishment of a European experimenters group which met regularly during the project and published its collective results in an ESA Special Publication (ref. 1).

Another activity of European cooperation in propagation research was initiated in the framework of the COST (Cooperation Scientifique et Technique) project of the European Commission. From 1972 to 1977, in "Action COST 25/4" results of propagation experiments above 10 GHz obtained in 13 different countries were collectively analysed in order to obtain better understanding of the variations of propagation effects with climate (ref. 2). In this project mainly analysed results of individual experiments were put together and compared. It was realised that a higher level of collective analysis would be possible, if statistics obtained from measurements were put into a common data base and made available for collective analysis. This was carried out in the subsequent action COST 205 (1978-1984), where 11/14/18 GHz propagation data obtained with the ESA satellite OTS and the Italian satellite SIRIO were collated and analysed (ref. 3). This required a higher level of cooperation, including agreements on standard formats for presenting the various statistics obtained.

The OTS experiments themselves were coordinated by ESA and Eutelsat together. The habit of convening the coordination meetings of experimenters at the different participating institutes across Europe, which was established in the COST 25/4 project and since then followed by many other COST projects, has led to an intensive exchange of information which has proven to be indispensable for cooperation "at working level". Collective European results of the satellite propagation experiments have been made available to the International Telecommunications Union (ITU) and form a major part of the data bank of CCIR Study Group 5 on Earth-Satellite propagation statistics.

Organisation of OPEX

Thus in the previous 15 years an active European community of researchers in the field of radio propagation was established. When in the late seventies plans for a large satellite carrying a number of experimental telecommunications payloads were taking shape, this community was called upon to input their requirements for a propagation experiment. ESA specifications were drawn up in consultation with prospective experimenters. Soon it became clear that there was wide interest in such experiments and a need existed for regular information exchange in the preparatory stages. Starting as early as 1980 regular meetings of interested parties (researchers and industry) were held. Based on the experience from the COST projects the general opinion was that collective development of specifications for earth station hardware as well as procedures for data acquisition, preprocessing and analysis would be very beneficial for experimenters and greatly enhance the results to be obtained. In 1984 this work was started by the establishments of three working groups:

- W.G. 1 - Earth station requirements.
Chairman: Mr. S.K. Barton (UK)
- W.G. 2 - Data acquisition and preprocessing
Chairman: Mr. F. Zelders (NL)
- W.G. 3 - Data analysis
Chairman: Prof. A. Paraboni (I)

The overall objective of the preparatory stage of the OPEX project thus established was to arrive at a level of standardization that allows direct comparison of results of experiments without the usual uncertainties regarding equipment quality and compatibility of data analysis procedures. Detailed discussions were held in the working groups of all aspects of the experiments and the results envisaged. The work of these groups resulted in the issuing of three handbooks, specifying quality objectives and defining interfaces for data acquisition, preprocessing and analysis, respectively.

Participation in the OPEX meetings has been very encouraging and a good measure of the high level of interest. Attendance to the meeting is at a constant level of some 40 people from all ESA member states. The possibility to carry out experiments from the N. American continent has generated interest also from U.S. experimenters and resulted in regular contact with the NAPEX group. The table on next page lists the organisations that are actively involved in the OPEX work.

Table of participants in OPEX

Organisation -----	Location -----
Technical University Graz	Graz, Austria
ASSA	Vienna, Austria
BTMC	Antwerpen, Belgium
Newtech	Antwerpen, Belgium
E.B.U.	Brussels, Belgium
U.C.L./Lab. de Telecomm.	Louvain-la-Neuve, Belgium
C.R.C./Radio Prop. Lab.	Ottawa, Canada
FTZ	Darmstadt, W.Germany
Dornier System	Friedrichshafen, W.Germany
Inst. Fuer Rundfunktechnik	Muenchen, W.Germany
DFVLR	Oberpfaffenhofen, W.German
P. and T./Radio Comms.	Copenhagen, Denmark
ElektronikCentralen	Copenhagen, Denmark
T.U.D./Electromagn. Inst.	Copenhagen, Denmark
ETSI Telecomunicacion	Barcelona, Spain
ETSI Telecomunicacion	Madrid, Spain
CNET	Paris, France
I.R.A.M.	Grenoble, France
Eutelsat	Paris, France
March Microwave	Braintree, U.K.
Univ. Bradford	Bradford, U.K.
Signal Processors	Cambridge, U.K.
Rutherford Appleton Lab.	Chilton, U.K.
Univ. Essex	Colchester, U.K.
CSR	Ilkley, U.K.
BTRL	Martlesham, u.k.
Portsmouth Polyt.	Portsmouth, U.K.
BaE	Stevenage, U.K.
Politecnico di Milano	Milano, Italy
CNR / PSN	Roma, Italy
Fond. Ugo Bordoni	Roma, Italy
SeleniaSpazio	Roma, Italy
Telespazio	Roma, Italy
CSELT	Torino, Italy
Telecomm. Research Est.	Kjeller, Norway
ELAB	Trondheim, Norway
NIVR	Delft, Netherlands
Technical Univ. Delft	Delft, Netherlands
Technical Univ. Eindhoven	Eindhoven, Netherlands
APT	Huizen, Netherlands
Dr, Neherlab. PTT	Leidschendam, Netherlands
Universidade Aveiro	Aveiro, Portugal
Swedish Telecom Radio	Farsta, Sweden
Helsinki Univ. of Technol.	Espoo, Finland
Virginia Tech	Blacksburg, U.S.A.
JPL	Pasadena, U.S.A.
NASA	Washington, U.S.A.

Results

Major results of discussions of beacon receiver design have been in the area of standardization of output specifications of receivers and a thorough discussion of calibration principles. For the output interface of the receiver hardware a digital output has been recommended presenting 100 samples/second of I and Q channels of the receiver. Principles of oversampling of signals in the presence of noise have been discussed and resulted in some novel design ideas for digital beacon receivers. A digital receiver has been developed by Signal Processors Ltd in Cambridge, U.K., based on frequency feed-forward control, using digital signal processing techniques in software.

In the areas of preprocessing and analysis of data the OPEX Handbooks produced by the Working Groups have been the basis for the specification of a software system, the development of which is now taking place under contract to ESA by Siemens Austria (Vienna) and CSR Ltd. (Ilkley, U.K.). This processing system is intended to become the European reference system for the treatment of propagation data. CSR have already delivered a complete Olympus propagation station, including a data acquisition and processing system, to the German Post Office Research Centre FTZ.

It has been emphasized as a result of the studies by the OPEX group, that for an accurate measurement of fading an independent measurement of total attenuation under conditions of clear sky or light rain by means of radiometers is indispensable. The development of a low-cost 20/30 GHz dual-frequency radiometer for this purpose is being pursued under contract to ESA by Farran Ltd (Ireland). The instrument which has been named Atmospheric Water Radiometer (AWR) will have a variety of other applications (remote sensing, meteorology) by virtue of its capability to measure total atmospheric water vapour content and liquid water content separately through a well-proven inversion process.

In the area of scientific analysis a major decision facilitating a comparison of results among experimenters concerned the treatment of crosspolar data. As the polarisation orientation at the groundstation is dependent on its location, crosspolarisation results cannot be compared directly. The common analysis specified as a standard is in terms of the tilt angle of the principal axes of the medium itself and the differential attenuation along these axes.

To facilitate an exchange of calibrated time-series data on a bilateral basis, a specification of a standard file format for the storage of "events" has been made. This "standard event tape" (which, physically, most likely will be an optical disk) at the same time serves as the "reference" interface between the data acquisition and preprocessing system and the data analysis system.

Anticipating a large amount of statistical information to result from propagation research in the nineties, ESA also started, in collaboration with Intelsat, the development of an intelligent data base management system for the production of propagation predictions and the evaluation of prediction methods that use large-scale statistics of propagation and meteorological data. A contract to study the feasibility of a DBMS using modern software techniques is carried out by Bradford University under contract with ESA and Intelsat.

Propagation measurements using millimeter waves will be possible in a few years in Europe with the Italsat satellite (40/50 GHz). Looking ever further ahead, ESA has now started the development of a small, light-weight 45/90/135 GHz beacon payload by letting a contract to assess feasibility and critical technology for such an instrument to Contraves Italiana (Rome).

Conclusion

The OPEX project was started as a voluntary coordination activity under ESA guidance. Its success is marked by industrial activities now taking place in Europe to implement the recommendations of the European experimenters. As a result there exists now a very positive outlook for an unprecedented level of cooperation and exchange of information in the area of propagation research. Large-scale pooling of results appears to be the only way to make progress in the development of global prediction methods that can be used effectively in the planning of new satellite communication systems.

Marking the conclusion of the preparatory phase of the OPEX project will be the 11th OPEX meeting mid June in Copenhagen, where status of user preparations and current research are reviewed, as well as progress in the software development contract on data processing.

A symposium on the utilisation of Olympus, covering all planned experiments with the four payloads, will be organised by ESA in collaboration with the Austrian Solar and Space Agency (ASSA) next year April in Vienna, hopefully marking the successful launch of the satellite.

References

1. G. Brussaard and B. Battrick (editors), "ATS-6 propagation experiments in Europe", ESA SP-131, October 1977
2. F. Fedi (editor), "The Eurocop-COST 25/4 project on radiopropagation above 10 GHz", Alta Frequenza, April 1979
3. F. Fedi (editor), "Special Issue on the COST 205 project on Earth-Satellite radio propagation above 10 GHz", Alta Frequenza, May/June 1985

ACTS and OLYMPUS Propagation Experiments

Charles W. Bostian
Kenneth R. Baker

Satellite Communications Group
Bradley Department of Electrical Engineering
Virginia Polytechnic Institute and State University
Blacksburg, VA 24061

Abstract - The OLYMPUS and ACTS satellites both provide opportunities for 10-30 GHz propagation measurements. The spacecraft are sufficiently alike that OLYMPUS can be used to test some prototype ACTS equipment and experiments. Data are particularly needed on short term signal behavior and in support of uplink power control and adaptive FEC techniques. The VA Tech Satellite Communications Group has proposed a set of OLYMPUS experiments including attenuation and fade rate measurements, data communications, uplink power control, rain scatter interference, and small-scale site diversity operation. We are also developing a digital signal processing receiver for the OLYMPUS and ACTS beacon signals.

1. Introduction

This paper describes a set of experiments that our group has proposed for OLYMPUS and ACTS. The spacecraft are similar in that both support communications and propagation research in the 10-30 GHz band. In describing our proposed experiments we invite comments from the NAPEX community and hope to interest other groups in similar studies.

OLYMPUS provides an opportunity to test techniques and equipment that will be important in the ACTS program before ACTS is launched. For example, OLYMPUS measurements will provide propagation information needed by the ACTS adaptive FEC system. Prototype ACTS-program equipment debugged with OLYMPUS can be duplicated and distributed to measurement sites around the U.S. Planning experiments with both satellites insures against launch delays on either one.

2. The Satellites

2.1 OLYMPUS

OLYMPUS is an ESA satellite offering coherent beacons at nominal frequencies of 12, 20, and 30 GHz and 30/20 GHz transponders. After a January 1989 launch it will be located at 19 deg. w, and we will see it at 14 deg. elevation. This relatively low angle will create interesting propagation effects without being unrepresentative of commercial links.

The propagation package includes beacons at 12.5 GHz (12501.866 MHz), 20 GHz (19770.393 MHz) and 30 GHz (29655.589 MHz) derived from a common oscillator. See Fig. 1. Experimenters may lock all receivers to the 12.5 GHz beacon and extend their 20 and 30 GHz dynamic range.

The 12.5 GHz earth coverage beacon will provide a +6 dBW EIRP toward our site with Y polarization (normal to the equator). The 20 and 30 GHz European coverage beacons will radiate +16 dBW toward Blacksburg. The 30 GHz beacon will transmit Y polarization and the 20 GHz beacon may be switched between X or Y polarization at 1866 Hz. ESA plans to operate the spacecraft predominantly in the switched mode for cross polarization discrimination (XPD) measurements. The U.S. is too far from boresight for reliable XPD measurements.

2.2 ACTS

ACTS is a NASA satellite intended to develop and prove advanced 30/20 GHz communications technology and to offer an opportunity for propagation experiments. It will provide a 30/20 GHz communication package to test hardware and operating procedures for a TDMA (time division multiple access)/DAMA(demand access multiple access) system for commercial satellites. Its adaptive FEC will make ACTS the first satellite to compensate for propagation effects in real time.

The ACTS beacon package consists of two beacons at 20 GHz which also transmit telemetry information and a 30 GHz CW beacon which will be useful for detecting uplink fades. The 20 GHz beacons are not optimum for propagation work because of their modulation. In addition, since the ACTS beacons are not derived from a common source, they offer less fade margin than OLYMPUS. The ACTS beacons have much better polarization purity than OLYMPUS for U.S. sites; ACTS is suitable for depolarization measurements.

3. Proposed VA Tech Experiments for OLYMPUS and ACTS

3.1 Background: Why Experiments are Needed

The reader may legitimately ask "After ATS-5, ATS-6, CTS, COMSTAR, and SIRIO, what could we still need to know about 30/20 GHz propagation? If there is something, why can't we get it from further analysis of the old data?" There are several reasons why more work is needed.

Virtually all of the 20/30 GHz and most of the 14/11 GHz propagation data available from U.S. sites were collected at high angles to determine worst-month and annual attenuation and depolarization statistics. They were not recorded with a time resolution suitable for analyzing fade rates and durations. While valuable for their intended purposes, these data cannot tell us much about short-term signal phenomena that are important to digital links or about real-time attenuation scaling for uplink power control or adaptive FEC. This is reflected in Science Review of the NASA Radio Propagation Program, Science and Technology Corporation Report STC-2127, February 1987, where a 1986 NASA review panel makes a cogent case for further work in 10-30 GHz propagation, emphasizing studies of fade rates and fade durations and such intersystem questions as rain scatter interference.

In a further attempt to assess the need for additional 20/30 GHz propagation, our group surveyed 19 people representing both satellite users and propagation researchers. Their replies indicated three important needs:

- (a) Data that would be useful for developing some kind of adaptive control to mitigate the effects of rain fades on 20/30 GHz satellite links.
- (b) Fade statistics for a broad range of climates.
- (c) Simultaneous multiple and higher frequency measurements.

In summary, we feel that the greatest operational need is for short-term fade prediction for uplink power control and adaptive FEC. These processes both involve short-term prediction of signal behavior at one frequency and scaling this prediction to a (higher) uplink frequency.

3.2 Proposed VA Tech Experiments

Fig. 2 illustrates our proposed experiments. These are described in the sections which follow.

3.2.1 Basic OLYMPUS Propagation Measurements

We will construct a receive-only terminal to collect 12, 20, and 30 GHz attenuation data with OLYMPUS and a build prototype data acquisition system for use with both OLYMPUS and ACTS. We intend to measure fade duration with a time resolution of 100 ms. Data on short-term OLYMPUS signal behavior will fill gaps in the current understanding of 10-30 GHz propagation and support the ACTS communications experiments.

3.2.2 The OLYMPUS CODE Experiment.

CODE, an acronym for COoperative Data Exchange, refers to a system that provides high speed data (up to 2 Mbps) into a remote earth station and low speed data (9.6 kbps) out to a hub station. The CODE system requires only 150 mW of transmitter power into a 0.9 m antenna at 29 GHz. We propose to build a CODE terminal to communicate with the European experimenters and to use it to operate a "live" uplink power control experiment with OLYMPUS. Our system will obtain an extra 8 dB of margin by using a 600 mW transmitter and a 1.2 m antenna.

3.2.3 Uplink Power Control Experiment.

We propose to develop hardware and software for a simulated uplink power controller. This device will make real time predictions of 30 GHz fading from 12 GHz and/or 20 GHz fade measurements. This unit, a self contained and independent addition to the OLYMPUS experiment, will operate under microprocessor control. This will allow immediate testing and optimization of uplink power control algorithms.

A 29 GHz waveguide attenuator, fitted with a stepper motor and controlled by a microprocessor, will be our uplink power control device. This should provide about 7 dB of control range, which is as large as most systems can handle. The algorithms developed from the propagation experiment will be used in the microprocessor during CODE experiment transmissions, and the bit error rate (BER) of the link will be monitored.

The availability of the OLYMPUS 20 and 30 GHz steerable spot beams provides a unique opportunity to test the ACTS baseband processor under operational conditions. We propose to use a double-hop configuration and our CODE equipment to transmit data through OLYMPUS to a receiving earth station connected to an ACTS baseband processor. The earth station will format the received CODE data into a TDM frame compatible with ACTS, send them through the baseband processor, and reformat the data back to a CODE format and retransmit them back through OLYMPUS. The general configuration for this experiment is shown in Figs.3 and 4.

The ACTS TDMA system is designed around data frames with 64 bit bursts at 110 Mbps. A data reformat operation will be required before data can be passed to the ACTS processor. Additional words can be added to the TDM frame to indicate the measured BER on the uplink and to provide a new sequence for downlink BER measurement. Control signals for the uplink power control, uplink FEC, and downlink FEC also need to be added into the data frame. The transmission from our earth station will be at the CODE 9.6 kbps rate. We propose to use a BER test set to generate a pseudo-random bit sequence so that the uplink BER can be measured by the receiving earth station. We understand that the Canadians plan a similar experiment using a double hop through a laboratory baseband processor.

3.2.4 Rain-Scatter Interference at 30 GHz

This experiment and the small-scale diversity experiment which follows are semi-independent measurements that will fill gaps in current knowledge of 10-30 GHz propagation as identified by the NASA Review Panel. Tests with OLYMPUS will determine whether these should be replicated on a large scale with ACTS.

A potential interference problem exists if an earth terminal illuminates a satellite in an adjacent orbital slot via rain scattering of the uplink signal. The probability of this happening increases if the earth station increases its uplink power to compensate for the attenuation due to the rain. The geometry of this problem is illustrated by Fig. 5(a). We propose to investigate this by placing a second 30 GHz antenna pointed 2 degrees off axis from the primary antenna. This inverted geometry is shown in Fig. 5(b). We will observe the common volume containing the rain using our 2.8 GHz multiple polarization radar and simultaneously measure power scattered into the second antenna.

3.2.5 A Small-Scale Diversity Experiment

There is some evidence for fine scale structure in heavy rain. We believe that it may be possible to derive diversity gain from antenna spacings on the order of 50 m. Such antenna spacings would permit diversity reception by one site with two antennas. Since two complete and widely-separated sites are presently required to take advantage of diversity gain, this would result in a considerable savings in earth terminal costs.

We propose to test this hypothesis at 20 GHz by simply erecting a second receiving antenna approximately 50 m away from the primary receiving antenna. By comparing the fading characteristics of the two receivers, it should be possible to evaluate the quality and quantity of diversity gain such a system would enjoy.

3.2.6 ACTS Propagation Experiments

The results of the experiments described above will determine which OLYMPUS propagation measurements should be continued with ACTS. We anticipate that those which are continued will be replicated at a number of sites.

For a widespread propagation experiment like that envisioned for ACTS to be meaningful, the receivers and data collection systems at each site should be made as alike as is possible, and the data from the various sites should be processed in exactly the same way using the same software and the same data format. For these reasons we have proposed to develop prototype receivers and data acquisition systems for distribution to participating ACTS sites. Digital receivers in particular should offer consistent performance and immunity to thermal effects.

4. Summary of Work Accomplished in Support of Proposed Experiments

4.1 Introduction

During the current fiscal year our group was asked by JPL to look at the fade rate question as it affects the ACTS program and to design a prototype receiver for OLYMPUS and ACTS. In the sections that follow, we will report briefly on these two activities.

4.2 Fade Rates

The question of how fast a 10 - 30 GHz signal can fade during rain has had a long and somewhat checkered history. Measurements reported in the literature differ significantly. These differences seem to be related both to the bandwidth and the dynamic characteristics of the measuring equipment and to the sampling rate, filter characteristics, and other details of the data acquisition and processing systems. One group argues on theoretical grounds that measured fade rates will always be limited by the dynamic response of the receiver, while older work on terrestrial paths indicates that the maximum fade rate is determined by how fast falling rain can fill the radio path. Since fade rate is very important to uplink power control and adaptive FEC systems, we have been investigating both its theoretical and experimental aspects with the idea of making definitive fade rate measurements on the OLYMPUS beacons. Our effort has included collecting and trying to rationalize all of the published literature on the subject.

Dennis Sweeney of our group has completed a preliminary evaluation of Ruthroff's (Ruthroff, 1970) expression for fade rate on a terrestrial link. To do this he used a hypothetical path 1.5 km long and modeled the rain as a step function of equal sized drops all falling at the same velocity. By step function we mean that the leading edge of the falling rain can be represented as a plane surface with rain above the plane and no rain below it. He evaluated the integral over the first Fresnel zone which represents the fade rate for frequencies of 30, 20, 15, and 10 GHz and rain rates of 10, 50 and 100 mm/hr. The following table is a sample of the results for 30 GHz.

Table 1. Predicted fade rates for a 1.5 km 30 GHz terrestrial path for step functions of rain at the rain rates shown.

Percent of volume intersected by rain	Fade rates in dB/s for step rate of		
	10 mm/hr	50 mm/hr	100 mm/hr
10%	0.146	0.730	1.461
30	0.622	3.110	6.219
50	0.934	4.670	9.340
70	0.622	3.109	6.219
90	0.146	0.730	1.460

The analysis produces a fade rate which is directly proportional to rain rate and symmetrical with respect to the center of the volume. This happens because after the rain reaches the center of the volume represented by the first Fresnel zone, rain is falling out of the volume as well as falling into it. When the volume is completely full of rain an equal amount falls out of the volume as falls into it and the net fade rate becomes zero.

While the values tabulated above seem reasonable, we have not yet been able to check them against the static attenuation values predicted by the ar^D relation for specific attenuation with coefficients published by Olsen, Rogers, and Hodge (1978).

4.3 Plans for ACTS and OLYMPUS Receivers

The section describes the fundamental OLYMPUS/ACTS receiver for propagation measurements. It will initially be configured to receive the OLYMPUS beacons; later it will become the heart of our ACTS receiver.

As Fig. 6 indicates, we plan a double conversion design with an 1120 MHz first IF and a 70 MHz second IF. The first frequency was chosen to facilitate coherent detection. The output of the second IF will feed either a quadrature detector or a digital signal processing (DSP) detector described below. The entire system is referenced to a single 70 MHz crystal. We plan to include an automatic calibration system and to achieve an overall measurement of plus or minus 0.1 dB.

Since the OLYMPUS beacons are coherent, the receivers will be linked by a common LO system that locks the 20 GHz and 30 GHz receivers to the 12 GHz beacon under normal operating conditions. The receivers may be switched to independent operation if a beacon fails or to permit testing of the digital detector to be developed for ACTS. During ACTS operation, all beacon receivers will operate independently.

By taking advantage of the coherent OLYMPUS beacons we will be able to measure 20 and 30 GHz fades down to the noise floor, providing a dynamic range of approximately 45 dB. Since the 12 GHz beacon is less susceptible to fading, the 20 and 30 GHz receivers will not lose lock during severe fades at those frequencies. This will lessen the inherent problem of most phase locked receivers -i.e. the inability to reacquire the carrier at the same fade depth as when lock was lost.

The link budgets for the three beacons are shown in Table 2. These calculations assume:

- system lock on the 12 GHz beacon
- 12 ft. dish for 12 GHz reception
- 4 ft. dishes for 20 GHz and 30 GHz reception
- antenna temperature 290 K as for deep fade conditions
- antenna aperture efficiency factor of .65
- LNA and mixer noise temperature of 440K for 12 GHz
- LNA and mixer noise temperature of 1540K for 20/30 GHz

Table 2. OLYMPUS Link Budget for Coherent Receiver

Quantity	Units	12.5 GHz	20 GHz	30 GHz
satellite EIRP	dBW	6	16	16
free space loss	dB	206.5	210.5	214.0
atmos. loss	dB	.2	.95	.78
other losses	dB	1	2	2
antenna gain	dB	51.7	46.2	49.6
receiver NF	dB	4	8	8
system noise temp	dBK	28.6	32.6	32.6
G/T	dB/K	23.1	13.6	17.0
C/No	dBHz	50.0	44.8	44.8
C/N in 10 Hz BW	dB	30.0	-	-
C/N @ PLL thresh.	dB	10.0	-	-
Fade margin	dB	20.0	43.7	44.8

Note that the fade margin calculated for the 20 GHz and 30 GHz beacon is derived from the fade margin of the 12 GHz beacon. This was done by frequency scaling the 12 GHz fade margin to 20 GHz and to 30 GHz using the CCIR formula.

Table 3 shows link budgets for a system where the receivers are independent. That is, they lock individually to their respective carriers. The link budget for the 12 GHz beacon is the same as Table 1 and is not repeated here. Therefore Table 2 shows the link budgets for only the 20 GHz and 30 GHz receivers. Comparison of the two tables shows that phase locking the receivers achieves potentially 30 dB more dynamic range for the 20 GHz and 30 GHz systems.

Table 3. OLYMPUS Link Budget for Non-coherent Receiver

Quantity	Units	20 GHz	30 GHz
satellite EIRP	dBW	16	16
free space loss	dB	210.5	214.0
atmos. loss	dB	.95	.78
other losses	dB	2	2
antenna gain	dB	46.2	49.6
receiver NF	dB	8	8
system noise temp	dBK	32.6	32.6
G/T	dB/K	13.6	17.0
C/No	dBHz	44.8	44.8
C/N in 10 Hz BW	dB	24.8	24.8
C/N @ PLL thresh.	dB	10.0	10.0
Fade margin	dB	14.8	14.8

Figure 7 shows this receiver reconfigured for ACTS. The 20 and 30 GHz receivers individually acquire the incoming signals. The overall receiver design is not as complex as the coherent OLYMPUS receiver, but many major components are the same. Since the ACTS 20 GHz beacon is modulated, the receiver must be able to measure signal strength in the presence of this modulation.

Fig. 8 presents a block diagram of our ACTS digital signal processing (DSP) detector. Designed around one of the new DSP chips, the detector will feature (1) the ability to find and lock to the carrier rather than a sideband and (2) the ability to measure signal power in the presence of modulation. It works by downconverting the incoming 70 MHz IF signal to 67.5 kHz. The signal is then bandlimited to 135 kHz and sampled at 300 kHz and fed to the DSP portion of the receiver, here shown simply as a block. Using digital filtering and spectral estimation techniques the DSP block determines the carrier frequency, the type and depth of modulation, and the received power.

All of the various operations will be under the control of a microprocessor. As the signal drifts, it will be tracked by tuning the direct digital synthesis (DDS) LO used in the initial down conversion. The processor will also control the serial and parallel output ports. The first will deliver measurement data while the second will control the receiver and pass status information.

5. References

- Olsen, R.L., D.V. Rogers, and D.B. Hodge, "The aR^b Relation in the Calculation of Rain Attenuation," IEEE Trans. AP-S, Vol. AP-26, pp. 318-329, March 1978.
- Ruthroff, C.L., "Rain Attenuation and Radio Path Design," BSTJ, Vol. 49, pp. 121-135, January 1970.

6. Acknowledgments

This paper summarizes the ideas and work of many members of the VA Tech Satellite Communications Group who have worked on plans for ACTS and OLYMPUS experiments. In particular we would like to acknowledge the contributions of Warren Stutzman (propagation measurements), Tim Pratt (uplink power control and the CODE Experiment), John McKeeman (data collection), Robert Porter (data collection and processing), Dennis Sweeney (fade rates, receiver design), and Sandra Fitzhugh (receiver design). Cynthia Marshall prepared the manuscript for printing. Richard Campbell of Michigan Tech has served as a consultant on receiver design.

OLYMPUS
Beacon Block Diagram

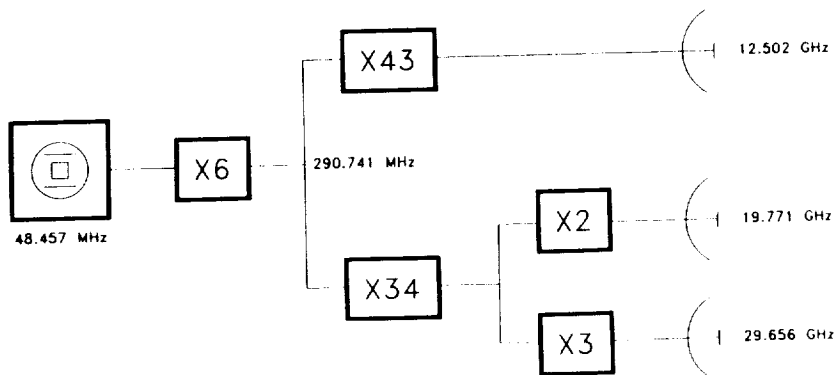


Figure 1. Derivation of the OLYMPUS beacon frequencies.

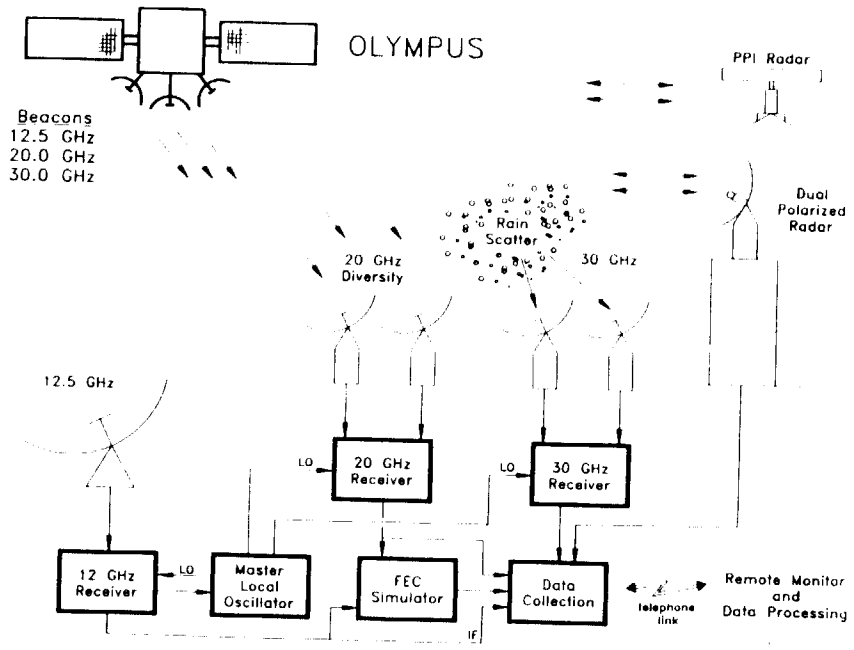


Figure 2. Schematic picture of the proposed experiments.

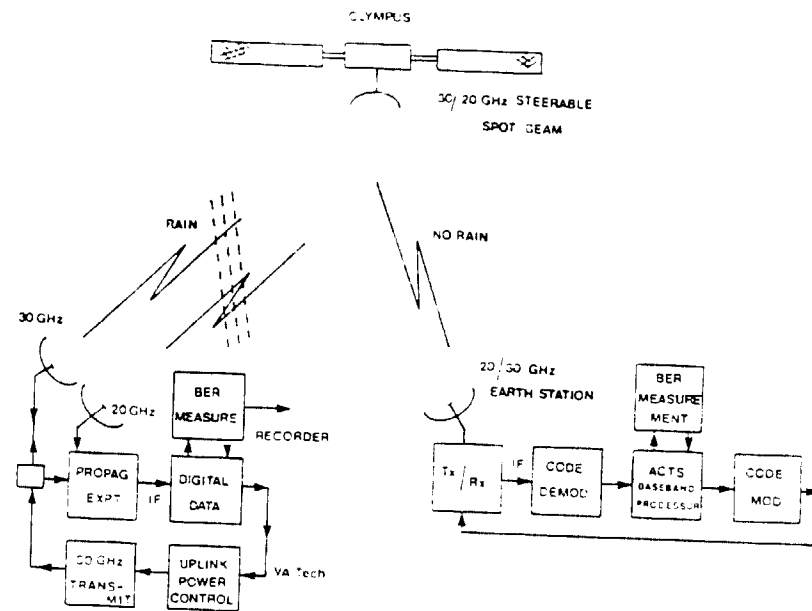


Figure 3. Uplink power control experiment using OLYMPUS.

IMPROVED DATA TO
 OF poorer quality

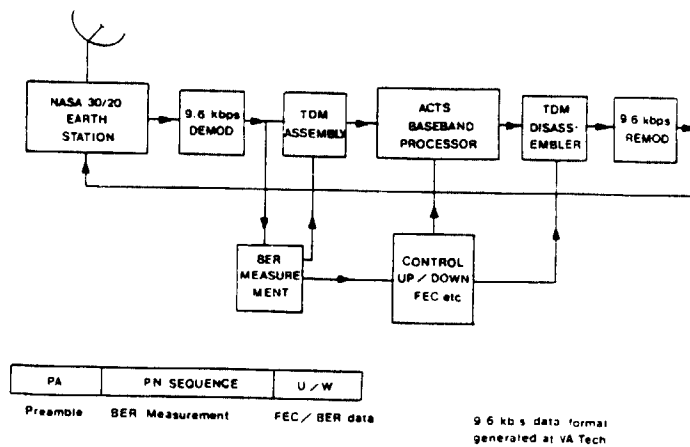


Figure 4. Data formatting in the uplink power control experiment.

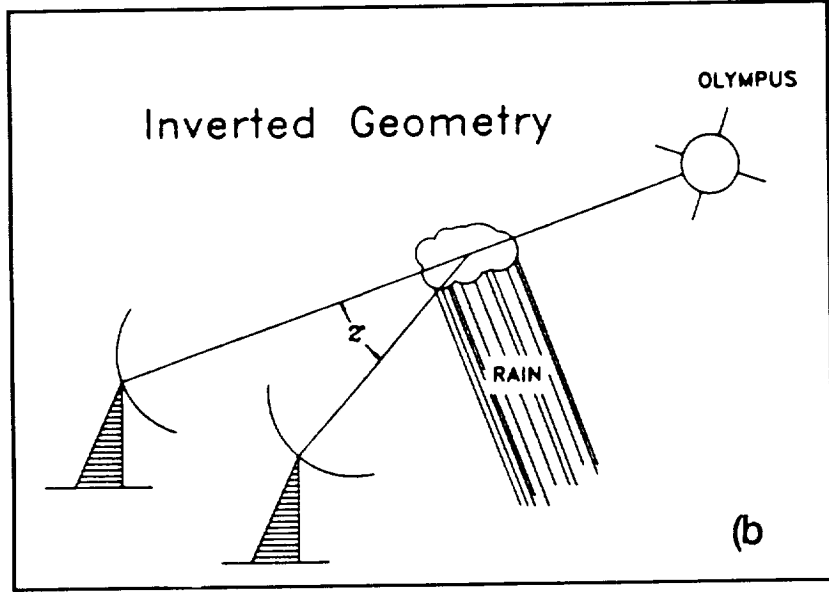
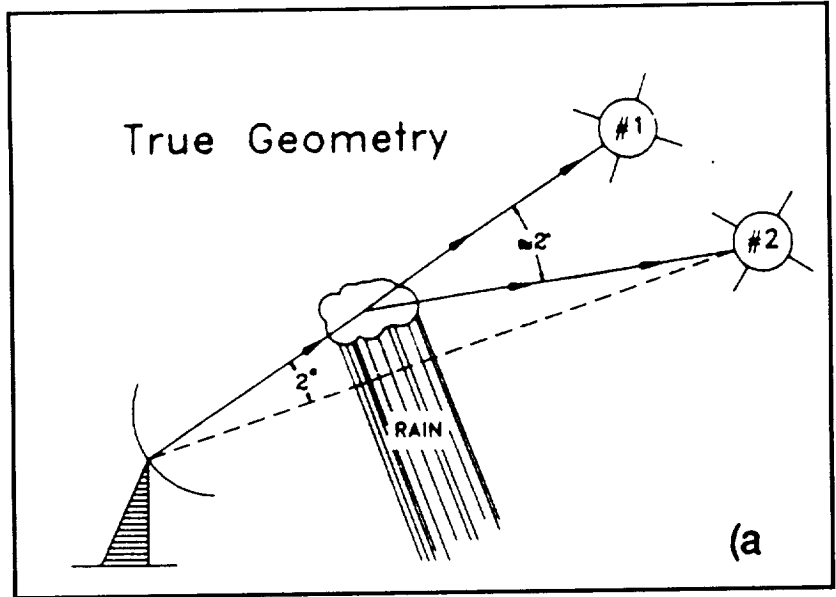


Figure 5. Rain scatter experiment.

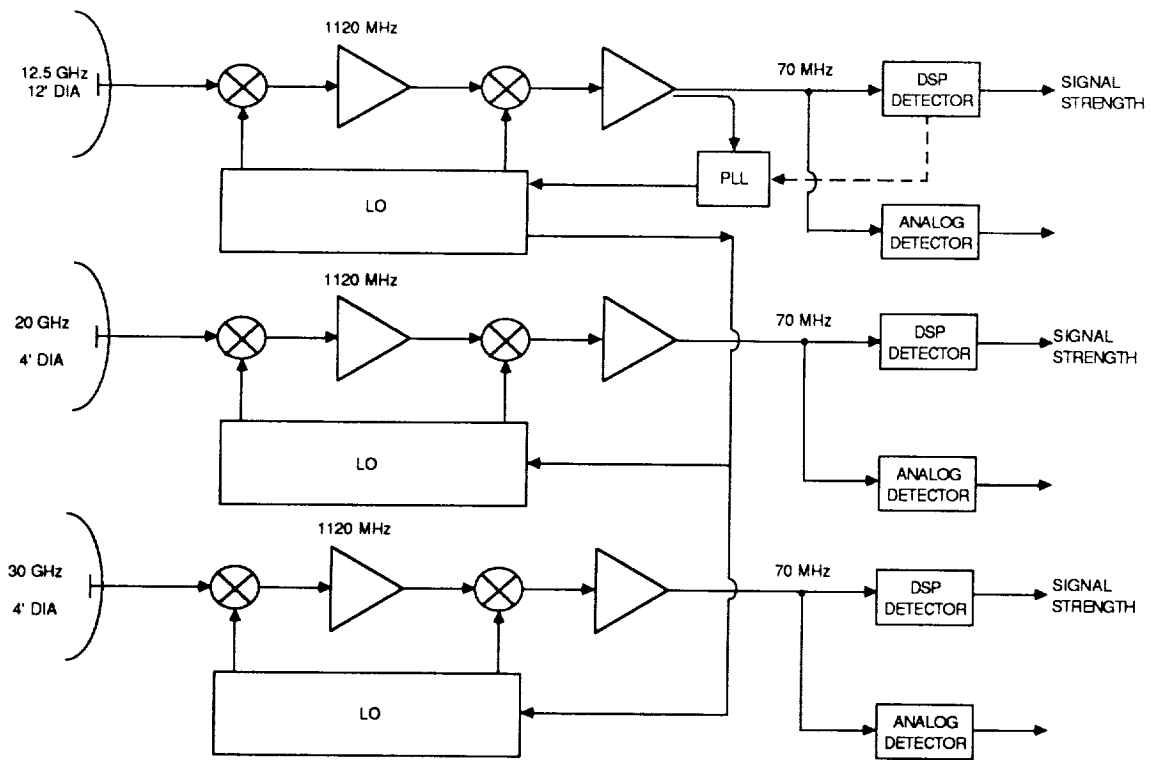


Figure 6. Overview of the OLYMPUS receiver.

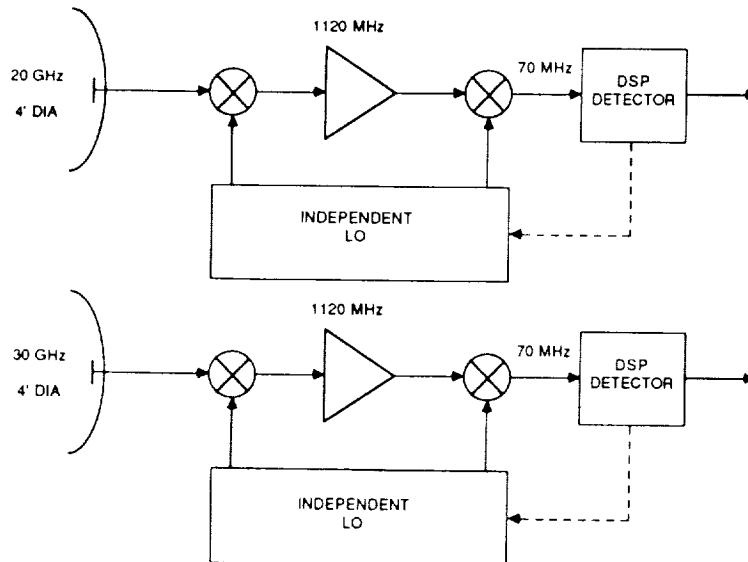


Figure 7. The ACTS receiver.

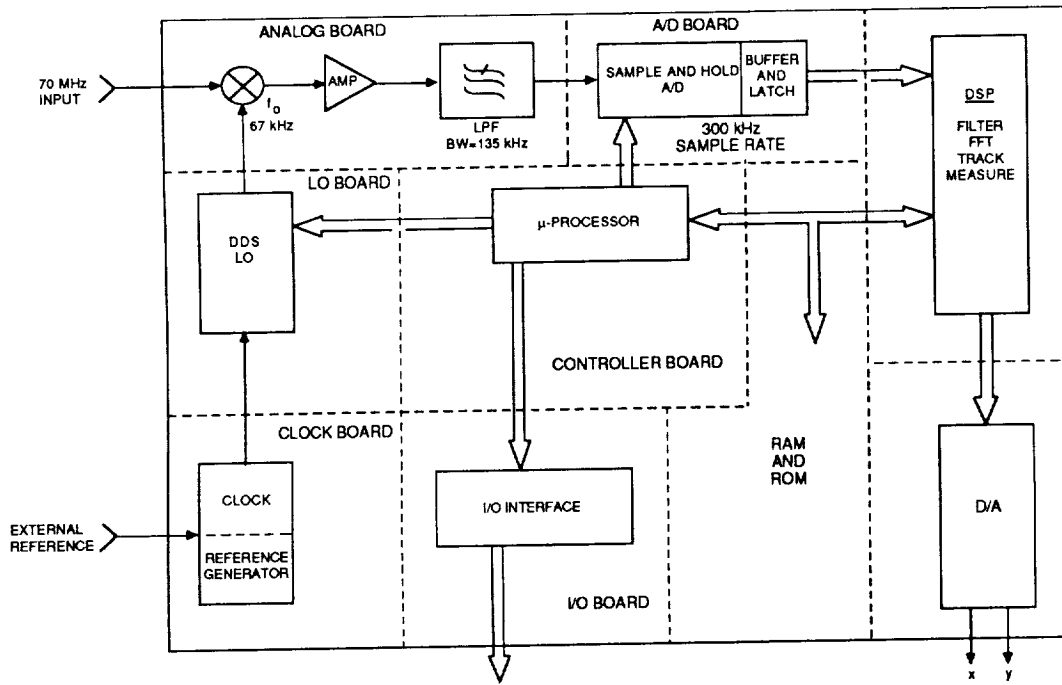
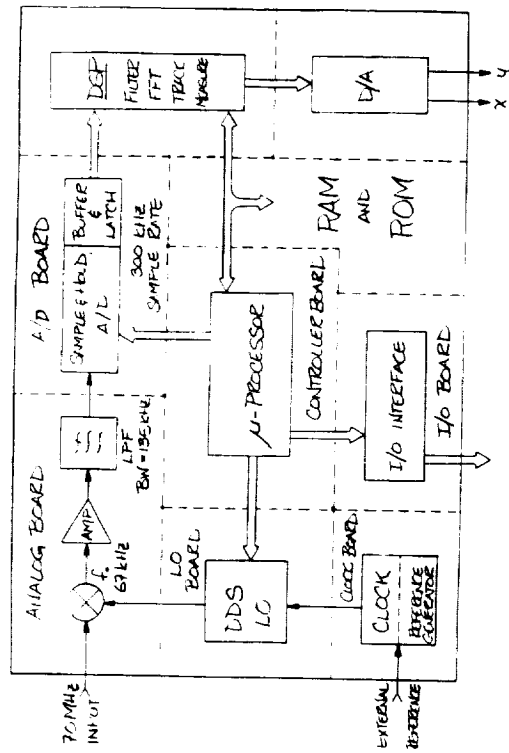
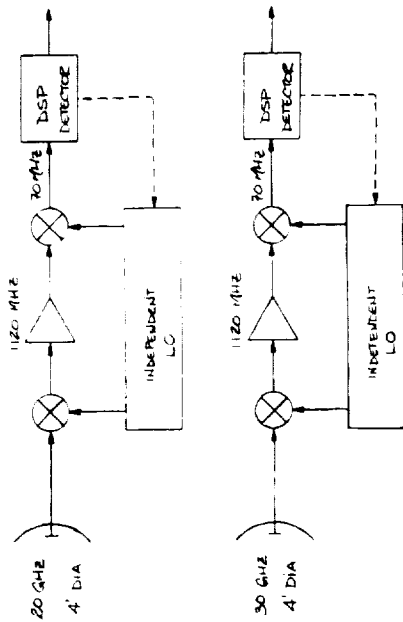
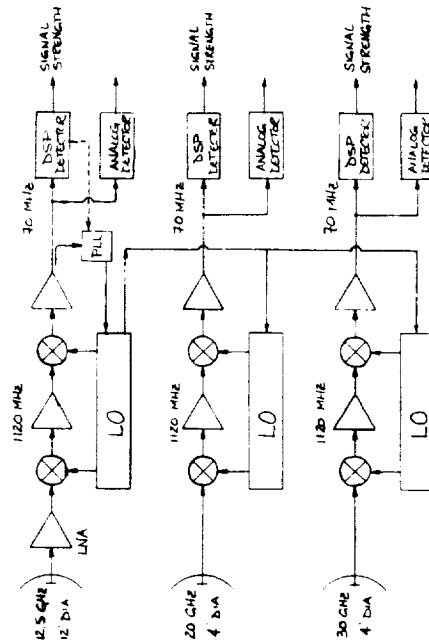
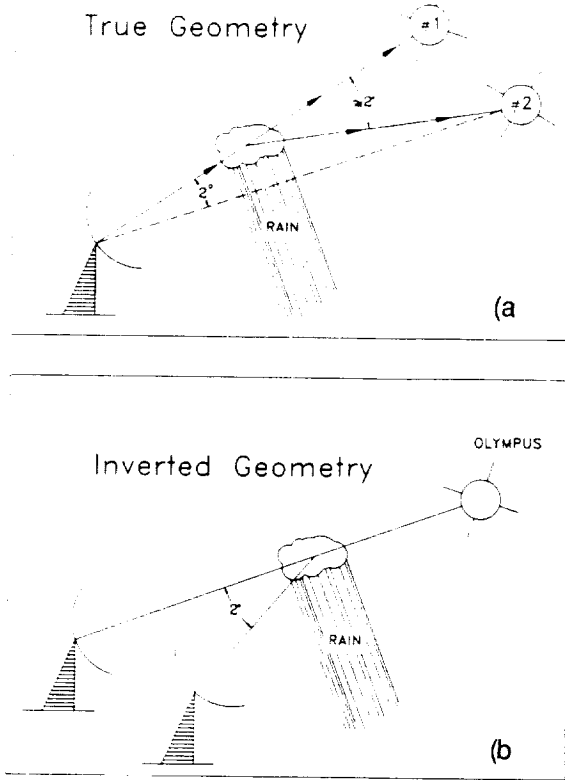


Figure 8. The ACTS digital signal processing (DSP) detector.



ORIGINAL PAGE IS
OF POOR QUALITY

ORIGINAL PAGE IS
OF POOR QUALITY

A DIGITAL BEACON RECEIVER

Peter D Ransome

Signal Processors Limited
Cambridge Science Park
Milton Road
Cambridge CB4 4GJ
England

Abstract

A digital satellite beacon receiver is described which provides measurement information down to a carrier/noise density ratio approximately 15 dB below that required by a conventional (phase locked loop) design. When the beacon signal fades, accuracy degrades gracefully, and is restored immediately (without hysteresis) on signal recovery, even if the signal has faded into the noise. Benefits of the digital processing approach used include the minimisation of operator adjustments, stability of the phase measuring circuits with time, repeatability between units, and compatibility with equipment not specifically designed for propagation measuring. The receiver has been developed for the European "Olympus" satellite which has CW beacons at 12.5 and 29.7 GHz, and a switched polarisation beacon at 19.8 GHz approximately, but the system can be reconfigured for CW and polarisation-switched beacons at other frequencies.

Introduction

It is of interest to various parties to gather propagation data at microwave frequencies for paths between ground stations and satellites in order to predict the performance of telecommunications systems within current and hitherto unused frequency bands. Conventional high performance satellite beacon receivers are complex (and therefore costly) units needing careful setting-up and maintenance.

At the occurrences of the most interesting(!) propagation events (i.e. deep fades), the performance of conventional phase locked loop receivers degrades catastrophically due to their inherent carrier/noise density threshold. Moreover, as the path recovers, the loop has to either reacquire (implying hysteresis of perhaps 4 dB and inability to measure during this time) or to have previously stored parameters of the unfaded signal in a complex unit, as an aid to reacquisition. The loop bandwidth of the PLL is typically 50 Hz, giving a carrier/noise density ratio (C/No) tracking threshold of 25 to 30 dB.

The beacon receiver developed by Signal Processors Limited (SPL) overcomes the hysteresis problem in addition to maintaining lock down to a point typically 15 dB below the C/No limit for a PLL, whilst gracefully losing accuracy. This is achieved by the elimination of feedback loops, a feedforward architecture being used. Digital processing implies stability, accuracy and repeatability. The tracking of the beacon carrier follows the ideas of (Barton, 1985), by tracking the carrier frequency independently of its phase. Instead of a PLL, the carrier frequency tracking is performed by a digital Fourier Transform Processor, with a box bandwidth of approximately 1 Hz.

System Overview

SPL's digital beacon receiver provides full transmission matrix measurement for signals from polarisation-switched beacons such as those carried by the ESA "Olympus" satellite. R.F. input to the receiver is taken at 70 MHz and output given at 100 Hz, consisting of cartesian digital data to twelve-bit resolution, and accompanying status information.

The receiver is contained in a 3U, 19 inch rack-mounting package, and consists of plug-in modules for R.F. synthesiser, I.F. channel and digitisation, digital signal processing, output interface and system control. The modular design eases the incorporation of special customer requirements. Figure 1 is a block diagram of the receiver.

The analogue stages of the receiver consist of the synthesiser and I.F. channel modules. The synthesiser generates the two local oscillators used by each I.F. channel module. The I.F. module uses a double down-conversion technique to translate the 70MHz receiver input to approximately 15 kHz I.F. at which point the signal is digitised with a 60 kHz sampling rate prior to further processing by the DSP sections of the receiver.

The DSP card removes the final 15 kHz I.F. to produce a (complex number) baseband signal for each received polarisation. Carrier tracking is performed by a spectral analysis of the signals to a resolution of approximately 1 Hz, and the use of an intelligent frequency-tracking algorithm to control a variable frequency digital oscillator to be mixed into the signal path. The sampling rate of the baseband signal can now be lowered (together with the application of a sampling phase correction for a polarisation-switched beacon). The final stage of the DSP work is to normalise all output data components to a phase reference derived from the incoming copolar signal.

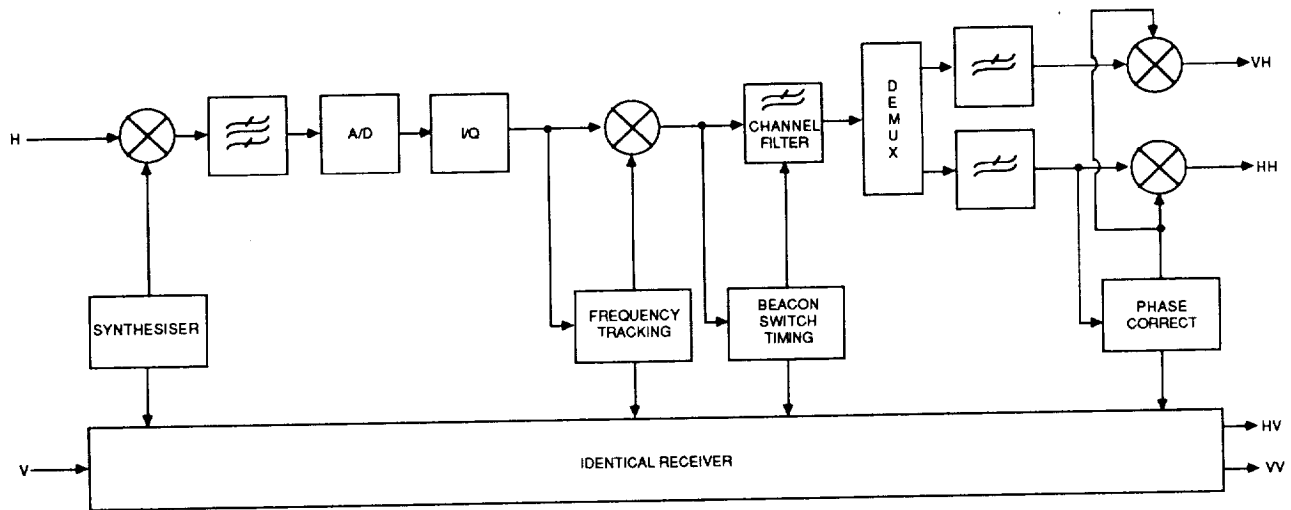


Figure 1. Dual Polarisation Beacon Receiver

The system control module formats the output data to the specified output interface option. Status information is interleaved with this data and also displayed on the receiver front panel. The control module will determine beacon carrier frequency to the accuracy of the station timekeeping, by calibrating its clocks in terms of a station reference frequency that may be provided to the receiver.

Summarised Performance Specification

Input Frequency	70 MHz
C/No Dynamic Range Limits	66 dB (overload) 15 dB (tracking fails)
Carrier Acquisition Level	38 dB C/No
+/- 2 degree Phase Accuracy Point	30 dB C/No
Carrier Phase Measurement Threshold	20 dB C/No
Carrier Freq Tracking Threshold	15 dB C/No
Output Signals	HHi HHq HVi HVq VHi VHq VVi VVq
Output Sample Rate	99.96 Hz (nominal)

Notes:

All figures refer to the 19.8 GHz Olympus Beacon

"C" is the level of the unswitched carrier

Output signal notation refers to: transmit polarisation
receive polarisation
phase measurement axis

The HHq output is non-zero when carrier phase tracking is no longer possible, i.e. below 20 dB C/No

The DBR-1 has been developed for use with the polarisation-switched 19.8 GHz Olympus beacon but is adaptable for use with other beacons on other satellites. When used with other transmitters with no polarisation switching, it should be noted that tracking performance is improved by 6 dB for a given beacon power.

Technical Description

Analogue Front End

The synthesiser reduces the bandwidth required in the digital section of the receiver by removing the bulk of the satellite beacon frequency drift. The synthesiser generates the two local oscillators (L.O.'s) used by the I.F. modules. The 1st L.O. at 59.3 MHz nominal is synthesised and the 2nd L.O. is derived from a temperature compensated crystal oscillator (TCXO) running at 10.685 MHz. Two phase coherent outputs at each frequency are provided, for use when both polarisations of a beacon are being measured (two IF modules fitted).

The I.F. module downconverts the 70 MHz receiver input to approximately 15 kHz I.F. at which point the signal is digitised for processing by the DSP module. A double down-conversion technique is employed, the 1st I.F. at 10.7 MHz and 2nd at 14.928 kHz (sixteen times the Olympus beacon's nominal switch rate). This approach accommodates the input frequency variation whilst allowing a relatively straightforward LC filter at 70 MHz to provide adequate front end selectivity. The 10.7 MHz I.F. is filtered by a custom designed crystal filter with bandwidth (-1 dB) of 15 kHz. This filter also provides adequate rejection of polarisation switching sidebands which can alias onto the carrier after digitisation. The ADC is a self-calibrating 14-bit successive approximation type, sampling at 59.712 kHz (four times the final I.F.).

The R.F. input and L.O. signals are connected via coaxial inserts through the backplane connectors. Milled aluminium boxes provide shielding of the analogue sections of the cards.

Digital Processing

The final I.F. is locked at one quarter of the ADC sampling rate, so its removal is simple (in the digital domain), to leave a complex data stream for each received polarisation. Carrier frequency tracking is accomplished by spectral analysis of the input signal in one received polarisation channel. An intelligent tracking algorithm allows frequency "boxes" of about 1 Hz width (a width well matched to the phase-noisy spectrum of signals at this point). Frequency tracking of a CW beacon can be maintained down to a C/No of 9 dB, and of a polarisation-switched beacon down to 15 dB (a higher figure since the sideband power is rejected in the tracking algorithm). The C/No at which tracking stops is operator-selectable, and the receiver holds its estimate of beacon carrier frequency at that point and waits for the signal level to recover, reacquiring with no hysteresis after short term "deep fades".

The carrier is removed to leave signals ready for polarisation tracking (analogous to symbol timing recovery). This is performed by decimating the sample rate to four times the beacon switch rate, and dumping the samples sequentially into four integrators. Analysis of the bin contents provides an indication of the phase of the (polarisation) modulation (if the C/No is high enough). Having determined the sampling points, a variable group delay filter provides correct sample phase (on a polarised signal), and a channel filter provides correct attenuation of switching sidebands. Finally the signals are decimated to a sample rate of approximately 100 Hz, normalised in phase to the HH component (if C/No is above 20 dB), formatted for the output interface, and sent.

Output Data Format

The twelve-bit output data wordlength and 100 Hz sampling rate have been agreed between OPEX working groups WG1 (Hardware), and WG2 (Data Pre-processing). The intention is that information of a 30-40 Hz bandwidth is to be retained during conditions of low fading in order to investigate scintillation effects, while the bandwidth will be dropped by a preprocessor during deep fades.

Operation

A serial link is provided for connection to a terminal used to set up receiver parameters and optionally to monitor status (the status information is also sent out with the output data). Receiver front panel display is minimal, consisting of lock indication and machine function/error status.

Trials

The receiver tracking performance has been developed with the aid of computer simulation. Field trials are scheduled for July 1988 at an open-air test site at the Rutherford Appleton Laboratory, Chilton, England. The site provides transmission and reception at 20 GHz, and test signals of realistic quality.

Acknowledgments

The DBR-1 receiver development has been funded in part by the European Space Agency (European Space Research and Technology Centre, Noordwijk, Netherlands) and the Science and Engineering Research Council (Rutherford Appleton Laboratory, Chilton, England. RAL will also provide field test facilities.)

References

Barton, S.K., "Section 6.4 : Alternative Digital Receivers" in OPEX Handbook for Beacon Receiver Design, Issue 1, January 1985

OLYMPUS BEACON RECEIVER

Jens Østergaard

ElektronikCentralen, DK-2970 Hørsholm, Denmark

A medium-size Beacon Receiving System for reception and processing of the B1 (20 GHz) and B2 (30 GHz) beacons from Olympus has been developed. Integration of B1 and B2 receiving equipments into one system using one antenna and a common computer for control and data processing provides the advantages of a compact configuration and synchronization of the two receiver chains. Range for co-polar signal attenuation measurement is about 30 dB for both beacons, increasing to 40 dB for B2 if the receivers are synchronized to B1. The accuracy is better than 0.5 dB. Cross-polarization discriminations of the order of 10 to 30 dB may be determined with an accuracy of 1 to 2 dB. A number of radiometers for complementary measurements of atmospheric attenuation from 13 to 30 GHz has also been constructed. A small multi-frequency system for operation around 22 GHz and 31 GHz is presently under development.

1. Introduction

For use in propagation experiments with signals transmitted from the upcoming ESA satellite Olympus, a dual-frequency Beacon Receiving System has been developed at ElektronikCentralen (EC), Denmark. It will receive and process the B1 (20 GHz) and B2 (30 GHz) satellite beacon signals.

The system is a self-contained equipment comprising an outdoor integrated antenna/receiver/detector part and a remotely placed computer. The compact configuration and rigid mechanical construction ensures safe transportation and easy installation. By tight temperature control of the receiver, stable and accurate operation is obtained even under extreme environmental conditions.

The computer and its dedicated software enables easy operation of the system and provides flexible data processing capabilities. Measured information on detected signals is displayed and printed out locally, and it may be transferred to a central computer for postprocessing, or to a data storage medium.

The system is primarily designed for measurement of B1 and B2 co-polar signal attenuation with large dynamic range and high accuracy. However, the crosspolarization discrimination of B1 - or rather the cross-polarization isolation - is also determined and reliable results for significant events are provided. The system can easily be expanded for measurement of the B2 cross-polar signal as well. Further, a high signal sampling rate makes the system well suited for investigation of scintillation phenomena.

Propagation experiments with beacons are usually complemented by parallel radiometer measurements. For this purpose, EC has developed a range of

radiometers for K_u-band and for 20 and 30 GHz. In the following sections the equipments are described.

2. Beacon Receiver

In the design of the Beacon Receiving System, it has been the objective to make a system which is compact, easy to install and operate, and suited for continuous, unattended operation - and which provides satisfactory measuring capability, e.g. dynamic range and accuracy, on the signals available.

Figure 1 shows the system configuration.

The antenna is comparatively small, 1.3 m diameter, so pointing will not be critical. The dual-frequency Cassegrain system has high efficiency and good polarization isolation properties, and it allows the receiver to be mounted on the back of the main reflector, close to the feed.

By imbedding the main reflector in a temperature controlled enclosure, the reflector may be heated and kept free from ice. At the same time the receiver and detector equipments which are mounted within the enclosure will be protected from exposure to extreme ambient temperatures. The internal temperature in the receiver and detector boxes is controlled to about $\pm 2^{\circ}\text{C}$ thereby eliminating the need for active gain drift determination by means of pilot signals.

The receiver comprises front end chains for the B1 and B2 signals. Each chain contains a low-noise preamplifier and provides double frequency conversion. The box containing the front ends is mounted directly on the feed assembly which can be rotated for precise polarization alignment.

The two front end chains are synchronized, the local oscillator signals being derived from a common reference oscillator. The local oscillator assembly has a performance similar to that of the satellite beacon generator as concerns frequency stability and phase noise. This means that the characteristics of the received beacon signals are not unduly degraded by the receiving system.

In the detector the received polarization-switched B1 signal is demodulated and co-polar and cross-polar signals detected. The VCO's of the B1 and B2 chains may be synchronized, either by locking to B1 or by locking to B2. This gives increased flexibility and extended dynamic range for B2 measurements.

Switching detectors produce I and Q components of the received signals. This will ensure maximum accuracy in the extraction of amplitude and phase information from the signals. I and Q components, as well as sensor and status signals are transmitted in digital form to a PC-type computer, which may be placed at a convenient indoor location.

The computer will provide efficient control and monitoring of the overall operation of the system and will give alarm in case of any malfunction.

It processes the data on received beacon signals and performs the transmission of the final results to a central computer or to a hard disk for storage. Local graphics display and printing of the results is made available.

The receiving system will have a G/T of 18 dB/K at 20 GHz and 20 dB/K at 30 GHz. In Europe this will ensure a dynamic range for attenuation measurements on co-polar signals of 29 dB for B1, and 31 dB for B2, if the two receivers are not synchronized. When B2 is synchronized to B1 its dynamic range is extended by about 10 dB. The accuracy is about 0.5 dB for maximum measurable attenuations, and 1-2 dB on the expected values of cross-polarization discrimination.

3. Radiometers

3.1 K_u-band Radiometer

The K_u-band radiometer is intended for operation at a single frequency in the band 13 to 18 GHz. It is a compact, self-supporting system with an outdoor integrated antenna/receiver part and a remotely placed controller/computer. Data processing facilities for calculation of results such as sky noise temperature and atmospheric attenuation are provided.

The basic configuration of the radiometer encompasses a 1 m Cassegrain antenna, a radiometer receiver of the noise injection type, and a PC. Figure 2 shows a block diagram of the radiometer.

The Cassegrain antenna provides minimum distance from feed horn to receiver which means small feed loss corrections. The feed horn is mechanically integrated in the receiver subsystem which is mounted on the main reflector. This arrangement permits easy replacement of receivers and change of polarization without need for recalibration. An insulated heated enclosure houses the receiver and all associated equipment. The main reflector forms one of the faces of the enclosure and may thus always be kept above freezing level. Warm air will be blown onto the feed horn window in order to keep it free from water and ice.

The noise injection type receiver yields a maximum of independence of gain variations and mismatches within the noise injection feedback loop thus ensuring a high long-term stability. The measurement accuracy depends mainly on the precise knowledge of the temperature of the internal reference load, which is easily controlled.

The receiver front end and detector is installed in a temperature regulated box. This box also contains a datalogger which registers the temperature of the key microwave components in the front end and feed assembly as well as antenna surface temperature. A variety of house-keeping data is also measured.

The detected noise power from the receiver and the temperature and house-keeping signals are digitized and transmitted to the computer which per-

forms the calculation of the sky noise temperature. In this calculation the effects of losses and reflections in the feed waveguide and horn are corrected for, as well as the ground noise pick-up through the antenna sidelobes. In an initial measurement and calibration, the antenna pattern has been determined and the power distribution table introduced in the computer software.

From the sky noise temperature the apparent atmospheric attenuation at the measuring frequency is found. By means of a scaling formula the attenuation at any frequency in the range 10 to 22 GHz may be calculated. On the computer's screen the found results are presented in graphical form, and a list of housekeeping data are displayed. Also, results from several months are stored in the computer.

The radiometer system has proved high measuring accuracy and stability. The absolute accuracy in sky noise temperature is better than 4 K at 30 deg. elevation. A high-performance cryogenic load is used in initial receiver calibrations and in recalibrations which are only required at 8 to 12 months intervals. More frequent calibration checks are performed by use of a computer-controlled tip-curve method.

3.2 20/30 GHz Radiometer

EC has previously supplied single-frequency radiometers for 20 and 30GHz at the same configuration as described above. Now a new 20/30 GHz radiometer system is under development. It is intended for a range of applications in satellite communication (signal attenuation correction), satellite ranging (path delay correction), and in scientific investigations of atmospheric properties (content of water and water vapor).

This dual frequency, or multi-frequency, system will measure sky noise temperature at one or several frequencies around 22 GHz and at one frequency around 31 GHz. High accuracy is a prime performance objective which imposes strict requirements on the antenna system. Sidelobes shall be extremely low in order to avoid ground noise pick-up, and equal beam-width at 20 and 30 GHz are desired. An offset reflector antenna with optimum performance will be developed. A compact selfcontained equipment with an absolute accuracy better than 4 K and great operational flexibility is aimed at.

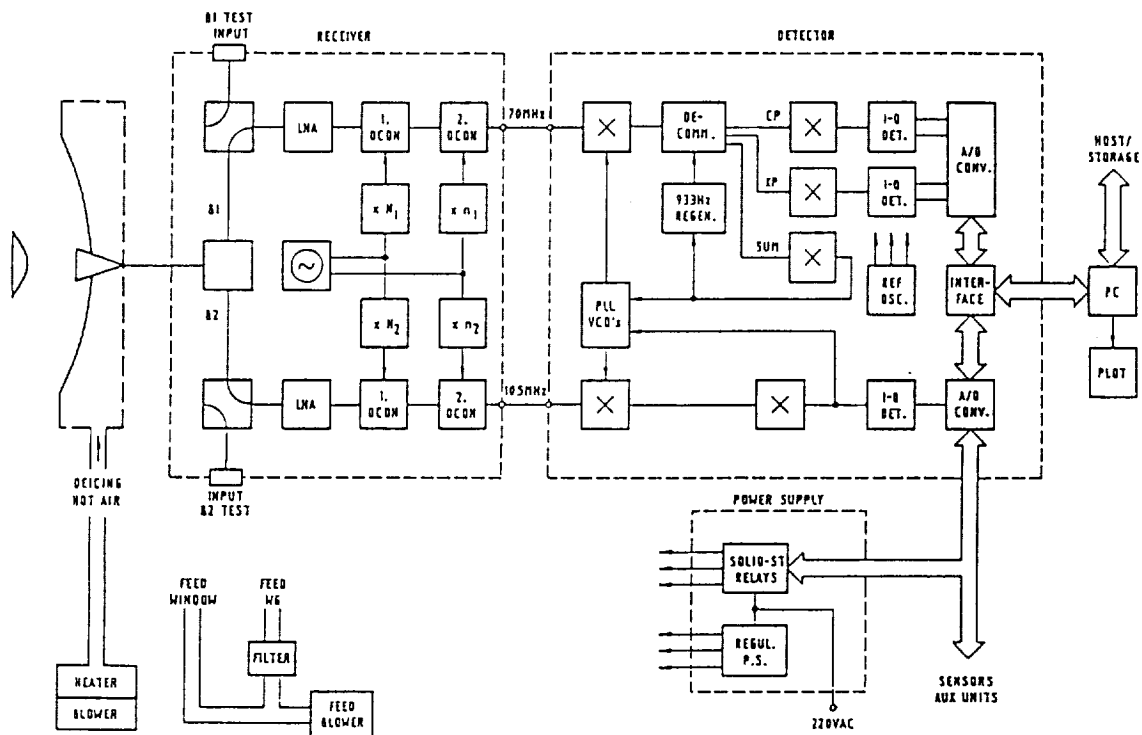


Figure 1 Simplified B1/B2 Receiving System, Simplified Block Diagram

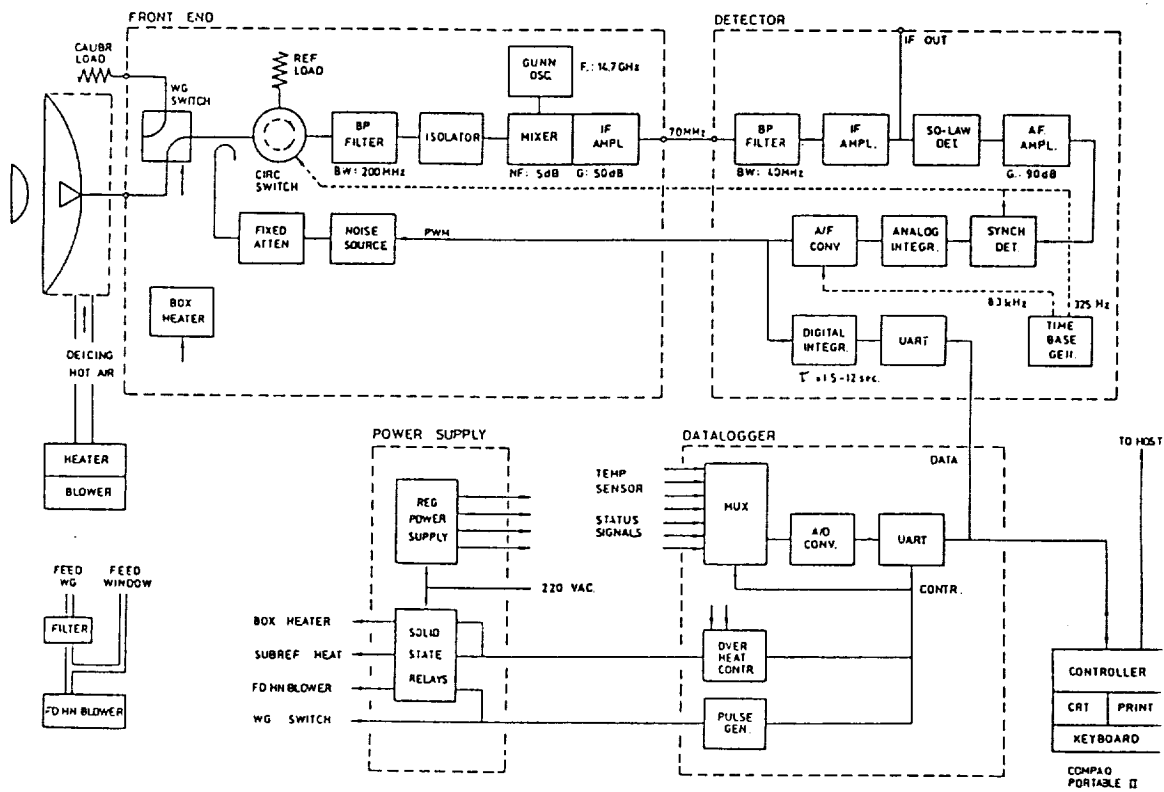


Figure 2 Ku-band Radiometer, Block Diagram.

ORIGINAL PAGE IS
OF POOR QUALITY

THE PROPAGATION INFORMATION CENTER AT THE UNIVERSITY OF COLORADO

ERNEST K. SMITH and WARREN L. FLOCK
Department of Electrical and Computer Engineering
Campus Box 425, University of Colorado
Boulder, CO 80309

Abstract--A Propagation Information Center is in the process of being established at the University of Colorado with connections to NAFEX and to the NASA program at CU for Interdisciplinary Research in Telecommunications Policy and Technology Issues. The Propagation Information Center was conceived as a response to several items in the Science Review of the NASA Propagation Program carried out in September of 1986 by a distinguished panel of experts. E. K. Smith joined W. L. Flock at the University of Colorado in July 1987. In preparation for the opening of the Information Center one or the other (or both) has attended six national or international meetings related to the work of the Center. The program for the Center is conceived as including archival aspects: a memory of past work by NAFEX members; accounts of relevant research activities around the world; papers published in pertinent areas of propagation; and pertinent propagation data files. Duties of the Center should include: exchanging information as to future plans with research organizations around the world; scanning the literature for possible CCIR SG-5 contributions; carrying out quick response studies as requested by program management; conducting customer surveys of users of the NASA Propagation Programs products; preparing a quarterly newsletter to help maintain communication amongst program participants; and finally, assisting students and faculty at the University of Colorado working on policy issues for NASA with problems relating to propagation.

1. Introduction.

In September 1986, John Kiebler of the Communications and Information Division of NASA Headquarter (Code EC), conducted the first-ever formal program review of the NASA Propagation Program. He contracted with Science and Technology, Inc. to handle the arrangements and a panel of experts, namely Prof. Henry G. Booker, chairman, Dr. Gert Brussaard, Dr. K. S. McCormick, and Dr. David V. Rogers, was enlisted. Among their recommendations (Booker et al., 1987) were the following:

- The effectiveness of the program would be enhanced by cooperative projects with other organizations.
- There should be a mechanism for monitoring propagation research of other governmental and industrial organizations.
- The "acclaimed" Propagation Handbooks should be updated periodically, preferably in coordination with the 4-year CCIR cycle.
- The CCIR support activities should be maintained within the propagation program.

With these points in mind and, with the recognition that institutional memory is short, and hence an archiving function would be useful, the concept of a propagation information center began to take

shape (Flock, 1987a). The University of Colorado at Boulder has some built in advantages as a site for the Center. The winter URSI/IEEE National Radio Science Meeting is traditionally held at the University of Colorado. Boulder is the home of the Institute for Telecommunication Sciences, the NOAA Environmental Research Laboratories, the NBS Radio Standards Laboratory, and the National Center for Atmospheric Research, each of which has ties with the University of Colorado.

Office space was made available to Ernest Smith in July and an appointment as Professor Adjunct in the Electrical and Computer Engineering Department was made official in November. Warren Flock became Professor Emeritus in December, 1986 and he and Smith now share an office with space reserved across the hall for a secretary. They bring complementary talents to the job. Warren Flock has just completed the second edition of the Propagation Handbook for frequencies below 10 GHz (Flock, 1987b) and has organized and taught a course on Earth-space propagation at CU. Ernie Smith is more the outside man with broad experience with the CCIR, URSI, the IEEE, and foreign propagation laboratories.

2. Recent Activity.

While the final hurdle for the Propagation Information Center is not yet surmounted, still the outcome has seemed sufficiently assured that it was appropriate to start making preparations. Keeping up to date on worldwide propagation research has seemed to be especially good. Towards this end we have attended the following conferences:

- URSI General Assembly, Israel, August/September, 1987. Ernie Smith was a delegate and organized and chaired an invited session on Planetary Noise Environment (Smith 1987). He also served as secretary for the USNC Young Scientist Selection Committee.
- International Conference on Communications Technology, Nanjing, November, 1987 was attended by Warren Flock who presented an invited paper (Flock and Smith, 1987) on mobile satellite propagation.
- USNC/URSI National Radio Science Meeting, Boulder, January 1988 was attended by Ernie Smith. Both Ernie and Warren are members of the IEEE Wave Propagation Standards Committee which was meeting during the same period and Warren is currently chairman of the Mini-review subcommittee. Ernie had looked after the interests of URSI Commissions E and F for the Program Committee in his capacity of member-at-large of USNC/URSI.
- 1988 International Symposium on Radio Propagation (ISRP'88, Beijing, sponsored by URSI and Chinese Institute of Engineers, and co-sponsored by IEEE AP-S) April 18-21, 1988, was attended by Ernie as IEEE AP-S representative and member of the program committee. Ernie delivered a plenary address in English and Chinese and a technical paper (Smith and Flock, 1988). He also attended part of the URSI Beacon Satellite Symposium (IBSS'88) which was co-located with ISRP'88.
- Mobile Satellite Symposium, Pasadena, May 3-5, 1988, was attended by Warren, who delivered a paper (Flock and Smith, 1988).
- 1988 AP-S International Symposium and URSI Radio Science Meeting, Syracuse, June 6-10, was attended in part by Warren and Ernie.

Other preparations for the opening of the Propagation Information Center (CUPIC) include:

- Preparation of mailing lists for the Propagation Handbooks.
- Reviewing the Propagation Handbooks.
- Acquiring a Macintosh SE and LaserWriter.
- Acquiring answering machines on Ernie's lines (303) 492-7123 office, and (303) 530-3440 home.
- Improving ties with the Center for Space and Geosciences Policies (also supported by NASA Code EC) which has long had a propagation interest.

3. Program and Structure of the Propagation Information Center (CUPIC).

CUPIC is conceived of as an evolving entity which will provide a service to NAPEX participants and to NASA and JPL management. Current staffing is two-thirds of a man-year, covering Professors Smith and Flock, and a part-time secretary/programmer. Present plans include developing the the following services and archives as time permits:

- Serve as a memory for past work of NAPEX. CUPIC will maintain a master copy of each final report and paper produced under NAPEX and will contract with a local organization to reproduce copies upon request.
- Maintain indices of current propagation papers cross-referenced by subject, author, and year. Copies of current propagation papers will be maintained either in our periodical holdings (Radio Science, IEEE Proceedings, and AP-S and COM-Soc Transactions and journals) or reprint copies.
- Possibly maintain certain propagation data files (e.g. LMSS shadowed data samples, rain impaired data sample at 20 GHz) produced by the NAPEX participants.
- Exchange research products with other research organizations engaging in Earth-space propagation research in the US and abroad, and keep abreast of their current, and, if possible, future plans.
- Participate in the work of USPC/CCIR Study Groups 5 and 6, scan current literature for possible contributions to relevant areas of SG 5/6. Prepare submissions as appropriate.
- Undertake customer surveys of the recipients of NAPEX products.
- Prepare a newsletter about activities of NAPEX participants and about research in radio-wave propagation in general. Short articles will be solicited from NAPEX participants and cooperating organizations.
- Collaborate with the Center for Space and Geoscience Policy at the University of Colorado to develop information which may be helpful to NASA and JPL management in determining future directions for the NAPEX program.

References

Booker, H. G., G. Brussaard, K. S. McCormick, and D. V. Rogers, "Science Review of the NASA Radio Propagation Program; Report of a Panel Convened in Columbia, Maryland 3-5 September, 1986," STC-2127, Science and Technology Corporation, Hampton, VA, February 1987.

Flock, W. L., "An Information Center for Propagation Studies", pp 10, 11, Proceedings of NAFEX XI, Virginia Tech, June 1987, F. Davarian Ed., JPL D-4647, August 1987a (JPL internal document).

Flock, W. L., "Propagation Effects on Satellite Systems at Frequencies Below 10 GHz; A Handbook for Satellite System Design", NASA Reference Publication 1108(02), Second Edition, December 1987b.

Flock, W. L. and E. K. Smith, "Propagation Impairments in Mobile Satellite Transmission", Proceedings of the 1987 Conference on Communications Technology (ICCT'87), November 9-11, 1987, Nanjing, China, pp 810-813, World Scientific, Singapore, November 1987.

Flock, W. L. and E. K. Smith, "Propagation Effects on Spread-Spectrum Mobile-Satellite Systems," Proceedings of the Mobile Satellite Conference, pp 133-139, JPL Publication 88-9, May 1988.

Smith, E. K., "Introductory Comments" to Session E.9 Satellite and Planetary Noise Environments, Abstract Book, page 398, XXII URSI General Assembly of the International Union of Radio Science, Tel Aviv, Israel, August 24 - September 2, 1987.

Smith, E. K. and W. L. Flock, "Some Current Problems in Earth-Space Propagation," Proceeding of the International Symposium on Radio Propagation, pp 123-126, Beijing, April 18-21, 1988; International Information Exchange Service Co., Kowloon, Hong Kong, April, 1988.

**ORIGINAL PAGE IS
OF POOR QUALITY**



